Molecular dissection of the spindle and kinetochore associated Astrin/SKAP complex

Inaugural-Dissertation
zur Erlangung des Doktorgrades
Dr. rer. nat.

an der Fakultät für Chemie
und Chemische Biologie der

Technischen Universität Dortmund

angefertigt am

Max-Planck-Institut für molekulare Physiologie

Dortmund

vorgelegt von

Alexandra Friese

Dortmund

August 2015

Die der vorliegenden Arbeit zugrunde liegenden Experimente wurde in der Zeit von Oktober 2011 bis August 2015 am Max-Planck-Institut für molekulare Physiologie, Dortmund, in der Abteilung für mechanistische Zellbiologie unter der Anleitung von Prof. Dr. Andrea Musacchio durchgeführt.

1. Gutachter: Prof. Dr. Andrea Musacchio
2. Gutachter: Prof. Dr. Roland Winter

Table of Contents

Abbreviations

+TIPs	plus end tracking proteins
3C	PreScission protease cleavage site
APC/C	anaphase-promoting complex/cyclosome
ATP	adenosine triphosphate
AU	absorbance units
AUC	analytical ultracentrifugation
BS2G	bis(sulfosuccinimidyl)glutarate
BSA	bovine serum albumin
CCAN	constitutive centromere associated network
Cdk	cyclin dependent kinase
CH domain	calponin homology domain
CPC	chromosomal passenger complex
CREST	calcinosis, Raynaud's syndrome, esophageal dysmotility, scleroderdactyly, telangiectasia
DAPI	4,6-diamidin-2-phenylindoldihydrochlorid
DMEM	Dulbecco's modified eagle's medium
DNA	deoxyribonucleic acid
DSS	di(succinimidyl)suberate
EB protein	end binding protein
EM	electron microscopy
f.l.	full-length
FBS	fetal bovine serum
GDP	guanosine diphosphate
GFP	green fluorescent protein
GMPCCP	guanosine-5'-[(α,β)-methyleno]triphosphate
GST	glutathione-S-transferase
GTP	guanosine triphosphate
IF	immunofluorescence
K_d	dissociation constant
KMN	Knl1 complex/Mis12 complex/Ndc80 complex
MAP	microtubule associated protein
MCAK	mitotic centromere-associated kinesin
MCC	mitotic checkpoint complex
MS	mass spectrometry

MST	microscale thermophoresis
MT	microtubule
MTBD	microtubule-binding domain
MW	molecular weight
PBS	phosphate buffered saline
PEG	polyethylene glycol
PP1	protein phosphatase 1
RNA	ribonucleic acid
RZZ	Rod/Zwilch/ZW10
SAC	spindle assembly checkpoint
SDS-PAGE	sodium dodecyl sulfate polyacrylamide gel electrophoresis
SEC	size exclusion chromatography
SeMet	seleno-methionine
siRNA	small interfering ribonucleic acid
Ska complex	spindle and kinetochore associated complex
SKAP	small kinetochore associated protein
SLS	Swiss Light Source
TEV	tobacco etch virus
TIRF	total internal reflection fluorescence
TTL	tubulin tyrosin ligase
Tub	tubulin
WB	western blot
WT	wild type

One- and three-letter amino acid codes were used according to the nomenclature recommendations of the International Union of Pure and Applied Chemistry (IUPAC) and the International Union of Biochemistry and Molecular Biology (IUB).

List of Figures

List of Tables

ABSTRACT

Faithful chromosome segregation is crucial for cells. To achieve it, large protein complexes called kinetochores form a link between chromosomes and the mitotic spindle. The mechanisms of the recruitment and regulation of kinetochore components leading to functional kinetochore-microtubule attachments are still poorly understood. The work described in this thesis takes a step towards understanding this complex process by analyzing the interactions of the spindle and kinetochore associated Astrin/SKAP complex that is essential for mitotic progression and chromosome biorientation. A combinatorial approach including biochemical, biophysical, cell biological and structural methods was used to elucidate the structure and the functional role of the Astrin/SKAP complex during mitosis.

Studies on the intersubunit interaction of the Astrin/SKAP complex identified the domains encompassing amino acids 482 to 850 in Astrin and 159 to 316 in SKAP as minimal interaction domains. The microtubule-binding domain of SKAP was mapped to amino acids 135 to 225, while no microtubule-targeting domain could be identified in Astrin, suggesting that the Astrin/SKAP complex binds microtubules through SKAP. Microtubule binding of SKAP requires several conserved positively charged residues that interact with microtubules at both the inter- and intra-tubulin dimer interface. The microtubule-binding sites of SKAP at least partly overlap with those of the Ndc80 complex, the major microtubule binder of the kinetochore. SKAP binds tubulin in solution and bundles microtubules. This work suggests that SKAP is a microtubule-stabilizing factor that facilitates microtubule nucleation and growth, explaining the functions of the Astrin/SKAP complex in spindle organization and stabilization of kinetochore-microtubule attachments. Functional inactivation of the microtubule-binding domain of SKAP prevents rescuing the significant defects in spindle formation, chromosome congression and mitotic progression that are caused by depletion of SKAP. Furthermore, this study shows that the kinetochore localization of the Astrin/SKAP complex does not depend on the presence of microtubules. First insights into the structural organization of the Astrin/SKAP complex reveal a highly elongated and flexible structure. A promising step towards the crystal structure of SKAP could be achieved by successful crystallization of different SKAP constructs.

In summary, this work provides a first thorough *in vitro* analysis of the structure and function of the Astrin/SKAP complex. The obtained results significantly advance our understanding of the functional role of the Astrin/SKAP complex during mitosis and the mechanisms leading to functional kinetochore-microtubule attachments.

ZUSAMMENFASSUNG

Die ordnungsgemäße Trennung der Chromosomen ist entscheidend für Zellen. Um dies zu erreichen, bilden große Proteinkomplexe, sogenannte Kinetochore, eine Verbindung zwischen den Chromosomen und der mitotischen Spindel. Die Mechanismen der Rekrutierung und Regulation von Kinetochor-komponenten, welche zu funktionellen Kinetochor-Mikrotubuli-Anbindungen führen, sind nach wie vor unzureichend erforscht. Die in der vorliegenden Dissertation beschriebene Arbeit erweitert das Verständnis dieses komplexen Prozesses durch die Analyse der Interaktionen des Spindel- und Kinetochor-assoziierten Astrin/SKAP-Komplexes, welcher essenziell für den mitotischen Verlauf und die Biorientierung der Chromosomen ist. Ein kombinatorischer Ansatz aus biochemischen, biophysikalischen, zellbiologischen und strukturellen Methoden wurde angewendet, um die Struktur und die funktionelle Rolle des Astrin/SKAP-Komplexes während der Mitose aufzuklären.

Untersuchungen der Interaktionen zwischen den Untereinheiten des Astrin/SKAP-Komplexes identifizierten die Domänen, welche die Aminosäuren 482 bis 850 in Astrin sowie 159 bis 316 in SKAP umfassen, als minimale Interaktionsdomänen. Die Mikrotubuli-bindende Domäne von SKAP wurde auf die Region von Aminosäure 135 bis 225 eingegrenzt, während keine Mikrotubuli-bindende Domäne in Astrin identifiziert werden konnte. Dies deutet darauf hin, dass der Astrin/SKAP-Komplex durch SKAP an Mikrotubuli bindet. Die Mikrotubulibindung von SKAP erfordert mehrere konservierte positiv geladene Reste, welche mit Mikrotubuli sowohl an der Inter- als auch der Intra-Tubulindimer-Oberfläche interagieren. Die Mikrotubulibindestellen von SKAP überlappen sich zumindest teilweise mit denen des Ndc80-Komplexes, welcher der Hauptbinder für Mikrotubuli ist. SKAP bindet Tubulin in Lösung und bündelt Mikrotubuli. Diese Arbeit deutet darauf hin, dass es sich bei SKAP um einen Mikrotubuli-stabilisierenden Faktor handelt, welcher die Nukleation und das Wachstum von Mikrotubuli erleichtert, wodurch die Funktionen des Astrin/SKAP-Komplexes in der Spindelorganisation und Stabilisierung von Mikrotubuli-Kinetochor-Anbindungen erklärt werden können. Die funktionelle Inaktivierung der Mikrotubuli-bindenden Domäne von SKAP unterbindet die „Rettung“ signifikanter Defekte in der Spindelausbildung, der Chromosomenkongression und dem mitotischen Verlauf, welche durch die Degradation von SKAP verursacht werden. Weiterhin zeigt diese Studie, dass die Kinetochorlokalisierung des Astrin/SKAP-Komplexes nicht von der Anwesenheit von Mikrotubuli abhängig ist. Erste Einblicke in die strukturelle Organisation des Astrin/SKAP-Komplexes lassen

eine stark elongierte und flexible Struktur erkennen. Ein vielversprechender Schritt zur Kristallstruktur von SKAP konnte durch die erfolgreiche Kristallisation verschiedener SKAP-Konstrukte erreicht werden.

Zusammenfassend liefert diese Arbeit eine erste sorgfältige *in vitro* Analyse der Struktur und Funktion des Astrin/SKAP-Komplexes. Die erhaltenen Ergebnisse leisten einen signifikanten Beitrag zur Verbesserung unseres Verständnisses der funktionellen Rolle des Astrin/SKAP-Komplexes während der Mitose und der Mechanismen, welche zu funktionellen Kinetochor-Mikrotubuli-Anbindungen führen.

1 INTRODUCTION

1.1 The cell cycle

The cell cycle describes the fundamental and highly regulated series of events, including DNA duplication and cell division, by which all cells reproduce their genetic material in order to generate two identical daughter cells (Alberts et al., 2008; Morgan, 2007). The eukaryotic cell cycle is divided into four phases. In S phase - S stands for DNA synthesis - the replication of DNA and the duplication of chromosomes take place. The duplicated chromosomes are called sister chromatids. They are tightly linked by a protein complex called cohesin until the latter is cleaved by the protease separase during mitosis (Waizenegger et al., 2000). Mitosis is the process of nuclear division and together with the division of the cell itself, also known as cytokinesis, represents one of two major events of M phase, in which the segregation of chromosomes to two daughter cells occurs (Alberts et al., 2008; Morgan, 2007). Between the M and S phases most cells pass through two so-called gap phases, the G1 phase between M and S phase and the G2 phase between S and M phase. These additional phases provide enough time for cell growth and duplication of proteins and cell organelles. The phases G1, S and G2 are summarized as interphase.

The term mitosis was coined by Walther Flemming in the early 1880s (Flemming, 1882; Mitchison & Salmon, 2001). It summarizes all processes that are required to faithfully segregate the sister chromatids, so that both daughter cells contain an identical set of chromosomes (Alberts et al., 2008). This extremely complex process is tightly regulated, as it is crucial for the viability of cells to maintain the integrity of their genomes. Defects in the accuracy of mitotic events can result in aberrations of the chromosome number, so-called aneuploidy, and genetic instability often leading to cell death or cancer (Lengauer et al., 1998).

Mitosis can be subdivided into five phases called pro-, prometa-, meta-, ana- and telophase (Alberts et al., 2008; Morgan, 2007). The processes that take place during these phases are schematically shown in figure 1.1. In prophase, chromosomes condense into a compact flexible form and the centrosomes, the starting points of the spindle, mature, so that the assembly of the spindle can be initialized. In prometaphase, the nuclear envelope breaks down and the chromosomes become attached to the spindle microtubules at their centromere regions via large protein complexes known as kinetochores. In metaphase, all chromosomes are aligned at the spindle midzone, the so-called metaphase plate, in a state called biorientation

with both sister chromatids connected to spindle microtubules emanating from opposite spindle poles. In anaphase, the sister chromatids are separated and pulled towards the opposite spindle poles. After these early events at the onset of anaphase, also known as anaphase A, the spindle poles themselves move apart from each other in anaphase B. In telophase, the two sets of chromosomes are repackaged into the daughter nuclei completing the process of mitosis.

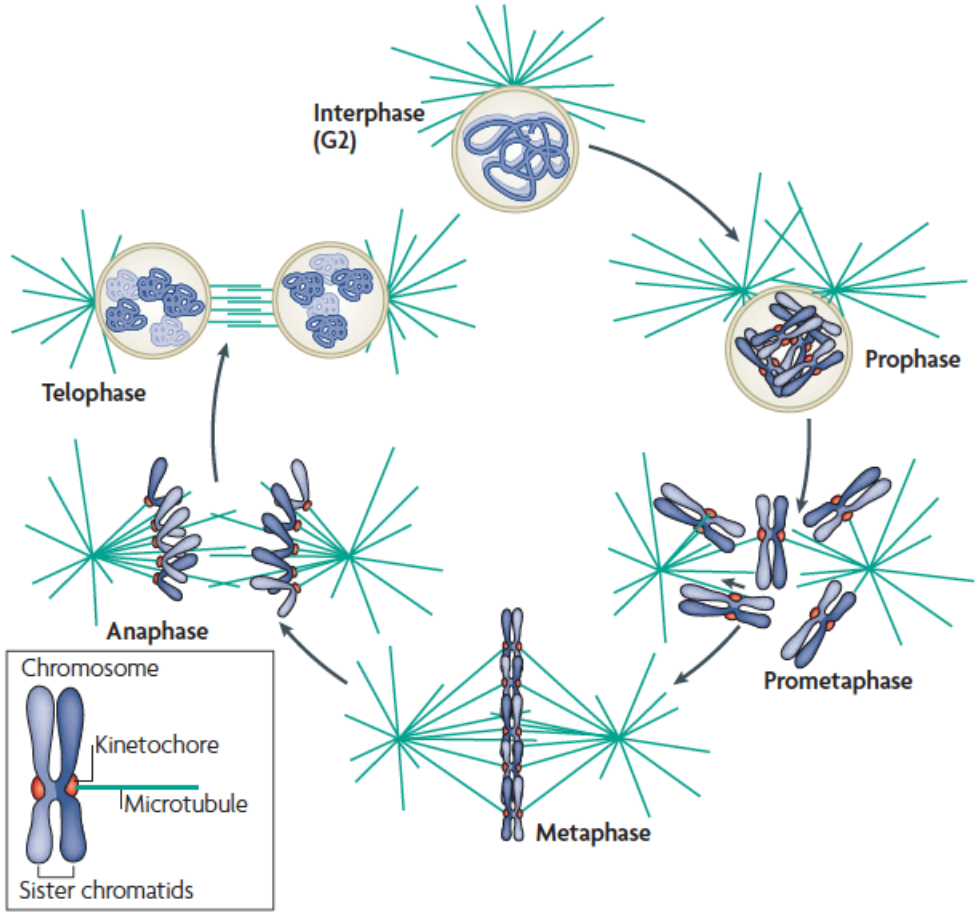

Figure 1.1: Overview of mitotic cell division. During prophase, replicated chromatin is condensed. During prometaphase, the nuclear envelope breaks down and chromosomes get attached to spindle microtubules via kinetochores. In metaphase, all chromosomes are bioriented and aligned at the metaphase plate. During anaphase, sister chromatids become separated and are pulled towards opposite spindle poles. During telophase, two daughter nuclei are generated. The cell cycle is completed by cytokinesis (not shown here). Figure adapted from Cheeseman & Desai, 2008.

Because of the need for accuracy, cell cycle progression is strictly controlled by a series of so-called checkpoints that ensure initiation of specific cell cycle events in the correct order and only upon successful completion of the previous event (Coudreuse & Nurse, 2010; Morgan, 2007). This cell cycle control system is based on the oscillating activities of a family of enzymes called the cyclin dependent

kinases (Cdks) that regulate cell cycle progression at three major checkpoints. The first checkpoint, the G1/S checkpoint or Start, makes sure that DNA replication only starts if the conditions for cell proliferation are ideal. The G2/M checkpoint regulates the entry into mitosis. The third checkpoint is the metaphase-to-anaphase transition, which is regulated by the spindle assembly checkpoint (SAC) that stimulates the separation of sister chromatids only after biorientation of all chromosomes (Musacchio & Salmon, 2007).

1.2 Microtubules and the mitotic spindle

Besides the function of microtubules in forming the mitotic spindle during cell division, microtubules exert several functions in non-dividing cells including organization of the cytoplasm, positioning of the nucleus and organelles as well as forming flagella and cilia (Desai & Mitchison, 1997). In the 1960s, it was discovered that the mitotic spindle is an array of long microtubule fibers consisting of tubulin as building block (Kiefer et al., 1966). Microtubules are hollow cylindrical polymers, 25 nm in diameter, comprised of 12 to 15 protofilaments with a heterodimer of α- and β-tubulin as its building block (Desai & Mitchison, 1997). These α-/β-tubulin heterodimers associate in a head-to-tail conformation to form a polar lattice with a slowly growing minus end, exposing α-tubulin, and a fast growing plus end, exposing β-tubulin (Wittmann et al., 2001). The assembly of microtubules proceeds in two phases, nucleation and growth or elongation (Johnson & Borisy, 1977). The barrier to initiate microtubule growth by formation of nuclei is much higher than to elongate an existing polymer, but this nucleation barrier can be overcome in the presence of certain proteins (Murphy & Borisy, 1975). Indeed, several microtubule-associated proteins (MAPs) are implicated in the active control of the polymerization state of microtubules by promoting either their polymerization or depolymerization (Cheeseman & Desai, 2008), as further described below.

As shown in figure 1.2, microtubules are highly dynamic structures exhibiting fast transitions from polymerization to depolymerization, so-called catastrophes, and reverse transitions from depolymerization to polymerization, also known as rescue. This non-equilibrium polymerization behavior is known as dynamic instability (Desai & Mitchison, 1997) and the hydrolysis of GTP at the exchangeable or E-site of β-tubulin serves as its energy source (Weisenberg et al., 1976; David-Pfeuty et al., 1977). The GTP-binding site on α-tubulin, the so-called N-site, is nonexchangeable and constitutively bound to GTP, because it is buried within the tubulin dimer

interface. The E-site of β-tubulin is exposed at the surface of the microtubule plus end and contacted by a newly incorporated tubulin dimer, which completes the binding pocket and enables hydrolysis, thereby forming a link between microtubule polymerization and GTP hydrolysis (Nogales et al., 1999). The resulting GDP after GTP hydrolysis is locked in the polymer lattice, so that microtubules predominantly contain GDP-tubulin. The polymerizing microtubule end is stabilized by a 'GTP cap', which has been postulated because of the much slower off rate of GTP-tubulin from a GTP-lattice compared to the off rate of GDP-tubulin from a GDP-lattice during depolymerization (Mitchison & Kirschner, 1984). Upon loss of the 'GTP cap', depolymerization with very rapid loss of GDP-tubulin subunits takes place. The released GDP-tubulin is then reprimed for another polymerization cycle by nucleotide exchange from GDP to GTP.

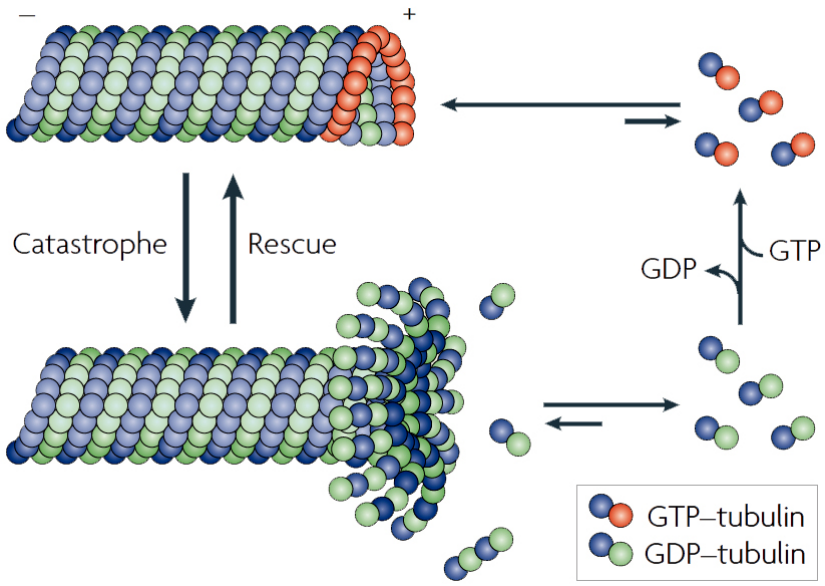

Figure 1.2: Microtubule dynamics. Microtubules form a polar lattice by head-to-tail association of α-/β-tubulin dimers. Their dynamic structure shows fast transition from polymerization to depolymerization, called catastrophe, and reverse transition, called rescue. Figure adapted from Cheeseman & Desai, 2008.

Microtubule dynamics are crucial for chromosome movement, and chromosome separation is mainly driven by microtubule depolymerization (Desai & Mitchison, 1997). Confirming the importance of microtubule dynamics *in vivo*, many successful anticancer drugs, such as taxol, bind to tubulin and suppress microtubule dynamics by either increasing or decreasing microtubule polymerization (Dumontet & Jordan, 2010). Although several studies have revealed a connection between tubulin

conformation and its polymerization state - with a straight tubulin conformation within the microtubule lattice and a curved conformation at depolymerizing ends -, a correlation with its nucleotide state has been challenging. Recent high-resolution cryo electron microscopy studies on microtubules that are either dynamic or stabilized by taxol or the slowly hydrolyzable GTP analog GMPCPP provide further insight into the mechanism of dynamic instability (Alushin et al., 2014; Zhang et al, 2015). These experiments suggest that GTP hydrolysis leads to a compaction around the E-site nucleotide at the longitudinal interfaces as well as a rearrangement of α-tubulin, thereby generating a destabilizing strain within the microtubule lattice that is released by tubulin bending during depolymerization. Taxol inhibits these conformational changes, thereby allosterically inducing a GTP-like state, indicating that the structural transitions are responsible for destabilization upon nucleotide hydrolysis. Since lateral contacts are not significantly affected by the nucleotide state or drug binding, the stability of the microtubule lattice seems to be mainly modulated at longitudinal interfaces.

As briefly mentioned above, several microtubule-associated proteins can actively control the polymerization state of microtubules, which is important for fast remodeling of the microtubule cytoskeleton in response to cellular signals (Desai & Mitchison, 1997). Some proteins influence microtubule dynamics by acting as microtubule-depolymerizing factors, such as the kinesin-13 familiy including the mitotic centromere-associated kinesin (MCAK) that induces catastrophes (Desai et al., 1999). Others act as microtubule-stabilizing factors, such as the cytoplasmic linker protein (CLIP)-associated protein (CLASP) (Mimori-Kiyosue et al., 2005) and XMAP215, which promotes microtubule growth (Brouhard et al., 2008). Several proteins that regulate microtubule dynamics are plus-end tracking proteins, so called +TIPs. The end binding (EB) protein family acts as central hub for these +TIPs (Akhmanova & Steinmetz, 2010). EB proteins possess an N-terminal calponin homology (CH) domain that is important for the direct interaction with microtubules and autonomous tracking of growing microtubule plus ends (Hayashi & Ikura, 2003). The C-terminal dimerization domain mediates the recruitment of several other +TIPs that do not track microtubule plus ends autonomously, but through binding of EB proteins (Honnappa et al., 2009; Akhmanova & Steinmetz, 2010). The recognized features within the EB C-terminal domain are the EB homology domain and the acidic tail comprising an EEY/F motif. The EB homology domain is recognized by +TIPs through a small four-residue motif containing the sequence serine-X-isoleucine-proline (X stands for any amino acid), the so-called SXIP motif (Honnappa

et al., 2009). Other +TIPs possess a small globular cytoskeleton-associated protein glycine-rich (CAP-Gly) domain with a hydrophobic cavity to interact with the C-terminal EEY/F motif of EB proteins (Honnappa et al., 2006). Recent high-resolution cryo electron microscopy analysis of EB-bound microtubules provides new insight into the modulation of structural transitions at the growing microtubule end by EB proteins (Zhang et al., 2015). These experiments reveal that EB proteins preferentially recognize and promote an intermediate GDP-P_i state upon GTP hydrolysis, explaining their end-tracking behavior and their effect on microtubule dynamics including stimulation of microtubule growth as well as increase of catastrophe frequency. EB-bound microtubules exhibit a compacted lattice with a unique rotation between adjacent tubulin dimers compared to the untwisted compacted GDP-microtubule lattice. By generating this lattice compaction, EB proteins presumably promote rapid GTP hydrolysis. The stimulation of microtubule growth by EB proteins may be explained by EB binding between adjacent protofilaments and generation of a specific curvature that facilitate the establishment of lateral contacts and thereby seam closure.

Another group of microtubule-associated proteins are motor proteins, which move along the microtubules. There are two families of motor proteins: the dyneins, which move towards the minus end, and the kinesin superfamily, which mostly move towards the plus end (Morgan, 2007). These motor proteins are typically dimers with microtubule-binding head domains and additional domains that form a link to a cargo or other subcellular structures. The ATPase activity in their head domains allows the motor proteins to convert chemical energy contained in ATP into mechanical energy of movement along the microtubule lattice, so that they can transport a cargo along microtubules or move the microtubules past an anchor point. The polarity of microtubules, by which they can act as directional track for motor proteins, and their dynamic instability, which generates significant forces that carry out useful mechanical work *in vivo*, present the two major properties of microtubules that allow them to form the mitotic spindle (Wittmann et al., 2001). The mitotic spindle contains three distinct sub-populations of microtubules that have their minus ends focused at the spindle poles and the plus ends pointing towards the chromosomes (Morgan, 2007; Wittmann et al., 2001). A schematic view of these three microtubule types of the mitotic spindle is shown in figure 1.3. First, astral microtubules extend away from the centrosomes into the cytoplasm and help orienting and positioning the spindle within the cell. Second, interpolar microtubules emanate from opposite spindle poles and interact in an antiparallel manner at the spindle midzone, thereby stabilizing the

bipolar spindle. Third, kinetochore microtubules connect chromosomes to spindle poles and are responsible for pulling the sister chromatids apart towards opposite spindle poles during anaphase.

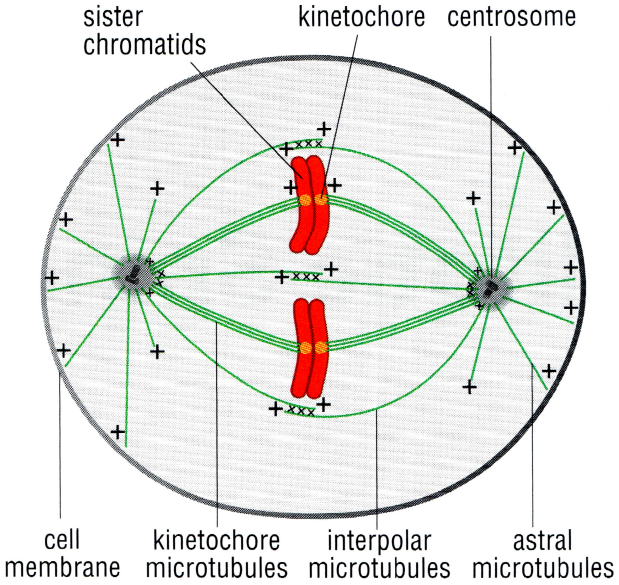

Figure 1.3: The mitotic spindle. Schematic overview of different microtubule types at the mitotic spindle in metaphase. Figure adapted from Morgan, 2007.

Mitotic microtubules exhibit a rapid turnover driven primarily by an increased catastrophe rate, which allows them to efficiently search for binding sites on the chromosomes in the surrounding cytosol, a mechanism also known as search-and-capture model (Kirschner & Mitchison, 1986; Holy & Leibler, 1994). Upon successful capture of a spindle microtubule by a kinetochore, the microtubules show increased half-lives and are thereby stabilized. Besides this stabilizing effect of kinetochores, their ability to keep the chromosomes attached to growing and shrinking microtubules is an essential feature for proper functioning of the spindle (Rieder & Salmon, 1998).

1.3 Organization and function of kinetochores

Kinetochores are complex protein networks that consist of over 100 individual proteins (DeLuca & Musacchio, 2012). First insights into the organization of a vertebrate kinetochore were obtained by electron microscopy (EM) studies revealing a trilaminar structure with electron dense inner and outer layers separated by an electron lucent middle layer (McEwen et al., 2007) as shown in figure 1.4. In the absence of microtubules, a fibrous corona is visible as dense array of fibers that extend from the outer plate.

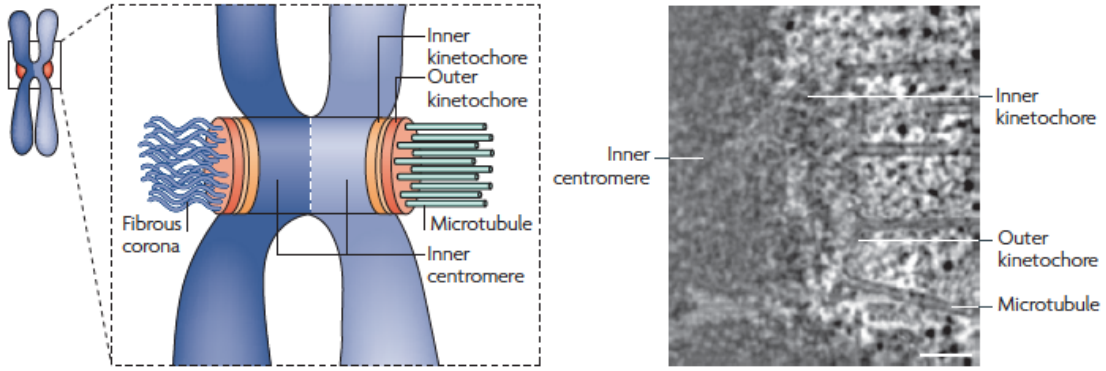

Figure 1.4: Vertebrate kinetochore ultrastructure. Left, schematic view of a mitotic chromosome with the sister chromatid on the right attached to spindle microtubules and the chromatid on the left unattached. Right, electron micrograph of a human kinetochore representing a single slice from a tomographic volume of a high-pressure frozen mitotic cell. Scale bar: 100 nm. Figure adapted from Cheeseman & Desai, 2008.

This organization of the centromere-kinetochore region reflects the main functions of kinetochores, which can be divided into four modules (Musacchio & Salmon, 2007; Welburn & Cheeseman, 2008; Santaguida & Musacchio, 2009). A schematic view of these modules within the kinetochore is shown in figure 1.5.

The first module is the inner kinetochore, which forms the interface with centromeric chromatin and appears as the electron dense inner layer in the EM image (see figure 1.4). It consists of a large complex comprising 16 subunits called the constitutive centromere associated network (CCAN). The CCAN builds a robust interface at the centromere region and serves as structural core for the recruitment of outer kinetochore components (Perpelescu & Fukagawa, 2011). Its members are identified as CENP - for centromere protein - followed by a letter. The association of the CCAN with centromeric DNA is the first step in kinetochore assembly. Two distinct pathways for the recruitment of the kinetochore based on the CCAN subunits CENP-C and CENP-T/W have been proposed. CENP-C directly binds to

nucleosomes containing the histone H3 variant CENP-A (Carroll et al., 2010), which defines the centromeric region together with epigenetic modifications (Black & Bassett, 2008). The CENP-T/W complex was found to associate with H3, but not CENP-A containing nucleosomes (Hori et al., 2008). The histone-fold containing complexes CENP-T/W and CENP-S/X form a stable CENP-T/W/S/X heterotetramer that is able to bind and supercoil DNA to form a nucleosome-like structure as scaffold for kinetochore assembly (Nishino et al., 2012). Furthermore, the CCAN was shown to be important for the deposition of new CENP-A at centromeres after mitosis, thus making it not only essential for recognition of centromeric chromatin, but also for its maintenance (Hori et al., 2013). Some organisms, like *Caenorhabditis elegans* or *Drosophila melanogaster*, seem to have lost many CCAN components and only rely on CENP-A and CENP-C for inner kinetochore assembly (Westermann & Schleiffer, 2013). Such simplified kinetochores retain the basic chromosome segregation function, but robust and high fidelity chromosome segregation requires the assembly of the entire protein network.

The second module is the outer kinetochore, which acts as attachment site for the plus ends of spindle microtubules and corresponds to the electron dense outer layer in the EM image (see figure 1.4). The central component of this outer plate is the KMN network, which contains the Knl1 complex, the Mis12 complex and the Ndc80 complex and is essential for the establishment of kinetochore-microtubule interactions. It is linked to the inner kinetochore through direct interactions with the two CCAN components CENP-C and CENP-T that bind to the Mis12 complex and the Ndc80 complex, respectively (Gascoigne et al., 2011; Screpanti et al., 2011). The outer kinetochore is discussed in more detail in section 1.4.

The third module is the spindle assembly checkpoint (SAC), which is recruited to outer kinetochore components. The SAC is a feedback control mechanism that monitors the state of kinetochore-microtubule attachments and coordinates it with the progression of the cell cycle. It delays anaphase onset by generating a ‘wait-anaphase’ signal until all sister chromatids are properly attached to opposite spindle poles. The SAC is further discussed in section 1.5.

The forth module, which is located at the inner centromere region, contains the chromosomal passenger complex (CPC). The CPC is responsible for discriminating between correct and incorrect kinetochore-microtubule attachments. It is believed that the CPC acts as tension sensor and thereby selectively stabilizes correct attachments, whereas it favors the correction of incorrect attachments. The CPC is discussed in more detail in section 1.5.

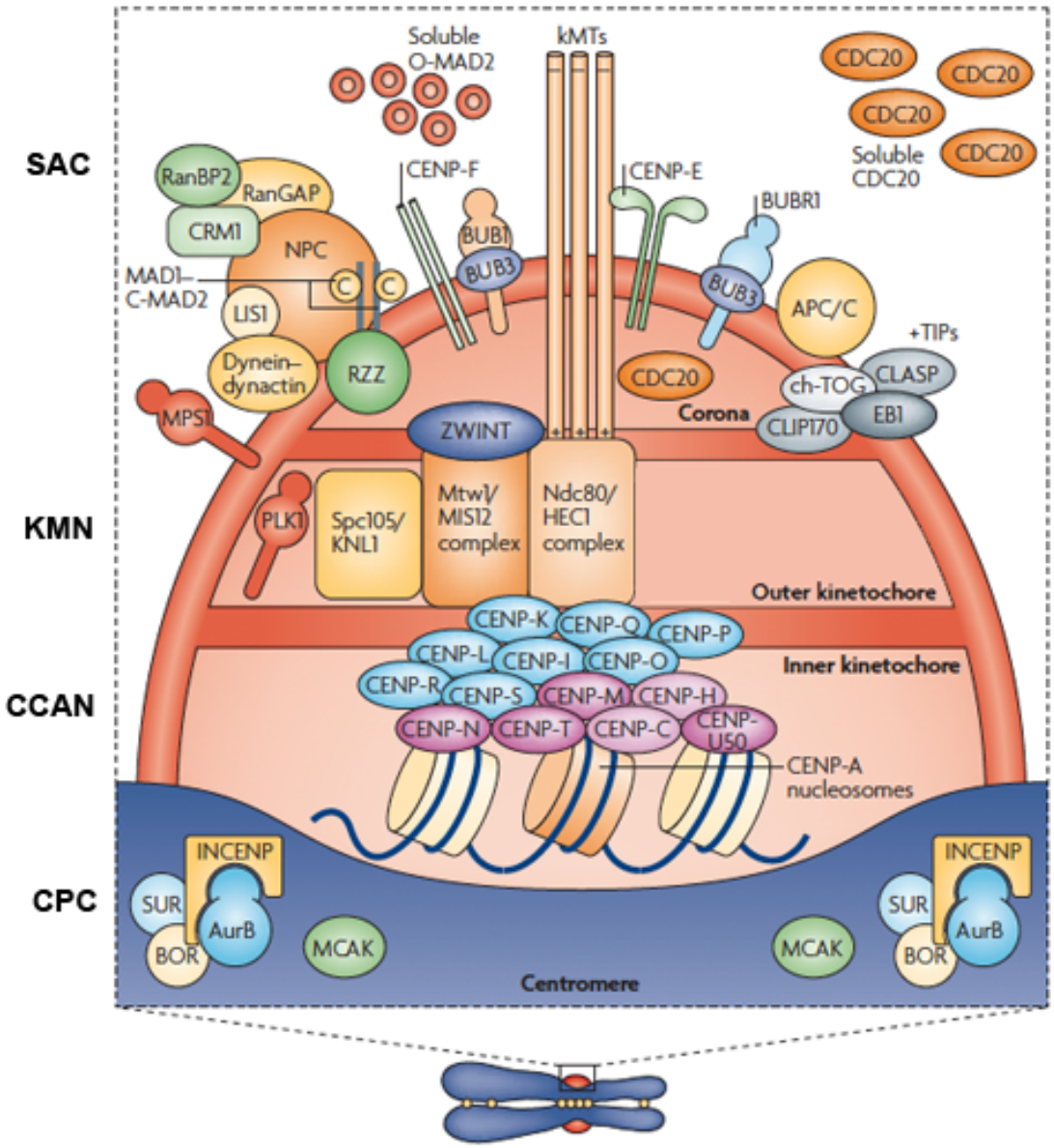

Figure 1.5: Organization of the centromere-kinetochore region. The kinetochore can be divided into four building blocks: 1.) The constitutive centromere associated network (CCAN), which is located at the inner kinetochore, is responsible for chromatin binding. 2.) The outer kinetochore, which contains the KMN (Knl1 complex/Mis12 complex/Ndc80 complex) network, is required for the establishment of kinetochore-microtubule attachments. 3.) The spindle assembly checkpoint (SAC), which is recruited to outer kinetochore components, synchronizes kinetochore-microtubule attachments and cell cycle progression. 4.) The chromosomal passenger complex (CPC), which associates with the inner centromere region, is required for correction of improper kinetochore-microtubule attachments. Figure adapted from Musacchio & Salmon, 2007.

The simplest kinetochore is found in the budding yeast *Saccharomyces cerevisiae* and binds a single microtubule (Westermann et al., 2007), whereas human kinetochores bind 15-20 microtubules (Cheeseman & Desai, 2008). With few exceptions, yeast kinetochore components have vertebrate homologs, suggesting that important features of kinetochore composition and organization are conserved

throughout evolution, despite some organism-specific differences (Kitagawa & Hieter, 2001; Cheeseman & Desai, 2008; Welburn & Cheeseman, 2008).

Although the overall network of kinetochore proteins is relatively well defined, the molecular details of the interactions between the different proteins and the dynamics of kinetochore-microtubule attachments during mitotic progression remain poorly understood.

1.4 The outer kinetochore

The outer kinetochore contains the 10-subunit KMN network consisting of the 2-subunit Knl1 complex, the 4-subunit Mis12 complex and the 4-subunit Ndc80 complex (Santaguida & Musacchio, 2009; Varma & Salmon, 2012). Whereas the CCAN components colocalize with CENP-A nucleosomes throughout the cell cycle, the KMN network is only recruited to kinetochores during late interphase-prophase and dissociates again during late anaphase-telophase (Cheeseman & Desai, 2008).

The KMN network exhibits two main functions. First, it provides the main microtubule-binding interface and therefore couples kinetochores to assembling and disassembling microtubules, which is crucial to align chromosomes at the metaphase plate and to pull them towards the spindle poles in anaphase (Maiato et al., 2004). Second, the KMN network is involved in the recruitment of all SAC components, with the possible exception of Aurora B, and thereby plays an important role in SAC control and the regulation of kinetochore dynamics (Martin-LLuesma et al., 2002; Kiyomitsu et al., 2007).

Significant progress in the *in vitro* reconstitution of the KMN network and its interaction with the inner kinetochore has been achieved in recent years (Ciferri et al., 2005; Cheeseman et al., 2006; Petrovic et al., 2010; Screpanti et al., 2011; Petrovic et al., 2014). A schematic overview of the molecular architecture of the KMN network is shown in figure 1.6.

The Mis12 complex comprises the four subunits Dsn1, Mis12, Nnf1 and Nsl1. It exhibits an elongated rod-shaped structure with a length of about 22 nm (Petrovic et al., 2010; Varma & Salmon, 2012). Its subunits are linearly aligned with Nnf1 at the inside, followed by Mis12 and Dsn1 and Nsl1 at the outside. The Mis12 complex forms a link to the inner kinetochore by binding directly to CENP-T and CENP-C (Gascoigne et al., 2011; Screpanti et al., 2011; DeLuca & Musacchio, 2012). It acts as a scaffold for the assembly of the outer kinetochore by binding both the Ndc80

and the Knl1 complex with the C-terminal tail of the Nsl1 subunit (Cheeseman & Desai, 2008; Petrovic et al., 2010). In agreement with the function of the Mis12 complex as platform for outer kinetochore assembly, depletion of its subunits results in reduced kinetochore localization of Ndc80 and defects in chromosome biorientation and segregation (Kline et al., 2006).

The Knl1 complex is a heterodimer formed by the two subunits Knl1 and Zwint (Varma & Salmon, 2012). The ~300 kD multidomain protein Knl1 has an elongated structure with its N-terminal region pointing outwards and binding to microtubules (Cheeseman et al., 2006), whereas its C-terminal region is associated with the Mis12

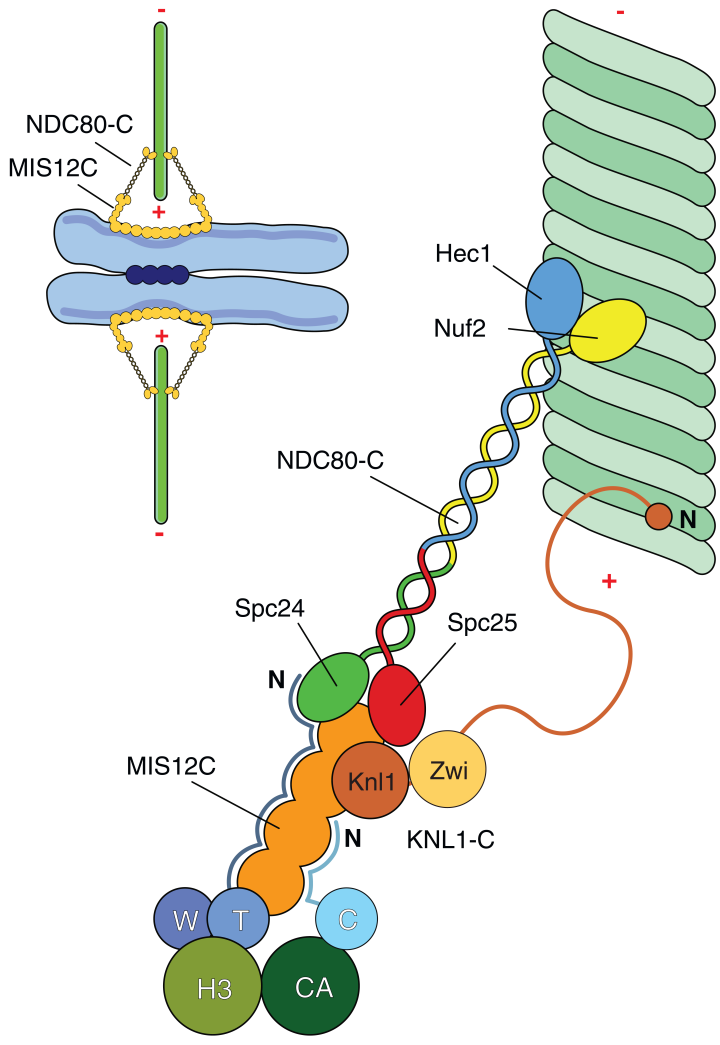

Figure 1.6: Schematic view of the molecular architecture of the KMN network. With the exception of CENP-T, W and C all CCAN subunits have been omitted. CENP-T/W associates with H3 nucleosomes (H3), whereas CENP-C associates with CENP-A nucleosomes (CA). The Mis12 complex forms a bridge between inner and outer kinetochore by binding CENP-T and C as well as the Spc24/Spc25 subcomplex of the Ndc80 complex. The Ndc80/Hec1 and Nuf2 subunits of the Ndc80 complex interact with microtubules and the N-terminal region of Knl1 also possesses microtubule-binding abilities. Figure adapted from DeLuca & Musacchio, 2012.

complex (Petrovic et al., 2010; Varma & Salmon, 2012). This interaction with the Mis12 complex recruits Knl1 to kinetochores. The N-terminal region of Knl1 contains 10-12 amino acids long helical motifs, the so-called KI motifs, which contribute to the function of Knl1 as scaffold for the recruitment of the SAC components Bub1 and BubR1, thereby indicating an important role of Knl1 in maintaining SAC activity in human cells (Krenn et al., 2012). However, the main contribution to the kinetochore recruitment of Bub1 and BubR1 does not come from the KI motifs, but from phosphorylated MELT repeats (Krenn et al., 2014). Consistent with these findings, depletion of Knl1 displaces Bub1 and BubR1 from kinetochores and results in cells that undergo accelerated mitosis and enter anaphase with misaligned chromosomes due to a checkpoint failure (Kiyomitsu et al., 2007). Furthermore, Knl1 is important for the recruitment of protein phosphatase 1 (PP1) to the outer kinetochore. PP1 counteracts the activity of the Aurora B kinase, which is part of the chromosomal passenger complex (CPC) and is involved in regulation of kinetochore-microtubule attachments as discussed in more detail in section 1.5. The C-terminal coiled-coil domain of Knl1 forms a tight interaction with a binding partner named Zwint, thereby recruiting it to kinetochores (Kiyomitsu et al., 2007; Petrovic et al., 2010). Zwint is involved in the kinetochore recruitment of ZW10 (Starr et al., 2000), a component of the Rod-Zwilch-ZW10 (RZZ) complex. The RZZ is another outer kinetochore protein complex that is essential for both SAC activation, by recruiting the crucial SAC component Mad1/Mad2 to unattached kinetochores (Kops et al., 2005), and SAC silencing, by recruiting Spindly that in turn recruits dynein/dynactin upon microtubule attachment (Starr et al., 1998; Griffis et al., 2007). The dynein/dynactin complex is a minus end directed motor protein complex that is required for a process called kinetochore shedding, during which RZZ and Mad1/Mad2 are removed from kinetochores and transported along the microtubules towards the spindle poles (Karess, 2005).

The 170 kD Ndc80 complex consists of the four proteins Ndc80 (Hec1), Nuf2, Spc24 and Spc25, which are associated as two subcomplexes, Ndc80/Nuf2 and Spc24/Spc25 (Cheeseman et al., 2006). The Ndc80 complex forms a 57 nm long dumbbell-like structure with the ends of the dumbbell separated by a long coiled-coil domain (Ciferri et al., 2005; Wei et al., 2005). The inner end of the Ndc80 complex comprising the Spc24/Spc25 subcomplex binds to the CCAN protein CENP-T as well as the Mis12 complex (Petrovic et al., 2010; Nishino et al., 2013; Malvezzi et al., 2013). The outward pointing end of the Ndc80 complex is formed by the Ndc80/Nuf2 subcomplex and serves as primary binding site for the plus ends of the spindle

microtubules (DeLuca & Musacchio, 2012). The interface for microtubule interaction is created by the N-terminal tail of the Ndc80 subunit and two calponin homology (CH) domains in the Ndc80 and Nuf2 subunits (Ciferri et al., 2008), although the CH domain of Nuf2 was found not to be directly involved in microtubule binding (Alushin et al., 2010). The 80 amino acid long, disordered and positively charged N-terminal tail of Ndc80 is important for its high-affinity microtubule binding by interacting with the negatively charged C-terminal tails of tubulin, the so-called E-hooks, and represents the site of phosphoregulation by Aurora B (Cheeseman et al., 2006). This interaction site is also involved in self-assembly of the Ndc80 complex into clusters upon microtubule binding (Alushin et al., 2010) explaining its cooperative binding to microtubules (Ciferri et al., 2008). A key microtubule-binding region of the Ndc80 complex is the so-called 'toe' located in the CH domain of Ndc80. It recognizes a site at the α-/β-tubulin interface of both intra- and inter-tubulin dimers, also known as 'toe print' (Alushin et al., 2010). Microtubule binding by the Ndc80 complex is sensitive to the conformation of tubulin, since the Ndc80 complex binds preferentially to straight microtubules. Recent studies have identified near the microtubule binding CH domain of Ndc80 a conserved loop domain that is important for stabilizing kinetochore-microtubule attachments (Maure et al., 2011), providing a third microtubule-binding feature within the Ndc80 complex. The function of the Ndc80 complex as key player of kinetochore-microtubule attachments is reflected in the phenotype from its ablation by RNA interference. Depletion of its components causes defects in the establishment of stable kinetochore-microtubule attachments and induces mitotic cells to undergo cell death making the Ndc80 complex essential for cell viability (DeLuca et al., 2002). Furthermore, a regulated interaction of the Ndc80 complex with the checkpoint kinase Mps1 is important for Mps1 recruitment to kinetochores, which is essential for SAC activity by subsequent recruitment of the SAC components Bub1/Bub3 and the Mad1/Mad2 complex (Martin-LLuesma et al., 2002; London et al., 2012; Shepperd et al., 2012; Yamagishi et al., 2012; Vleugel et al., 2014; Krenn et al., 2014; London & Biggins, 2014; Overlack et al., 2014).

The question how the KMN network couples chromosome movement to assembling and disassembling microtubules is an active area of research. Cooperative microtubule binding of Ndc80 and Knl1, which is further enhanced in presence of the complete KMN network (Cheeseman et al., 2006), only provides a partial answer, even if this core attachment site contributes significantly to the fidelity of chromosome segregation. The two attachment sites are arranged in a high-density array to build

multiple contacts on a single microtubule. Quantitative fluorescence microscopy revealed that there might be eight Ndc80 complexes per microtubule in budding yeast (Joglekar et al., 2006). The specific arrangement of these complexes in defined clusters might contribute to increasing the strength of microtubule binding (Alushin et al., 2010).

Other proteins like the motor proteins dynein and CENP-E as well as the large coiled-coil protein CENP-F, which shows weak microtubule-binding activity (Feng et al., 2006), might function in parallel to Ndc80 and Knl1 (Cheeseman & Desai, 2008). In budding yeast, the Dam1/Dash complex is also involved in kinetochore-microtubule attachments. This 10-subunit complex, which is present with 16-20 copies per microtubule (Joglekar et al., 2006), forms a ring-like structure around microtubules and can move processively at the end of depolymerizing microtubules (Westermann et al., 2005; Westermann et al., 2006). Since the Dam1 complex is able to couple the energy of microtubule disassembly with motion of a cargo along the microtubules, it has been suggested to function as processive coupler of chromosome movement (Asbury et al., 2006; Grishchuk et al., 2008). The Dam1 complex directly interacts with the Ndc80 complex, which enhances the ability of the Ndc80 complex to track dynamic microtubule ends and is regulated by yeast Aurora B kinase Ipl1 (Tien et al., 2010). No structural homolog of the Dam1 complex has been discovered in higher eukaryotes, but the spindle and kinetochore associated (Ska) complex has been proposed as its functional homolog in vertebrates (Hanisch et al., 2006; Varma & Salmon, 2012). The Ska complex consists of the three subunits Ska1, Ska2 and Ska3/Rama1 and is important for the formation of kinetochore-microtubule attachments in human cells (Hanisch et al., 2006; Daum et al., 2009; Gaitanos et al., 2009; Theis et al., 2009). The Ska complex forms a 35 nm wide W-shaped dimer with two copies of each subunit (Jeyaprakash et al., 2012). The N-terminal ends of the subunits build the dimerization interphase, whereas the C-terminal domains of Ska1 and Ska3, which exhibit microtubule-binding ability, form the ends of the two arms of the ‘W’ thereby creating four putative microtubule-binding sites of the Ska complex. Although the human Ska complex and the yeast Dam1 complex exhibit a completely different structure, their functional properties are similar. The Ska complex binds cooperatively to microtubules and forms oligomers that track depolymerizing microtubule ends (Welburn et al., 2009; Schmidt et al., 2012). In contrast to the Ndc80 complex, which preferably binds straight microtubules, the Ska complex can bind both the straight microtubule lattice and curved protofilaments (Schmidt et al., 2012; Abad et al, 2014). It recognizes the globular regions of tubulin monomers by

interacting with the microtubules in multiple orientations through several positively charged amino acid clusters (Abad et al., 2012). The Ska complex promotes the association of the Ndc80 complex with disassembling microtubule ends and their synergistic interaction maintains the movement of cargo along the depolymerizing microtubule (Schmidt et al., 2012). The localization of the Ska complex to kinetochores depends on all three members of the KMN network and the phosphorylation by Aurora B negatively regulates its interaction with the KMN network and thereby its kinetochore recruitment (Chan et al., 2012). A model showing the functional homology of the Ska complex and the Dam1 complex in stabilizing kinetochore-microtubule attachments together with the Ndc80 complex is presented in figure 1.7.

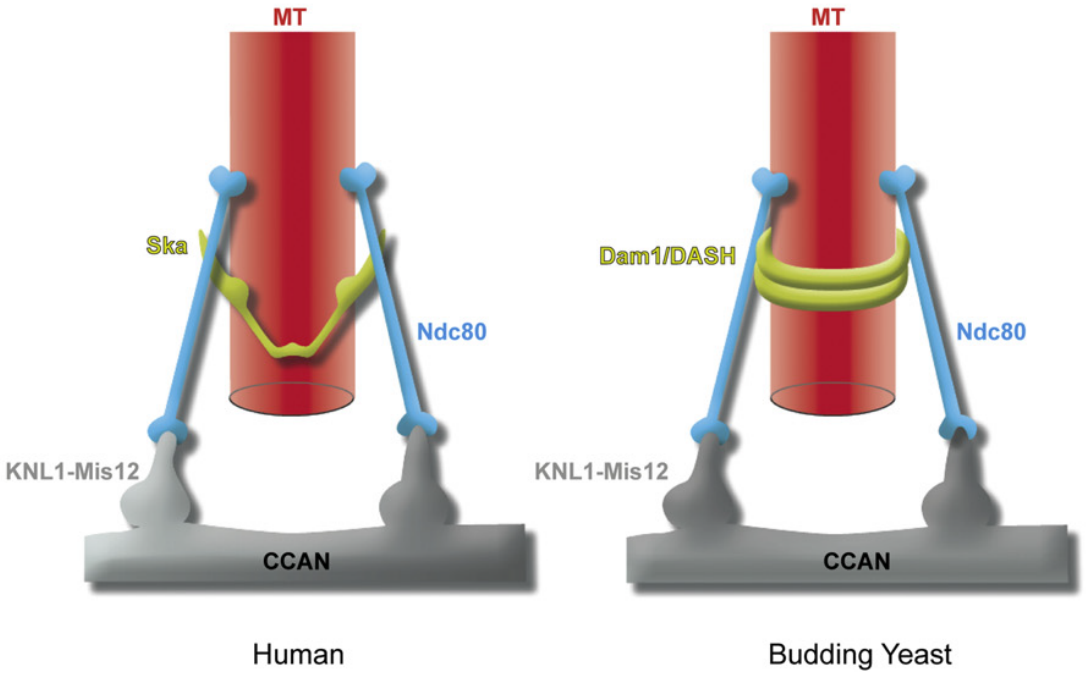

Figure 1.7: Model showing the functional homology of the human Ska complex and the yeast Dam1 complex. Both the W-shaped Ska complex and the ring-shaped Dam1 complex function together with the Ndc80 complex to stabilize kinetochore-microtubule attachments. Figure is adapted from Jeyaprakash et al., 2012.

1.5 Establishment and regulation of kinetochore-microtubule attachments

Since biorientation of all sister chromatids to kinetochore microtubules is crucial for the fidelity of chromosome segregation, this complex process is highly regulated. The establishment of kinetochore-microtubule attachments takes place stepwise (Tanaka, 2008; Tanaka, 2010). First, a kinetochore interacts with the lateral surface of a single microtubule. Then it is transported along the microtubule towards the spindle pole and subsequently gets tethered at the plus end of the microtubule thereby converting the lateral attachment to an end-on attachment. Finally, the sister kinetochore attaches to microtubules emanating from the opposite spindle pole. In case the chromosomes get attached with an improper orientation, such as in syntelic attachments in which both sister chromatids are connected to the same spindle pole, these erroneous attachments need to be corrected before the cell goes into anaphase.

The initial interaction of kinetochores with the lateral surface of astral microtubules was first discovered in newt lung cells (Hayden et al., 1990) and subsequently in yeast (Tanaka et al., 2005). This lateral capture is due to the much larger contact surface of the lattice compared to the microtubule tip. The proposed search-and-capture model (Kirschner & Mitchison, 1986; Holy & Leibler, 1994), describing a random search for kinetochores by the dynamic microtubules, is not efficient enough to explain the typical duration of prometaphase (Wollman et al., 2005). Another mechanism that contributes to the establishment of initial kinetochore-microtubule attachments involves the small GTPase Ran, which also functions in nuclear trafficking (Moore & Blobel, 1994). A concentration gradient of Ran-GTP is supposed to form around chromosomes, which acts as guide for microtubules towards chromosomes (Tanaka, 2010). Since this Ran-dependent mechanism is - due to the fast diffusion of Ran - only effective over relatively long distances (e.g. 10 µm), but not within short distances, a contribution of kinetochore-derived microtubules to initial kinetochore-microtubule attachments has been proposed (Khodjakov et al., 2003). Kinetochore fibers initiate from the centromere region and subsequently interact with spindle pole microtubules facilitating attachment of kinetochores to spindle microtubules. After the lateral attachment kinetochores slide along the microtubule towards the spindle pole, which is promoted by the minus-end directed motor protein dynein (Sharp et al., 2000). When the plus end of the shrinking microtubules reaches the kinetochore, the lateral attachment is converted to an end-on attachment, which

stabilizes the kinetochore-microtubule attachment. This conversion probably requires the association of the Ndc80 with the Dam1 complex (Tien et al., 2010) as described in section 1.4. Finally, the sister chromatid becomes attached to spindle microtubules emanating from the opposite pole.

In order to achieve biorientation, erroneous kinetochore-microtubule attachments need to be corrected. In 1969, it was first discovered in meiosis I that tension plays an important role in such an error correction mechanism (Nicklas & Koch, 1969). During meiosis I, kinetochores undergo repeated connection to and disconnection from spindle microtubules until the two homologous kinetochores are bioriented. Micro-needle manipulation in grasshopper spermatocytes revealed that erroneous kinetochore-microtubule attachments known as syntelic attachments could be stabilized, when tension was artificially applied on chromosomes away from the poles to which both kinetochores are attached. In the absence of tension, these erroneous configurations were invariably corrected.

The conserved serine/threonine kinase Aurora B was identified as crucial component of the error correction machinery. It is involved in destabilization of kinetochore-microtubule attachments thereby promoting chromosome biorientation and alignment (Tanaka et al., 2002; Welburn et al., 2010; Carmena et al. 2012). Aurora B is a subunit of the CPC, which also contains INCENP, Survivin and Borealin. The location of the CPC changes in the course of mitosis in order to ensure spatially restricted substrate phosphorylation and thereby regulation of different key events including correction of kinetochore-microtubule attachment errors, activation of the SAC as well as construction and regulation of the contractile apparatus during cytokinesis (Carmena et al., 2012). In prometaphase, Aurora B localizes to centromeres and phosphorylates kinetochore components to weaken kinetochore-microtubule attachments and facilitate their turnover. Important targets of Aurora B phosphorylation are the Ndc80 complex, the Dsn1 subunit of the Mis12 complex and Knl1. Phosphorylation of the Ndc80 complex modulates the microtubule binding affinity of the KMN network (Cheeseman et al., 2006; De Luca et al., 2006; Alushin et al., 2012; Welburn et al., 2010). The nine Aurora B phosphorylation sites on Ndc80 (Guimaraes et al., 2008) are located in two segments in the N-terminal tail, one at the tubulin binding interface and the other at the binding interface with an adjacent microtubule bound Ndc80 complex (Alushin et al., 2012). Phosphorylation by Aurora B at these target sites serves to fine-tune the interaction of the Ndc80 complex with microtubules and with neighboring Ndc80 complexes. In budding yeast, phosphorylation of the Dam1 complex is important for the regulation of its interaction

with the Ndc80 complex (Cheeseman et al., 2002; Tien et al., 2010). In agreement with these findings, non-phosphorylatable mutants of the Dam1 complex, the Ndc80 complex and Knl1 exhibit defects in chromosome alignment suggesting that Aurora B phosphorylation is crucial for proper establishment of biorientation (Cheeseman et al., 2002; DeLuca et al., 2006; Welburn et al., 2010).

Upon biorientation, the turnover of kinetochore-microtubule attachments needs to be prevented to ensure the stability of attachments. Indeed, when sister kinetochores are bioriented and tension is applied, Aurora B substrates are dephosphorylated (Welburn et al., 2010). A model explaining the phosphorylation of Aurora B targets in absence of tension and their dephosphorylation in presence of tension is shown in figure 1.8. When no tension is present in prometaphase, kinetochore components are phosphorylated by Aurora B leading to SAC activation and destabilization of kinetochore-microtubule attachments. Upon biorientation, when tension is applied, intrakinetochore stretch spatially separates outer kinetochore components from the reach of Aurora B leading to stabilization of kinetochore-microtubule attachments through dephosphorylation by phosphatases, such as PP1 and PP2A (Santaguida & Musacchio, 2009). In agreement with this model, Aurora B substrates become dephosphorylated when placed within the kinetochore at a sufficiently large distance from the centromere, while positioning Aurora B closer to the kinetochore prevented stabilization of kinetochore-microtubule attachments (Liu et al., 2009). Indeed, the distance along the intra-kinetochore longitudinal axis between the C-terminus of Ndc80 and CENP-A increases from 65 nm, when chromosomes are not under tension, to 102 nm in the presence of tension upon biorientation (Maresca & Salmon, 2009). However, the separation model would predict that unattached kinetochores, which lack tension, would be permanently prevented from forming stable attachments. The actual situation is probably that Aurora B generates a state of initial labile attachments to prevent premature stabilization of attachments, which remain amenable to become corrected if tension fails to manifest because of the lack of biorientation (Santaguida & Musacchio, 2009). Thus, current models of attachment and biorientation are oversimplifications, while the complete correction mechanism and the question how kinetochores create stable attachments in the first place remain unclear.

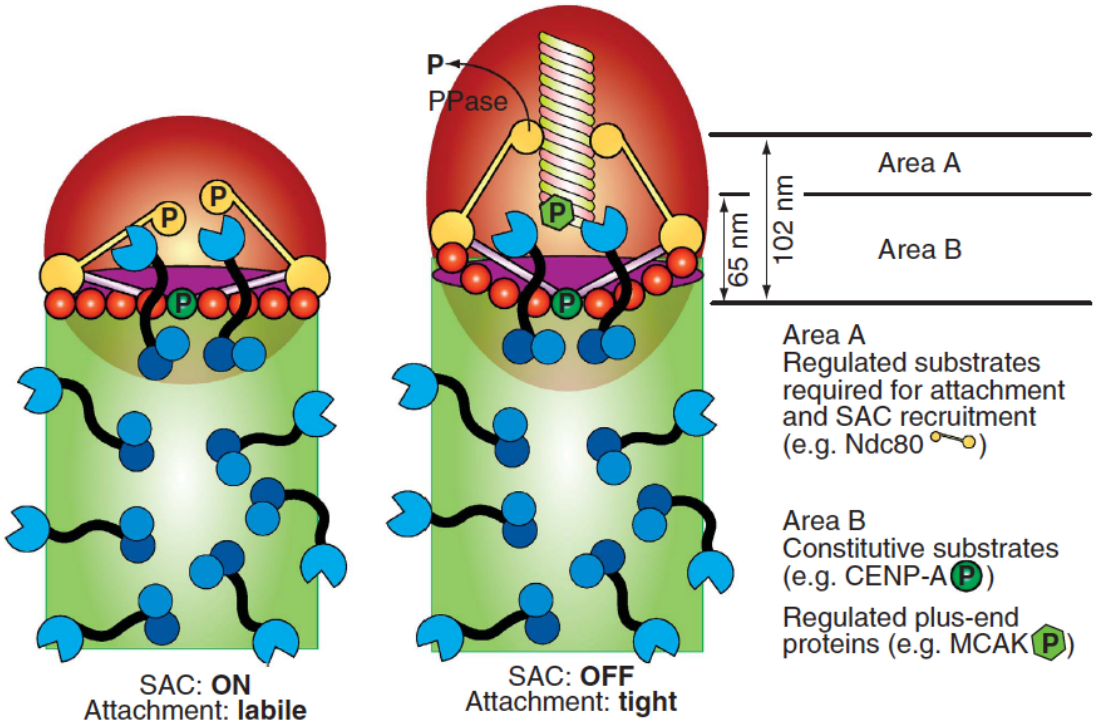

Figure 1.8: Model of error correction. In the absence of tension (left), kinetochore components are phosphorylated by Aurora B, leading to SAC activation and destabilization of kinetochore-microtubule attachments. In the presence of tension (right), outer kinetochore components are removed from the reach of Aurora B, leading to stabilization of kinetochore-microtubule attachments through dephosphorylation by a phosphatase (PPase). Figure adapted from Santaguida & Musacchio, 2009.

There is a close interplay between the error correction and the SAC, since the destabilization of improper kinetochore-microtubule attachments by the error correction machinery creates unattached kinetochores that recruit checkpoint proteins and induce SAC signaling (Santaguida & Musacchio, 2009). However, error correction and SAC are distinct mechanisms with different functions. Error correction promotes biorientation, whereas the SAC monitors the state of kinetochore-microtubule attachments and coordinates it with the progression of the cell cycle by delaying anaphase onset until all sister chromatids are properly attached to opposite spindle poles (Musacchio & Salmon, 2007; Welburn & Cheeseman, 2008; Santaguida & Musacchio, 2009). In addition to its crucial role in error correction, the Aurora B kinase plays a direct role also in SAC control. In the presence of microtubule-depolymerizing drugs, and therefore in the absence of microtubules, Aurora B is required for the kinetochore recruitment of SAC proteins and its inhibition severely impairs SAC signaling (Hauf et al., 2003; Santaguida et al., 2011), showing that the role of Aurora B in the SAC is not limited to creating unattached kintochores. The link between error correction and SAC control is underlined by the importance of intrakinetochore stretch both in controlling Aurora B phosphorylation of kinetochore

components and in determining the state of checkpoint signaling (Maresca & Salmon, 2009).

Besides Aurora B, several other proteins are involved in the SAC, including Mad1, Mad2, Bub1, BubR1, Bub3 and the kinase Mps1 (Musacchio & Salmon, 2007; Nezi & Musacchio, 2009). Aurora B and Mps1 are the key players in the recruitment of downstream SAC components. Mps1 is recruited through phosphorylation of Ndc80 by Aurora B (Saurin et al., 2011; Nijenhuis et al., 2013). Subsequently, Mps1 recruits Bub1 through phosphorylation of Knl1 and further phosphorylation of Bub1 by Mps1 recruits the Mad1/Mad2 complex (Brady & Hardwick, 2000; Krenn et al., 2014; Overlack et al., 2014; London & Biggins, 2014; Moyle et al., 2014). When SAC proteins are recruited to unattached kinetochores, they generate a 'wait-anaphase' signal corresponding to the formation of an anaphase inhibitor, the mitotic checkpoint complex (MCC). The MCC consists of the three SAC proteins Mad2, BubR1 and Bub3 as well as its target Cdc20, whose incorporation in the MCC prevents it from binding and activating the anaphase promoting complex or cyclosome (APC/C), which is required for anaphase onset. The APC/C is an E3 ubiquitin ligase that mediates polyubiquitylation and thereby proteasomal degradation of its two key substrates cyclin B and securin (Peters, 2006). Cyclin B is an activator of the major mitotic kinase Cdk1, whose inactivation promotes exit from mitosis. Securin is an inactivator of separase, which cleaves sister chromatid cohesions during anaphase. The initial step in the generation of the MCC is described in the Mad2 template model (De Antoni et al., 2005). Mad2 is a two-state protein that adopts distinct topologies known as closed and open Mad2. A closed conformer of Mad2 bound to Mad1 acts as kinetochore receptor for cytosolic open Mad2 and converts it into closed Mad2 thereby allowing it to bind to Cdc20. The formed closed Mad2/Cdc20 may subsequently amplify the conformational change of open Mad2 in the cytosol by acting itself as template, but this remains hypothetical. As long as the MCC remains bound to the APC/C, the latter is unable to initiate anaphase onset, which ensures enough time for the establishment of proper kinetochore-microtubule attachments. The RZZ recruits Spindly and dynein/dynactin (Starr et al., 1998; Griffis et al., 2007), which removes RZZ and Mad1/Mad2 from kinetochores upon microtubule attachment (Karess, 2005). Furthermore, APC/C dependent non-degradative autoubiquitylation of Cdc20 and binding of $p31^{comet}$ to closed Mad2 promote MCC disassembly and release of Cdc20 from the MCC (Foley & Kapoor, 2013) resulting in SAC silencing and thereby allowing mitotic exit. The relationship between the SAC and the cell cycle machinery is schematically shown in figure 1.9.

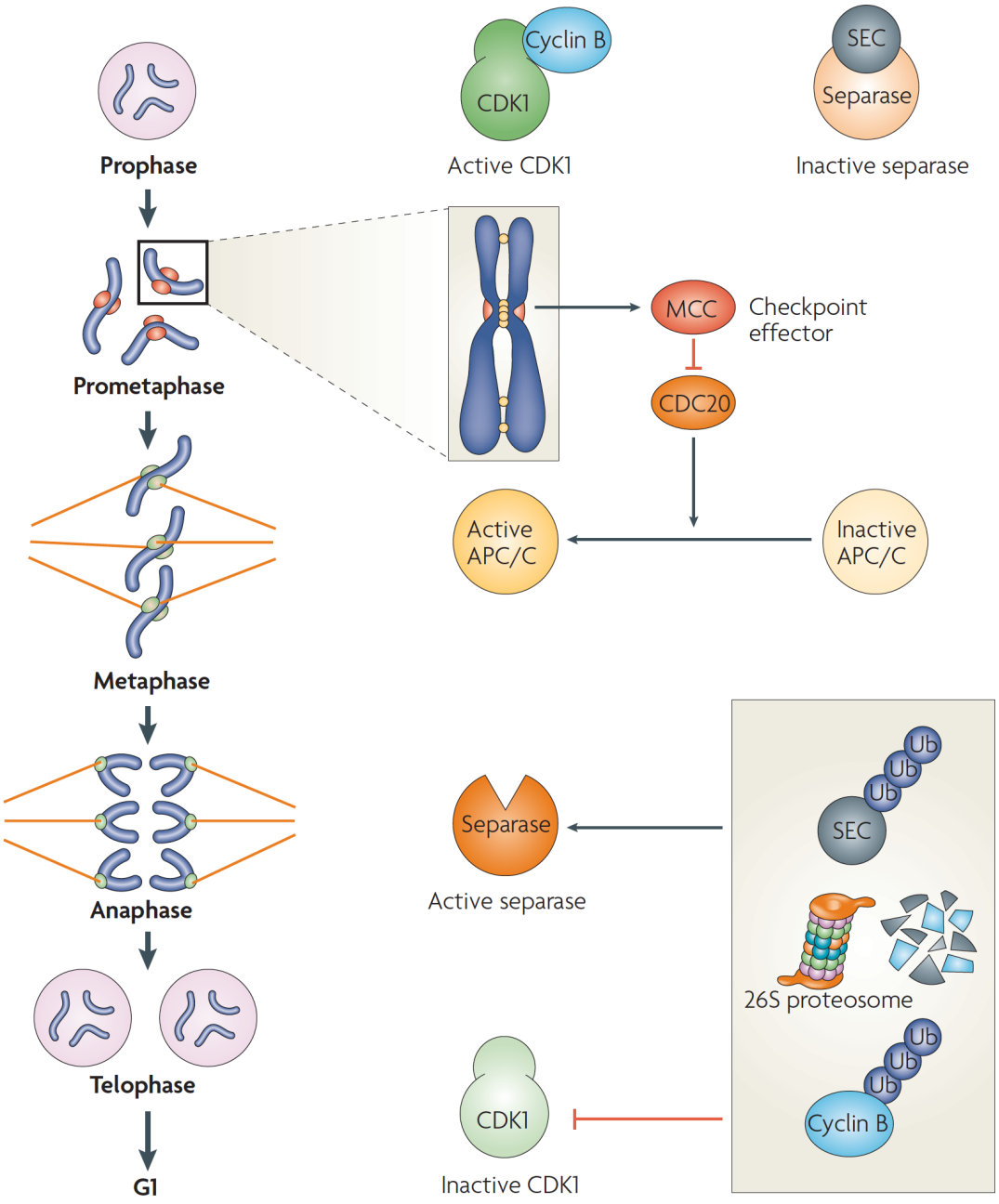

Figure 1.9: Function of the SAC. To enter mitosis, activity of Cdk1 by binding to cyclin B is required. Prior to anaphase, separase is kept inactive by binding of securin. Unattached kinetochores contribute to generation of the MCC, which prevents Cdc20 from activating the APC/C. Biorientation silences the SAC leading to MCC disassembly and Cdc20 release. Subsequent activation of the APC/C results in ubiquitylation and degradation of securin and cyclin B, thereby activating separase and inactivating Cdk1, which leads to mitotic exit. Figure adapted from Musacchio & Salmon, 2007.

Figure 1.10 schematically summarizes the complexity of the kinetochore-microtubule attachment process, which requires a close interplay of the microtubule-attachment machinery, error correction and the SAC, as discussed in sections 1.4 and 1.5, but it is still not entirely understood.

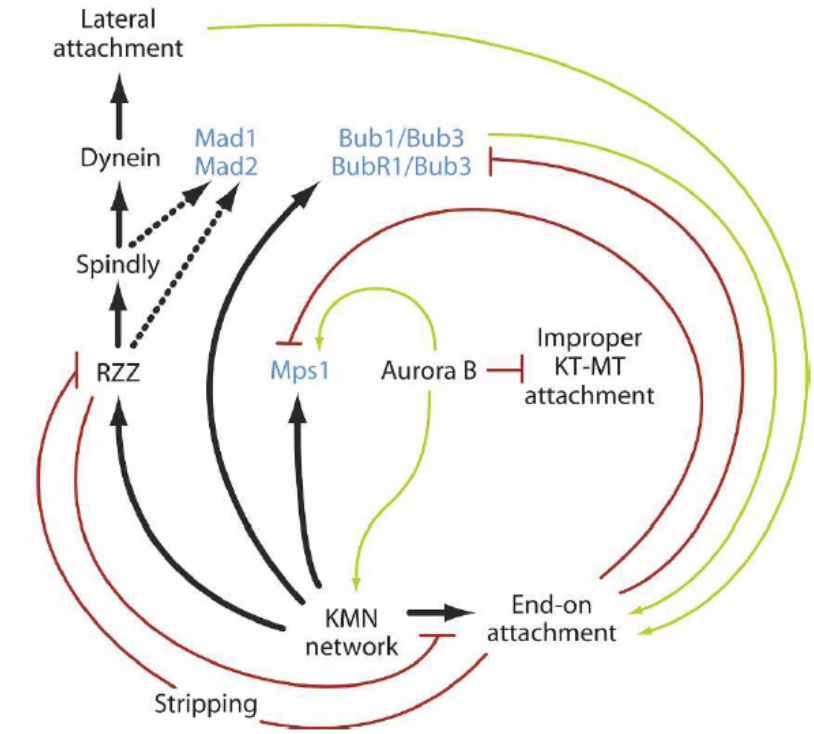

Figure 1.10: Complexity of the kinetochore-microtubule attachment process. Black arrows indicate an action, such as recruitment or microtubule binding. Dotted black arrows suggest an uncertainty regarding the functional significance of the involved species. Green arrows define positive regulation, whereas red lines with a small perpendicular line indicate negative regulation. The KMN network mediates several actions, including kinetochore recruitment of the RZZ complex and of the SAC proteins Mps1, Bub1, BubR1 and Bub3, and the formation of stable end-on microtubule attachments. The actions of the KMN network are positively regulated by Aurora B. Aurora B also suppresses improper kinetochore-microtubule attachments. The checkpoint proteins (in blue) positively regulate the process of end-on attachment. Aurora B recruits Mps1, which is required for subsequent recruitment of the SAC components Bub1/Bub3 and Mad1/Mad2. After recruitment to prometaphase kinetochores, the RZZ complex recruits Spindly, dynein, Mad1 and Mad2. Dynein mediates lateral attachment to microtubules, which in turn favors end-on attachment. The establishment of end-on attachment suppresses the kinetochore accumulation of the RZZ and of the other proteins whose kinetochore localization depends on the RZZ, due to their stripping from kinetochores. Figure modified from Civril & Musacchio, 2008.

1.6 The Astrin/SKAP complex

Yet another protein complex playing a role in mitotic progression is the Astrin/SKAP complex. The 134 kD protein Astrin (also called SPAG5 or MAP126) was identified in 2001 as a spindle associated protein and a component of sperm flagella (Mack & Compton, 2001; Chang et al., 2001; Shao et al., 2001). The 35 kD small kinetochore associated protein SKAP (also called Kinastrin or TRAF4-associated factor 1) was independently identified in 2009 as the product of a gene (*FLJ14502*) whose transcription is induced at the G2/M transition of the cell cycle (Fang et al., 2009). Later, it was discovered that Astrin and SKAP form a tight complex that may comprise sub-stoichiometric amounts of the dynein light chain LC8, Polo-like kinase 1 (Plk1) and Shugoshin 2 (Sgo2) (Schmidt et al., 2010; Dunsch et al., 2011).

Astrin and SKAP show identical cellular localizations (Mack & Compton, 2001; Thein et al., 2007; Fang et al., 2009; Schmidt et al., 2010; Dunsch et al., 2011). During interphase, they associate with centrosomes; in prophase, they localize to the spindle, concentrating at spindle poles; in metaphase and anaphase, they localize throughout the spindle and to kinetochore; and in anaphase and telophase, they are at the spindle midzone. At metaphase, when biorientation is established, the Astrin/SKAP complex is recruited to outer kinetochores of properly aligned chromosomes. In early mitosis, its localization to kinetochores is counteracted by Aurora B activity, so that the Astrin/SKAP complex only becomes recruited to kinetochores in case of correct chromosome alignment (Schmidt et al., 2010). Therefore, the presence of the Astrin/SKAP complex at kinetochores indicates a mature end-on attachment (Shrestha et al., 2013). Furthermore, the Astrin/SKAP complex was found to localize to the plus ends of growing microtubules (Dunsch et al., 2011; Wang et al., 2012; Tamura et al., 2015).

Several interactions have been proposed to account for the complex cellular localization of the Astrin/SKAP complex and its function in mitotic progression and chromosome alignment. Targeting of the Astrin/SKAP complex to centrosomes in the S and G2 phases may be due to an interaction with Ninein, which is implicated in centrosomal microtubule nucleation and microtubule anchoring (Cheng et al., 2007). Phosphorylation of Astrin by glycogen synthase kinase 3β, which is involved in several pathways including regulation of cell fate, mitosis and apoptosis, was found to be important for Astrin association with spindle microtubules and kinetochores (Cheng et al., 2008). The two motor proteins CENP-E and Kif18a have also been implicated in the kinetochore recruitment of the Astrin/SKAP complex (Manning et al.,

2010; Huang et al., 2012). Furthermore, the KMN network was shown to be essential for kinetochore localization of SKAP, since depletion of subunits of the Ndc80 complex or the Mis12 complex significantly decreases SKAP levels at the kinetochore, possibly through a direct interaction with the Dsn1 subunit of the Mis12 complex (Wang et al., 2012). Astrin and SKAP were both found to bind microtubules *in vitro* (Schmidt et al., 2010; Dunsch et al., 2011). *In vitro*, microtubule binding by SKAP may be mediated through its C-terminal coiled-coil domains, ranging from amino acid 159 to 316, which is consistent with its minimal microtubule-binding domain *in vivo* and the failure of SKAP N-terminus comprising amino acids 1 to 158 to localize to the spindle (Dunsch et al., 2011). On the other hand, the N-terminal region of SKAP was also proposed to be a major determinant of the localization of SKAP to the mitotic spindle (Tamura et al., 2015; Wang et al., 2012). Astrin was shown to bind microtubules *in vitro* with its C-terminal domain encompassing amino acids 955 to 1193 (Schmidt et al., 2010), but this C-terminal region is unable to associate with the spindle *in vivo*, while a construct comprising amino acids 482 to 850 and lacking the C-terminal region retains spindle localization (Dunsch et al., 2011; Mack & Compton, 2001). The regions encompassing amino acids 482 to 850 in Astrin and 159 to 316 in SKAP may not only be the minimal microtubule-binding domains *in vivo*, but also the minimal interaction sites of the two subunits within the Astrin/SKAP complex (Dunsch et al., 2011). An interaction between SKAP and the kinesin CENP-E was found to synergistically enhance the microtubule binding of SKAP (Huang et al., 2012). The plus end tracking properties of the Astrin/SKAP complex depend on a SXIP-motif in the N-terminal domain of SKAP (Tamura et al., 2015; Wang et al., 2012), which, as discussed above, is known to mediate the interaction of many microtubule-associated proteins with EB proteins that track microtubule plus ends (Honnappa et al., 2009). Indeed, SKAP directly interacts with EB1 and EB3 in a SXIP-dependent manner and this interaction is important for SKAP function in controlling microtubule growth rates and anaphase onset (Wang et al., 2012; Tamura et al., 2015). In cells, SKAP may exist in two distinct pools: a spindle microtubule associated pool that influences microtubule growth in a SXIP-motif dependent manner and a kinetochore associated pool that binds congressed kinetochores in a SXIP-motif independent manner (Tamura et al., 2015).

Cells that are depleted of either Astrin or SKAP behave normally during interphase, but are unable to progress through mitosis resulting in a mitotic delay and finally ending in apoptotic cell death (Gruber et al., 2002). The Astrin/SKAP complex is suggested to play a role in the assembly and orientation of the bipolar spindle

structure, since a depletion of either of its subunits leads to the formation of multipolar and highly disordered spindles (Gruber et al., 2002; Thein et al., 2007; Schmidt et al., 2010; Dunsch et al., 2011). The formation of multipolar spindles is mainly caused by a premature disengagement of the two centrioles of each centrosome. In addition, Astrin depletion causes the loss of sister chromatid cohesion before anaphase onset. These two processes involve the activity of separase, indicating that a subpopulation of separase can be activated despite the general mitotic arrest in these cells (Thein et al., 2007; Dunsch et al., 2011). Thus, Astrin may contribute to the regulatory network that controls separase activity. The N-terminal domain of Astrin encompassing amino acids 4 to 239 may interact with the centrosomal kinase Aurora A to regulate its localization to mitotic spindles, microtubule organization and spindle pole integrity (Du et al., 2008). Aurora A was also found to phosphorylate Astrin at serine 115 (Chiu et al., 2014). A phosphorylation-deficient mutant of Astrin appears to activate the SAC and to decrease spindle stability, and it fails to bind its interaction partners including SKAP, whereas a phospho-mimicking mutant may bind securin and induce its ubiquitylation and degradation. This suggests a role of Astrin in separase activation, since the degradation of securin leads to activation of separase. In rotary shadowing electron microscopy (EM), a sample of Astrin refolded from bacterial inclusion bodies was shown to build an 80 nm large 'lollipop'-shaped structure with a 15 nm N-terminal globular head domain and a 65 nm rod predicted to encompass the C-terminal coiled-coil domains (Gruber et al., 2002). The 2-fold symmetry of this 'lollipop' structure suggests that Astrin forms parallel dimers that oligomerize through the globular head domain to form aster-like structures. This oligomerization may allow Astrin to bundle microtubules and crosslink other binding partners, thereby providing a scaffold for crosslinking regulatory and structural components of the mitotic spindle (Gruber et al., 2002).

The Astrin/SKAP complex is also suggested to promote metaphase-to-anaphase transition by contributing to chromosome alignment and stabilizing kinetochore-microtubule attachments, since depletion of its subunits leads to an impaired chromosome alignment and a SAC-dependent mitotic arrest (Thein et al., 2007; Fang et al., 2009; Schmidt et al., 2010; Dunsch et al., 2011). The stabilizing effect of the Astrin/SKAP complex on microtubule plus end dynamics may be due to participation of Astrin, together with CLASP1 and Kif2b, in a functional switch at outer kinetochores that temporally regulates kinetochore-microtubule attachments (Manning et al., 2010). Kif2b is a member of the kinesin-13 family with microtubule

depolymerizing activity (Manning et al., 2007). In early mitosis, the Kif2b/CLASP1 complex is recruited to kinetochores, where it promotes chromosome movement, kinetochore-microtubule turnover and maintenance of SAC signaling. During metaphase, this complex is replaced by an Astrin/CLASP1 complex that promotes kinetochore-microtubule stability, chromosome alignment and SAC silencing (Manning et al., 2010). In late mitosis, the interaction of Astrin/SKAP and dynein may promote dynein-mediated transport of kinetochore components required for chromosome congression from microtubule plus ends toward spindle poles. It may also promote kinetochore-microtubule attachment and SAC regulation (Dunsch et al., 2011). Besides its function in mitosis, Astrin was also found to be important for spindle organization and cell cycle progression in meiosis (Yuan et al., 2009).

Taken together, the Astrin/SKAP complex is essential for spindle organization, chromosome alignment, stabilization of kinetochore-microtubule attachments and mitotic progression. However, the required protein interactions and the molecular mechanisms underlying its complex cellular localization and its diverse functions remain elusive.

2 OBJECTIVE

As accurate chromosome segregation is crucial for cell viability, it is important to understand this complex process on the molecular level. In order to elucidate the underlying mechanisms, the essential protein interactions have to be identified and characterized in detail. This thesis deals with the molecular dissection of the spindle and kinetochore associated Astrin/SKAP complex, which is essential for mitotic progression and chromosome alignment. The overall goal of this project is to characterize the interactions of the Astrin/SKAP complex within the complex and with other kinetochore components. First of all, Astrin and SKAP will be expressed recombinantly in order to obtain soluble constructs of the two proteins and to reconstitute the protein complex *in vitro*. These recombinant proteins will be used to identify the minimal binding domains for the interactions of the Astrin/SKAP complex, which will be functionally investigated in more detail both *in vitro* and *in vivo* using a combinatorial approach of biochemical, biophysical and cell biological methods. Furthermore, attempts will be made to structurally characterize the reconstituted Astrin/SKAP complex as well as the individual proteins by means of electron microscopy and X-ray crystallography in order to obtain more detailed information about their molecular architecture. The results will advance our understanding of the functional role of the Astrin/SKAP complex during mitosis and give closer insights into the mechanisms leading to the establishment of functional kinetochore-microtubule attachments.

3 RESULTS

3.1 Domain organization of the Astrin/SKAP complex

A bioinformatic characterization of Astrin and SKAP was performed in order to obtain initial hints regarding the structural and functional organization of the two proteins. The secondary structure predictions of Astrin and SKAP by PSIPRED (Buchan et al., 2013) can be found in supplementary figures 6.1 and 6.3. The models of Astrin and SKAP with the highest confidence, i.e. with the highest probability that the sequence and the template match, predicted by Phyre2 (Kelley & Sternberg, 2009) are depicted in figures 3.1 and 3.2. For Astrin, the central 462 residues (39 % of the total sequence) were modeled with a confidence of 99.5 % by the single highest scoring template. The remaining residues could be modeled with > 90 % confidence using multiple templates. For SKAP, 310 residues (98 % of the total sequence) were modeled with a confidence of 98.4 % by the single highest scoring template.

The predictions by the servers and programs Jpred, PSIPRED, Phyre2 and I-TASSER (Cole et al., 2008; Buchan et al., 2013; Kelley & Sternberg, 2009; Roy et al., 2010; Zhang, 2008) suggest that both Astrin and SKAP consist mainly of disordered and helical regions. The N-terminal region of Astrin up to amino acid 481 is predicted to be mainly unstructured apart from several small helical sections. This region is followed by two long helical fragments comprising amino acids 482 to 903 and 966 to 1175 that are connected by a disordered linker region. The coiled-coil domains of Astrin that were predicted by Paircoil2 (McDonnell et al., 2006) as shown in supplementary figure 6.2 lie within these helical parts of the protein. For SKAP, the N-terminal domain comprising amino acid 1 to 158 is suggested to be mainly unstructured, whereas the central part ranging from amino acid 159 to 225 and the

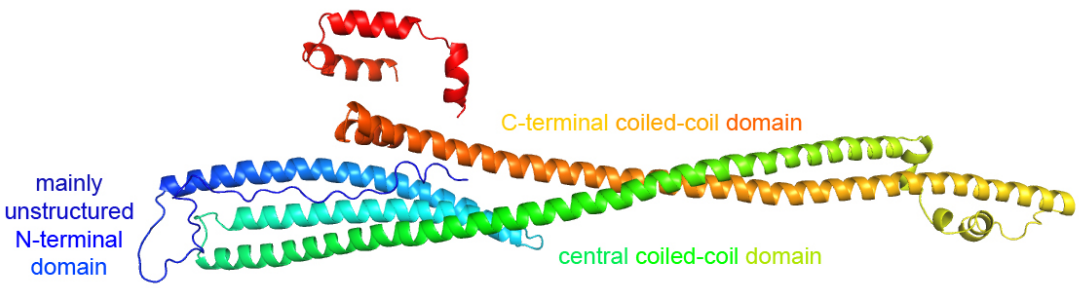

Figure 3.1: Model of the tertiary structure of Astrin predicted by the Phyre2 server. The illustration of the model was done with PyMOL (DeLano Scientific, San Francisco, US-CA). Coloring proceeds along the chain from blue (N-terminus) to red (C-terminus).

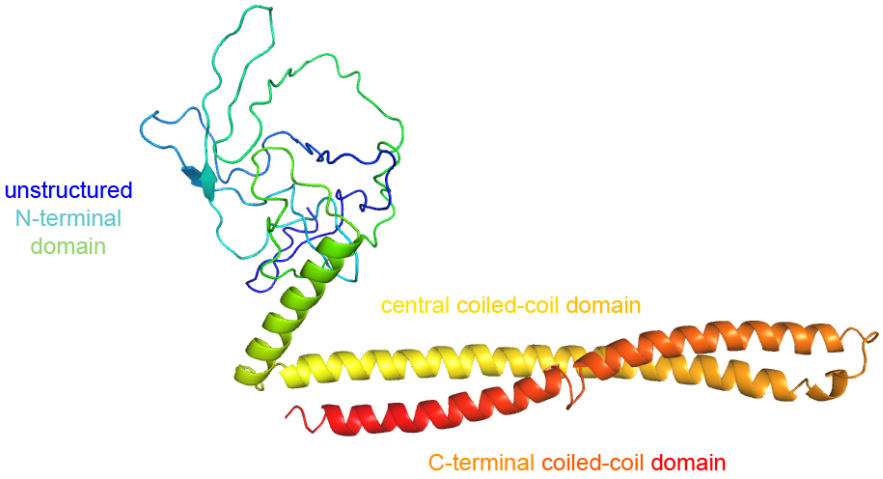

Figure 3.2: Model of the tertiary structure of SKAP predicted by the Phyre2 server. The illustration of the model was done with PyMOL (DeLano Scientific, San Francisco, US-CA). Coloring proceeds along the chain from blue (N-terminus) to red (C-terminus).

following C-terminal segment each consist of one long α-helix. These predicted helical regions are also consistent with the coiled-coil domain prediction by Paircoil2 (McDonnell et al., 2006) as shown in supplementary figure 6.4.

Although Astrin and SKAP have not been recognized for being homologous proteins, the bioinformatic characterization indicates that their overall domain organization, which is shown in figure 3.3, is similar, despite conspicuous size differences. Specifically, both Astrin and SKAP consist mainly of three domains: The N-terminal domain of both proteins is predicted to be mainly unstructured. In both proteins, this region is followed by two coiled-coil domains of different lengths, separated by predicted intervening gaps. These observations suggest that both Astrin and SKAP exhibit an elongated structure.

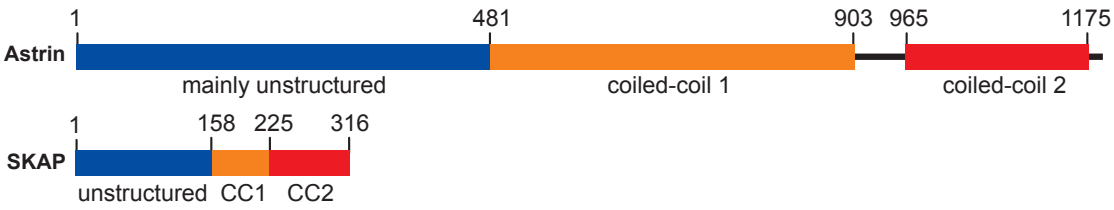

Figure 3.3: Domain organization of Astrin and SKAP. Domain organization is based on secondary structure predictions by Jpred, PSIPRED, Phyre2 and I-TASSER. CC: coiled-coil.

3.2 Expression and purification of Astrin and SKAP constructs

3.2.1 Expression of Astrin and SKAP full-length constructs

To allow the *in vitro* characterization of the Astrin/SKAP complex, attempts were made to produce recombinant forms of the two proteins. Therefore, wild type and codon-optimized coding sequences were subcloned into several expression vectors for individual expression as well as for coexpression. In case of the full-length proteins different affinity tags were tested including N- or C-terminal hexahistidine (His_6) tags and a glutathione S transferase (GST) tag. *Escherichia coli* and insect cells were used as expression systems.

A test expression of GST-Astrin is depicted in figure 3.4. The expression was performed in *E. coli* C41 cells at 18 °C for 16 h. The comparison of the whole cell extracts before (-) and after (+) induction with IPTG shows that GST-Astrin was expressed at a high level with the expected molecular weight of 160 kD. During the subsequent batch purification all the expressed protein was found in the pellet fraction (P) after clearing the cell lysate. No corresponding band was visible in the fraction of the washed beads, revealing that GST-Astrin was insoluble. Similarly, in other expression systems and with different affinity tags, Astrin full-length protein showed good expression levels, but could not be expressed in a soluble form.

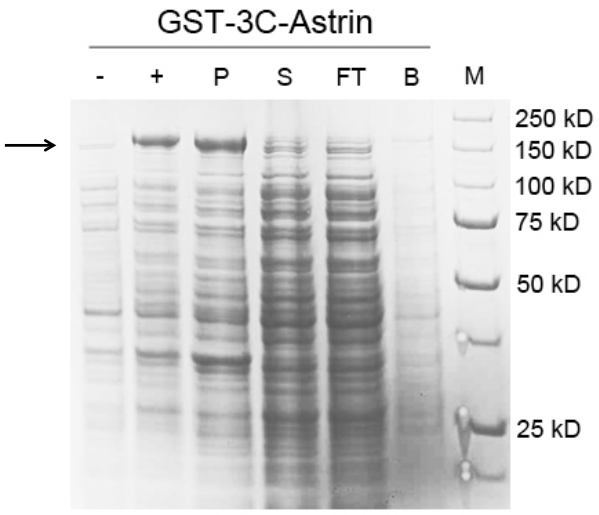

Figure 3.4: Test expression and batch purification of GST-Astrin full-length. Coomassie stained SDS-PAGE gel showing the test expression in C41 cells and batch purification of codon-optimized Astrin full-length with a PreScission cleavable (3C) GST tag. The arrow marks the expected position of GST-Astrin at a molecular weight of 160 kD. -: whole cell extract before induction, +: whole cell extract after induction, P: pellet after clearing the lysate, S: supernatant after clearing the lysate, B: sample of washed bead fraction, M: molecular weight standard with molecular weights indicated on the right.

Figure 3.5 shows a test expression of GST-SKAP full-length in *E. coli* C41 cells at 18 °C for 16 h. A band with the expected molecular weight of 61 kD could be found in the sample of the whole cell extract after induction of expression, indicating a high expression level of GST-SKAP. As for Astrin, the pellet fraction after clearing the cell lysate shows the corresponding band of GST-SKAP that could not be found in the soluble fraction, thus indicating that most of the expressed protein is insoluble. The sample of the washed beads reveals that a small fraction of GST-SKAP was soluble. However, during large-scale expression trials, GST-SKAP could not be expressed in a soluble form. Other expression systems and affinity tags as well as a coexpression strategy with Astrin full-length did not lead to soluble protein.

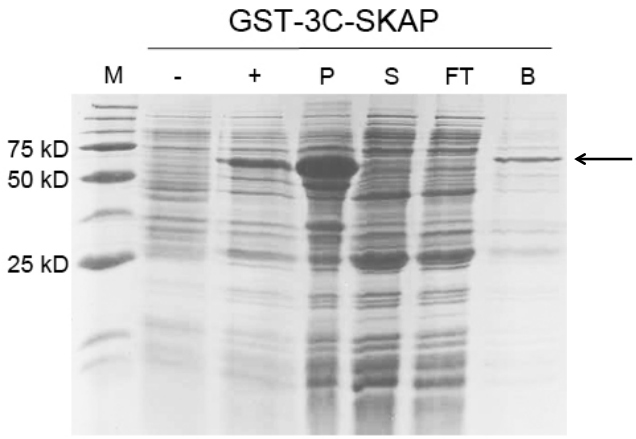

Figure 3.5: Test expression and batch purification of GST-SKAP full-length. Coomassie stained SDS-PAGE gel showing the test expression in C41 cells and batch purification of SKAP full-length with a PreScission cleavable (3C) GST-tag. The arrow marks the expected position of GST-SKAP at a molecular weight of 61 kD. -: whole cell extract before induction, +: whole cell extract after induction, P: pellet after clearing the lysate, S: supernatant after clearing the lysate, B: sample of washed bead fraction, M: molecular weight standard with molecular weights indicated on the left.

A summary of expression level and solubility from test expressions of the different Astrin and SKAP full-length constructs is shown in table 3.1. The highest expression levels of Astrin and SKAP could be obtained with the N-terminal GST-tag, whereas His_6-tags only resulted in lower amounts of expressed proteins. Also during coexpressions studies, the two proteins showed only low expression levels. In case of the C-terminal His_6-tags on Astrin and SKAP the test expressions of both proteins revealed additional protein bands at the expected molecular weights as well as bands with lower molecular weights, thus indicating degradation of the proteins when no affinity tags are placed at the N-terminus.

Table 3.1: Expression levels and solubility of Astrin and SKAP full-length constructs.

construct	expression level	solubility	comments
His_6-Astrin	+	-	
His_6-TEV-Astrin	+	-	
Astrin-His_6	+	-	degradation
GST-3C-Astrin	+++	-	
His_6-SKAP	++	-	
His_6-TEV-SKAP	++	-	
SKAP-His_6	++	-	degradation
GST-3C-SKAP	+++	(✓)	small amounts of soluble protein only in test expression in C41 at 18 °C for 16 h
His_6-Astrin/SKAP	+	-	
His_6-SKAP/Astrin	+	-	
GST-3C-Astrin/SKAP	+	-	
GST-3C-SKAP/Astrin	+	-	

3.2.2 Expression and purification of Astrin and SKAP truncation constructs

Based on the bioinformatic characterization discussed in section 3.1 different truncation constructs of Astrin and SKAP, in addition to the full-length proteins, were generated by subcloning and tested for their solubility. Purification protocols were successfully established for the soluble constructs as described in section 5.4.1.4.

The designed truncation constructs for Astrin are depicted in figure 3.6. The three domains, combinations of them, and two truncations based on previously published results were tested. These two constructs are a truncated version of the central coiled-coil domain ranging from amino acid 482 to 850, which has been suggested to be the SKAP binding domain of Astrin (Dunsch et al., 2011), and the Aurora A binding domain comprising amino acids 1 to 239 (Du et al., 2008).

As an example of a successful purification, the size exclusion chromatography of Astrin$^{1\text{-}239}$ that was expressed in *E. coli* C41 cells at 18 °C for 14 h and purified by a two step procedure including affinity and ion-exchange chromatography is shown in figure 3.7. The chromatogram reveals four peaks, of which the first three contain Astrin$^{1\text{-}239}$. The front peak belongs to a fraction of Astrin$^{1\text{-}239}$ that is contaminated with

DNA as judged by the ratio of absorbance at 260 nm to 280 nm of 2.1. The following two peaks correspond to Astrin$^{1-239}$, which shows the expected molecular weight of 26 kD and is free of contaminants based on the SDS-PAGE gel and absorption spectra of the pooled sample. The fact that, despite its small molecular weight of 26 kD, Astrin$^{1-239}$ elutes very early during size exclusion chromatography with elution volumes corresponding to molecular weights of more than 150 kD suggests that it exists in an oligomeric state, or alternatively, and not exclusively, that it may have an elongated structure. The presence of two peaks is an indication for different oligomeric states of Astrin$^{1-239}$.

A summary of the expression levels, solubility and yields of the truncated Astrin constructs is listed in table 3.2. Apart from this truncated N-terminal domain of Astrin, a GST fusion of the whole N-terminal domain as well as the C-terminal coiled-coil domain could be expressed in a soluble form and purified with yields between 0.2 mg and 0.5 mg per liter of expression culture. All constructs containing the central coiled-coil domain of Astrin, which is believed to interact with SKAP, were expressed in an insoluble form, indicating that the interaction partner is required for stabilization.

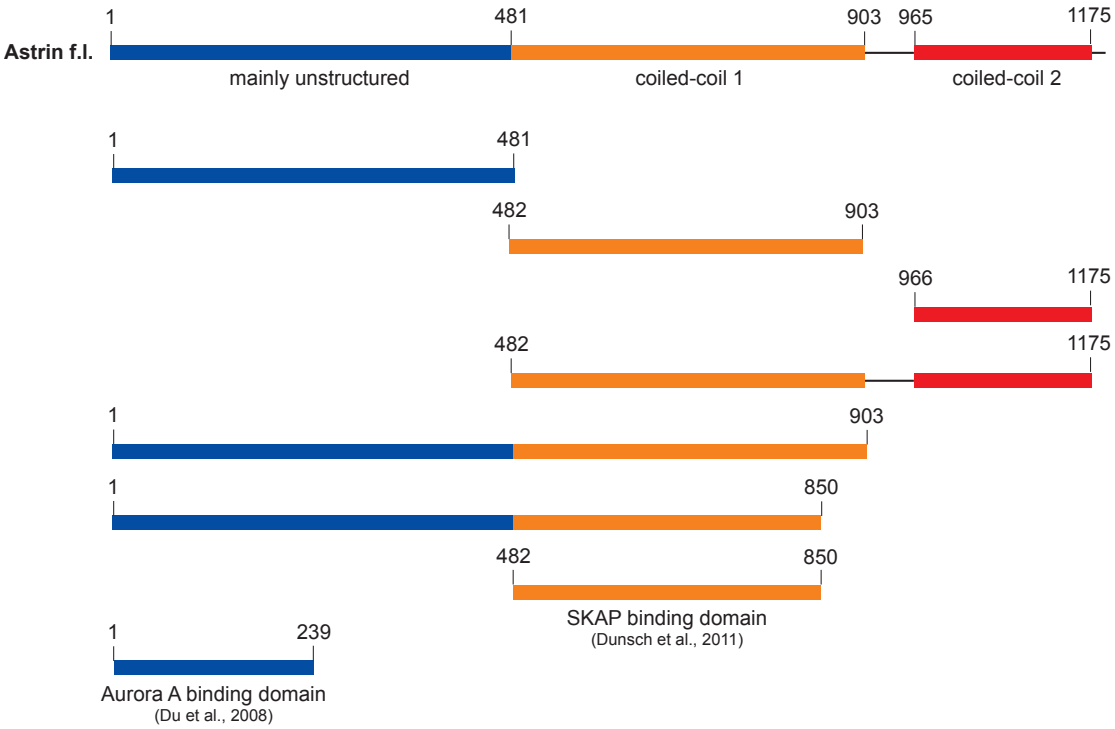

Figure 3.6: Truncations constructs of Astrin. Constructs were designed based on the domain organization depicted on top and previously published results.

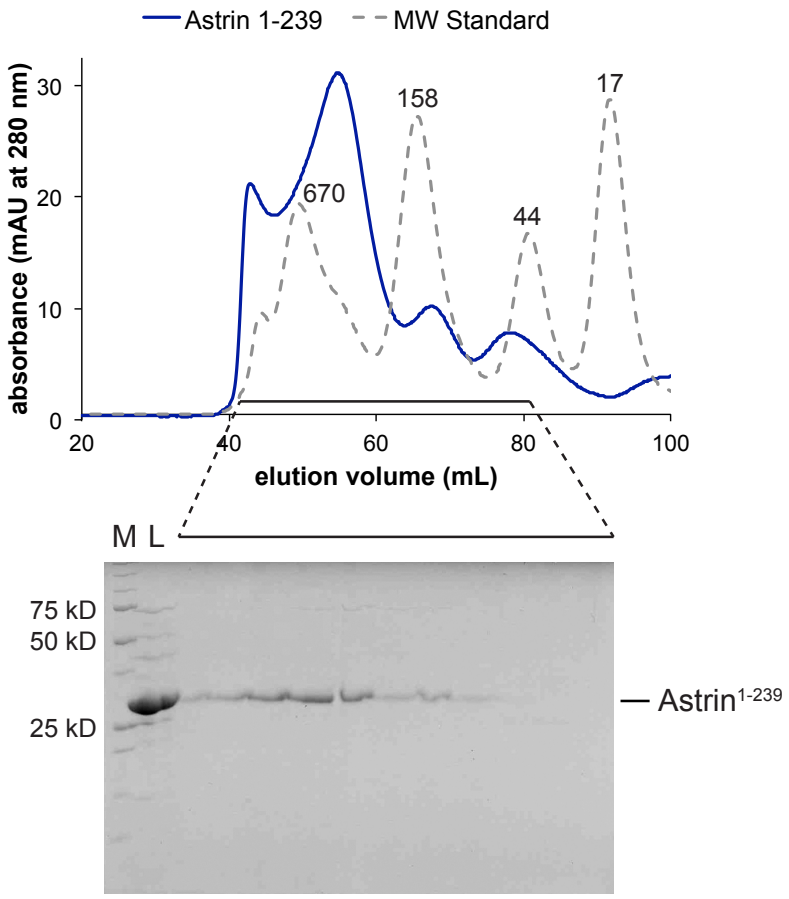

Figure 3.7: Purification of Astrin$^{1-239}$. Top, elution profile of Astrin$^{1-239}$ during size exclusion chromatography. Dashed line indicates elution profile of a molecular weight marker with the indicated molecular weights of the proteins in kD. Bottom, Coomassie stained SDS-PAGE gel with samples of indicated fractions from the size exclusion chromatography depicted on top. M: molecular weight standard with molecular weights indicated on the left, L: appearance of the sample loaded on the size exclusion chromatography column.

Table 3.2: Expression levels, solubility and yields of Astrin truncation constructs. All constructs were tagged with an N-terminal, PreScission cleavable GST-tag.

construct	expression level	solubility	yield
Astrin$^{1-481}$	++	✓	0.2 mg/L (only soluble as GST fusion)
Astrin$^{1-239}$	++	✓	0.3 mg/L
Astrin$^{482-850}$	+++	-	
Astrin$^{482-903}$	+++	-	
Astrin$^{966-1175}$	+++	✓	0.5 mg/L
Astrin$^{482-1175}$	+	-	
Astrin$^{1-850}$	+	-	
Astrin$^{1-903}$	+	-	

The truncation constructs for SKAP shown in figure 3.8 are the three isolated domains and their combinations. In order to map the microtubule-binding domain of SKAP (see section 3.3.2) several constructs were designed based on the predicted secondary structure of SKAP that consist of the central coiled-coil domain and N-terminal extensions of different lengths.

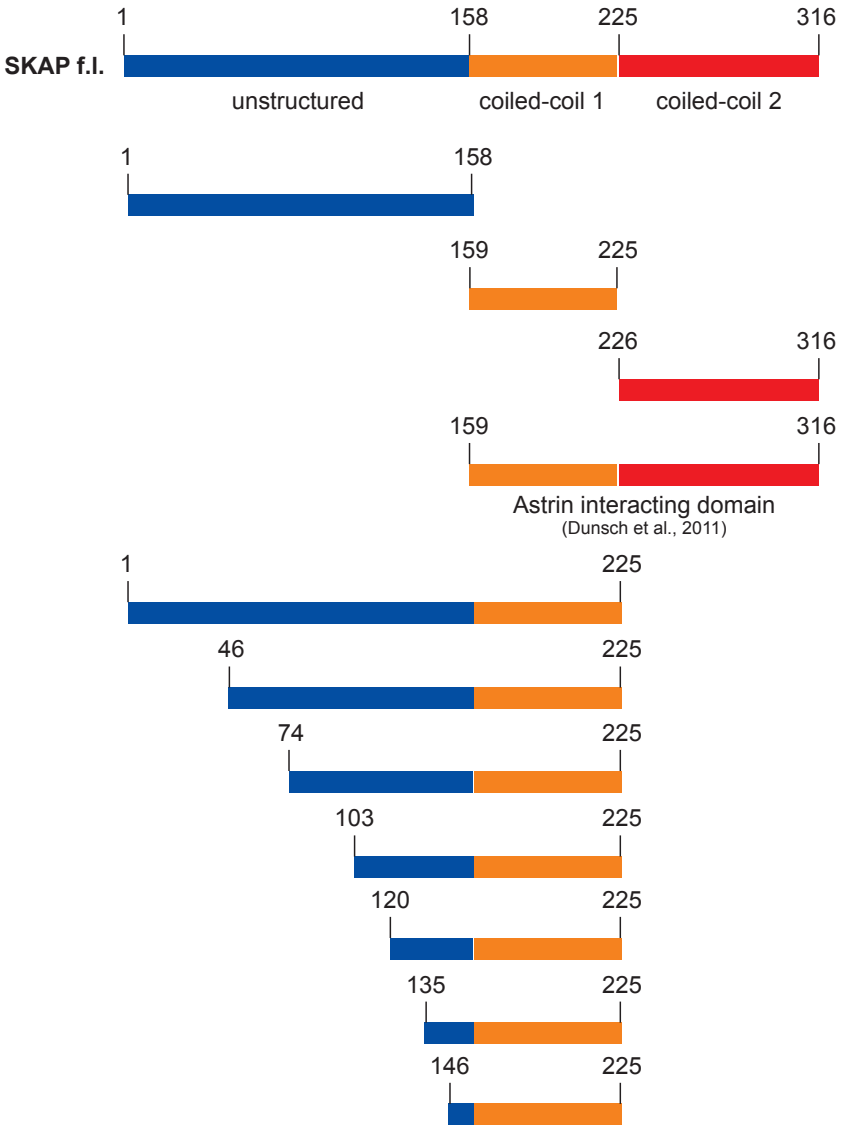

Figure 3.8: Truncations constructs of SKAP. Constructs were designed based on the domain organization depicted on top and predicted secondary structure.

Figure 3.9 presents the size exclusion chromatography of SKAP$^{159-316}$ that was expressed in *E. coli* C41 cells at 18 °C for 16 h and purified by affinity and ion-exchange chromatography. The chromatogram reveals a single peak, which shows that SKAP$^{159-316}$ was successfully purified to homogeneity. This is confirmed by the

SDS-PAGE gel that displays a single band at the expected molecular weight of 19 kD. As already seen in the elution profile of Astrin$^{1-239}$, SKAP$^{159-316}$ eluted from the size exclusion chromatography column at low elution volumes corresponding to molecular weights of more than 150 kD. This suggests that SKAP$^{159-316}$ has an elongated structure or that it exists in a dimeric or oligomeric state. This elongated structure is in agreement with the secondary structure predictions that suggest the existence of two coiled-coil domains in this region of SKAP.

A summary of the expression levels, solubility and yields of the tested SKAP truncations is listed in table 3.3. In addition to SKAP$^{159-316}$, all single domains as well as the N-terminal extension constructs of the central coiled-coil domain up to amino acid 103 could be expressed in a soluble form. The purifications of these constructs resulted in yields between 2 mg and 9 mg per liter of expression culture.

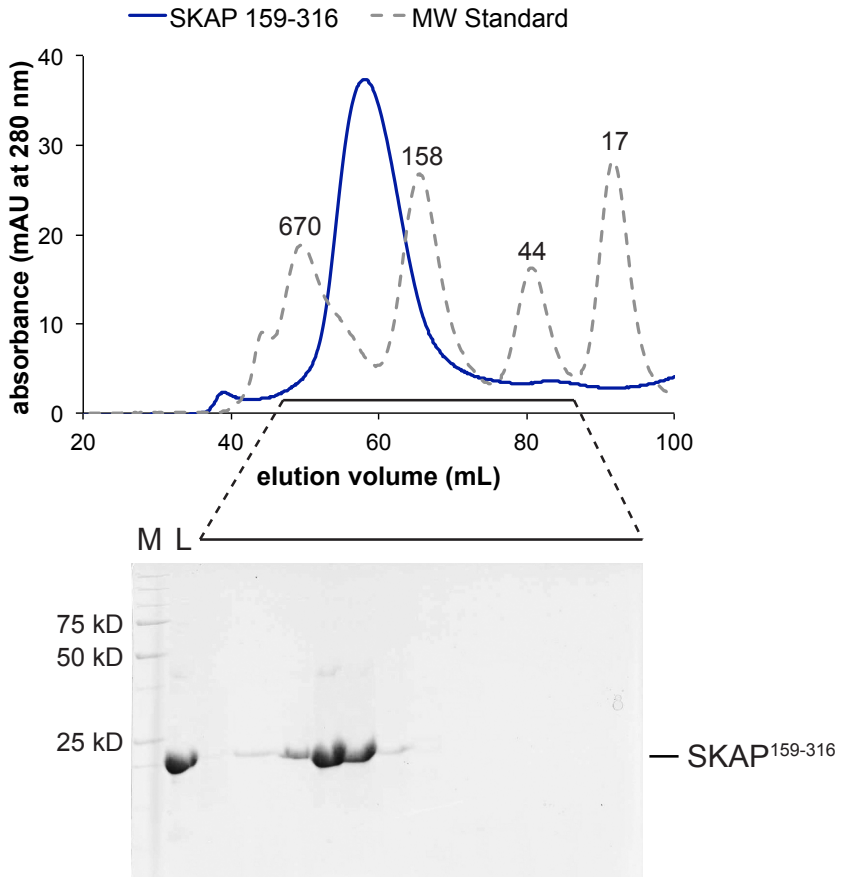

Figure 3.9: Purification of SKAP$^{159-316}$. Top, elution profile of SKAP$^{159-316}$ during size exclusion chromatography. Dashed line indicates elution profile of a molecular weight marker with the indicated molecular weights of the proteins in kD. Bottom, Coomassie stained SDS-PAGE gel with samples of indicated fractions from the size exclusion chromatography depicted on top. M: molecular weight standard with molecular weights indicated on the left, L: appearance of the sample loaded on the size exclusion chromatography column.

Table 3.3: Expression levels, solubility and yields of SKAP truncation constructs. All constructs were tagged with an N-terminal, PreScission cleavable GST-tag.

construct	expression level	solubility	yield
$SKAP^{1-158}$	++	✓	2 mg/L (only soluble as GST fusion)
$SKAP^{159-225}$	+++	✓	4 mg/L
$SKAP^{226-316}$	+	✓	9 mg/L
$SKAP^{159-316}$	+++	✓	3 mg/L
$SKAP^{1-225}$	+	-	
$SKAP^{46-225}$	++	-	
$SKAP^{74-225}$	++	-	
$SKAP^{103-225}$	+++	✓	2 mg/L
$SKAP^{120-225}$	+++	✓	3 mg/L
$SKAP^{135-225}$	+++	✓	3 mg/L
$SKAP^{146-225}$	+++	✓	4 mg/L

3.2.3 Expression and purification of $SKAP^{135-225}$

Since the SKAP construct comprising amino acids 135 to 225 plays a major role in this study, a more detailed purification procedure of this construct is discussed below. The established purification protocol is explained in section 5.4.1.4. In brief, the construct was expressed in *E. coli* C41 cells at 18 °C for 16 h after induction with 0.1 mM IPTG. The cleared lysate was loaded onto a GSH column for affinity purification. After extensive washes the GST tag was cleaved on the column with PreScission protease for 16 h at 4 °C in order to obtain untagged $SKAP^{135-225}$. The eluate was subsequently purified by anion exchange chromatography to remove DNA and other protein contaminants. As a final purification step, the concentrated protein was loaded onto a S200 size exclusion chromatography column. A representative chromatogram can be found in figure 3.10. As for $SKAP^{159-316}$, the low elution volume of $SKAP^{135-225}$ suggests an elongated structure, which is in agreement with the predicted coiled-coil structure. The SDS-PAGE gels of the size exclusion chromatography and of the pooled fraction show two bands. The more intense protein band corresponds to $SKAP^{135-225}$, whose expected molecular weight is 11 kD, whereas the less intense band at about 25 kD probably consists of a GST contamination that could not be removed during purification. The purity of $SKAP^{135-225}$ amounts to over 90 % as quantified by band intensity and it could be purified with yields of 3 mg per liter of expression culture.

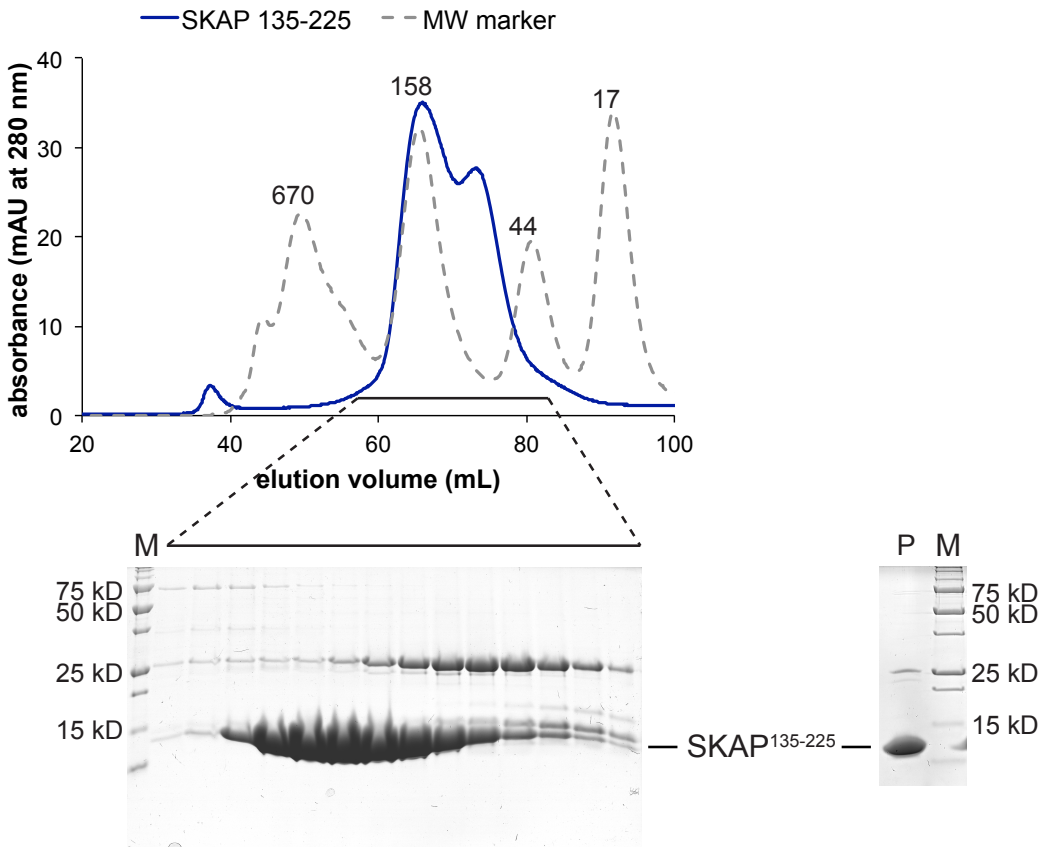

Figure 3.10: Purification of SKAP$^{135-225}$. Top, elution profile of SKAP$^{135-225}$ during size exclusion chromatography. Dashed line indicates elution profile of a molecular weight marker with the indicated molecular weights of proteins in kD. Bottom left, Coomassie stained SDS-PAGE gel with samples of indicated fractions from the size exclusion chromatography shown on top. Bottom right, pooled and concentrated sample of SKAP$^{135-225}$ after final size exclusion chromatography (P). M: molecular weight standard with molecular weights indicated on the right.

In order to determine the molecular weight and thereby the oligomeric state of SKAP$^{135-225}$, analytical ultracentrifugation (AUC) experiments were performed. Figure 3.11 A shows the sedimentation coefficient distribution of a sample containing SKAP$^{135-225}$. The distribution is based on the radial signals of the sedimentation velocity experiment depicted in figure 3.11 B. The sedimentation coefficient distribution reveals two peaks. The smaller peak with a sedimentation coefficient of 2.2 S belongs to a contamination of the sample with a molecular weight of 80.6 kD. The larger peak, with a sedimentation coefficient of 1.2 S and a frictional ratio of 2.7, belongs to SKAP$^{135-225}$. This peaks corresponds to a molecular weight of 32.84 kD indicating that SKAP$^{135-225}$ - which has a monomeric size of 11 kD - forms a trimer. The frictional ratio takes the shape-dependent hydrodynamics of the molecule into account. A perfect sphere has a frictional ratio of 1, whereas elongated structures have values over 2. A frictional ratio of the analyzed molecule of 2.7 suggests that SKAP$^{135-225}$ exhibits a very elongated structure, which is in agreement with the high

predicted coiled-coil content. The result that SKAP$^{135-225}$ forms a trimer is also supported by crosslinking analysis (see figure 3.11 C). In this experiment a sample containing SKAP$^{135-225}$ was incubated with the crosslinker bis(sulfosuccinimidyl)-glutarate (BS2G), which covalently links primary amines of lysine side chains that are within a distance compatible with the crosslinker length of 7.7 Å. It can be seen that with increasing amounts of the crosslinker two bands appeared apart from the monomeric band of SKAP$^{135-225}$ at 11 kD. The lower of these bands, with an apparent molecular weight of 22 kD, corresponds to a SKAP dimer, whereas the upper band at around 33 kD corresponds to a SKAP trimer.

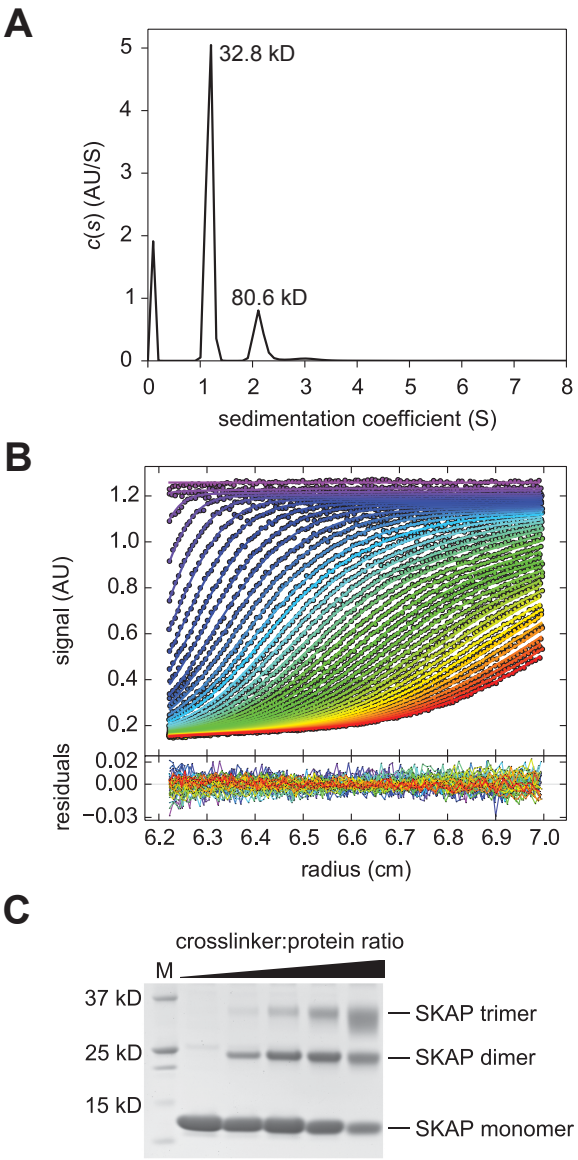

Figure 3.11: SKAP$^{135-225}$ forms a trimer. (**A**) Sedimentation coefficient distribution c(*S*) of sedimentation velocity experiments of SKAP$^{135-225}$. (**B**) Top, plot of radial signals of the AUC of SKAP$^{135-225}$. Bottom, residuals of the fit showing the deviation of the c(*S*) model from the observed signals. (**C**) Detail of supplementary figure 8.13 A showing the crosslinking of SKAP$^{135-225}$ in presence of increasing amounts of crosslinker BS2G.

3.2.4 Expression and purification of a truncated Astrin/SKAP complex

Since the individual expression of Astrin constructs that contain its central coiled-coil domain resulted in insoluble protein, attempts were made to solubilize this Astrin domain by coexpression with SKAP$^{159-316}$ in insect cells. Figure 3.12 shows the constructs of Astrin and SKAP that were tested in these coexpression trials.

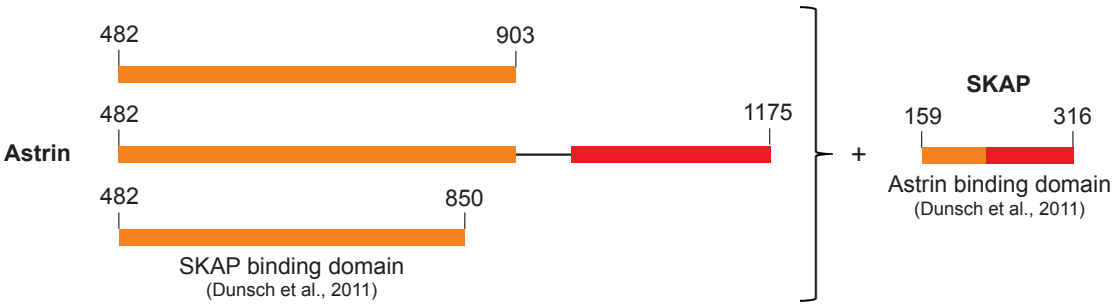

Figure 3.12: Constructs of Astrin and SKAP for coexpression in insect cells.

All constructs were expressed, but only the Astrin construct comprising amino acids 482 to 850 could be expressed in a soluble form upon coexpression with SKAP$^{159-316}$ (see table 3.4) suggesting that the two proteins interact directly via these minimal interaction domains in the absence of other binding partners. In case of the N-terminal His_6-tag on Astrin, the complex could not be enriched by affinity purification (see supplementary figure 6.5) suggesting that the N-terminus of Astrin$^{482-850}$ is buried within the complex and thereby not accessible to the affinity matrix. With a C-terminal His_6 tag on Astrin and untagged SKAP an expression and purification protocol was established for the Astrin$^{482-850}$/SKAP$^{159-316}$ complex (see sections 5.4.1.3.3 and 5.4.1.5).

Figure 3.13 shows a representative chromatogram and the corresponding SDS-PAGE gel of the final size exclusion chromatography purification step of the Astrin$^{482-850}$/SKAP$^{159-316}$ complex. It can be seen that the complex reveals two dominant protein bands at the expected molecular weights of 43 kD for Astrin$^{482-850}$ and 19 kD for SKAP$^{159-316}$. Other bands in the SDS-PAGE gel and several peaks in the chromatogram point to the contaminations of the sample. Therefore, only the purest fractions were pooled resulting in low yields of about 50 µg per liter of insect cell culture.

To find out whether SKAP$^{159-316}$ is the minimal interaction domain for Astrin, coexpression trials in insect cells of Astrin$^{482-850}$-His_6 with the single domains of SKAP

were tested. All coexpressions with the single SKAP domains resulted in insoluble Astrin$^{482-850}$ and only SKAP$^{159-316}$ was able to solubilize Astrin$^{482-850}$.

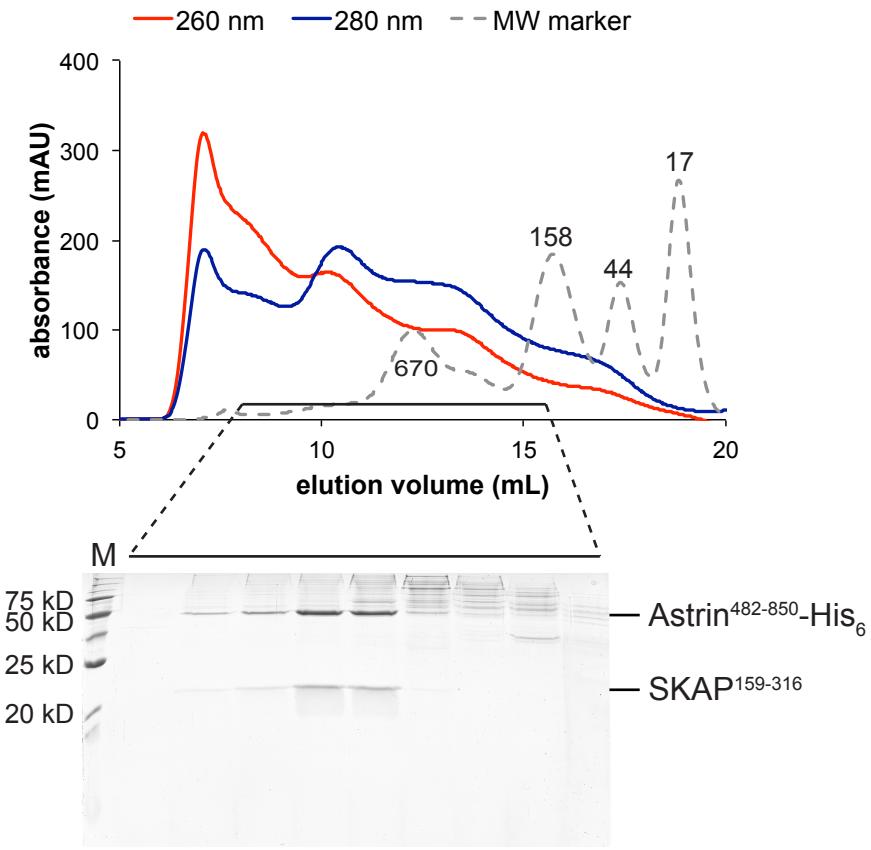

Figure 3.13: Purification of Astrin$^{482-850}$-His$_6$/SKAP$^{159-316}$. Top, elution profile of Astrin$^{482-850}$-His$_6$/SKAP$^{159-316}$ during size exclusion chromatography. Dashed line indicates elution profile of a molecular weight marker with the indicated molecular weights of proteins in kD. Bottom, Coomassie stained SDS-PAGE gel with samples of indicated fractions from the size exclusion chromatography depicted on top. M: molecular weight standard with molecular weights indicated on the left.

Table 3.4: Summary of coexpression tests in insect cells with different Astrin and SKAP constructs. n.t.: not tested.

		SKAP			
		1-158	159-225	226-316	159-316
Astrin	482-850	only SKAP soluble	only SKAP soluble	only SKAP soluble	+
	482-903	n.t.	n.t.	n.t.	only SKAP soluble
	482-1175	n.t.	n.t.	n.t.	only SKAP soluble

3.3 Interaction of the Astrin/SKAP complex with tubulin

3.3.1 The Astrin/SKAP complex binds to microtubules through SKAP

As mentioned in chapter 1.6, the Astrin/SKAP complex is able to bind to microtubules. In order to map the binding sites in more detail, the microtubule-binding properties of the recombinant Astrin and SKAP constructs were analyzed in microtubule cosedimentation assays. In these assays the protein of interest is incubated with taxol-stabilized microtubules and, after ultracentrifugation, the supernatant and pellet fractions are analyzed by SDS-PAGE. The supernatant contains unpolymerized tubulin and the proteins that do not bind to microtubules, whereas the pellet consists of the microtubules and bound proteins. In a control experiment without microtubules the proteins are treated in the same way as in the actual experiment in order to check their pelleting behavior under the assay conditions.

Figure 3.14 shows the microtubule cosedimentation assays with the single domains of SKAP. In case of the SKAP$^{1-158}$ N-terminal domain (see figure 3.14 A), it can be seen that in the absence of microtubules (- MT) most of the protein was found in the supernatant (S), whereas the pellet (P) only contained a small fraction of SKAP$^{1-158}$. In comparison to this, in the experiment together with microtubules (+ MT) the amount of SKAP$^{1-158}$ was shifted from the supernatant to the pellet fraction. Under these conditions, 42 % of SKAP$^{1-158}$ was bound to the microtubules indicating that the N-terminal domain of SKAP is able to bind to microtubules. The central coiled-coil domain of SKAP comprising amino acids 159 to 225 showed similar microtubule-binding properties as SKAP$^{1-158}$ (see figure 3.14 B). While SKAP$^{159-225}$ hardly pelleted in the control experiment without microtubules, the assays in the presence of microtubules revealed that 53 % of the protein was found in the pellet fraction. This suggests that the central coiled-coil domain of SKAP can also bind to microtubules. In contrast to the N-terminal domain and the central coiled-coil domain of SKAP, the C-terminal coiled-coil domain of SKAP ranging from amino acid 226 to 316 did not pellet in the presence of microtubules indicating that this domain is not able to bind to microtubules.

Next, the N- and C-terminal domains of Astrin were tested for their microtubule binding. As it can be seen in figure 3.15, both Astrin$^{1-239}$ and Astrin$^{966-1175}$ could only be found in the supernatant fractions, thus demonstrating lack of microtubule-binding affinity.

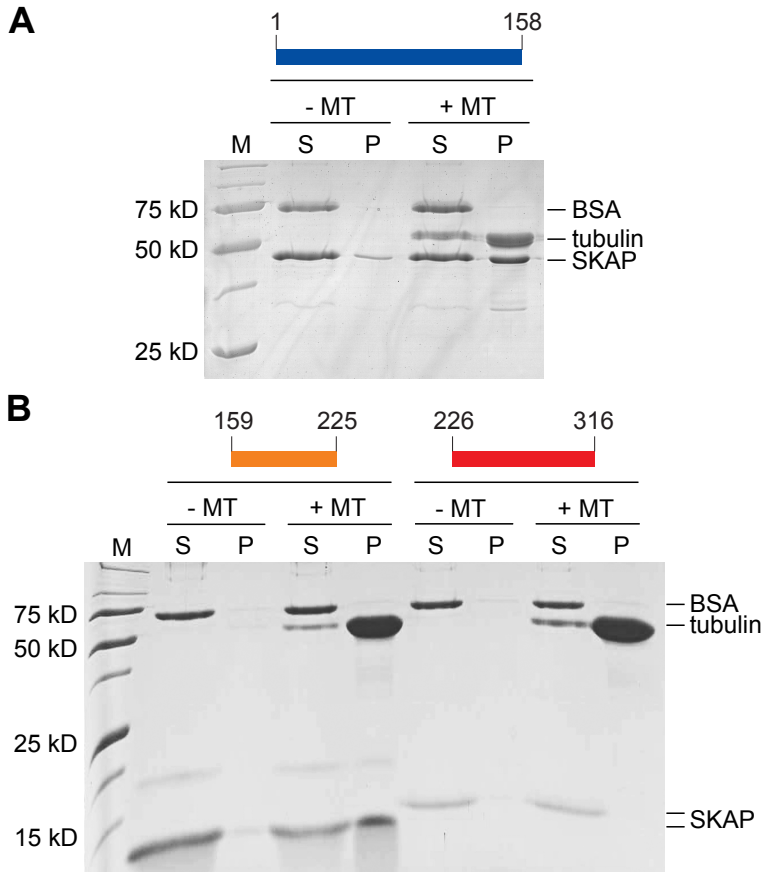

Figure 3.14: SKAP binds to microtubules with its N-terminal domain and central coiled-coil domain. Representative SDS-PAGE gels of microtubule cosedimentation assays with 3 µM taxol-stabilized microtubules (MT), 1 µM BSA and 3 µM GST-SKAP$^{1-158}$ (**A**), SKAP$^{159-225}$ or SKAP$^{226-316}$ (**B**). S: soluble fraction with proteins not bound to microtubules. P: pellet fraction with microtubules and bound proteins. M: molecular weight marker with molecular weights indicated on the left.

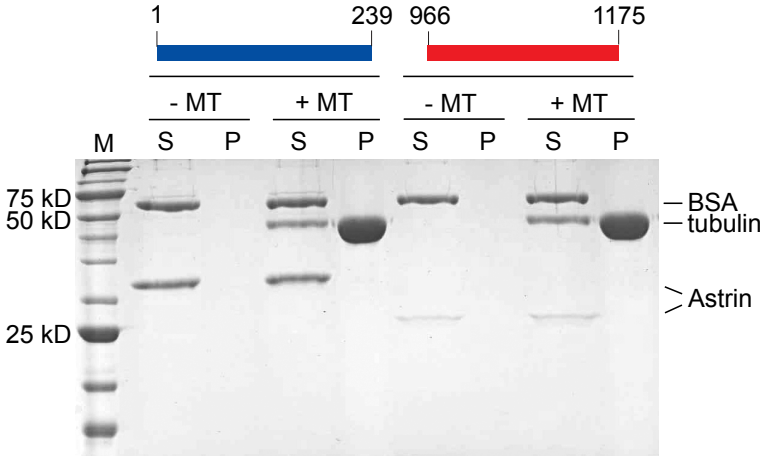

Figure 3.15: Astrin does not bind to microtubules. Representative SDS-PAGE gel of microtubule cosedimentation assays with 3 µM taxol-stabilized microtubules (MT), 1 µM BSA and 3 µM Astrin$^{1-239}$ or Astrin$^{966-1175}$. S: soluble fraction with proteins not bound to microtubules. P: pellet fraction with microtubules and bound proteins. M: molecular weight marker with molecular weights indicated on the left.

Since the tested Astrin constructs were not able to bind to microtubules on their own, it was tested if they show pelleting in the presence of SKAP$^{159-316}$, the Astrin interacting domain of SKAP. Therefore, the N- and C-terminal domains of Astrin were incubated together with microtubules and SKAP$^{159-316}$ in microtubule cosedimentation assays as shown in figure 3.16. As in the experiments lacking SKAP, the Astrin constructs showed no binding to microtubules when SKAP$^{159-316}$ was present. This suggests that SKAP$^{159-316}$ only binds to the central coiled-coil domain of Astrin and has no additional interaction site on the N- and C-terminal domains of Astrin.

The results of the microtubule cosedimentation assays with the single Astrin and SKAP constructs and the combination of them are summarized in table 3.5.

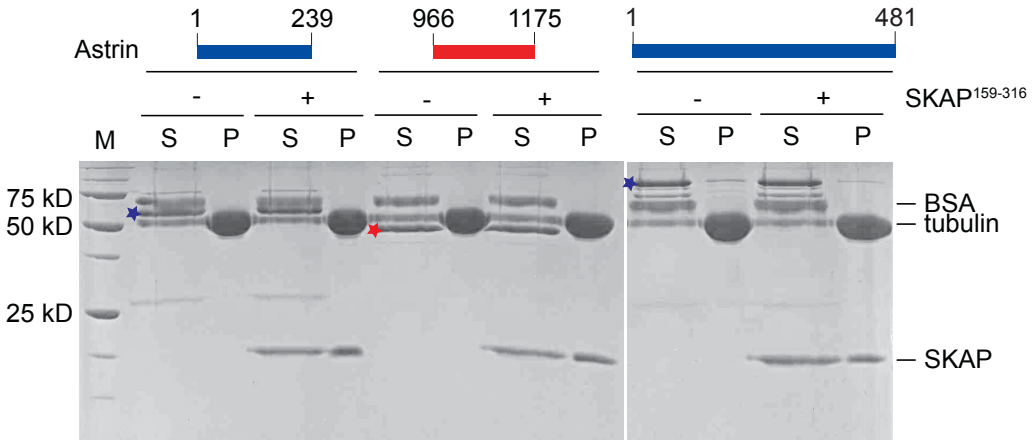

Figure 3.16: The N- and C-terminal domains of Astrin do not interact with SKAP bound to microtubules. Representative SDS-PAGE gels of microtubule cosedimentation assays with 3 µM taxol-stabilized microtubules, 1 µM BSA, 3 µM SKAP$^{159-316}$ and 3 µM Astrin$^{1-239}$, Astrin$^{966-1175}$ or Astrin$^{1-481}$. Blue and red starlets mark the protein bands corresponding to Astrin. S: soluble fraction with proteins not bound to microtubules. P: pellet fraction with microtubules and bound proteins. M: molecular weight marker with molecular weights indicated on the left.

Table 3.5: Summary of microtubule binding of Astrin and SKAP constructs. n.t.: not tested.

		Astrin			
		none	1-239	1-481	966-1175
SKAP	none		-	-	-
	1-158	+	n.t.	n.t.	n.t.
	159-225	+	n.t.	n.t.	n.t.
	226-316	-	n.t.	n.t.	n.t.
	159-316	+	only SKAP binding	only SKAP binding	only SKAP binding

To analyze if Astrin contributes to the microtubule binding of the Astrin/SKAP complex, the Astrin$^{482-850}$/SKAP$^{159-316}$ complex was compared to SKAP$^{159-316}$ alone in microtubule cosedimentation assays. For this purpose either 1 µM Astrin$^{482-850}$/SKAP$^{159-316}$ complex or 1 µM SKAP$^{159-316}$ was titrated with 0-10 µM taxol-stabilized microtubules. The SDS-PAGE gels of these experiments are depicted in figure 3.17 A and B. The corresponding amounts of protein in the supernatant and the pellet were quantified using ImageJ 1.49 (NIH). The fraction of protein that was bound to the microtubules was calculated by dividing the amount of protein in the pellet by the sum of protein in the supernatant and the pellet. Bound fractions were plotted against the microtubule concentration and the one-site binding curves were fitted with Origin7.0 (OriginLab, Northampton, US-MA) as described in section 5.4.2. The results of this quantification and fitting analysis are shown in figure 3.17 C and table 3.6. It can be seen from the SDS-PAGE gels and the corresponding quantification that the pelleting behavior of Astrin$^{482-850}$/SKAP$^{159-316}$ and SKAP$^{159-316}$ was very similar. Both showed concentration dependent microtubule binding with apparent dissociation constants (K_d) of 1.56 µM for the Astrin$^{482-850}$/SKAP$^{159-316}$ complex and 1.62 µM for SKAP$^{159-316}$. The maximal bound fractions that are reached when all binding sites are saturated amounted to comparable levels of 49 % and 35 %, respectively. The similar behavior of Astrin$^{482-850}$/SKAP$^{159-316}$ and SKAP$^{159-316}$ in microtubule binding indicates that Astrin$^{482-850}$ does not contribute to the microtubule binding of the Astrin$^{482-850}$/SKAP$^{159-316}$ complex. Since the N- and C-terminal domains of Astrin also failed to show affinity for microtubules, the Astrin/SKAP complex presumably binds to microtubules through SKAP.

Table 3.6: Summary of fitting analysis of microtubule cosedimentation assays with Astrin$^{482-850}$/SKAP$^{159-316}$ and SKAP$^{159-316}$. Microtubule cosedimentation assays were performed with 0-10 µM taxol-stabilized microtubules and 1 µM Astrin$^{482-850}$/SKAP$^{159-316}$ or SKAP$^{159-316}$. Quantification was done with ImageJ 1.49 (NIH). Data were fitted with Origin7.0 (OriginLab, Northampton, US-MA) as described in section 5.4.2.

construct	apparent dissociation constant K_d (µM)	maximal bound fraction
SKAP$^{159-316}$	1.62 ± 0.17	0.35 ± 0.02
Astrin$^{482-850}$/SKAP$^{159-316}$	1.56 ± 0.14	0.49 ± 0.02

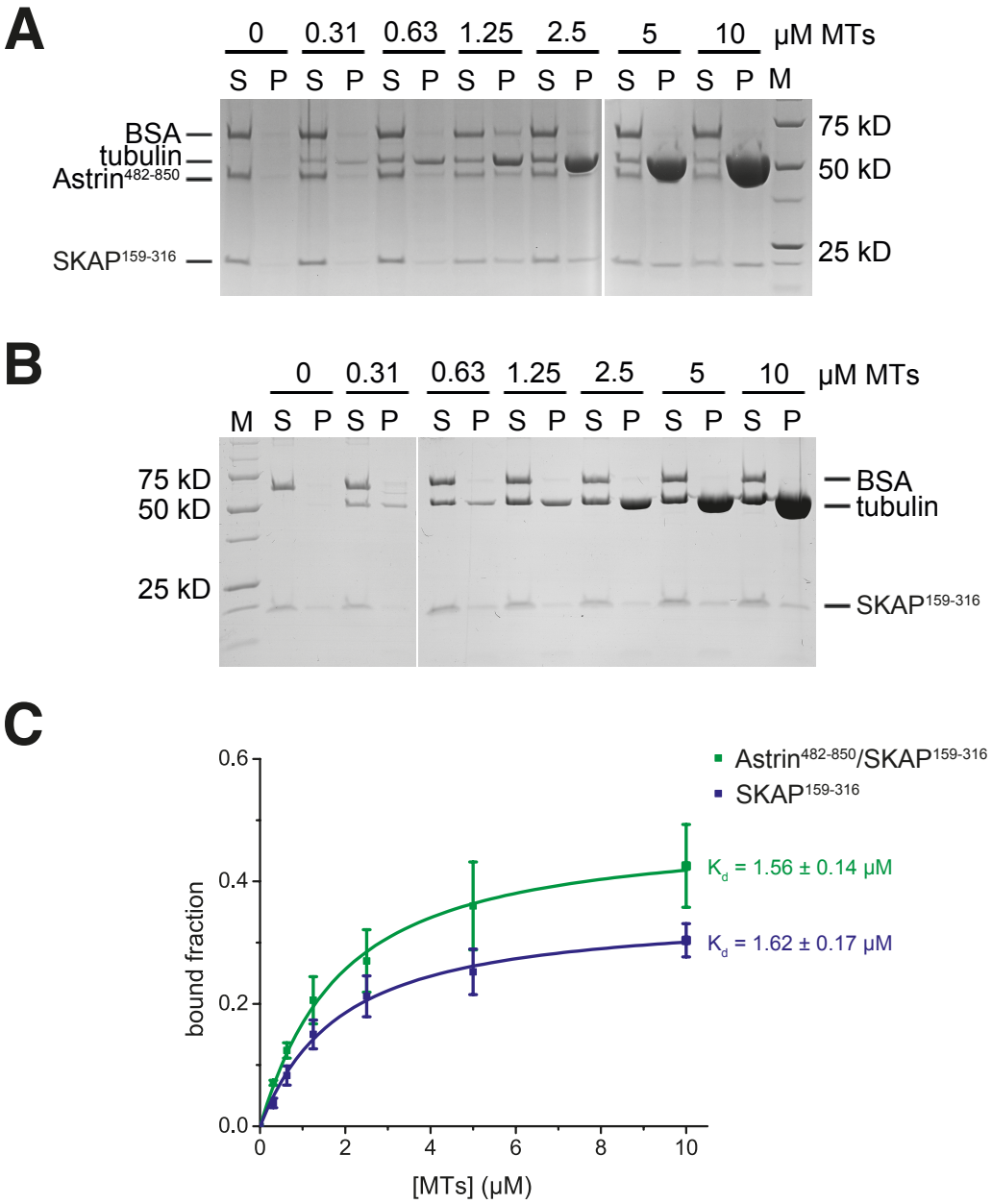

Figure 3.17: The Astrin/SKAP complex binds to microtubules through SKAP. Representative SDS-PAGE gels of microtubule cosedimentation assays with 0-10 µM taxol-stabilized microtubules (MTs), 1 µM BSA and 1 µM Astrin$^{482-850}$/SKAP$^{159-316}$ (**A**) or SKAP$^{159-316}$ (**B**). S: soluble fraction with proteins not bound to microtubules. P: pellet fraction with microtubules and bound proteins. M: molecular weight marker with molecular weights indicated at the side. (**C**) Quantification and fitting analysis of microtubule cosedimentation assays shown in (**A**) and (**B**). Quantification was done with ImageJ 1.49 (NIH). Data were fitted with Origin7.0 (OriginLab, Northampton, US-MA) as described in section 5.4.2.

3.3.2 The microtubule-binding domain of SKAP is located at amino acids 135 to 225

In section 3.3.1 it was shown that SKAP is able to bind to microtubules both with its N-terminal domain and its central coiled-coil domain. In order to identify the complete microtubule-binding domain of SKAP, different constructs of SKAP that contain the central coiled-coil domain and varying extensions to the N-terminus were created and analyzed in microtubule cosedimentation experiments. As mentioned in section 3.3.1, 1 µM of the respective protein was titrated with 0-10 µM taxol-stabilized microtubules, the bound fractions were quantified with ImageJ (NIH), plotted against the microtubule concentration and fitted with Origin7.0 (OriginLab, Northampton, US-MA). The SDS-PAGE gels as well as the corresponding quantifications can be found in figure 3.18 and the results of the fitting analysis are summarized in table 3.7. It can be seen that SKAP$^{159-225}$ and SKAP$^{146-225}$ showed a very similar behavior in microtubule binding. The apparent dissociation constants obtained for these constructs were 2.5 µM and 2.4 µM, respectively. Also the maximal bound fractions that amounted to 77 % and 71 %, respectively, were comparable. The longer constructs SKAP$^{135-225}$ and SKAP$^{103-225}$ revealed higher affinities for microtubules and at a microtubule concentration of 10 µM complete binding of SKAP could be reached. The calculated apparent dissociation constants were 0.58 µM and 1.1 µM, respectively, indicating a four times higher affinity for microtubules of SKAP$^{135-225}$ and a two times higher one for SKAP$^{103-225}$ compared to the shorter SKAP constructs. The comparison of the microtubule cosedimentation assays of these SKAP constructs reveals that SKAP$^{135-225}$ possessed the highest affinity for microtubules and that additional amino acids at the N-terminus do not further increase the affinity.

The comparison of the microtubule-binding affinities of SKAP$^{159-225}$ and SKAP$^{159-316}$ shows that the apparent dissociation constant for SKAP$^{159-225}$ (2.5 µM) is only 1.5-times higher than the one of SKAP$^{159-316}$ (1.62 µM). Together with the observation that SKAP$^{226-316}$ does not bind microtubules (see section 3.3.1, figure 3.14), this indicates that the C-terminal coiled-coil domain of SKAP comprising residues 226 to 316 is neither sufficient nor necessary for microtubule binding.

Taken together, it can be concluded that the domain comprising amino acids 135 to 225 represents the microtubule-binding domain of SKAP.

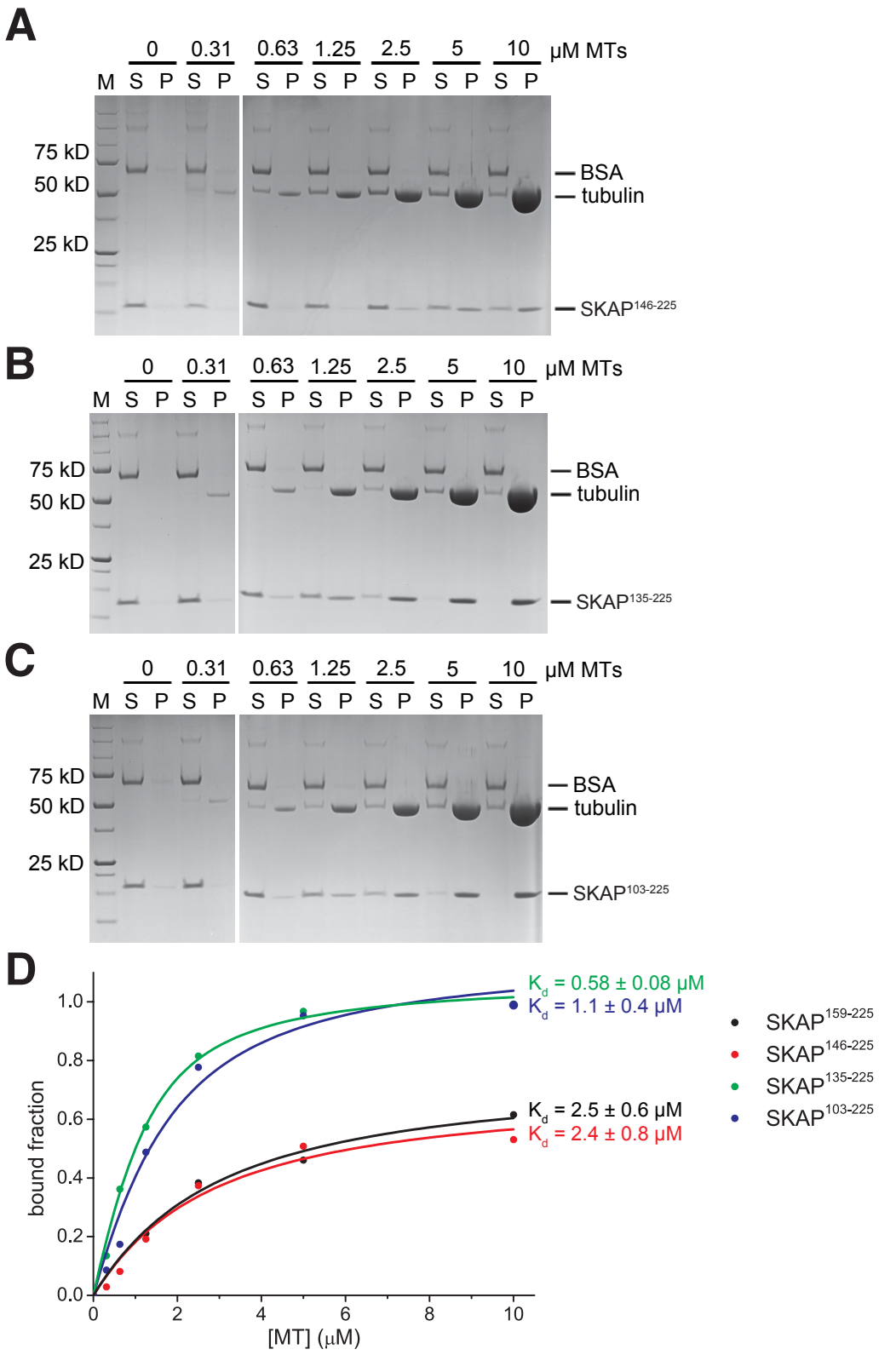

Figure 3.18: The microtubule-binding domain of SKAP is located at amino acids 135 to 225. Representative SDS-PAGE gels of microtubule cosedimentation assays with 0-10 µM taxol-stabilized microtubules (MTs), 1 µM BSA and 1 µM SKAP$^{146-225}$ (**A**), SKAP$^{135-225}$ (**B**) or SKAP$^{103-225}$(**C**). S: soluble fraction with proteins not bound to microtubules. P: pellet fraction with microtubules and bound proteins. M: molecular weight marker with molecular weights indicated on the left. (**D**) Quantification and fitting analysis of microtubule cosedimentation assays shown in (**A**)-(**C**). Quantification was done with ImageJ 1.49 (NIH). Data were fitted with Origin7.0 (OriginLab, Northampton, US-MA) as described in section 5.4.2.

Table 3.7: Summary of fitting analysis of microtubule cosedimentation assays with different SKAP constructs. Microtubule cosedimentation assays were performed with 0-10 µM taxol-stabilized microtubules and 1 µM $SKAP^{159-225}$, $SKAP^{146-225}$, $SKAP^{135-225}$ or $SKAP^{103-225}$. Quantification was done with ImageJ 1.49 (NIH). Data were fitted with Origin7.0 (OriginLab, Northampton, US-MA) as described in section 5.4.2.

construct	apparent dissociation constant K_d (µM)	maximal bound fraction
$SKAP^{159-225}$	2.5 ± 0.6	0.77 ± 0.07
$SKAP^{146-225}$	2.4 ± 0.8	0.71 ± 0.09
$SKAP^{135-225}$	0.58 ± 0.08	1.08 ± 0.03
$SKAP^{103-225}$	1.1 ± 0.4	1.17 ± 0.07

3.3.3 SKAP binds to the interface of α-/β-tubulin

After mapping the microtubule-binding domain of SKAP, the location of SKAP binding on the microtubules was investigated. For this purpose, a crosslinking analysis with microtubules and SKAP was performed in order to identify residues of both proteins that lie close to each other and point to proximate interfaces in the formed complex.

Bis(sulfosuccinimidyl)glutarate (BS2G) and di(succinimidyl)suberate (DSS), which covalently link primary amines of lysine side chains that are within a distance compatible with the length of the crosslinker of 7.7 Å and 11.4 Å, respectively, were used as crosslinkers. In an initial experiment, different ratios of crosslinker to protein were screened for the crosslinking of taxol-stabilized microtubules and $SKAP^{135-225}$ (see supplementary figure 6.13). The large scale crosslinking reactions with crosslinker:protein ratios of 1:1 for BS2G and 2.5:1 for DSS resulted in the crosslinks visualized in figure 3.19 A. Intermolecular crosslinks found between $SKAP^{135-225}$ and the ubiquitous tubulin isotypes α-1B and β-2B tubulin are colored in blue and intramolecular ones in red. A list of all identified crosslinks is shown in supplementary tables 6.1 and 6.2. Besides a high number of intramolecular crosslinks on $SKAP^{135-225}$, several intermolecular crosslinks could be identified between $SKAP^{135-225}$ and α-tubulin and a few between $SKAP^{135-225}$ and β-tubulin. These crosslinks occurred mainly with the N-terminal part of $SKAP^{135-225}$, suggesting that this part is important for microtubule binding (see section 3.3.5). In order to present the spatial distribution of the identified residues on tubulin, the crystal structure of tubulin (PDB-ID: 3RYC) was depicted in figure 3.19 B with tubulin residues involved in crosslinks with SKAP highlighted in stick representation. The font size of the indicated residues reflects their frequency of occurrence during mass spectrometric

analysis. Crosslinking of SKAP$^{135-225}$ to ten residues of tubulin was observed including nine residues on α-tubulin (K60, K96, K112, K163, K311, K336, K370,

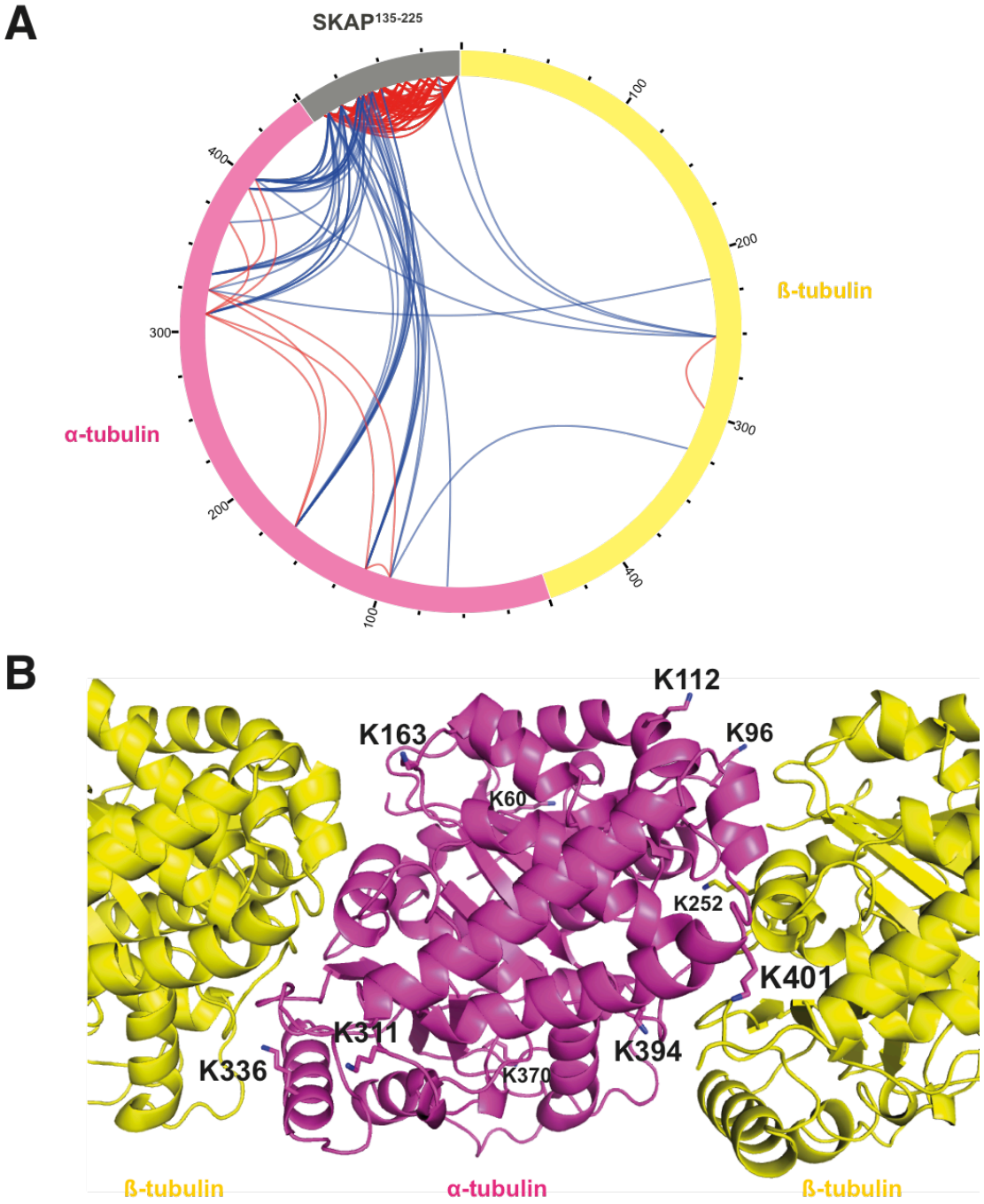

Figure 3.19: SKAP binds microtubules at the α-/β-tubulin interface. (**A**) Intermolecular (blue) and intramolecular (red) crosslinks found between SKAP$^{135-225}$ and α-1B and β-2B tubulin in crosslinking reactions with 10 µM SKAP$^{135-225}$ and 10 µM taxol-stabilized microtubules in presence of the crosslinkers DSS and BS2G. Crosslinks were visualized using the xVis web server (Grimm et al., 2015). (**B**) Cartoon representation of tubulin (PDB-ID: 3RYC) highlighting residues involved in crosslinking with SKAP$^{135-225}$. Respective residues are highlighted in stick representation. The font size reflects the frequency of occurrence of the crosslinks during mass spectrometric analysis. The illustration was done with PyMOL (DeLano Scientific, San Francisco, US-CA).

K394 and K401) and only one residue on β-tubulin (K252). Eight of these ten residues that showed the highest occurrence during mass spectrometric analysis are located at the intra- and inter-tubulin dimer interfaces (K96, K112, K163, K311, K336, K394 and K401 on α-tubulin and K252 on β-tubulin), whereas only two residues with low occurrence lie on the surface of α-tubulin (K60 and K370). These results indicate that SKAP is preferentially binding to the interface of α- and β-tubulin like the Ndc80 complex (Alushin et al., 2010; Ciferri et al., 2008), while it does not interact prominently with the globular regions of tubulin monomers like the Ska complex (Abad et al., 2014).

For validation of the crosslinking results, the inter- and intramolecular crosslinks of α- and β-tubulin were analyzed in context of the tubulin crystal structure (PDB-ID: 3RYC). Indeed, many of the crosslinked lysine residues lie within a short distance to each other. The remaining identified lysine residues are located further apart from each other, but at positions that are exposed on the surface and that presumably come into close proximity upon microtubule bundling through $SKAP^{135-225}$ (see section 3.3.6). Thus, all identified crosslinks of α- and β-tubulin are located at positions of the tubulin crystal structure that make for a consistent set, thereby validating the identified crosslinks between SKAP and tubulin.

To confirm SKAP binding to the dimeric interface of tubulin, microtubule cosedimentation assays were performed in which $SKAP^{135-225}$ was incubated either with taxol-stabilized microtubules or with subtilisin A-treated microtubules. Subtilisin A is a protease that cleaves the acidic C-termini of tubulin, the so-called E-hooks, a region often involved in interactions of tubulin with MAPs. The SDS-PAGE gel of this experiment and the corresponding quantification in figure 3.20 A and B show that cosedimentation of SKAP with subtilisin A-treated microtubules was decreased to 24 % in comparison to 64 % with taxol-stabilized microtubules. Since the E-hooks of tubulin are highly negatively charged, the interaction with SKAP is probably electrostatic. Therefore, it was tested if the addition of salt reduced microtubule binding of SKAP. Figure 3.20 C and D present the SDS-PAGE separation and quantification of the microtubule cosedimentation assay with taxol-stabilized microtubules and $SKAP^{135-225}$ in the presence of increasing concentrations of NaCl. There is a significant decrease of SKAP microtubule binding from 63 % in the presence of 150 mM NaCl to 24 % in the presence of 400 mM NaCl. In summary, these experiments show that SKAP binds to the E-hooks of tubulin in a salt-dependent manner.

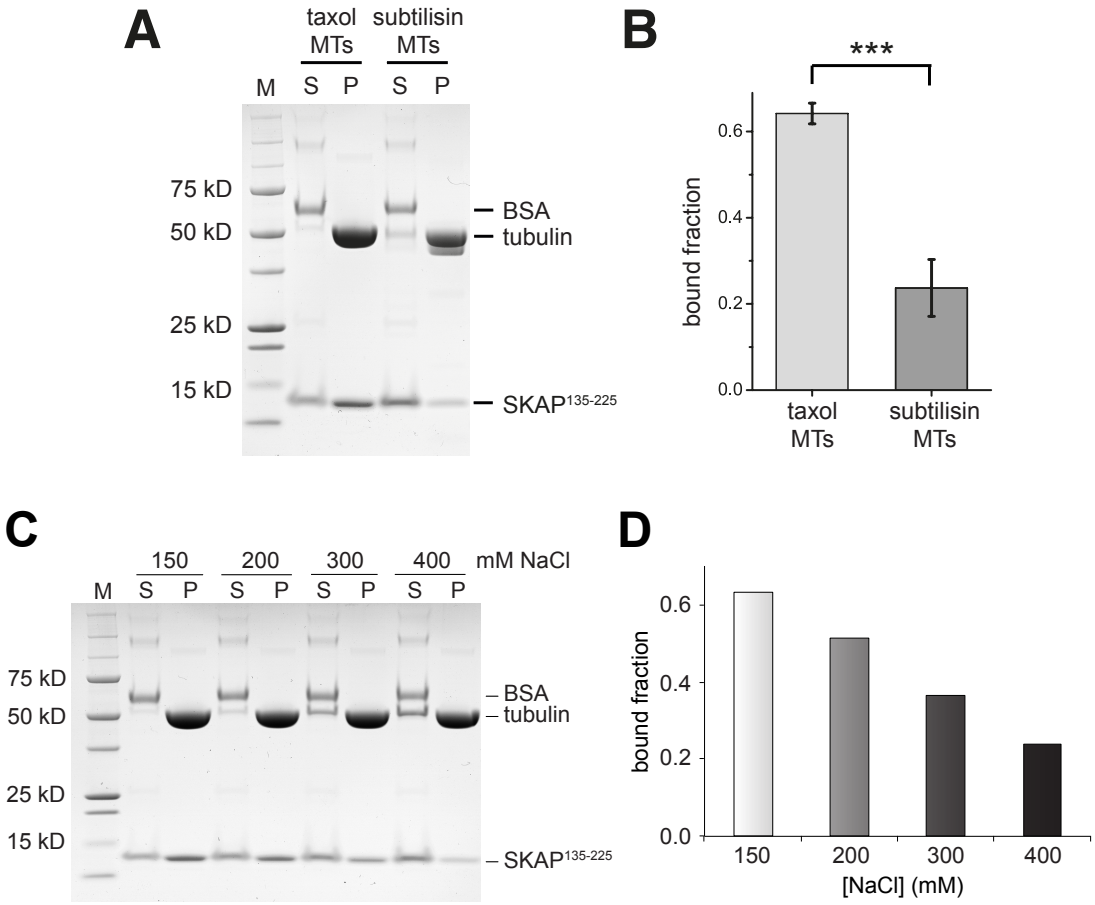

Figure 3.20: SKAP binds to the E-hooks of tubulin in a salt-dependent manner. (**A**-**B**) Representative SDS-PAGE (**A**) and quantification (**B**) of microtubule cosedimentation assays with 3 µM SKAP$^{135-225}$, 1 µM BSA and 3 µM taxol-stabilized or subtilisin A-treated microtubules (*t*-test: $p < 0.005$). (**C**-**D**) Representative SDS-PAGE (**C**) and quantification (**D**) of microtubule cosedimentation assays with 3 µM SKAP$^{135-225}$, 1 µM BSA and 3 µM taxol-stabilized microtubules in the presence of increasing concentrations of NaCl. S: soluble fraction with proteins not bound to microtubules. P: pellet fraction with microtubules and bound proteins. M: molecular weight marker with molecular weights indicated on the left. Quantification was done with ImageJ 1.49 (NIH).

3.3.4 SKAP competes with the Ndc80 complex for microtubule binding

As shown in the previous section, SKAP binds to the interface of α- and β-tubulin. Since this is also the binding site of the Ndc80 complex (Alushin et al., 2010), the question arose whether SKAP and the Ndc80 complex can bind simultaneously to microtubules, possibly through a cooperative binding mechanism, or rather compete for microtubule binding. This question was addressed with a microtubule cosedimentation assay, in which taxol-stabilized microtubules were first incubated with the Ndc80 complex and then increasing concentrations of SKAP$^{135-225}$ up to 80 µM were added. The SDS-PAGE gel of the pellet fraction and the corresponding quantification are shown in figures 3.21 A and B. By following the protein bands of

the 4-subunit Ndc80 complex, containing the Ndc80, Nuf2, Spc24 and Spc25 proteins, with increasing amounts of SKAP, it can be seen that the amount of Ndc80 complex bound to microtubules decreased with higher SKAP concentrations. This suggests that SKAP and the Ndc80 complex compete for an at least partly overlapping binding site on microtubules.

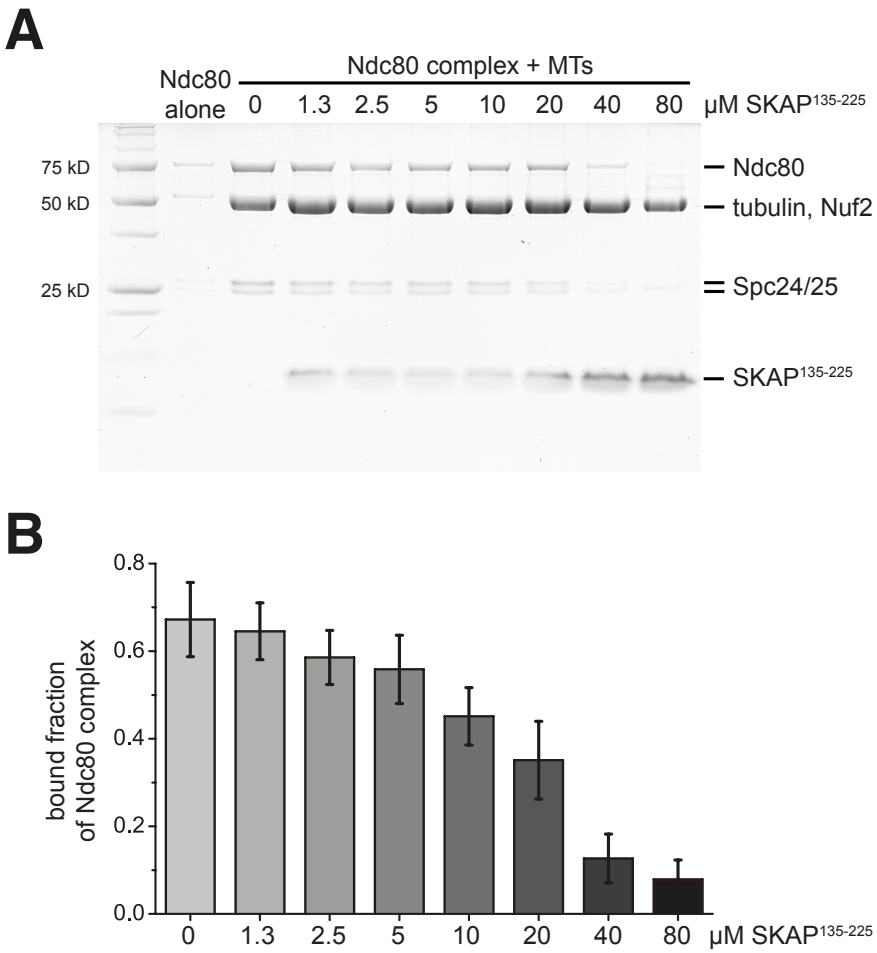

Figure 3.21: SKAP competes with the Ndc80 complex for microtubule binding. Representative SDS-PAGE of the pellet fraction (**A**) and quantification (**B**) of microtubule cosedimentation assay with 1 μM taxol-stabilized microtubules, 1 μM Ndc80 complex and 0-80 μM SKAP$^{135-225}$. Quantification was done with ImageJ 1.49 (NIH).

To analyze if the observed competition of SKAP and the Ndc80 complex for microtubule binding is also true at lower protein concentrations and thereby exclude a potential crowding-out effect of high SKAP concentrations on Ndc80 microtubule binding, a competition experiment was tested with fluorescence microtubule flow cell assays. In these assays, fluorescently labeled proteins are used so that the concentrations required for efficient detection are highly reduced. GFP-tagged Ndc80

complex was incubated with HiLyte 647-labeled microtubules in the presence of 0-4 µM mCherry-SKAP$^{135-225}$. The images and the quantification of these experiments, which are presented in figure 3.22, show that the fluorescence of the Ndc80 complex on the microtubules drops upon addition of SKAP$^{135-225}$. But the levels only decrease to about 50 %, and even with very high SKAP$^{135-225}$ concentrations the Ndc80 complex cannot be displaced completely from the microtubules. The detected decrease in Ndc80 intensity on microtubules confirms that there is competition between SKAP and the Ndc80 complex for microtubule binding at lower protein concentrations. The observation that SKAP is not able to displace the Ndc80 complex completely suggests that SKAP might bind to the intra- and inter-tubulin interface with different affinities. SKAP binding to one interface of tubulin might occur with higher affinity so that SKAP is able to displace the Ndc80 complex from this interaction site, whereas its binding to the other interface might be weaker and have no effect on Ndc80 binding at the low concentrations used in this experiment.

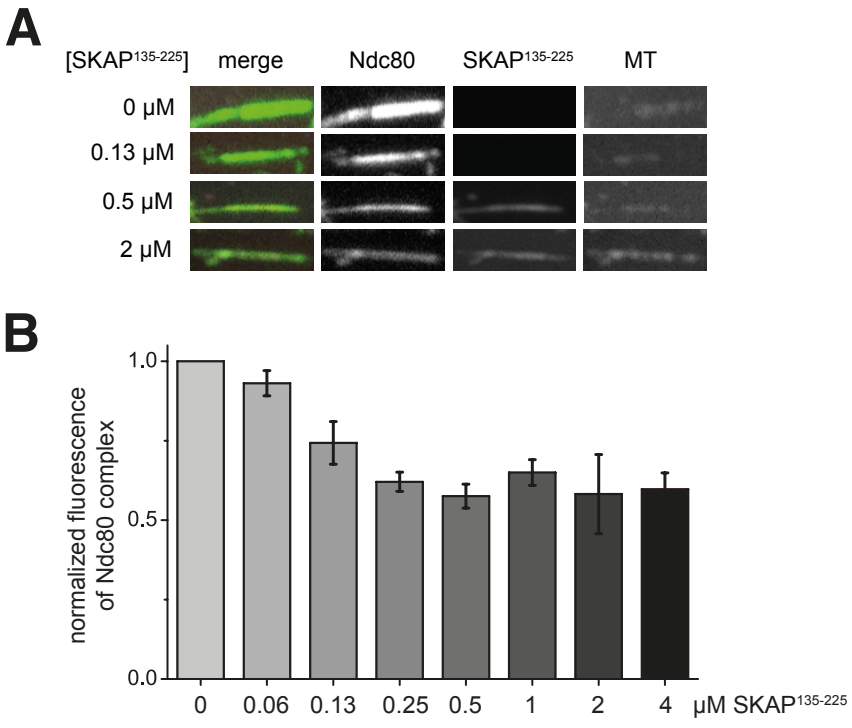

Figure 3.22: SKAP and the Ndc80 complex also compete for microtubule binding at lower protein concentrations. Representative images (**A**) and quantification (**B**) of fluorescence microtubule flow cell assays with 100 nM HiLyte 647-labeled microtubules, 35 nM GFP-tagged Ndc80 complex and 0-4 µM mCherry-SKAP$^{135-225}$. Quantification was done with ImageJ 1.49 (NIH).

Next, the binding of SKAP$^{135-225}$ to microtubules in flow cells was compared in the absence and presence of the Ndc80 complex. As it can be seen from figure 3.23, SKAP binding to microtubules occurred at lower concentrations in the absence of the Ndc80 complex. Also, its intensity on the microtubules increased in the absence of the Ndc80 complex. This strengthens the idea that SKAP$^{135-225}$ and the Ndc80 complex compete for microtubule binding and shows that there is no cooperative binding to microtubules.

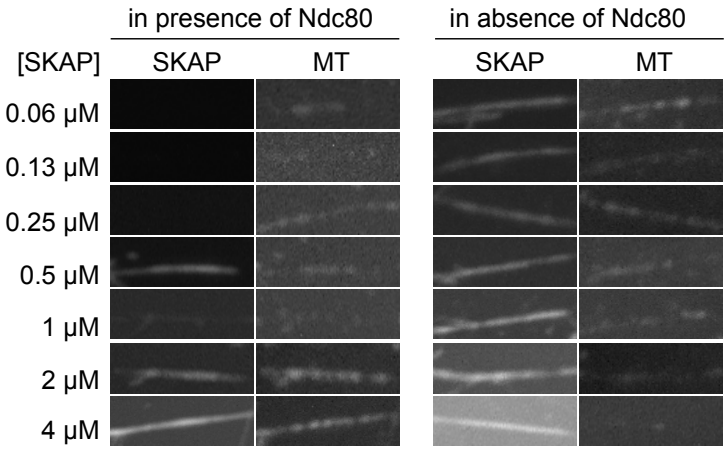

Figure 3.23: SKAP does not show cooperative microtubule binding in the presence of the Ndc80 complex. Representative images of fluorescence microtubule flow cell assays with 100 nM HiLyte 647-labeled microtubules and 0.06-4 µM mCherry-SKAP$^{135-225}$ in the presence or absence of 35 nM GFP tagged Ndc80 complex.

Next, it had to be verified that SKAP and the Ndc80 complex indeed bind to at least partly overlapping binding sites on microtubules and that their competition is not due to binding to each other, which might induce conformational changes or steric clashes preventing the Ndc80 complex from binding. Therefore, the interaction of SKAP$^{135-225}$ and the Ndc80 complex was analyzed by migration shift assays with size exclusion chromatography. For this purpose, the elution properties of SKAP$^{135-225}$ (black) and the Ndc80 complex (blue) were analyzed in comparison to a sample containing both together (red). The elution profile of the size exclusion chromatography and the corresponding SDS-PAGE gels in figure 3.24 reveal that there is no migration shift of either proteins, when they are loaded on the size exclusion chromatography column alone or together, indicating that SKAP$^{135-225}$ and the Ndc80 complex do not interact in solution. This confirms that SKAP and the Ndc80 complex indeed bind to at least partly overlapping binding sites on microtubules.

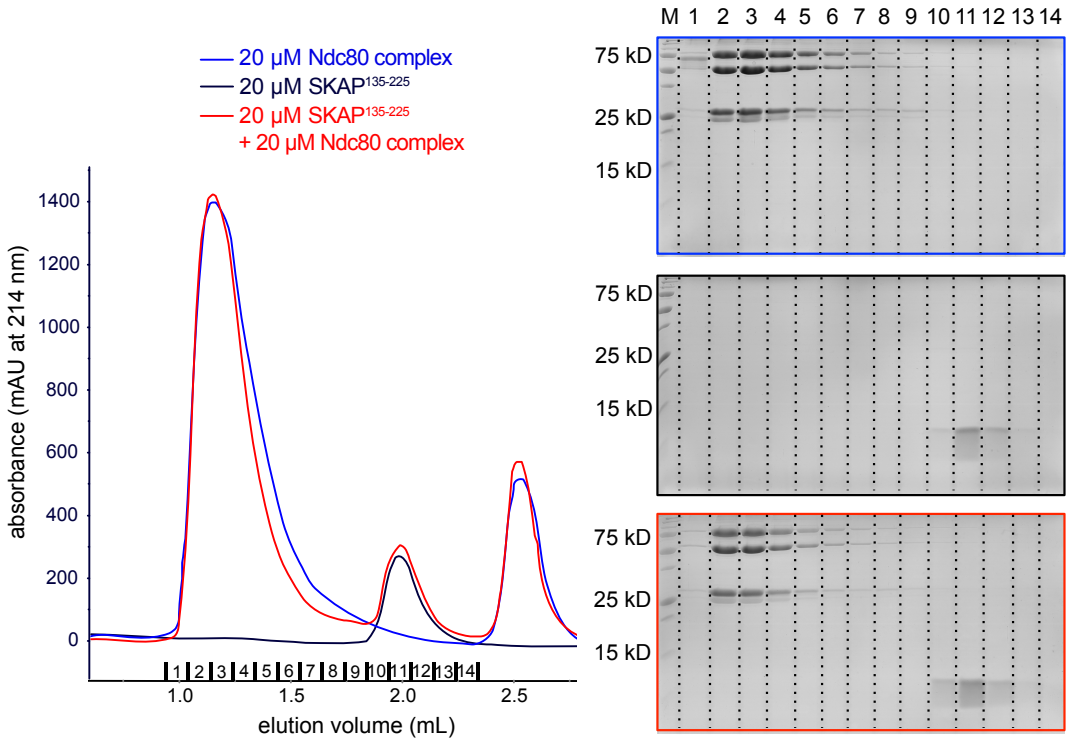

Figure 3.24: SKAP$^{135-225}$ and the Ndc80 complex do not interact in solution. Chromatogram (left) and SDS-PAGE gels (right) of migration shift size exclusion chromatography experiments on a Superdex 200 5/150 column with 20 µM SKAP$^{135-225}$ (black), Ndc80 complex (blue) or both together (red). M: molecular weight marker with molecular weights indicated on the left.

3.3.5 Multiple positively charged residues are important for microtubule binding of SKAP both *in vitro* and *in vivo*

After locating the binding sites of SKAP on microtubules, attempts were made to identify SKAP residues involved in microtubule binding. Therefore, a sequence alignment of SKAP from different species was performed in order to check for conserved residues. As shown in figure 3.25, this sequence alignment reveals a high degree of conservation within the microtubule-binding domain of SKAP. It can be seen that this domain contains several conserved charged residues (colored in green and red). Especially the N-terminal part of the microtubule-binding domain of SKAP, which was found to be involved in microtubule binding in crosslinking analysis (see section 3.3.3), possesses a high fraction - a third to be specific - of positively charged residues (colored in green). This conservation of positively charged residues supports the finding that SKAP binds electrostatically to the negatively charged E-hooks of tubulin (see section 3.3.3).

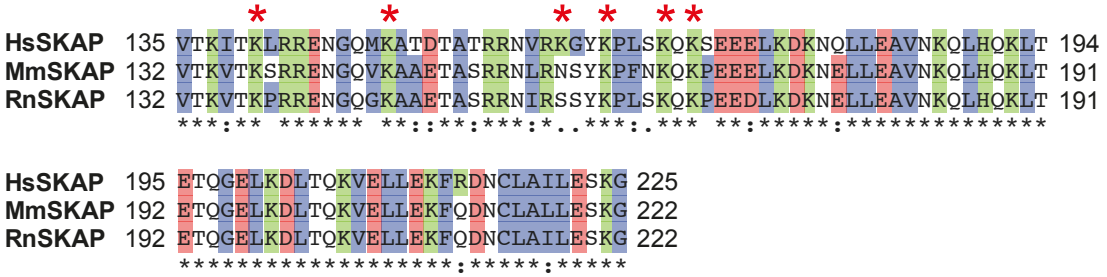

Figure 3.25: The microtubule-binding domain of SKAP possesses several conserved positively charged residues. Sequence alignment of the microtubule-binding domain of SKAP showing amino acid conservation between *Homo sapiens* (Hs), *Mus musculus* (Mm) and *Rattus norvegicus* (Rn). Alignment was performed with Clustal Omega (Sievers et al., 2011). Coloring: green: positively charged residues, red: negatively charged residues, purple: hydrophobic residues. Red asterisks indicate amino acids identified in crosslinking analysis and subjected to mutational analysis.

In order to identify specific residues of SKAP that are important for microtubule binding, positively charged residues that were found in the crosslinking analysis (see section 3.3.3) were mutated to alanine and analyzed for their microtubule binding properties. First, single mutations of the amino acids found with highest occurrence in the mass spectrometric analysis of the crosslinking experiments (K140A, K149A, K161A and K164A) were created. Figure 3.26 shows the quantification of microtubule cosedimentation assays with 1 µM of the indicated SKAP$^{135-225}$ construct and 0-10 µM taxol-stabilized microtubules. The corresponding SDS-PAGE gels can be found in supplementary figures 6.6 to 6.9. The results of the fitting analysis are summarized in table 3.8. These experiments reveal that all single mutants exhibited a decreased ability to bind microtubules compared to the wild type SKAP$^{135-225}$ construct. The mutants displayed apparent dissociation constants in the range of 1.7-2.9 µM, compared to 0.58 µM for the wild type, indicating a 3- to 5-fold lower affinity for microtubules. This suggests that these positively charged residues are important for microtubule binding of SKAP and that each contributes to microtubule binding to a similar extent.

Since all residues identified in the mutational analysis contribute to the microtubule binding of SKAP, it was tested next if a combination of these mutations had an additive effect on the microtubule-binding properties of SKAP. In addition to the already mentioned four residues, two more amino acids (K168 and K170) that were found in the mass spectrometric analysis of the crosslinking experiments were mutated to alanine. As combinations of the mutation sites, double (K161/164A), quadruple (K140/149/161/164A) and sextuple (K140/149/161/164/168/170A) mutants were created, which all showed identical behavior during purification compared to wild type SKAP$^{135-225}$.

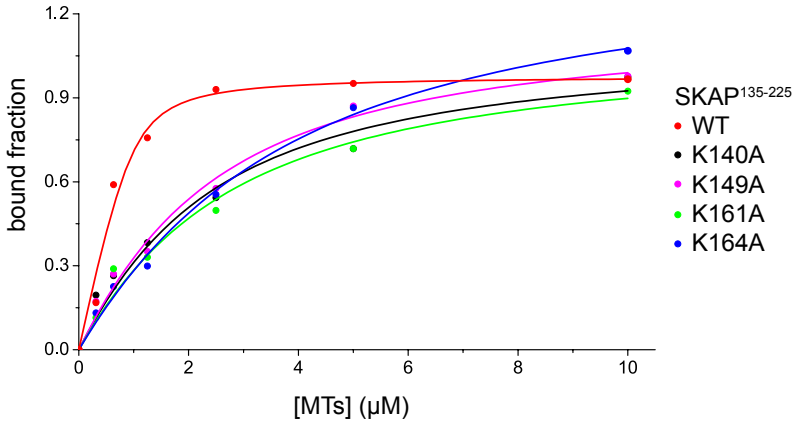

Figure 3.26: Multiple positively charged residues are important for microtubule binding of SKAP. Quantification and fitting analysis of microtubule cosedimentation assays with 0-10 µM taxol-stabilized microtubules and 1 µM SKAP$^{135-225}$ wild type (WT) or indicated mutants. Corresponding SDS-PAGE gels of the assays are shown in supplementary figures 6.6 to 6.9. Quantification was done with ImageJ 1.49 (NIH). Data were fitted with Origin7.0 (OriginLab, Northampton, US-MA) as described in section 5.4.2.

The different SKAP$^{135-225}$ mutants were analyzed for their microtubule-binding abilities in microtubule cosedimentation assays. A SDS-PAGE gel and the corresponding quantification of these experiments are presented in figure 3.27 A and B. It was found that the amount of SKAP bound to the microtubules was slightly decreased from 57 % for the wild type to 50 % for the double mutant, and significantly reduced to 31 % for the quadruple mutant and to 12 % for the sextuple mutant. These results clearly show an additive effect of the mutations on the microtubule binding of SKAP indicating that SKAP binds to microtubules with multiple positively charged residues. Interestingly, when comparing the amount of tubulin in the soluble and the pellet fractions it can be seen that the amount of polymerized tubulin was increased for the wild type construct compared to the mutants (see figure 3.27 A), even if the prepared microtubules belonged to the same batch. This suggests that SKAP has an effect on the stability and/or polymerization behavior of tubulin and that this effect is dependent on its ability to bind to microtubules (see section 3.3.6).

In order to determine the dissociation constants of the interactions of microtubules and the SKAP mutants, titration experiments with 1 µM of the respective mutant and 0-10 µM taxol-stabilized microtubules were performed. The quantification of these assays is shown in figure 3.27 C and the corresponding SDS-PAGE gels can be found in supplementary figures 6.10 to 6.12. The results of the fitting analysis are summarized in table 3.8. These quantifications confirm the additive effect of the mutations. Whereas the double mutant K161/164A showed an apparent dissociation

constant of 2.2 µM, the quadruple mutant K140/149/161/164A showed an about 8-fold higher apparent dissociation constant of 18.3 µM, and the sextuple mutant K140/149/161/164/168/170A showed nearly no microtubule binding, so that no fitting was possible. These findings indicate that multiple positively charged residues are important for the microtubule binding of SKAP *in vitro*.

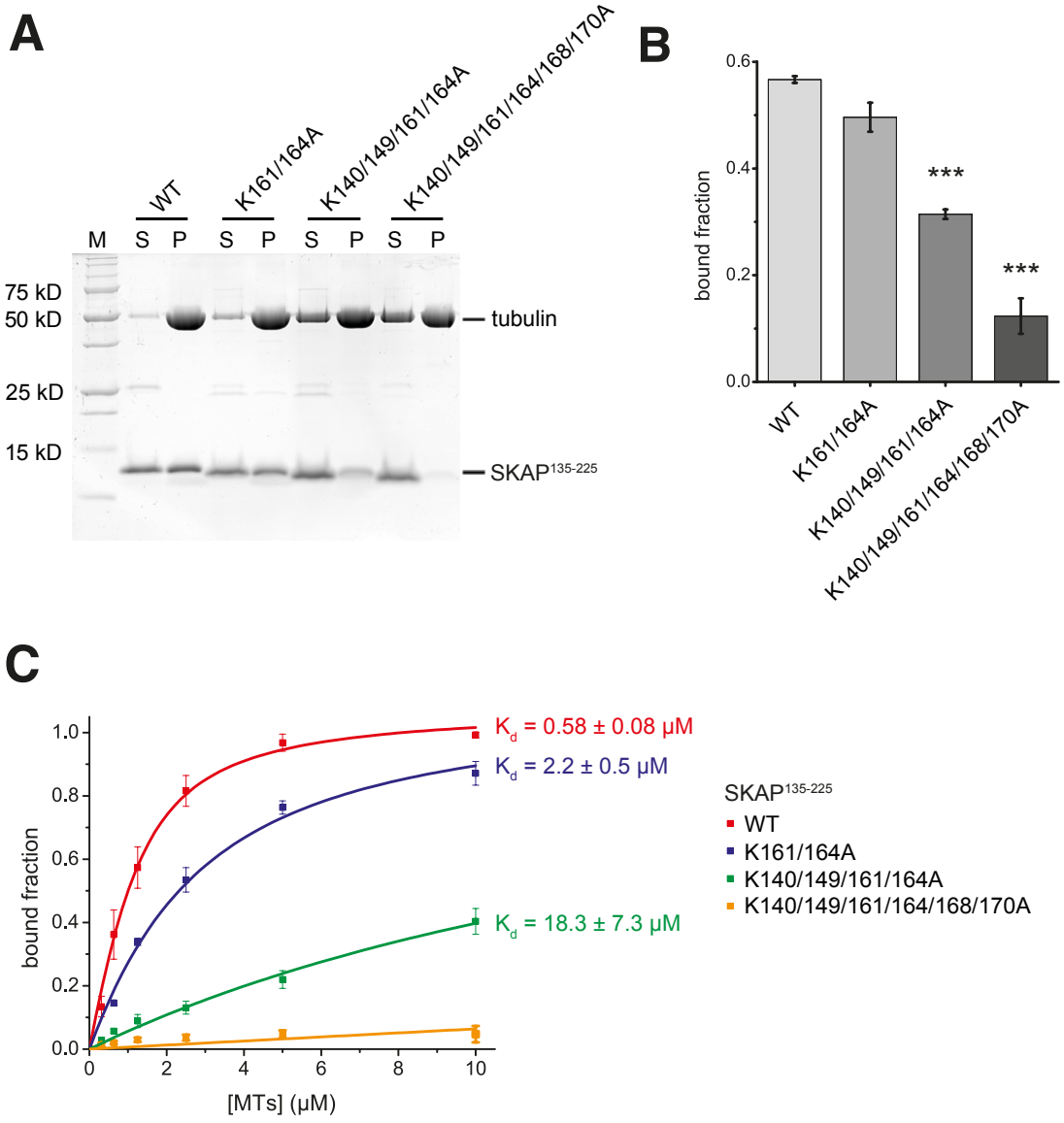

Figure 3.27: Multiple positively charged residues are required for microtubule binding of SKAP *in vitro*. (**A**-**B**) Representative SDS-PAGE (**A**) and quantification (**B**) of microtubule cosedimentation assays with 3 µM taxol-stabilized microtubules and 3 µM SKAP$^{135-225}$ wild type (WT) or indicated mutants (*t*-test: $p < 0.001$). S: soluble fraction with proteins not bound to microtubules. P: pellet fraction with microtubules and bound proteins. M: molecular weight marker with molecular weights indicated on the left. (**C**) Quantification and fitting analysis of microtubule cosedimentation assays with 0-10 µM taxol-stabilized microtubules and 1 µM SKAP$^{135-225}$ wild type (WT) or indicated mutants. Corresponding SDS-PAGE gels of the assays are shown in supplementary figures 6.10 to 6.12. Quantification was done with ImageJ 1.49 (NIH). Data were fitted with Origin7.0 (OriginLab, Northampton, US-MA) as described in section 5.4.2.

Table 3.8: Summary of fitting analysis of microtubule cosedimentation assays with SKAP$^{135-225}$ mutants. Microtubule cosedimentation assays were performed with 0-10 µM taxol-stabilized microtubules and 1 µM SKAP$^{159-225}$, SKAP$^{146-225}$, SKAP$^{135-225}$ or SKAP$^{103-225}$. Quantification was done with ImageJ 1.49 (NIH). Data were fitted with Origin7.0 (OriginLab, Northampton, US-MA) as described in section 5.4.2.

SKAP$^{135-225}$ construct	apparent dissociation constant K_d (µM)	maximal bound fraction
WT	0.58 ± 0.08	1.08 ± 0.03
K140A	1.7 ± 0.5	1.10 ± 0.11
K149A	1.8 ± 0.4	1.18 ± 0.08
K161A	2.1 ± 0.6	1.10 ± 0.10
K164A	2.9 ± 0.5	1.43 ± 0.09
K161/164A	2.2 ± 0.5	1.12 ± 0.09
K140/149/161/164A	18.3 ± 7.3	1.2 ± 0.4
K140/149/161/164/168/170A	no fitting possible	no fitting possible

Next, it was tested whether the region comprising the identified amino acids is only necessary or also sufficient for microtubule binding of SKAP. For this purpose, two constructs were created: one ranging from amino acid 135 to 174 and comprising the identified residues, and another ranging from amino acid 175 to 225. These two constructs were analyzed in microtubule cosedimentation assays and compared to the complete microtubule-binding domain. A representative SDS-PAGE gel and the corresponding quantification are depicted in figure 3.28. This experiment showed that in contrast to SKAP$^{135-225}$, both truncated constructs were hardly able to bind microtubules, since no significant protein amounts could be seen in the pellet fraction. The bound fractions of SKAP$^{135-174}$ and SKAP$^{175-225}$ were reduced to 10 % and 4 %, respectively, compared to 65 % of SKAP$^{135-225}$, suggesting that the identified residues are necessary, but not sufficient, for the microtubule binding by SKAP. This indicates that SKAP possesses a multipartite mode of microtubule binding, in which probably several other residues are involved in addition to the identified ones.

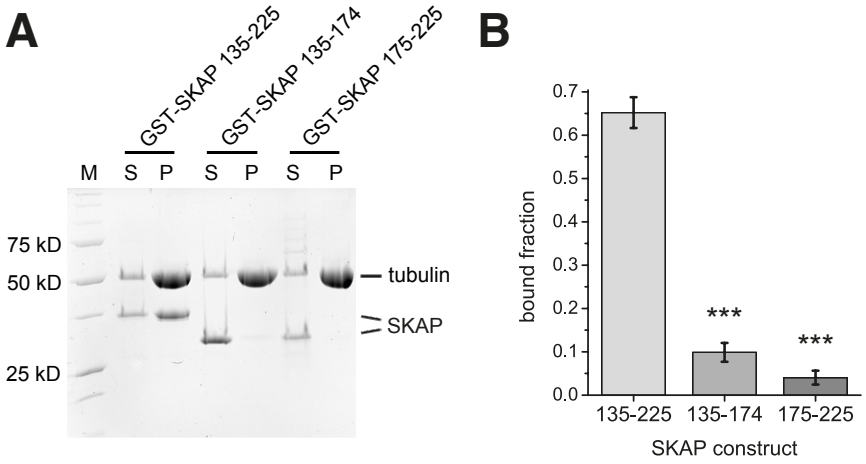

Figure 3.28: Amino acids 135 to 174 are necessary, but not sufficient for microtubule binding of SKAP. Representative SDS-PAGE (**A**) and quantification (**B**) of microtubule cosedimentation assays with 3 µM taxol-stabilized microtubules and 3 µM GST-SKAP$^{135-225}$, GST-SKAP$^{135-174}$ or GST-SKAP$^{175-225}$ (*t*-test: $p < 0.001$). S: soluble fraction with proteins not bound to microtubules. P: pellet fraction with microtubules and bound proteins. M: molecular weight marker with molecular weights indicated on the left. Quantification was done with ImageJ 1.49 (NIH).

To test if the SKAP residues involved in microtubule binding mediate SKAP localization *in vivo*, Flp-In T-REx cell lines expressing wild type or mutant full-length GFP-SKAP were generated. The levels of expression of wild type and mutant GFP-SKAP after doxycycline induction for 24 h were approximately equal (see supplementary figure 6.16). Cells were arrested in metaphase by treatment with the proteasome inhibitor MG132 and the cellular localization of GFP-SKAP to kinetochores and spindle microtubules was analyzed by immunofluorescence. Representative images and corresponding quantifications are presented in figure 3.29. GFP signals of the mutants were normalized to GFP signals of the wild type SKAP construct. As mentioned in the introductory section 1.6, wild type GFP-SKAP showed a dual localization to both spindle microtubules and - predominantly bioriented - kinetochores. When comparing the GFP intensity of wild type SKAP at kinetochores to those of the mutants, it can be seen that the intensities display only small variations, indicating that the mutations have no effect on the kinetochore localization of SKAP. In contrast to this, the mutants revealed reduced intensities at spindle microtubules compared to the wild type construct, and the degree of signal reduction corresponded to the number of inserted mutations. For the sextuple mutant, the localization to spindle microtubules was not abolished completely, but reduced to 45 %, indicating that the role in localization is not limited to the six identified residues. It is possible that interactions with other proteins are also important for the interaction of SKAP with microtubules. These results confirm that the mutation sites are necessary, but not sufficient for microtubule binding, both *in*

vivo and *in vitro*. In summary, these findings suggest that the identified residues of SKAP are not only required for its microtubule binding *in vitro*, but also *in vivo*, although other amino acids seem to play a role as well.

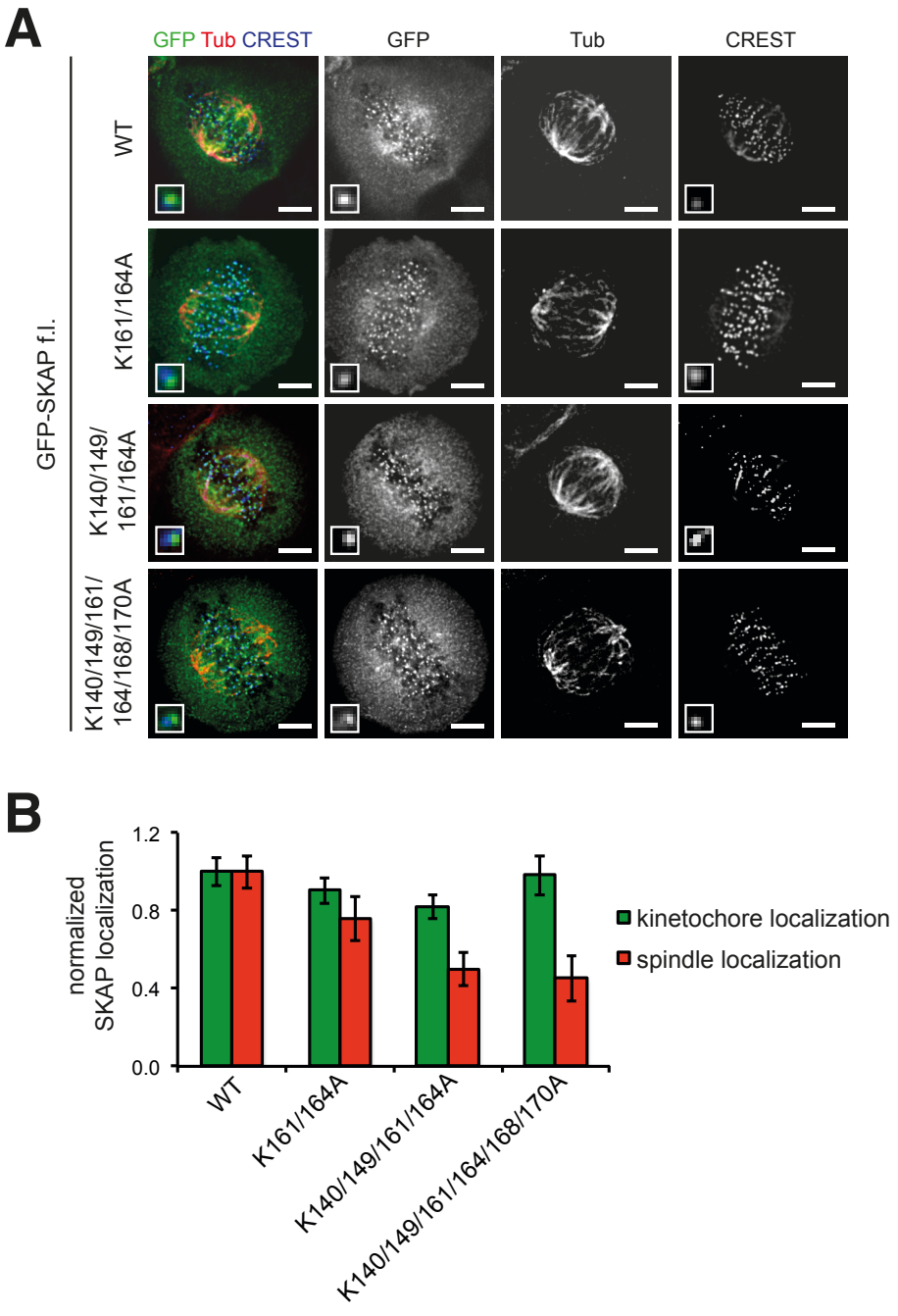

Figure 3.29: Multiple positively charged residues are required for microtubule binding of SKAP *in vivo*. (**A**) Representative immunofluorescence images of stable Flp-In T-REx cell lines expressing GFP-SKAP full-length (f.l.) wild type (WT) or indicated mutants. Cells were treated with 0.1 µg/mL doxycycline for 24 h and 10 µM MG132 for 1.5-2 h prior to fixation. Scale bar: 5 µm. (**B**) Plot of normalized GFP fluorescence at the kinetochores or the spindle microtubules for experiments shown in (**A**). Quantification was done with Imaris 7.3.4 (Bitplane, Zurich, CH).

Since cells expressing GFP-SKAP behaved comparably to control cells without expression, the overexpression of SKAP did not reveal any dominant phenotypic effect. Therefore, the phenotypic effects of depletion of SKAP by RNA interference were analyzed next. For this purpose, appropriate conditions for the RNA interference had to be established. Flp-In T-REx cells were transfected with two different siRNAs for 1, 2 or 3 days and the amounts of remaining endogenous SKAP were quantified by immunofluorescence and western blot as shown in figure 3.30.

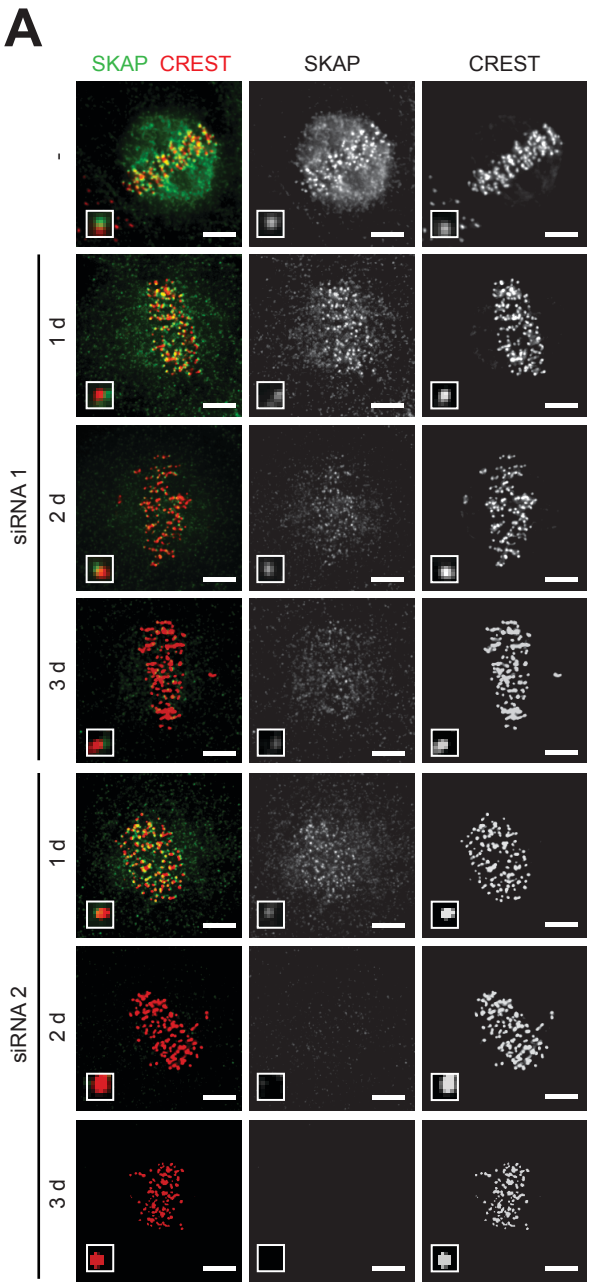

Figure 3.30: Test of SKAP siRNA. (**A**) Representative immunofluorescence images of RNA interference experiment with Flp-In T-REx cells incubated with two different SKAP siRNAs for 1,2 or 3 days. -: control without siRNA. Scale bar: 5 µm.

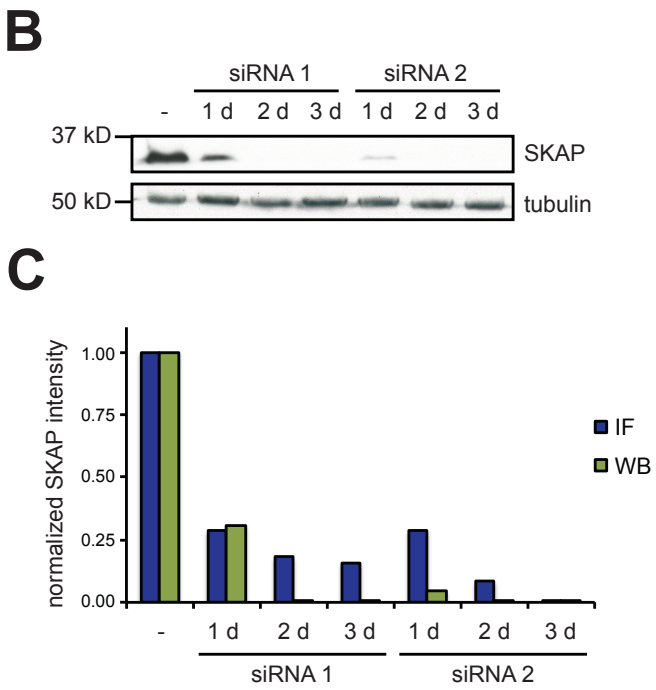

Figure 3.30 (continued)**: Test of SKAP siRNA.** (**B**) Western blots with cell lysates of Flp-In T-REx cells incubated with two different SKAP siRNAs for 1,2 or 3 days stained for SKAP and tubulin as loading control. (**C**) Quantification of SKAP intensities in immunofluorescence (IF) and western blot (WB) for experiments shown in (**A**) and (**B**). Quantification for immunofluorescence was done with Imaris 7.3.4 (Bitplane, Zurich, CH). The SKAP intensity at kinetochores was normalized to CREST signals. Quantification for western blot was done with ImageJ 1.49 (NIH). Intensities were normalized to those of control cells.

Whereas the western blot suggested a complete depletion of endogenous SKAP after 2 days of treatment with both SKAP siRNA 1 and 2, the immunofluorescence images revealed a less efficient depletion. After a 3-day treatment with SKAP siRNA 1 the level of endogenous SKAP was only reduced to 16 %. The transfection with SKAP siRNA 2, however, resulted in depletion to 9 % after 2 days and to < 1 % after 3 days. Therefore, the condition with 72 h transfection of SKAP siRNA 2 was chosen for further RNA interference and rescue experiments.

On closer observation of figure 3.30 A, it can be seen that the reduction of endogenous SKAP levels generated kinetochores that did not align to the metaphase plate. The RNA interference experiment depicted in the upper images of figure 3.31 also showed that SKAP depletion affected biorientation, since cells in a pseudo-metaphase state with several unattached kinetochores (indicated by white arrows) could be observed. These cells with disturbed biorientation amounted to 74 % of all metaphase or pseudo-metaphase cells. Another phenotype, which was observed in 31 % of SKAP depleted mitotic cells, was the formation of multipolar spindles, as

shown in the second image series in figure 3.31. This shows that SKAP is required for spindle organization and establishment of biorientation *in vivo*. The following image series of figure 3.31 display the rescue experiments in which wild type or mutant GFP-SKAP was expressed after treatment with SKAP siRNA to deplete endogenous SKAP. The quantification of observed phenotypes for the RNA interference and rescue experiments is summarized in table 3.9. Upon expression of wild type GFP-SKAP and GFP-SKAP K161/164A phenotypes were rescued completely, since these experiments showed only a very small fraction of cells with multipolar spindles and pseudo-metaphase states, comparable to control cells that

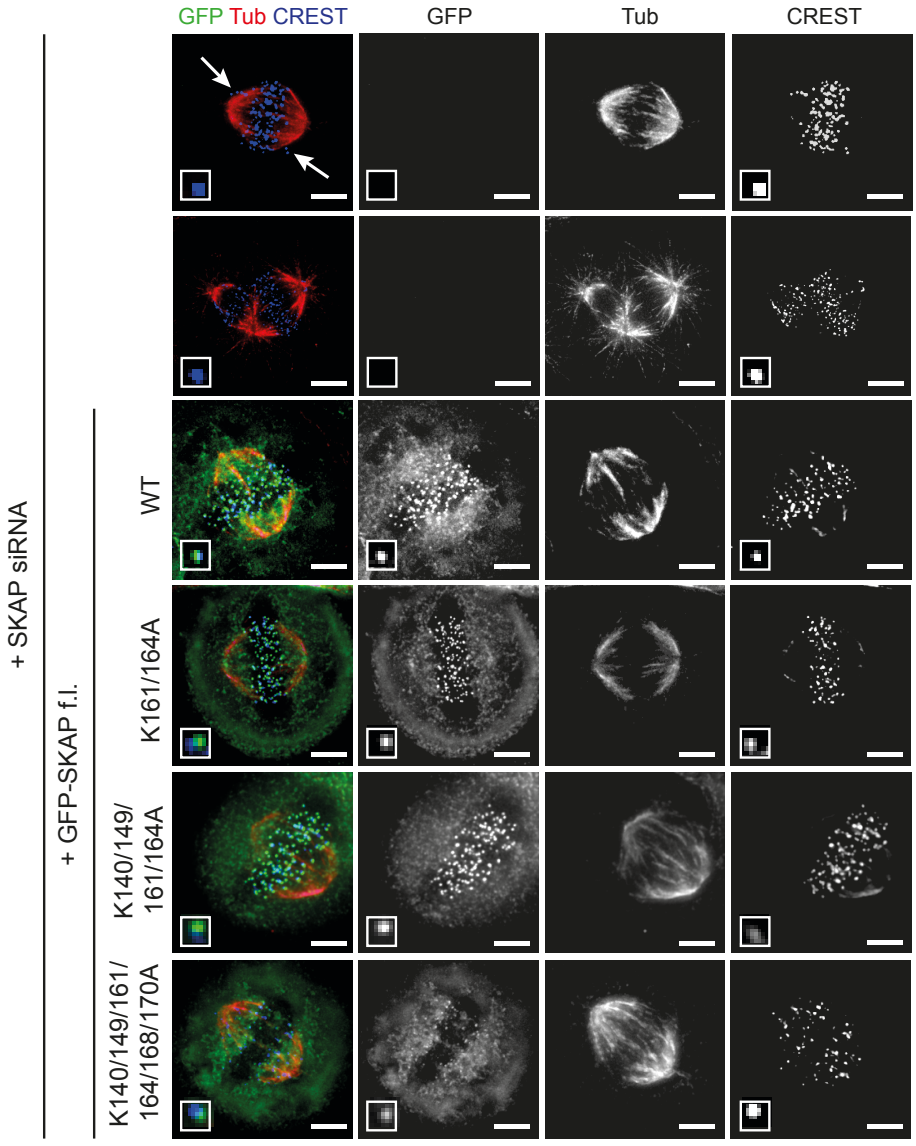

Figure 3.31: SKAP is required for spindle organization and establishment of biorientation *in vivo*. Representative immunofluorescence images of RNA interference and rescue experiments with stable Flp-In T-REx cell lines expressing GFP-SKAP full-length (f.l.) wild type (WT) or indicated mutants. Cells were treated with SKAP siRNA 2 for 72 h and gene expression was induced with 0.1 µg/mL doxycycline for 24 h. White arrows show unaligned kinetochores. Scale bar: 5 µm.

Table 3.9: Quantification of phenotypes observed in RNA interference and rescue experiments with GFP-SKAP expressing cells. Flp-In T-REx cell lines expressing GFP-SKAP full-length wild type (WT) or indicated mutants were treated with SKAP siRNA 2 for 72 h and GFP-SKAP expression was induced with 0.1 µg/mL doxycycline for 24 h.

SKAP siRNA	expressed SKAP construct	mitotic index (%)	mitotic cells with multipolar spindles (%)	(pseudo-) metaphase cells with unaligned kinetochores (%)
-	-	6	<1	5
+	-	42	31	74
+	WT	7	<1	4
+	K161/164A	7	<1	6
+	K140/149/161/164A	15	6	14
+	K140/149/161/164/ 168/170A	33	24	57

were not treated with SKAP siRNA. However, the quadruple and sextuple mutants of GFP-SKAP, which showed disturbed ability to bind microtubules, were only partly able to rescue the observed phenotypes. For the quadruple mutant, 6 % of mitotic cells revealed multipolar spindles and 14 % of metaphase cells exhibited unattached kinetochores, whereas for the sextuple mutant, these statistics amounted to 24 % and 57 %, respectively. These levels of perturbed mitosis were also reflected in the mitotic index, which specifies the percentage of cells that are in mitosis. An increased mitotic index indicates a delay in mitosis because of problems during mitotic progression. For control cells, the mitotic index amounts to 6 % and SKAP depleted cells expressing GFP-SKAP wild type or the double mutant show a comparable mitotic index of 7 %. In SKAP depleted cells, 42 % of all cells are in mitosis, indicating a mitotic delay. SKAP depleted cells that expressed quadruple and sextuple GFP-SKAP mutants showed more penetrant phenotypes, with a mitotic index of 15 % and 33 %, respectively. In summary, these findings show that the ability of SKAP to bind microtubules is important for its cellular function in spindle organization, biorientation and mitotic progression.

3.3.6 SKAP binds to tubulin in solution and can induce its polymerization

Since SKAP is able to bind to microtubules, as shown in the previous sections, the question arose if SKAP also binds to unpolymerized tubulin. This question was addressed with tubulin that formed a complex with either tubulin tyrosine ligase (TTL)

or with the stathmin-like domain of the RB3 protein (RB3), which prevent tubulin from polymerizing. TTL is an enzyme that posttranslationally tyrosinates detyrosinated α-tubulin. It binds to the C-terminal tail of α-tubulin in a tubulin dimer and only recognizes the curved conformation of tubulin dimers (Prota et al., 2013). The RB3 protein is part of the stathmin family whose members are known to have microtubule destabilizing activity (Gavet et al., 1998). The stathmin-like domain of RB3 binds two tubulin dimers and induces a curvature of the complex, while its N-terminal region binds a hydrophobic groove of α-tubulin that is involved in intermolecular contacts within microtubules (Gigant et al., 2000; Gigant et al., 2005). This stabilization of tubulin in a curved conformation and the binding to interfaces important for microtubule assembly cause inhibition of tubulin polymerization by TTL and RB3.

The binding of SKAP$^{135-225}$ to tubulin/TTL or tubulin/RB3 was analyzed by monitoring the elution volume in size exclusion chromatography experiments, as shown in figures 3.32 and 3.33. In these experiments, the elution of SKAP$^{135-225}$ (black) and tubulin/TTL or tubulin/RB3 (blue) was compared to samples containing both SKAP$^{135-225}$ and either of the tubulin complexes (red). The chromatograms and the corresponding SDS-PAGE gels reveal that in both cases there was a migration shift of the tubulin complex peak to lower elution volumes and thereby higher molecular weights in the presence of SKAP$^{135-225}$. Furthermore it can be seen on the SDS-PAGE gels that the peak fraction of SKAP$^{135-225}$ shifted from lane 10 in the control sample with SKAP$^{135-225}$ alone to lanes 8 or 6 in the presence of tubulin/TTL or tubulin/RB3, respectively. The comigration of SKAP$^{135-225}$ with the tubulin complexes at lower elution volumes than the single components indicate that SKAP$^{135-225}$ is able to bind to both the tubulin/TTL and the tubulin/RB3 complex in solution. In summary, these experiments show that SKAP is not only able to bind to polymerized microtubules, but also to unpolymerized tubulin.

Interestingly, both tubulin/TTL and tubulin/RB3 contained a fraction of free tubulin that peaked in lane 2 and that was not detectable after incubation of these samples with SKAP$^{135-225}$. When taking a closer look at the reaction mixtures, it could be seen that their turbidity was increased upon addition of SKAP$^{135-225}$ and after centrifugation a pellet was visible. Together with the absence of free tubulin upon addition of SKAP$^{135-225}$, this suggests that SKAP$^{135-225}$ polymerized the free tubulin. A similar effect was already mentioned during the description of figure 3.27 A in section 3.3.5, which showed an increased amount of polymerized tubulin when microtubules were incubated with wild type SKAP$^{135-225}$ compared to the mutants. These two observations give a first hint that SKAP may influence the polymerization of tubulin.

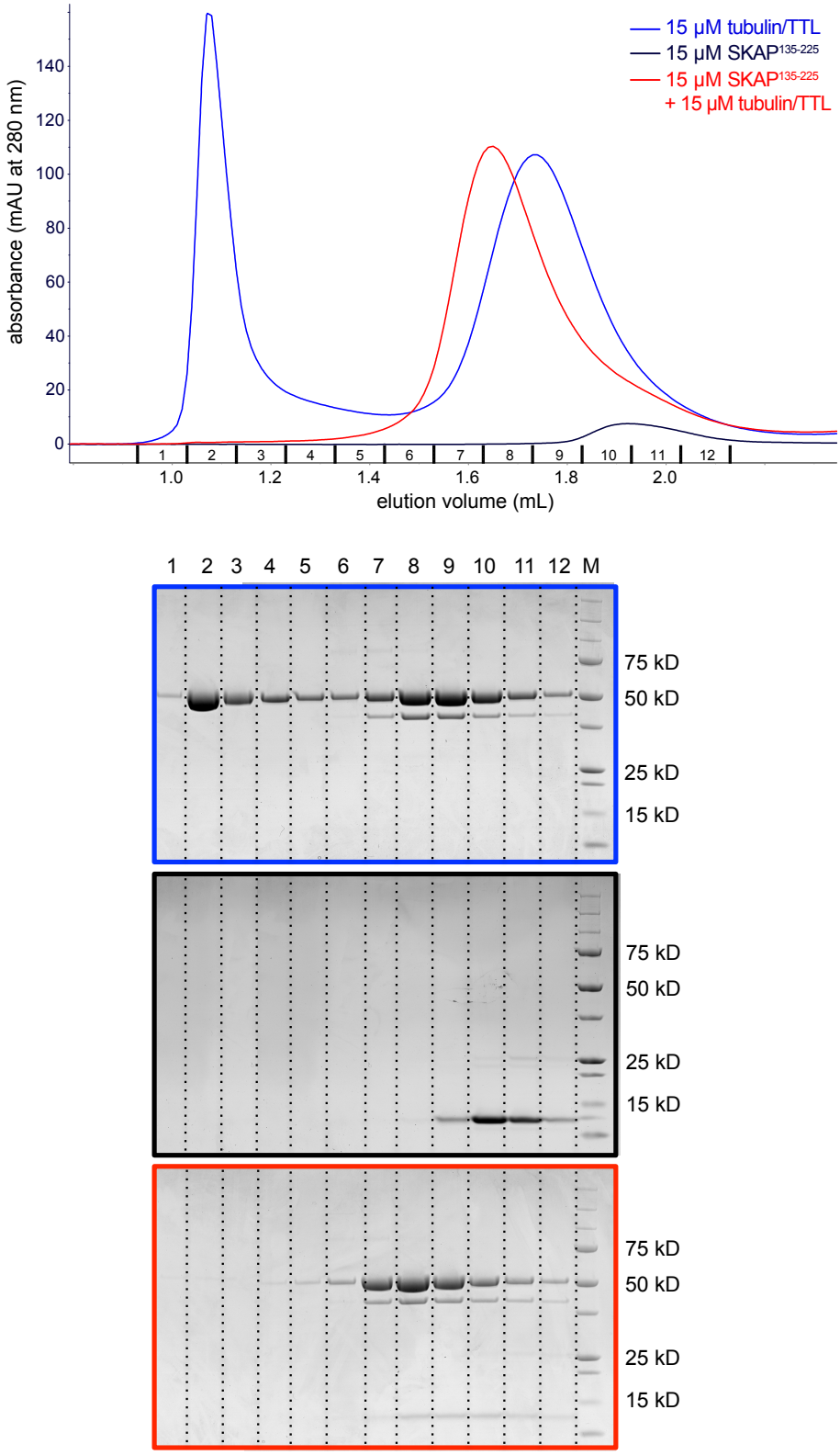

Figure 3.32: SKAP$^{135-225}$ binds to tubulin/TTL in solution. Chromatogram (top) and SDS-PAGE gels (bottom) of migration shift size exclusion chromatography experiments on a Superdex 200 5/150 column with 15 µM SKAP$^{135-225}$ (black), tubulin/TTL (blue) or both together (red). M: molecular weight marker with molecular weights indicated on the right.

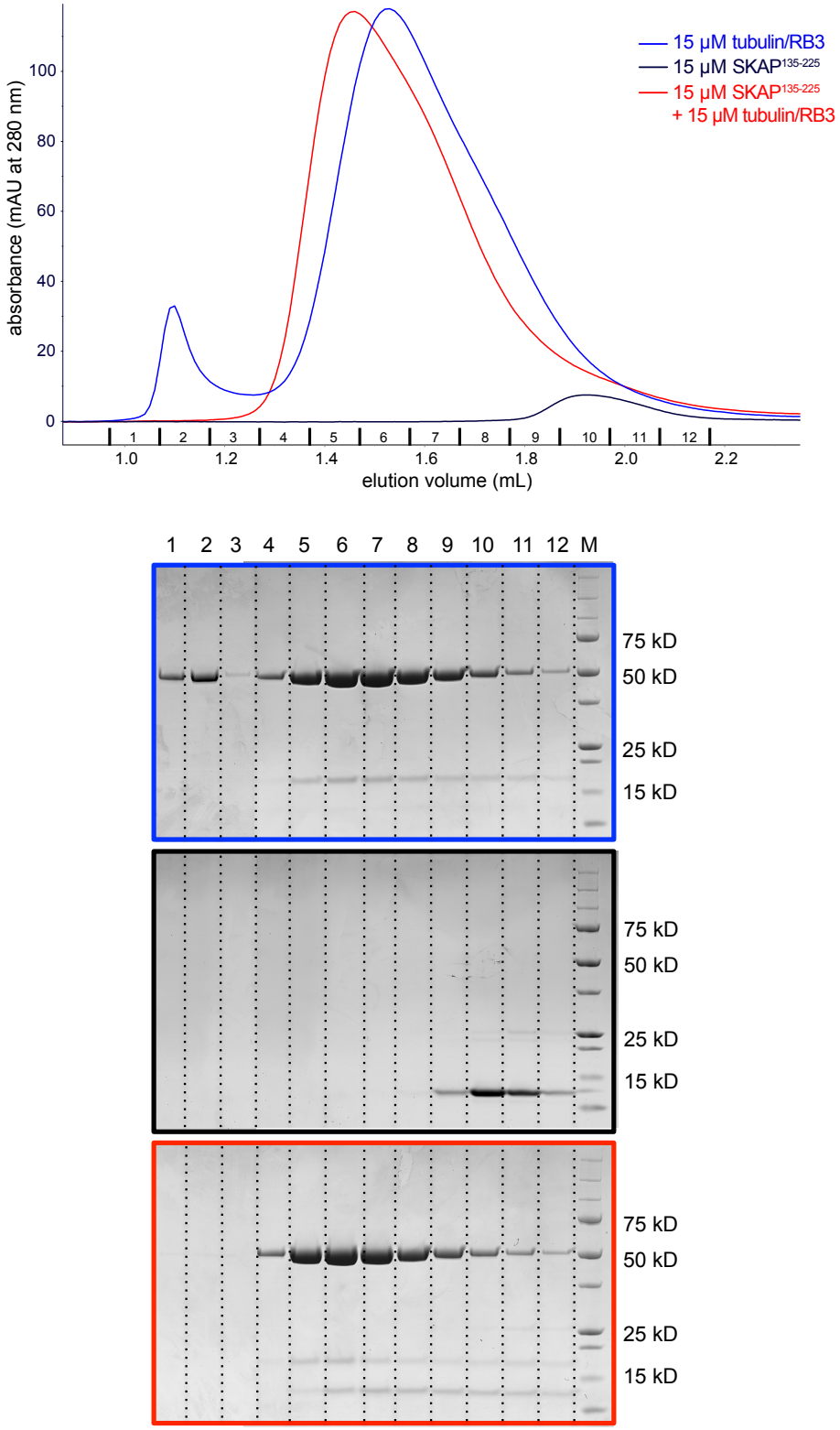

Figure 3.33: SKAP$^{135-225}$ binds to tubulin/RB3 in solution. Chromatogram (top) and SDS-PAGE gels (bottom) of migration shift size exclusion chromatography experiments on a Superdex 200 5/150 column with 15 µM SKAP$^{135-225}$ (black), tubulin/RB3 (blue) or both together (red). M: molecular weight marker with molecular weights indicated on the right.

In order to test whether SKAP indeed has an effect on the polymerization of tubulin, tubulin polymerization in the absence and presence of different SKAP constructs was analyzed in turbidity experiments by following the absorbance at 350 nm at a temperature of 37 °C (Mirigian et al., 2013). Hereby, a change in light scattering that is caused by the microtubule suspension can be measured. First, control experiments with tubulin alone and in the presence of BSA were performed. Tubulin concentrations up to 15 µM were tested and no polymerization was detected (see supplementary figure 6.14), indicating that the critical concentration, at which tubulin was able to polymerize on its own, lay above 15 µM under the assay conditions. To stay below the critical tubulin concentration, the assays with SKAP were performed at a tubulin concentration of 5 µM. Upon addition of SKAP$^{135-225}$, a concentration dependent increase in the absorbance at 350 nm could be observed, with the largest effects observed at a stoichiometric ratio (see figure 3.34 A), whereas the constructs SKAP$^{159-225}$ or SKAP$^{159-316}$ exhibited no ability to polymerize tubulin (see supplementary figure 6.15). This shows that SKAP$^{135-225}$ is able to promote tubulin polymerization *in vitro* and to lower its critical concentration, suggesting that SKAP is a microtubule-stabilizing factor with effects on tubulin nucleation.

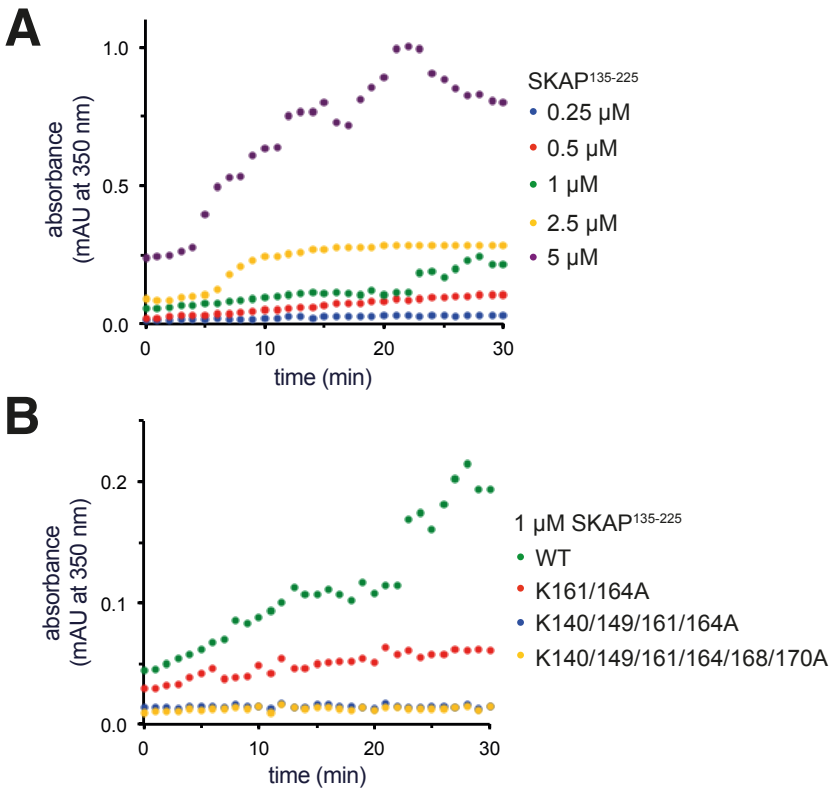

Figure 3.34: SKAP$^{135-225}$ promotes tubulin polymerization *in vitro*. Tubulin polymerization assays with 5 µM tubulin and 0.25-5 µM SKAP$^{135-225}$ (**A**) or 1 µM SKAP$^{135-225}$ wild type (WT) or indicated mutant (**B**). Tubulin polymerization was measured by following the absorbance at 350 nm at 37 °C.

Next, the mutants of SKAP$^{135-225}$ identified in section 3.3.5 were tested for their ability to polymerize tubulin. As it can be seen in figure 3.34 B, the double mutant K161/164A already showed a significant decrease in the amount of polymerized tubulin, whereas the samples with the quadruple mutant K140/149/161/164A and the sextuple mutant K140/149/161/164/168/170A even showed no tubulin polymerization at all. This indicates that the ability of SKAP$^{135-225}$ to promote tubulin polymerization corresponds with its ability to bind microtubules.

To quantify the effects of SKAP on tubulin polymerization, total internal reflection fluorescence (TIRF) microscopy experiments were performed. For this purpose, microtubule seeds stabilized with the slowly hydrolyzable GTP analog GMPCPP were attached to the surface of a coverslip and then incubated with unpolymerized tubulin in the absence and presence of SKAP. An assay condition with a tubulin concentration of 14 µM and a temperature of 25 °C was chosen, which showed a balanced ratio of polymerization and depolymerization in the control sample with tubulin alone, so that the influence of SKAP was easily detectable by a shift of this ratio towards polymerization.

Representative kymographs of microtubules and calculated growth rates in absence or presence of SKAP$^{135-225}$ wild type or mutants are presented in figure 3.35. The kymographs are composed of image series along the microtubule axis for each imaged time point. It can be seen that the microtubules in the tubulin control did not show significant growth during the observed period of 17 min, which was reflected in their low growth rate of 0.10 µm/min. In the presence of SKAP$^{135-225}$ wild type the microtubules grew up to 23 µm with an averaged growth rate of 0.78 µm/min, indicating that SKAP$^{135-225}$ was indeed able to shift the microtubule dynamics towards polymerization with an 8-fold higher microtubule growth rate than the tubulin control. Also the double mutant K161/164A revealed a significant increase of microtubule growth with a 5-fold higher growth rate of 0.47 µm/min compared to the tubulin control. However, with the quadruple mutant K140/149/161/164A and the sextuple mutant K140/149/161/164/168/170A comparable microtubule growth as with the tubulin control was observed with growth rates of 0.13 µm/min and 0.09 µm/min, respectively. These findings reveal that the mutants exhibited reduced abilities to favor tubulin polymerization *in vitro* compared to the wild type construct and the degree of reduction corresponded to the number of inserted mutations. In summary, the results of the TIRF analysis are comparable to those of the turbidity assays, and suggest that SKAP$^{135-225}$ is able to promote tubulin polymerization *in vitro*, in a way that requires its ability to bind to microtubules.

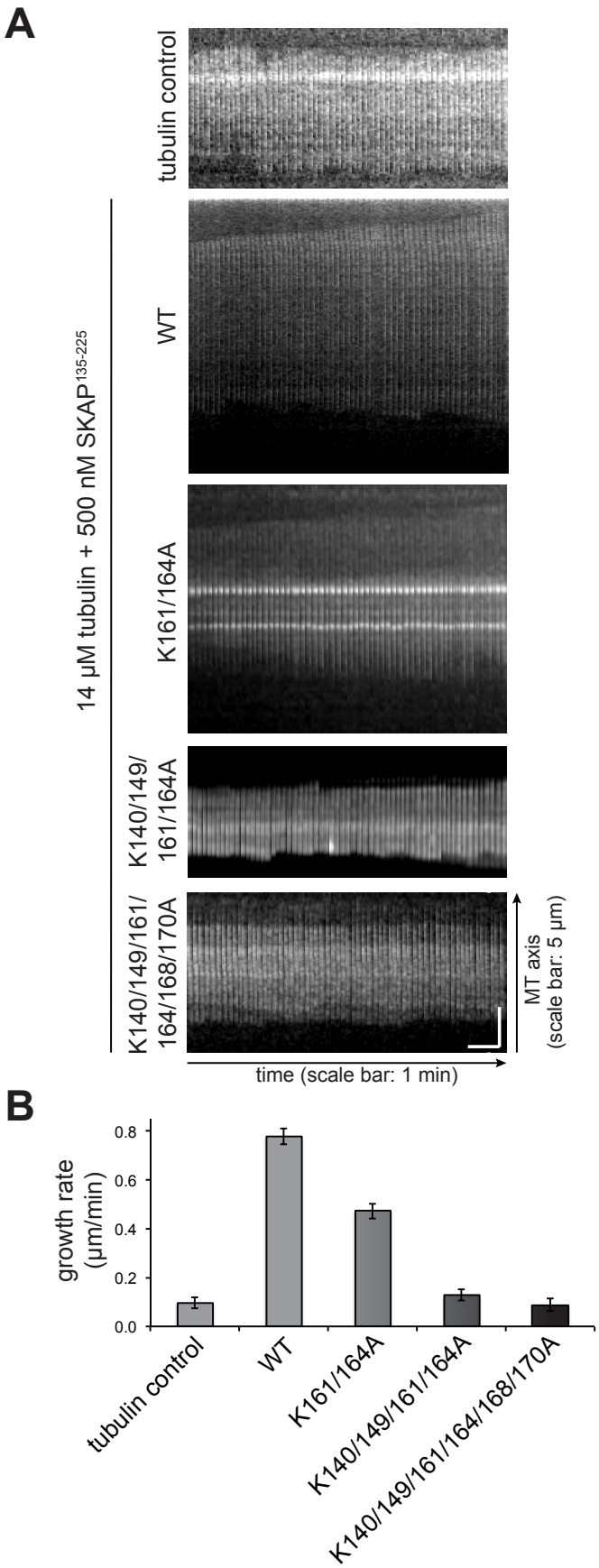

Figure 3.35: SKAP$^{135-225}$ favors microtubule growth *in vitro*. Representative kymographs of microtubules (**A**) and microtubule growth rates (**B**) observed in TIRF experiments in absence or presence of 500 nM SKAP$^{135-225}$ wild type or indicated mutants.

The TIRF experiments in the presence of SKAP$^{135-225}$ wild type not only revealed an effect of SKAP$^{135-225}$ on microtubule dynamics, but also on microtubule structure. As shown in figure 3.36, in addition to single microtubules, several microtubule bundles with different thickness and a length up to 60 µm could be observed, indicating that SKAP$^{135-225}$ promotes microtubule bundling *in vitro*.

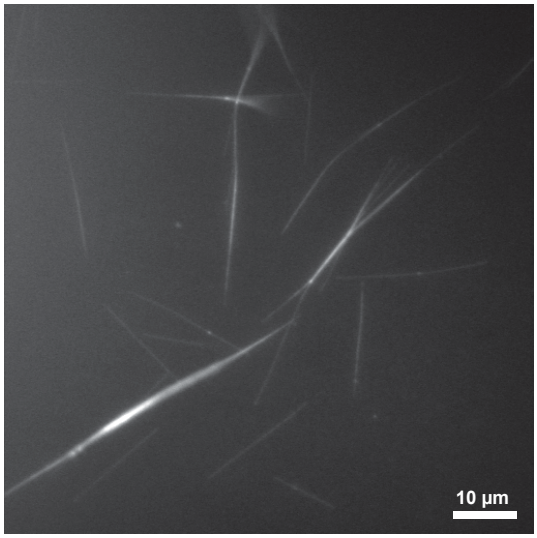

Figure 3.36: SKAP$^{135-225}$ promotes microtubule bundling *in vitro*. Representative TIRF image of microtubules in the presence of 500 nM SKAP$^{135-225}$ wild type and showing microtubule bundle formation.

To have a closer look on these microtubule bundles formed in the presence of SKAP$^{135-225}$, negative stain electron microscopy (EM) was performed. Therefore, samples of taxol-stabilized microtubules were polymerized at 34 °C in the absence and presence of SKAP$^{135-225}$ and directly imaged by EM. Figure 3.37 presents representative EM images of these samples at three different magnifications. In the absence of SKAP$^{135-225}$ a lot of single microtubules could be observed. Despite their high density, they did not form bundles or other higher-order structures. The sample with 0.5 µM SKAP$^{135-225}$ revealed huge polymeric tubulin structures that could clearly be identified as microtubule bundles in the higher magnifications. Even very short microtubules aligned into bundles. In the presence of 2 µM SKAP$^{135-225}$ these structures were even bigger and contained much thicker microtubule bundles. While in the background of the samples with less SKAP$^{135-225}$ several unpolymerized tubulin dimers could be seen, this sample revealed hardly any unpolymerized tubulin. Furthermore, in the presence of SKAP$^{135-225}$ a high amount of tubulin oligomers, reminiscent of microtubule nuclei, was visible (see bottom image series), indicating

that SKAP not only has an effect on microtubule bundling, but also on tubulin nucleation.

Taken together, the EM experiments confirm the findings of the TIRF analysis that SKAP$^{135-225}$ is able to bundle microtubules *in vitro* and - in addition to the observed lowered critical tubulin concentration in the turbidity assays - give a hint that SKAP$^{135-225}$ is able to nucleate tubulin and thereby promote its polymerization.

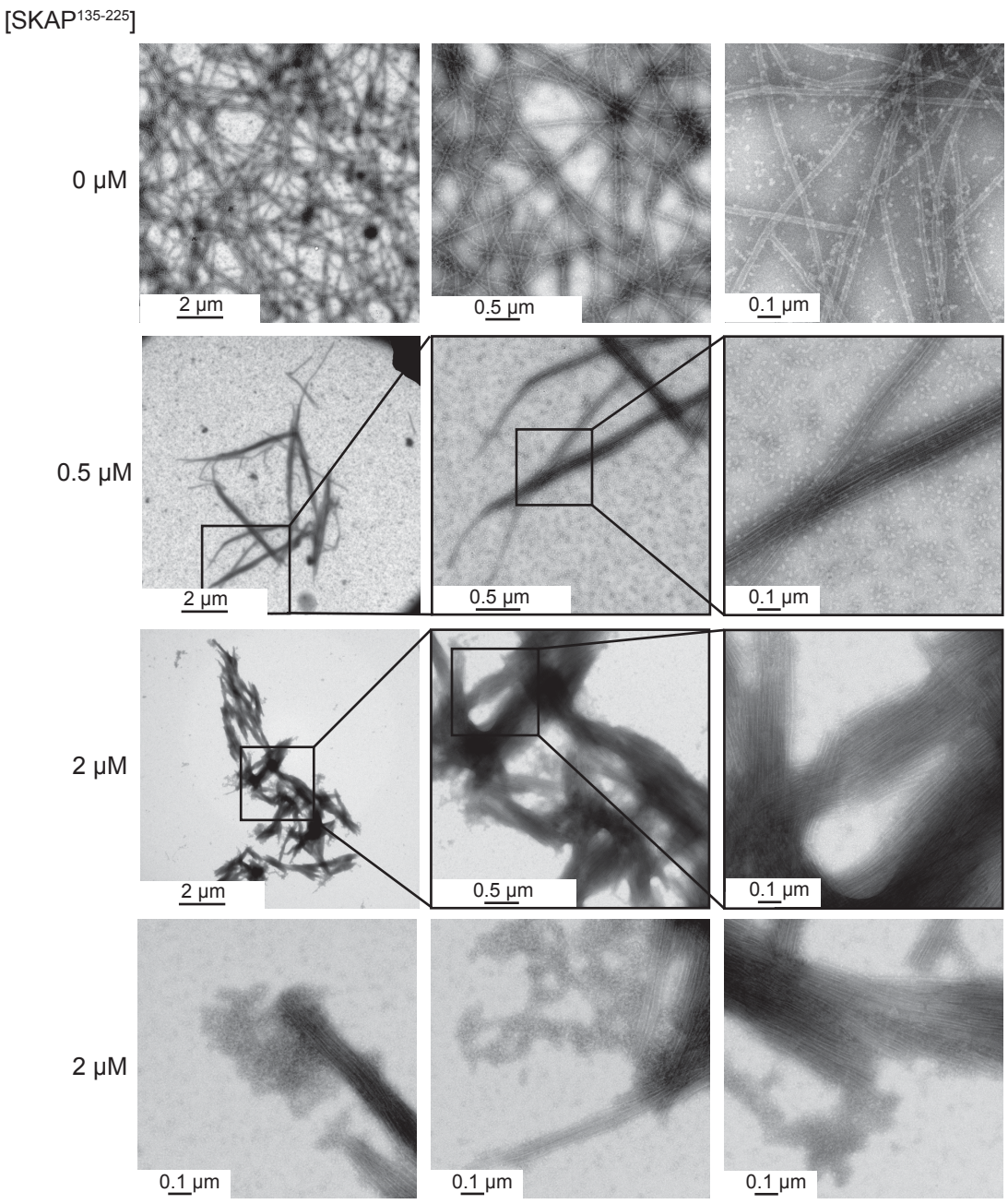

Figure 3.37: SKAP$^{135-225}$ promotes microtubule bundling *in vitro*. Representative negative stain EM images of microtubules in the absence and presence of SKAP$^{135-225}$. Samples with 10 µM tubulin and 0-2 µM SKAP$^{135-225}$ were incubated for 10 min at 34 °C and after addition of 50 µM taxol for another 30 min at 34 °C.

Next, the stability of microtubule bundles formed in the presence of SKAP$^{135-225}$ was analyzed. For this purpose, cold shock assays were performed, in which tubulin was polymerized at 34 °C in absence or presence of SKAP$^{135-225}$ wild type or mutants, followed by a cold shock on ice. Control samples were treated without cold shock. The SDS-PAGE gels of the supernatant and the pellet fractions after centrifugation and the corresponding quantification are shown in figure 3.38. The fraction of polymerized tubulin was determined by dividing the amount of tubulin in the pellet by its sum in supernatant and pellet. The control samples treated without cold shock confirm the observations of figure 3.27 A in section 3.3.5, which showed that the amount of polymerized tubulin was increased, when microtubules were incubated with the wild type SKAP$^{135-225}$ construct compared to the mutants. In this case, the polymerized tubulin fraction amounted to 63 % in presence of SKAP$^{135-225}$ wild type compared to 37 %, 30 % and 26 % in presence of the double, quadruple and sextuple mutants, respectively, revealing a correspondence of the ability of SKAP$^{135-225}$ to promote tubulin polymerization to the number of inserted mutations. The tubulin control sample treated without cold shock showed a polymerized tubulin fraction of 23 % comparable to the sextuple mutant. When comparing the samples treated with and without cold shock, it was found that the amount of polymerized tubulin in the tubulin control was decreased to only 6 %, indicating that microtubules formed in the absence of SKAP are not cold stable and therefore depolymerize upon cold treatment. The sextuple SKAP$^{135-225}$ mutant showed a similar reduction in the polymerized tubulin fraction to 9 %, suggesting that this mutant was not able to stabilize the formed microtubule during a cold shock. In contrast to this, SKAP$^{135-225}$ wild type as well as the double and quadruple mutants revealed comparable amounts of polymerized tubulin with and without cold shock, implying that these SKAP$^{135-225}$ constructs were able to stabilize the formed microtubules during the cold treatment.

In summary, these results suggest that SKAP$^{135-225}$ is able to prevent formed microtubule bundles from depolymerization upon cold treatment by acting as microtubule-stabilizing factor.

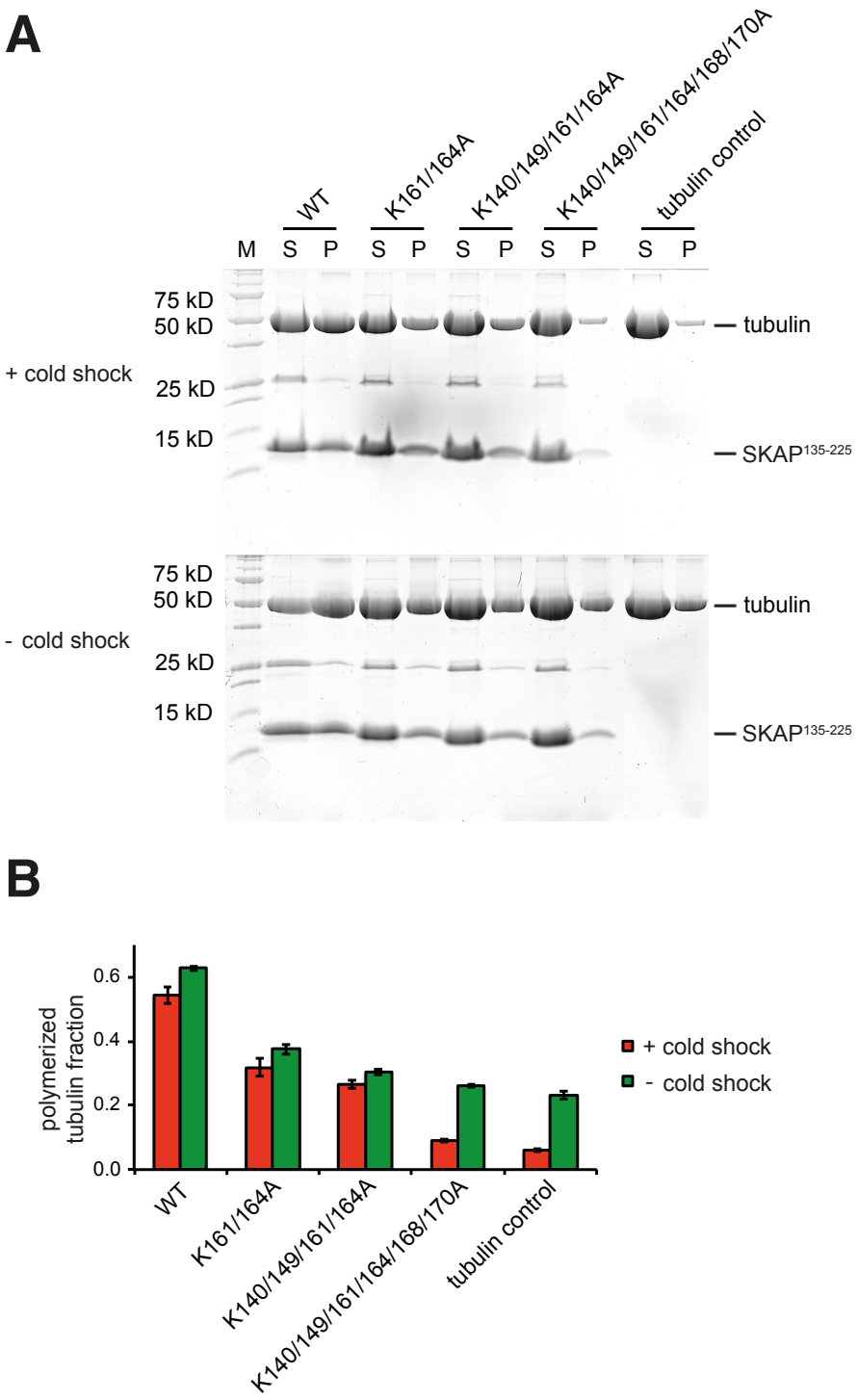

Figure 3.38: Microtubule bundles formed in the presence of SKAP$^{135-225}$ are cold stable. Representative SDS-PAGE gels (**A**) and quantification (**B**) of microtubule cold shock assays with 10 µM tubulin in absence or presence of 10 µM SKAP$^{135-225}$ wild type or indicated mutants. Samples were incubated for 30 min at 34 °C followed by a cold shock for 10 min on ice. Control samples were treated without cold shock. S: soluble fraction with proteins not bound to microtubules. P: pellet fraction with microtubules and bound proteins. M: molecular weight marker with molecular weights indicated on the left. Quantification was done with ImageJ 1.49 (NIH).

3.4 Kinetochore recruitment of the Astrin/SKAP complex

3.4.1 SKAP localizes to kinetochores in the absence of microtubules

As described in the introductory section 1.6, the localization of SKAP at kinetochores depends on the presence of microtubules and is counteracted by the activity of Aurora B kinase (Schmidt et al., 2010). In order to analyze the necessity of microtubules on the kinetochore localization of SKAP, immunofluorescence experiments with HeLa cells treated with different small molecule inhibitors were performed. MG132 is a proteasome inhibitor that blocks cells in metaphase. Hesperadin is an inhibitor of Aurora B kinase. Since Aurora B is important for correcting improper kinetochore-microtubule attachments and maintaining the spindle assembly checkpoint, an inhibition of this kinase leads to cells entering anaphase with a high amount of monooriented chromosomes because of missing correction mechanisms (Hauf et al., 2003). Nocodazole disrupts microtubule dynamics and thereby arrests cells in prometaphase, due to the lack of microtubules, which prevents kinetochores from accomplishing biorientation.

Representative immunofluorescence images and the corresponding quantification of the kinetochore localization of SKAP can be found in figure 3.39. HeLa cells treated only with MG132 established metaphase plates and showed no unattached kinetochores. In those cells, SKAP was found at both spindle microtubules and kinetochores with high intensity. As expected, in the presence of both MG132 and Hesperadin, HeLa cells were unable to align chromosomes to a metaphase plate and showed a high number of monooriented kinetochores. SKAP showed increased kinetochore localization in these cells and also localized to misattached kinetochores, indicating that Aurora B counteracts the kinetochore localization of SKAP. Next, these localization experiments were performed in the presence of nocodazole instead of MG132. The missing signal in the tubulin channel of the images with nocodazole treated cells reveals the absence of microtubules arresting cells in prometaphase. In these cells, SKAP levels at kinetochores were decreased to below 1 %, suggesting that SKAP was not able to localize to unattached kinetochores if Aurora B kinase was still functional. When HeLa cells were treated with Hesperadin in addition to nocodazole, kinetochore localization of SKAP could be restored to 51 % compared to cells treated with MG132, showing that SKAP could also localize to unattached kinetochores if Aurora B is inhibited.

In summary, these localization studies suggest that, although the intensity of SKAP at kinetochores is increased in the presence of spindle microtubules, SKAP does not

need microtubules to localize to kinetochores. Therefore, not only the attachment to microtubules brings SKAP to kinetochores, but there has to be an additional kinetochore receptor for SKAP.

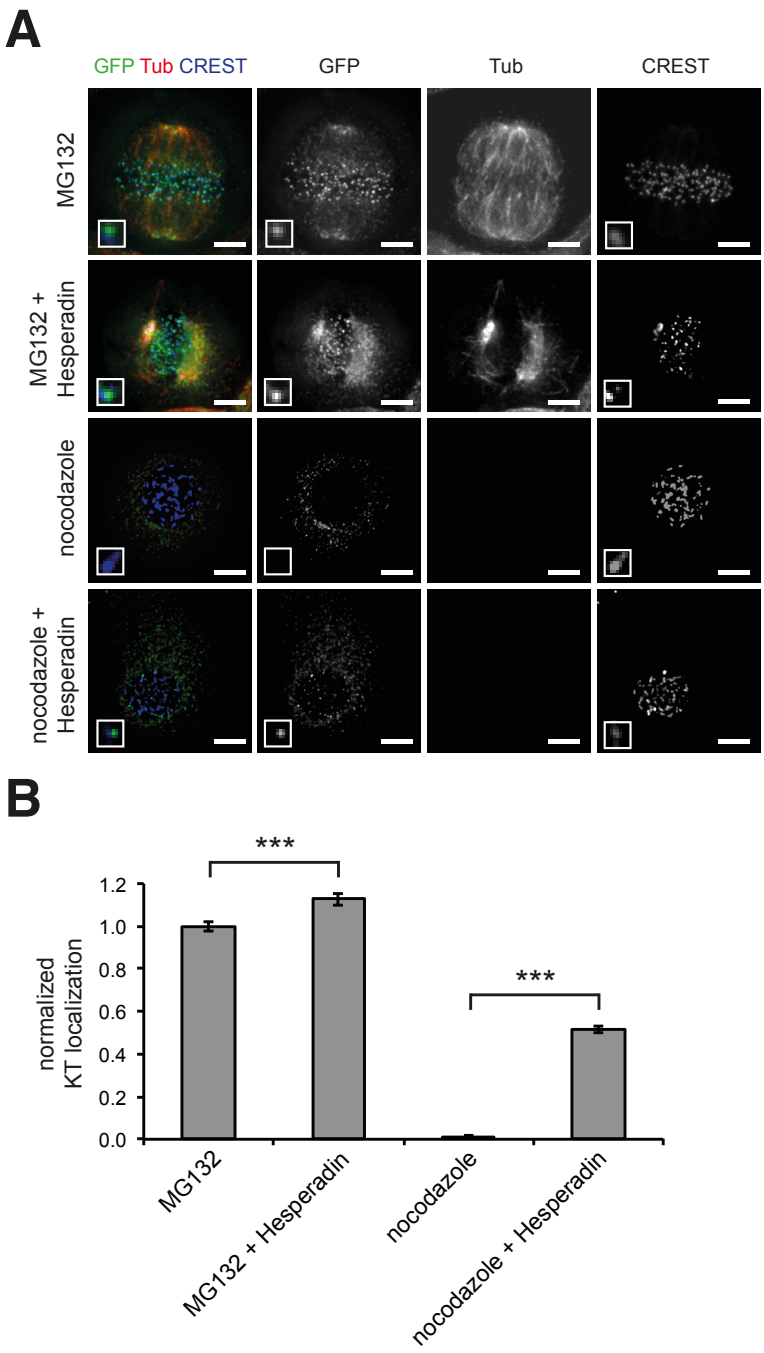

Figure 3.39: SKAP localizes to kinetochores in the absence of microtubules. (**A**) Representative immunofluorescence images of HeLa cells. Cells were treated with MG132 or nocodazole for 3 h and Hesperadin for 1.5 h prior to fixation. Scale bar: 5 µm. (**B**) Plot of endogenous SKAP signals at kinetochores for experiments shown in (**A**). Quantification was done with Imaris 7.3.4 (Bitplane, Zurich, CH). SKAP intensity was normalized to CREST signals (*t*-test: $p < 0.001$).

3.4.2 *In vitro* interaction studies to identify a kinetochore receptor for the Astrin/SKAP complex

Since the KMN network is important for the kinetochore localization of SKAP (Wang et al., 2012), *in vitro* interaction studies with SKAP and different components of the KMN network were performed. The SKAP construct ranging from amino acid 159 to 316 was used, because this region represents the minimal kinetochore localization domain of SKAP (Dunsch et al., 2011). Its localization with the KMN network proteins was investigated in GST pull-down experiments (see figure 3.40), migration shift assays by size exclusion chromatography (see figures 3.41 to 3.43) and with microscale thermophoresis (MST, see figure 3.44).

For GST pull-down experiments, GST-Knl1$^{2000-2311}$ was loaded onto GSH beads and subsequently incubated with SKAP$^{159-316}$ in absence or presence of the Mis12 and the Ndc80 complexes, as shown in figure 3.40 A. A protein band at a molecular weight of 20 kD, corresponding to SKAP$^{159-316}$, was visible in the binding experiment with GST-Knl1$^{2000-2311}$. This band was still detectable when GST-Knl1$^{2000-2311}$ was in complex with the Mis12 complex or the Mis12 and Ndc80 complexes. The control experiment with GST bound to the beads showed no corresponding protein band, indicating that SKAP$^{159-316}$ is able to bind to GST-Knl1$^{2000-2311}$ on solid phase. However, in pull-down assays with the slightly shorter GST-Knl1$^{2106-2316}$, as shown in figure 3.40 B, the band of SKAP$^{159-316}$ was not visible, neither with Knl1 alone nor with Knl1 in complex with the Mis12 and Ndc80 complexes. This suggests that there is no interaction between SKAP and Knl1, the Mis12 complex or the Ndc80 complex. The binding of SKAP$^{159-316}$ to the longer Knl1$^{2000-2311}$ construct was probably due to an unspecific interaction with the unpaired coiled-coil region of this Knl1 construct. The pull-down experiments with SKAP$^{159-316}$ and Zwint presented in figure 3.40 C revealed a protein band at a molecular weight of 20 kD corresponding to SKAP$^{159-316}$ in the assay with GST-Zwint as well as when Zwint was in complex with its binding partner Knl1, indicating an interaction between SKAP$^{159-316}$ and Zwint on solid phase.

Figure 3.41 shows the binding assays on size exclusion chromatography with SKAP$^{159-316}$ and the Mis12 complex. As seen in the chromatograms and the SDS-PAGE gels, SKAP$^{159-316}$ and the Mis12 complex showed the same elution properties when loaded onto the size exclusion chromatography column alone (red and blue) or together (black) and did not comigrate, suggesting that they do not interact in solution. In the experiment with SKAP$^{159-316}$ and GST-Knl1$^{2000-2311}$ depicted in figure 3.42, no migration shift or comigration could be observed, either. This confirms that

the interaction seen for these proteins on solid phase was probably due to a weak unspecific interaction. As shown in figure 3.43, Zwint and SKAP$^{159-316}$ shifted from lane 6 in the control samples to lanes 4 and 5 when loaded together. However, when the Zwint interaction partner Knl1$^{2000-2311}$ was added as well, a tight complex between Zwint and Knl1$^{2000-2311}$, but only a minor comigration of SKAP$^{159-316}$ could be observed, indicating only a weak interaction of SKAP$^{159-316}$ with the Zwint/Knl1 complex. Taken together, apart from a possible interaction with Zwint no kinetochore receptor of SKAP could be clearly identified by means of GST pull-downs and size exclusion chromatography.

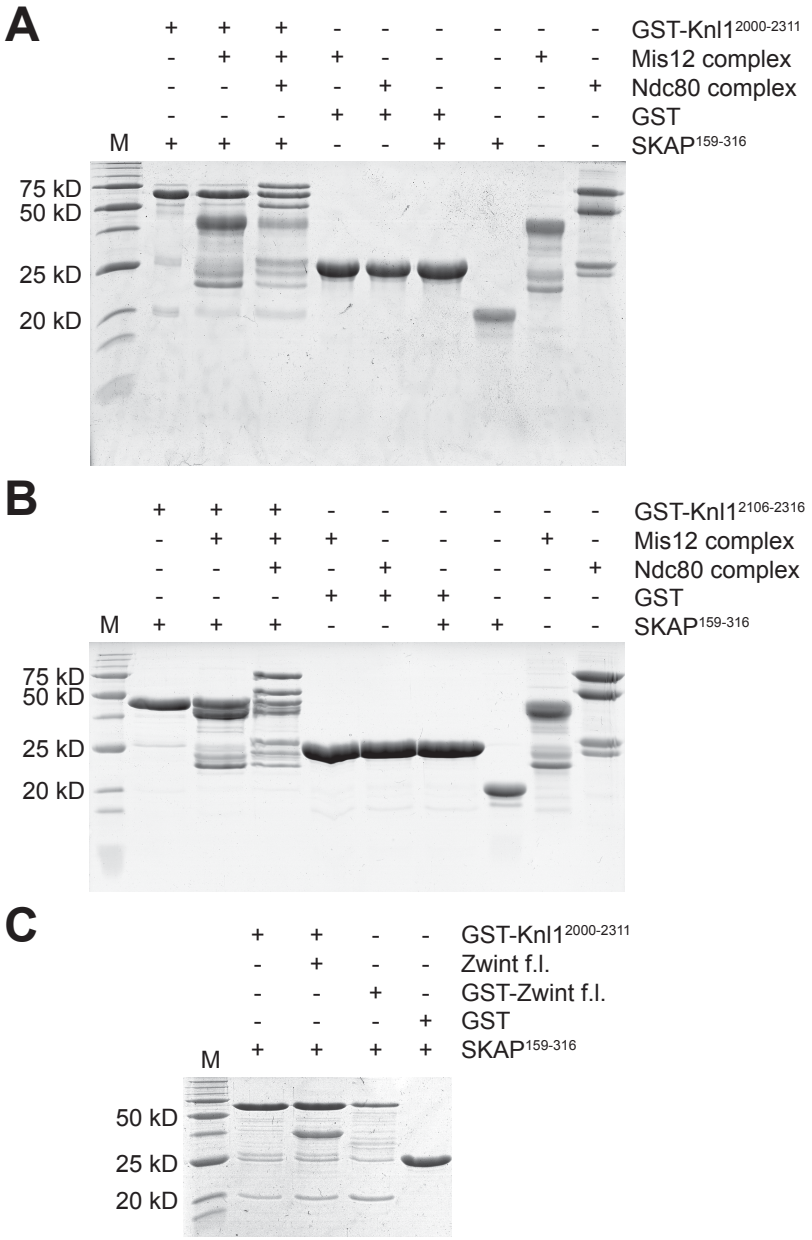

Figure 3.40: SKAP$^{159-316}$ interacts with Knl1$^{2000-2311}$ and Zwint in GST pull-down experiments. SDS-PAGE gels of GST pull-down experiments with Knl1$^{2000-2311}$, Knl1$^{2106-2316}$, the Mis12 complex, the Ndc80 complex, Zwint and SKAP$^{159-316}$. M: molecular weight marker with molecular weight indicated on the left.

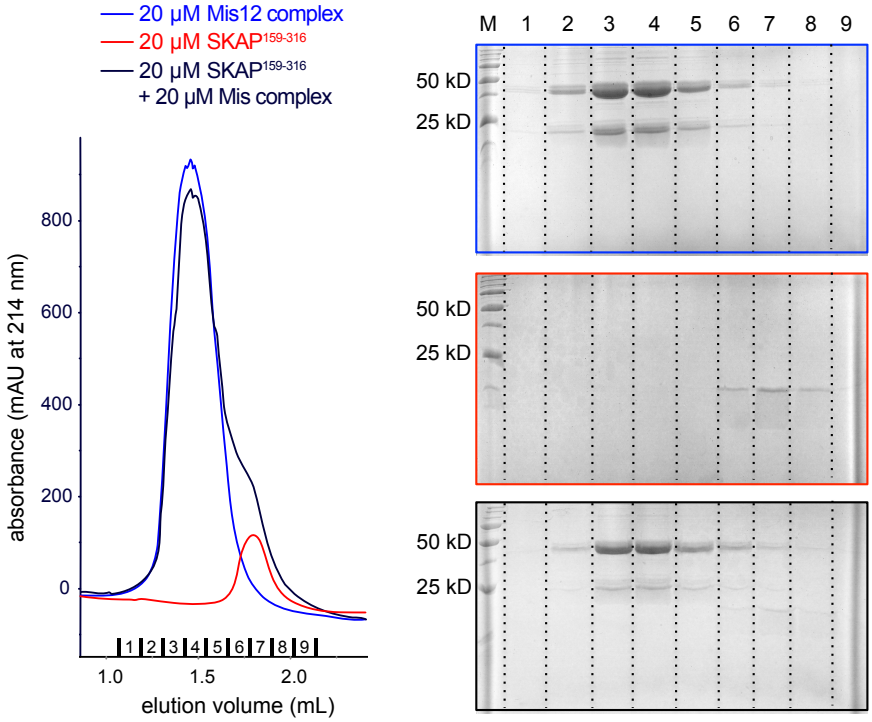

Figure 3.41: SKAP$^{159-316}$ does not bind to the Mis12 complex in solution. Chromatograms (left) and SDS-PAGE gels (right) of migration shift size exclusion chromatography experiments on a Superdex 200 5/150 column with 20 µM SKAP$^{159-316}$ (red), the Mis12 complex (blue) or both together (black). M: molecular weight marker with molecular weights indicated on the left.

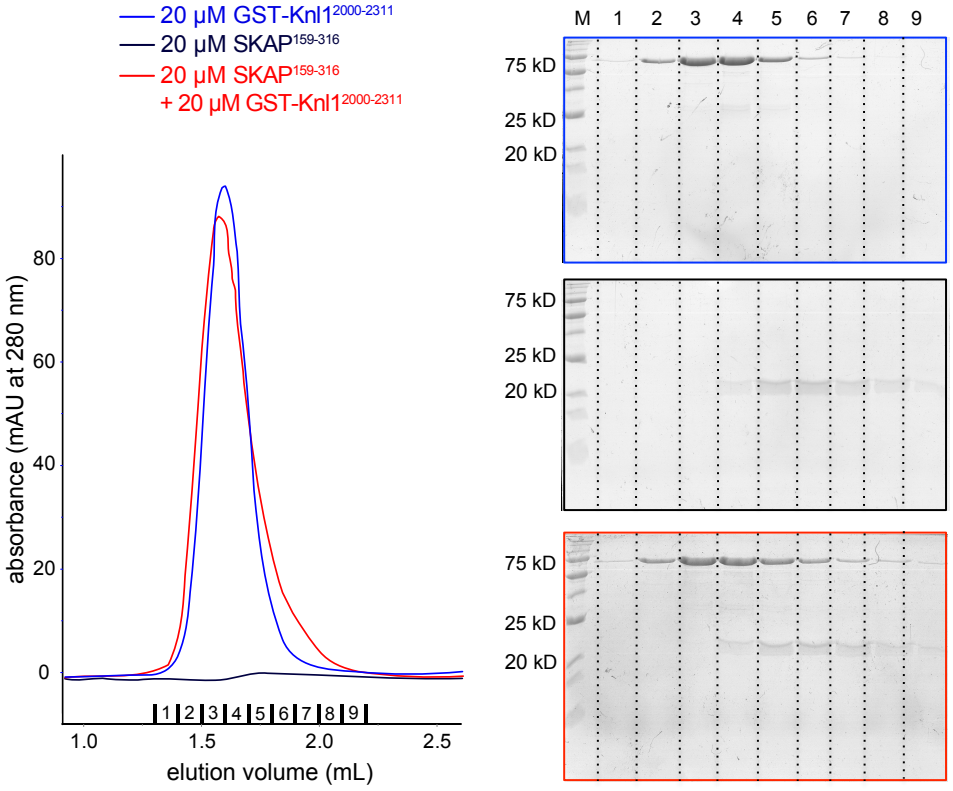

Figure 3.42: SKAP$^{159-316}$ does not bind to Knl1$^{2000-2311}$ in solution. Chromatograms (left) and SDS-PAGE gels (right) of migration shift size exclusion chromatography experiments on a Superdex 200 5/150 column with 20 µM SKAP$^{159-316}$ (black), GST-Knl1$^{2000-2311}$ (blue) or both together (red). M: molecular weight marker with molecular weights indicated on the left.

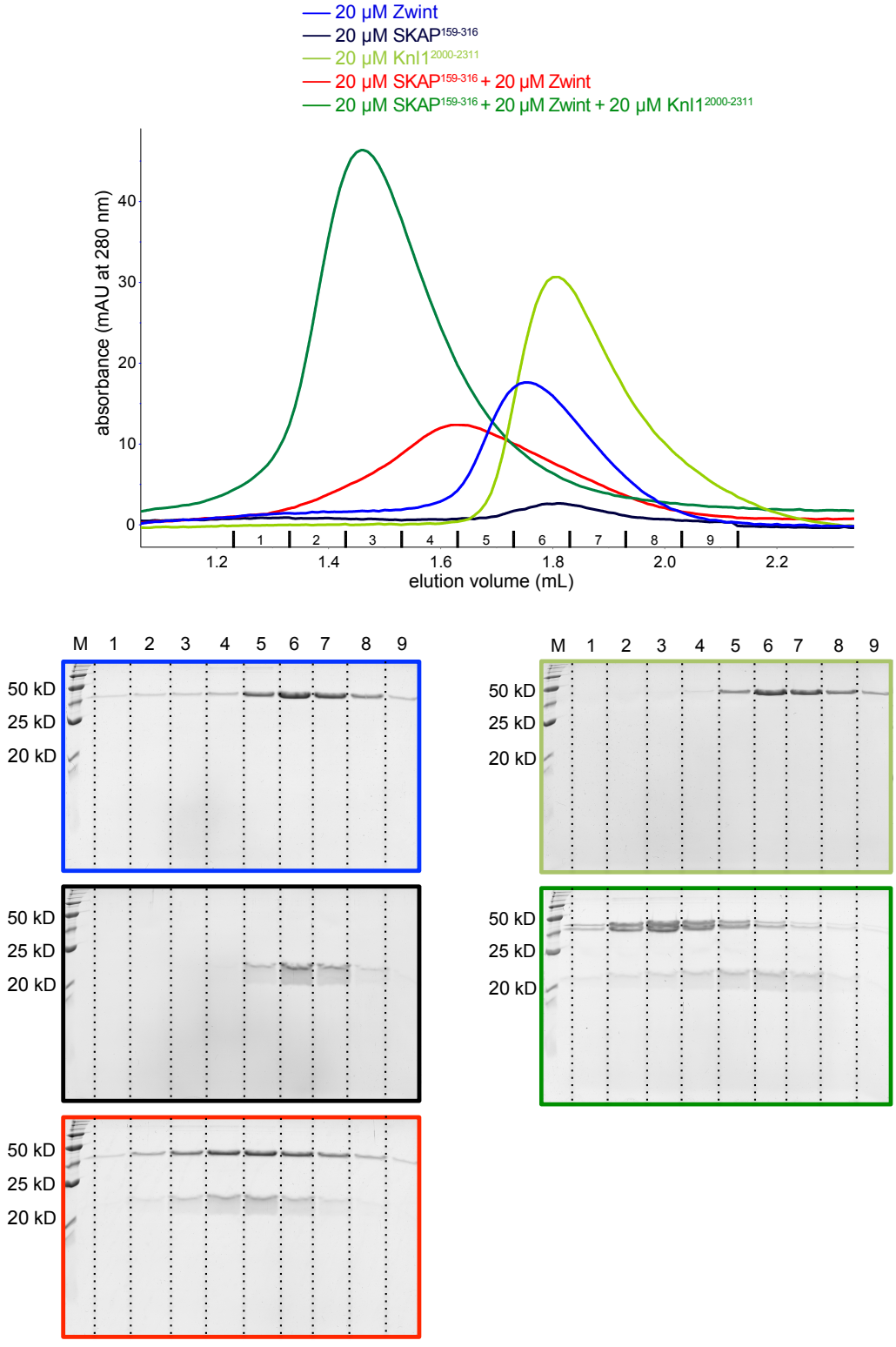

Figure 3.43: SKAP$^{159-316}$ binds to Zwint in solution. Chromatograms (top) and SDS-PAGE gels (bottom) of migration shift size exclusion chromatography experiments on a Superdex 200 5/150 column with 20 µM Zwint (blue), SKAP$^{159-316}$ (black), both together (red), Knl1$^{2000-2311}$ (light green) or all three together (dark green). M: molecular weight marker with molecular weights indicated on the left.

As a third method to analyze the interaction of SKAP and the KMN network, MST experiments were performed. With MST, the migration of biomolecules in a local temperature gradient is analyzed (Jerabek-Willemsen et al., 2011). This depends on the size, charge and solvation shell of the observed molecules. Since upon binding of two or more molecules their size, charge and conformation is altered, this structural change can be observed via a thermophoretic change.

Figure 3.44 shows the results of the MST experiments with fluorescent mCherry-SKAP$^{159-316}$ titrated with unlabeled Mis12 complex (A), Ndc80 complex (B) or Zwint (C), respectively. Fluorescence signals were analyzed with the NT Analysis software (NanoTemper Technologies GmbH, Munich, DE). The left panel of figure 3.44 depicts the changes in the initial fluorescence for the different concentrations of unlabeled protein, whereas the right panel shows the normalized difference in fluorescence for the thermophoresis and the temperature jump signal. Plotted signals were fitted with Origin7.0 (OriginLab, Northampton, US-MA) as mentioned in section 5.6.1. It can be seen that the initial fluorescence signal of mCherry-SKAP$^{159-316}$ increased upon addition of the Mis12 complex, the Ndc80 complex as well as Zwint. The fitting analysis revealed very similar dissociation constants for the three observed interactions amounting to 65 nM for the Mis12 complex, 56 nM for the Ndc80 complex and 66 nM for Zwint. The analysis of the thermophoresis and the temperature jump signals resulted in a decrease of signal corresponding to the increase in initial fluorescence. The dissociation constants obtained by the fitting analysis were 37 nM for the Mis12 complex, 59 nM for the Ndc80 complex and 35 nM for Zwint. Since the analysis of the thermophoresis and the temperature jump signals is based on a constant initial fluorescence for all titration points, the fitting of the fluorescence changes is supposed to be more accurate. Strikingly, the fitting of all shown interactions resulted in very similar dissociation constants between 35 nM and 66 nM. Since these calculated dissociation constants in the nM range assume very tight interactions and the interactions of SKAP$^{159-316}$ with the Mis12 complex or the Ndc80 complex could not be detected with other methods, i.e. GST pull-downs and size exclusion chromatography, the MST experiments probably do not show real interactions, as discussed in section 4.3.

Taken together, no receptor of the Astrin/SKAP complex could be identified by means of MST and the results suggest a cautious interpretation of binding data obtained from a single approach.

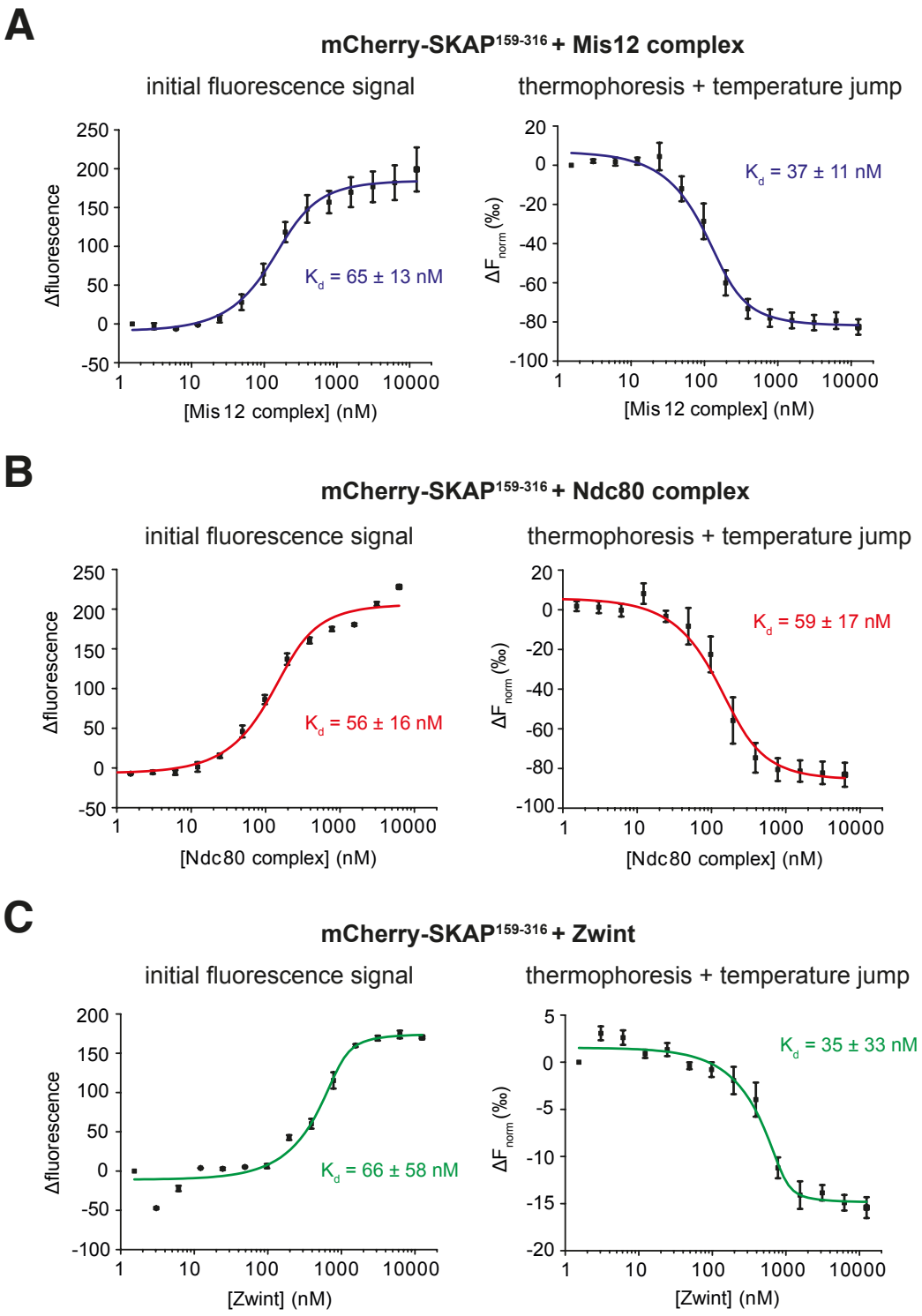

Figure 3.44: SKAP$^{159-316}$ shows an interaction with the Mis12 complex, the Ndc80 complex and Zwint in MST experiments. Quantification of microscale thermophoresis assays with 150 nM mCherry-SKAP$^{159-316}$ and the Mis12 complex (**A**), the Ndc80 complex (**B**) or Zwint (**C**). Left, change in initial fluorescence. Right, normalized difference in fluorescence for the thermophoresis and the temperature jump signal. Signals were analyzed with the NT Analysis software (NanoTemper Technologies GmbH, Munich, DE) and fitted with Origin7.0 (OriginLab, Northampton, US-MA) as mentioned in section 5.6.1.

3.5 Structural characterization of the Astrin/SKAP complex

3.5.1 The Astrin/SKAP complex is highly elongated and flexible

In order to look closer at the structure of the Astrin/SKAP complex, the truncated version of this complex containing Astrin$^{482-850}$ and SKAP$^{159-316}$ was analyzed with negative stain electron microscopy. As it can be seen in figure 3.45, the Astrin$^{482-850}$/SKAP$^{159-316}$ complex showed a highly elongated structure with several conformations indicating a high degree of flexibility. The calculated length of the complex is about 40-50 nm. The EM images in the bottom panel of figure 3.45 reveal ring-like structures, implying that the Astrin$^{482-850}$/SKAP$^{159-316}$ complex is able to form higher-order structures. Because of the high flexibility of the complex, a single particle analysis was not possible.

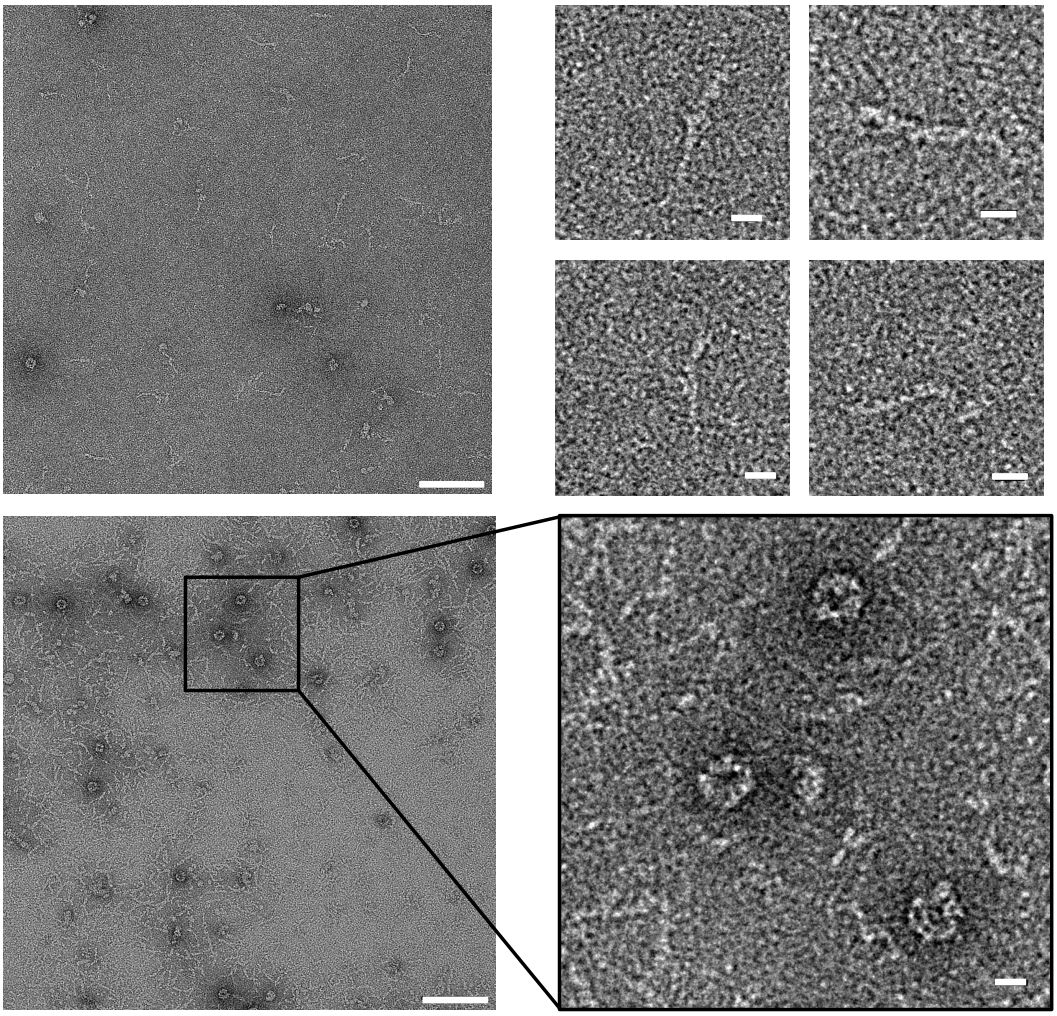

Figure 3.45: The Astrin$^{482-850}$/SKAP$^{159-316}$ is highly elongated and flexible. Representative negative-stain EM images of Astrin$^{482-850}$/SKAP$^{159-316}$. Scale bars: 100 nm (left) and 10 nm (magnifications on the right).

Next, attempts were made to decorate microtubules with the Astrin$^{482-850}$/SKAP$^{159-316}$ complex in order to investigate the binding mode. The binding to microtubules might reduce the flexibility of the complex and thereby allow a single particle analysis of the complex. The resulting EM images are depicted in figure 3.46. Panel A shows the images of microtubules together with the Astrin$^{482-850}$/SKAP$^{159-316}$ complex, panel B shows the control sample with undecorated microtubules. The comparison of these EM images reveals that the microtubules looked the same in both conditions, indicating that the Astrin$^{482-850}$/SKAP$^{159-316}$ complex did not bind to the microtubules under the assay conditions. Attempts with higher protein concentrations and different procedures to form the microtubules did not lead to a decoration of the microtubules, either, suggesting that the binding affinity of the Astrin$^{482-850}$/SKAP$^{159-316}$ complex for microtubules is too low to achieve binding under conditions suitable for EM analysis.

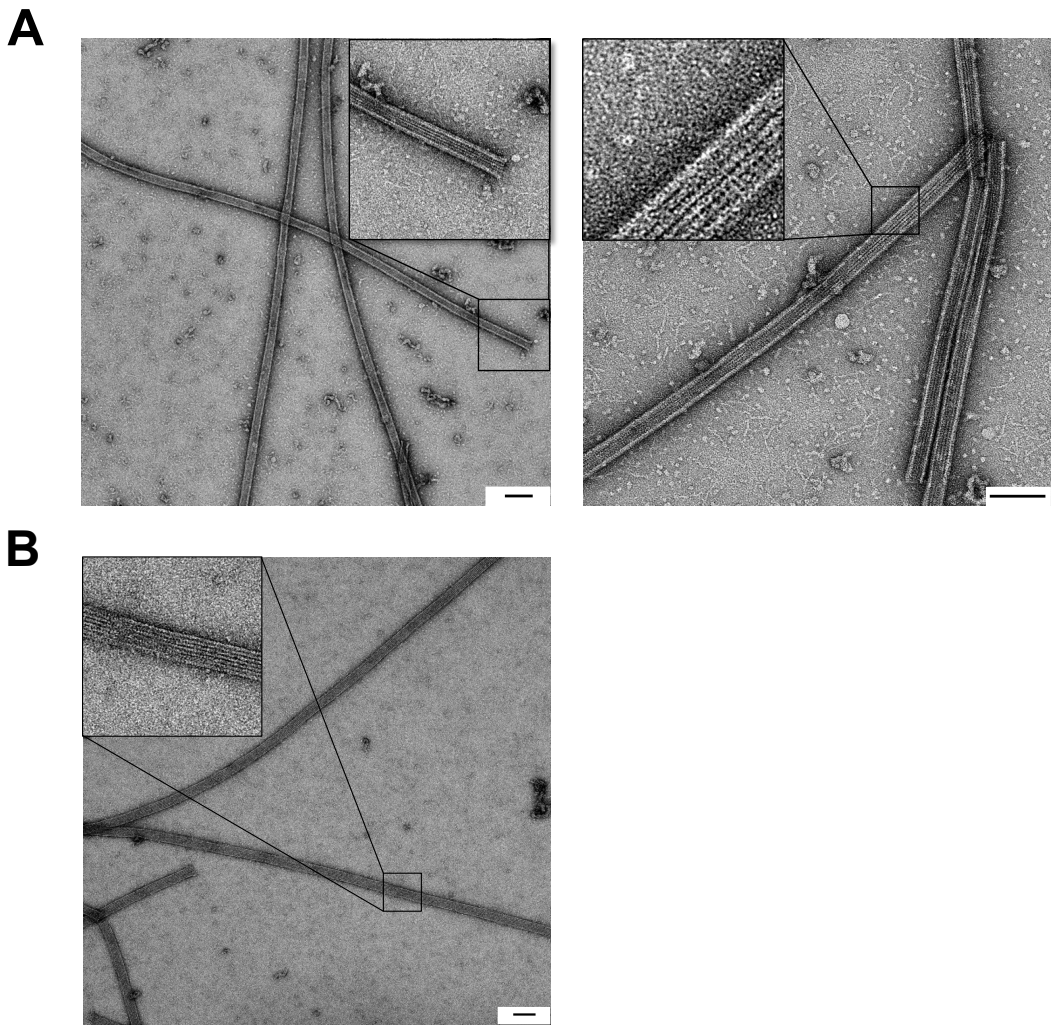

Figure 3.46: Negative stain EM images of microtubules in absence and presence of Astrin$^{482-850}$/SKAP$^{159-316}$. GMPCPP-stabilized microtubule seeds were incubated either in presence of Astrin$^{482-850}$/SKAP$^{159-316}$ (**A**) or alone (**B**) for 5 min at 37 °C on the grid. Scale bars: 100 nm.

3.5.2 Towards the crystal structure of SKAP

In order to gain insight into the atomic structure of SKAP, attempts were made to solve the structure of truncated SKAP constructs by means of X-ray crystallography. For this purpose, different SKAP constructs were crystallized via the vapor diffusion method with the sitting- and hanging-drop implementation.

For the microtubule-binding domain SKAP$^{135-225}$, one successful crystallization condition was identified. The obtained crystals, which are presented in figure 3.47, were rod-like and very tiny, with a maximal size of 30 µm, but they showed a clearly defined structure with sharp edges. The diffraction pattern of one of these crystals in figure 3.48 revealed a very anisotropic diffraction, which is typical for highly elongated structures such as coiled-coil proteins.

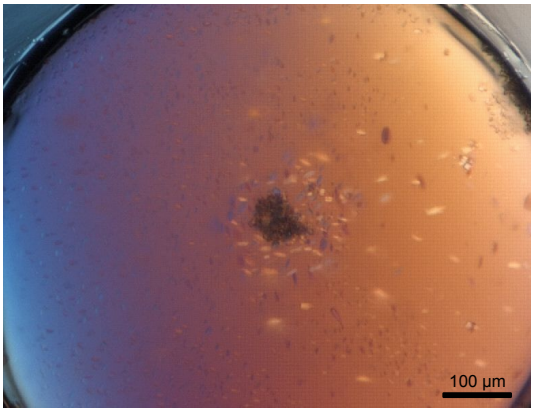

Figure 3.47: Crystals of SKAP$^{135-225}$. Crystals were grown at 20 °C via the sitting drop vapor diffusion method with reservoir solution containing 0.1 M Hepes, pH 7.0 and 30 % (w/v) PEG 6000.

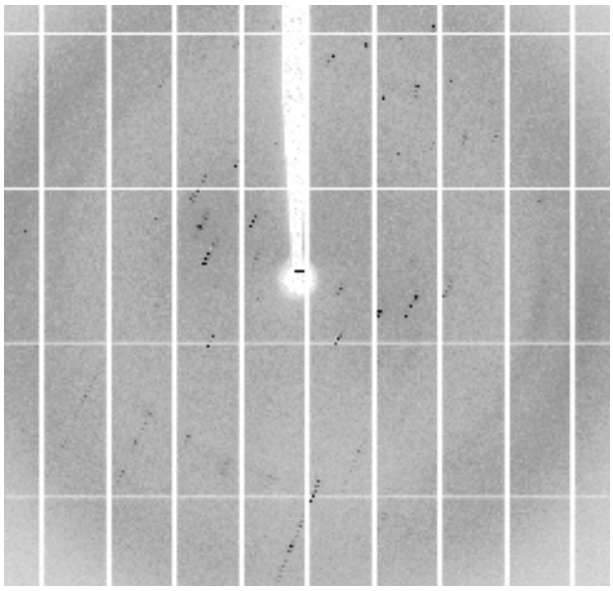

Figure 3.48: Diffraction image of a crystal of SKAP$^{135-225}$. Diffraction image was collected on beamline PXII of the Swiss Light Source (Paul Scherrer Institute, Villigen, CH).

In addition to the wild type form of SKAP$^{135-225}$, a seleno-methionine labeled version of this SKAP construct was crystallized for the purpose of obtaining phase information for computing initial electron density maps. As it can be seen in figure 3.49, these crystals show a rod-like form with a size of up to 40 µm comparable to the wild type SKAP$^{135-225}$ crystals. Furthermore, the introduction of heavy atoms for solving the phase problem was achieved by soaking native SKAP$^{135-225}$ crystals with different heavy atom derivatives including K_2PtCl_4 or $Pb(CH_3COO)_2$.

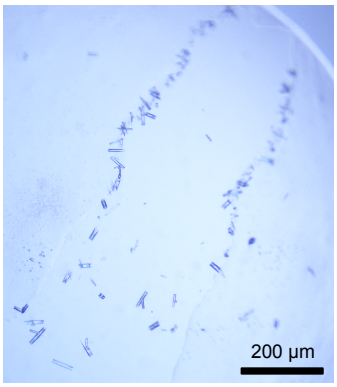

Figure 3.49: Crystals of seleno-methionine labeled SKAP$^{135-225}$. Crystals of seleno-methionine labeled SKAP$^{135-225}$ were grown at 20 °C via the hanging drop vapor diffusion method with reservoir solution containing 0.1 M Hepes, pH 7.5 and 20 % (w/v) PEG 6000.

Collection of X-ray diffraction data from these crystals resulted in five data sets of native SKAP$^{135-225}$ crystals, one data set of a seleno-methionine labeled SKAP$^{135-225}$ crystal and six data sets of SKAP$^{135-225}$ crystals soaked with different heavy atom derivatives. The statistics of the data sets for the native crystal with the best resolution of about 2.9 Å and the seleno-methionine labeled crystal with a resolution of 3.6 Å are summarized in tables 3.10. The statistics of two data sets with platinum and lead soaks that showed an anomalous signal below 4 Å and resolutions of 3.7 Å and 3.0 Å, respectively, are presented in table 3.11. Processing of all these data sets was compatible with a tetragonal space group - either $P4_1$ 2 2 or $P4_3$ 2 2 - and cell dimensions with two short axes of 37 Å and one long axis of 201-203 Å, revealing a very elongated unit cell. These cell constants are in agreement with the anisotropic diffraction and the predicted coiled-coil structure of SKAP$^{135-225}$. The data set of the seleno-methionine labeled crystal showed no significant anomalous signal, indicating that the seleno-methionine was probably located in a flexible loop. Attempts were made to solve the structure of SKAP$^{135-225}$ by isomorphous replacement with the

Phenix AutoSol, but no model could be build, probably due to problems with high anisotropic diffraction and insufficient resolution.

Table 3.10: Statistics of data collection of a wild type and a seleno-methionine (SeMet) labeled SKAP$^{135-225}$ crystal. Values in parenthesis correspond to the highest resolution shell. All data sets were collected from one single crystal on beamline PXII of the Swiss Light Source (Paul Scherrer Institute, Villigen, CH).

	SKAP$^{135-225}$	**SeMet-SKAP$^{135-225}$**
Space group	$P4_1$ 2 2 or $P4_3$ 2 2	$P4_1$ 2 2 or $P4_3$ 2 2
Cell dimensions		
a, *b*, *c* (Å)	37.24, 37.24, 203.25	37.15, 37.15, 201.37
α, β, γ (°)	90, 90, 90	90, 90, 90
Wavelength (Å)	1.00719	0.98013
Resolution (Å)	50.0 – 2.9 (3.0 – 2.9)	50.0 – 3.6 (3.7 – 3.6)
$R_{mrgd\text{-}F}$	8.7 (170.4)	14.4 (245.6)
I/σ(I)	11.2 (2.0)	14.4 (2.0)
Completeness (%)	99.8 (100.0)	99.9 (100.0)
Redundancy	11.4 (11.8)	26.8 (28.9)

Table 3.11: Statistics of data collection of SKAP$^{135-225}$ crystals soaked with K_2PtCl_4 or $Pb(CH_3COO)_2$. Values in parenthesis correspond to the highest resolution shell. All data sets were collected from one single crystal on beamline PXII of the Swiss Light Source (Paul Scherrer Institute, Villigen, CH).

	SKAP$^{135-225}$-Pt soak	**SKAP$^{135-225}$-Pb soak**
Space group	$P4_1$ 2 2 or $P4_3$ 2 2	$P4_1$ 2 2 or $P4_3$ 2 2
Cell dimensions		
a, *b*, *c* (Å)	37.43, 37.43, 201.91	37.31, 37.31, 201.97
α, β, γ (°)	90, 90, 90	90, 90, 90
Wavelength (Å)	1.07183	0.95107
Resolution (Å)	50.0 – 3.7 (3.8 – 3.7)	50.0 – 3.0 (3.1 – 3.0)
$R_{mrgd\text{-}F}$	14.9 (321.6)	13.9 (293.4)
I/σ(I)	16.1 (2.3)	17.3 (2.5)
Completeness (%)	99.9 (100.0)	99.9 (100.0)
Redundancy	26.5 (27.7)	26.7 (28.7)

In order to solve the structure of SKAP via molecular replacement, a mCherry-SKAP$^{135-225}$ fusion protein was crystallized. As shown in figure 3.50, the obtained rod-like crystals had a long axis of 50-300 µm and possessed sharp edges.

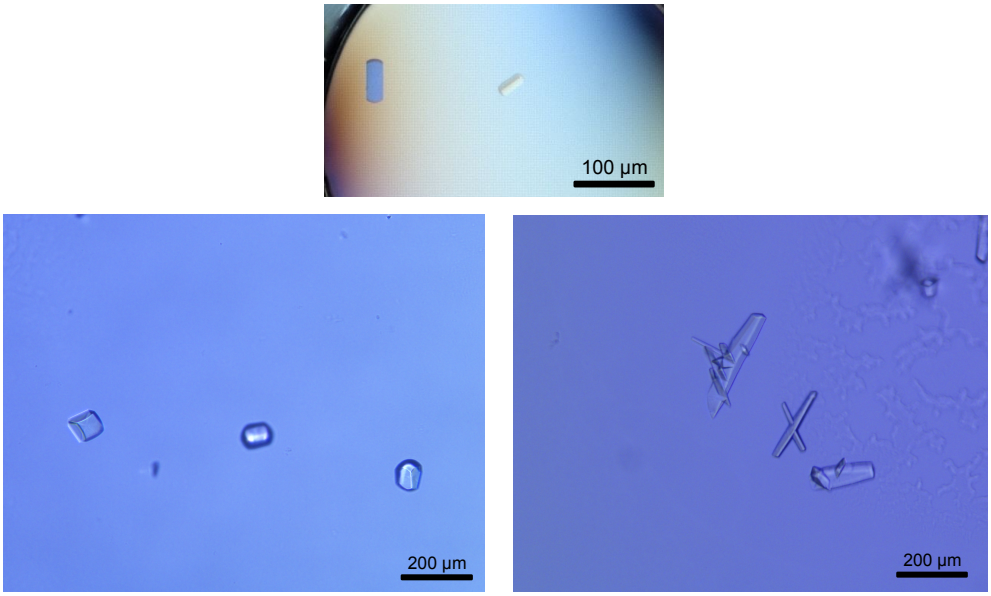

Figure 3.50: Crystals of mCherry-SKAP$^{135-225}$. Crystals of mCherry-SKAP$^{135-225}$ were grown at 20 °C via the sitting drop (top) and the hanging drop (bottom) vapor diffusion method with reservoir solutions containing 0.2 M KH_2PO_4, 20 % (w/v) PEG 3350.

Strikingly, the data collection of these crystals resulted in the same space group and cell parameters that were obtained for the wild type SKAP$^{135-225}$ crystals. This suggests the possibility that the mCherry-SKAP$^{135-225}$ fusion protein is cleaved during the crystallization process. Therefore, a SDS-PAGE analysis of a crystallization drop containing mCherry-SKAP$^{135-225}$ was performed. Figure 3.51 reveals that the fusion protein was indeed cleaved into mCherry and SKAP$^{135-225}$, so that no data set of the fusion protein could be obtained.

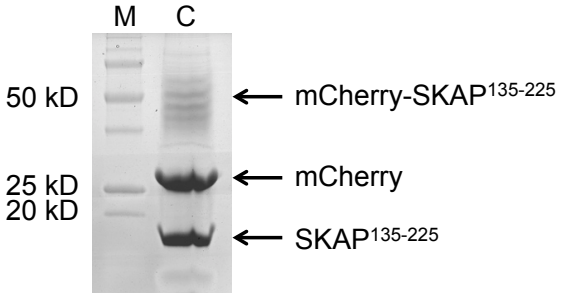

Figure 3.51: mCherry-SKAP$^{135-225}$ is cleaved during crystallization. SDS-PAGE gel of a crystallization drop containing mCherry-SKAP$^{135-225}$ crystals.

Since no higher resolution of the SKAP$^{135-225}$ crystals could be achieved with crystal optimization, the sextuple mutant SKAP$^{135-225}$ K140/149/161/164/168/170A was also crystallized. The mutations of lysine to alanine might facilitate the crystallization process, because lysines are known to be highly flexible and thereby might disturb crystal packing. SKAP$^{135-225}$ K140/149/161/164/168/170A indeed crystallized in six crystallization conditions instead of just one condition for the wild type protein. Crystals from two different conditions are shown in figure 3.52. With a size up to 200 µm these crystals grew much larger than the wild type crystals and they also showed clear defined structures with sharp edges. Different crystal forms including very thin needles and thicker rods could be obtained. However, these crystals only diffracted up to a resolution of about 5-6 Å.

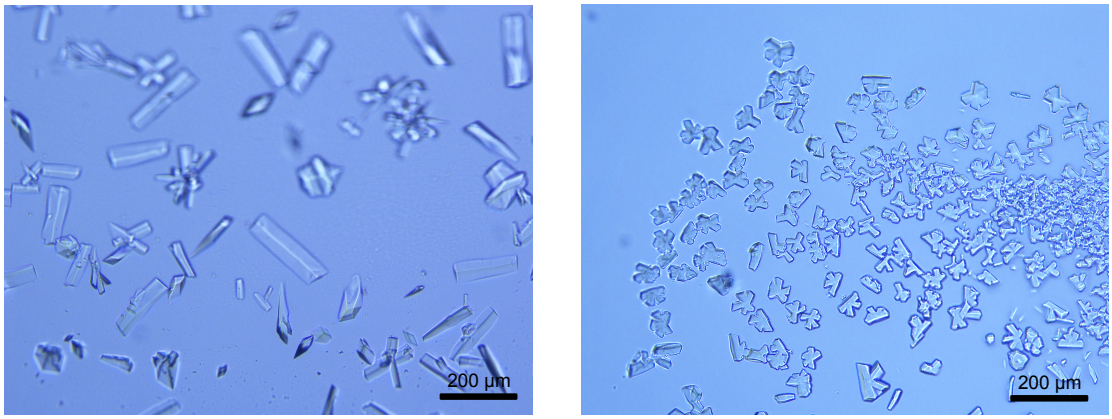

Figure 3.52: Crystals of SKAP$^{135-225}$ K140/149/161/164/168/170A. Crystals of SKAP$^{135-225}$ K140/149/161/164/168/170A were grown at 20 °C via the hanging drop vapor diffusion method with reservoir solutions containing 0.1 M MES, pH 6.0 and 20 % (w/v) PEG 6000 (left) or 0.04 M KH_2PO_4, 16 % (w/v) PEG 8000 and 20 % (v/v) glycerol (right).

In addition to SKAP$^{135-225}$ only the central coiled-coil domain ranging from amino acid 159 to 225 was crystallized. After first crystallization trials that led to crystals in huge clusters (see figure 3.53 left), the SKAP$^{159-225}$ crystals could be optimized to individually growing crystals with sharp edges and a size up to 200 µm (see figure 3.53 right). Two data sets were collected for these crystals and the statistics of the data set with the best resolution of 3.6 Å are summarized in table 3.12. The space group - $P4_1$ 2 2 or $P4_3$ 2 2 - is the same as for SKAP$^{135-225}$ and the cell dimensions containing two short axes of 54 Å and one long axis of 199 Å are similar to those of SKAP$^{135-225}$, indicating a very elongated structure.

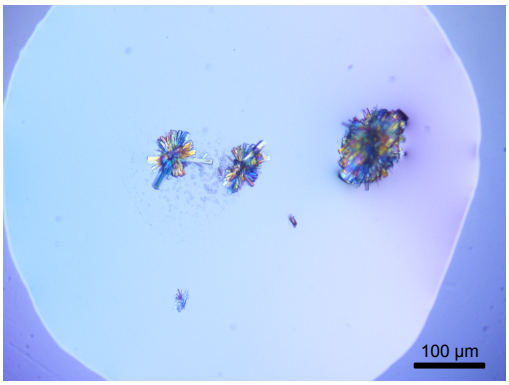

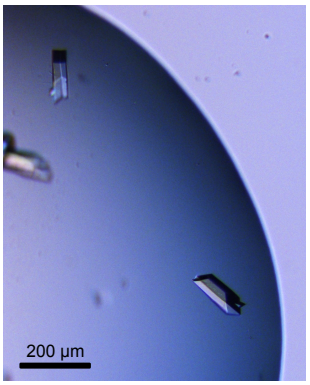

Figure 3.53: Crystals of SKAP$^{159-225}$. Crystals of SKAP$^{159-225}$ were grown at 20 °C via the hanging drop vapor diffusion method with reservoir solutions containing 0.15 M $MgSO_4$ and 15 % (w/v) PEG 3350 (left) or 0.2 M $MgSO_4$ and 20 % (w/v) PEG 3350 (right).

Table 3.12: Statistic of data collection of a SKAP$^{159-225}$ crystal. Values in parenthesis correspond to the highest resolution shell. The data set was collected from one single crystal on beamline PXII of the Swiss Light Source (Paul Scherrer Institute, Villigen, CH).

	SKAP$^{159-225}$
Space group	$P4_1$ 2 2 or $P4_3$ 2 2
Cell dimensions	
a, *b*, *c* (Å)	53.55, 53.55, 199.40
α, β, γ (°)	90, 90, 90
Wavelength (Å)	0.92045
Resolution (Å)	50.0 – 3.59 (3.68 – 3.59)
R_{mrgd-F}	7.0 (146.6)
I/σ(I)	21.5 (3.0)
Completeness (%)	99.0 (99.2)
Redundancy	23.0 (21.2)

In order to get insight into the binding mode of SKAP to microtubules on the atomic level and as alternative way to solve the SKAP structure via molecular replacement, crystallization experiments with the SKAP$^{135-225}$/tubulin/RB3 complex were performed. During the crystallization of this complex, one successful crystallization condition could be identified, in which the SKAP$^{135-225}$/tubulin/RB3 complex crystallized as very thin and clustered needles (see figure 3.54 left). The crushed needle clusters were used for microseeding experiments that resulted in small box-like crystals with a size of about 20 µm (see figure 3.54 right). The diffraction analysis of these crystals showed no diffraction.

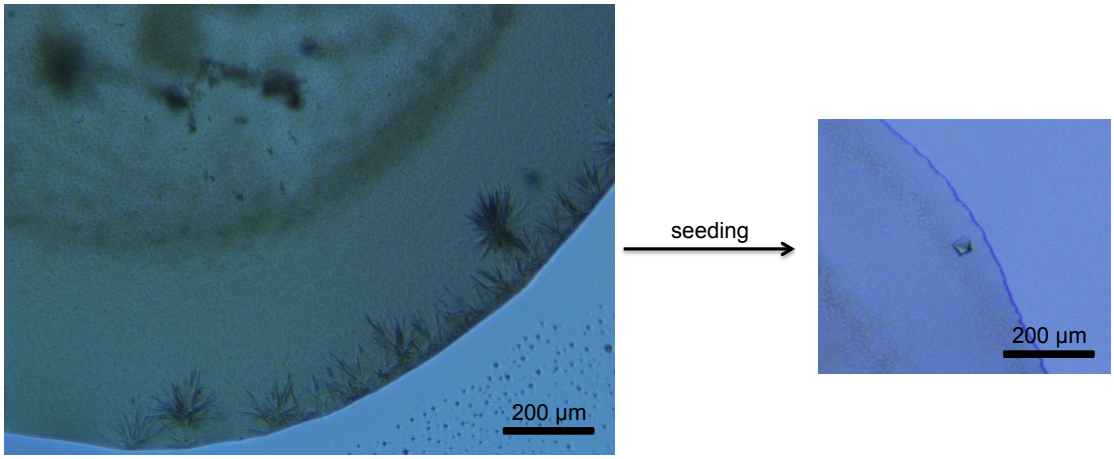

Figure 3.54: Crystals of the SKAP$^{135-225}$/tubulin/RB3 complex. Crystals of the SKAP$^{135-225}$/tubulin/RB3 complex were grown at 20 °C via the hanging drop vapor diffusion method with reservoir solutions containing 0.1 M MES, pH 6.0 and 30 % (w/v) PEG 200. The crystal on the right was obtained by microseeding with crushed clustered needle-like crystals as shown on the left.

In summary, the structure of SKAP could not be solved by means of X-ray crystallography, but several successful attempts to crystallize different SKAP constructs as well as the microtubule-binding domain of SKAP in complex with tubulin and the RB3 protein were made.

4 DISCUSSION

4.1 Domain organization of the Astrin/SKAP complex

Studies on the intersubunit interaction of the Astrin/SKAP complex (see sections 3.2.4 and 3.3.1.) showed that the domains encompassing amino acids 482 to 850 in Astrin and 159 to 316 in SKAP constitute the minimal interaction domains that are necessary to form a tight complex. This is in agreement with a previous analysis in which constructs with similar boundaries were expressed in mammalian cells and analyzed by immunoprecipitation (Dunsch et al., 2011).

Analyses on the oligomeric state of SKAP by AUC and cross-linking experiments revealed that SKAP$^{135-225}$ behaves as a trimer (see section 3.2.3, figure 3.11). Previously reported rotary shadowing EM analysis of full-length Astrin, refolded from bacterial inclusion bodies, showed a two-fold symmetry of Astrin indicating dimer formation (Gruber et al., 2002). Taken together with the observation that SKAP may form trimeric assemblies, the overall stoichiometry of the Astrin/SKAP complex may be expected to be 2:6. However, label-free mass spectrometric analysis of Astrin and SKAP immunoprecipitates from mitotic mammalian cells predicts a 1:2 stoichiometry of the Astrin/SKAP complex (Dunsch et al., 2011). Attempts to verify the oligomeric state of the Astrin$^{482-850}$/SKAP$^{159-316}$ complex in analytical ultracentrifugation sedimentation velocity experiments were hampered by the limited solubility of the complex. Furthermore, the N-terminal domain of Astrin seems to exist in different oligomeric states (see section 3.2.2, figure 3.7), which is in agreement with the findings by Gruber et al., 2002, according to which Astrin is able to oligomerize with its N-terminal domain. This suggests that the Astrin/SKAP complex with its potential 2:6 stoichiometry may in addition show higher-order oligomerization via the N-terminal domain of Astrin.

More extensive *in vitro* analyses of the Astrin/SKAP complex will require the production of more stable versions of the complex as well as stable soluble larger segments of the two proteins, which could not be achieved in this study because of the poor solubility of most Astrin constructs. Attempts to obtain full-length Astrin through the previously described refolding approach (Gruber et al., 2002) were unsuccessful. Future expression and purification trials may include a modification of the reported refolding approach, testing of new boundaries for truncation constructs as well as protein purification from human cell extracts.

Besides the identification of the intersubunit interaction domains, the microtubule-binding region of the Astrin/SKAP complex was mapped within SKAP to the region comprising amino acids 135 to 225 (see section 3.3.1 and 3.3.2). An updated domain organization of the Astrin/SKAP complex showing these functional domains in addition to its structural domains is presented in figure 4.1. Furthermore, the SXIP motif of SKAP, required for its interaction with EB proteins, and its adjacent Aurora B targeting site (Tamura et al., 2015; Wang et al., 2012), which are discussed in sections 4.2 and 4.3, are indicated.

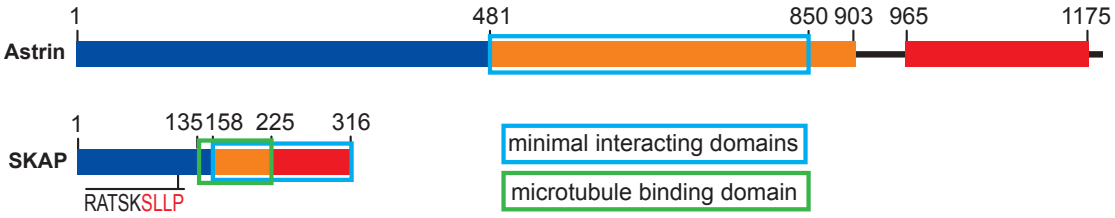

Figure 4.1: Domain organization of the Astrin/SKAP complex. In addition to the structural domain organization of the Astrin and SKAP subunits based on a bioinformatic characterization, functional domains identified in section 4 are indicated. The SXIP motif of SKAP (sequence in red) and its adjacent Aurora B consensus site (sequence in black) are indicated as well.

4.2 Interaction of the Astrin/SKAP complex with tubulin

It was proposed that the N-terminal region of SKAP, which contains the SXIP motif, mainly determines the localization of SKAP to the mitotic spindle (Tamura et al., 2015; Wang et al., 2012). However, a SKAP construct comprising amino acids 159 to 317, which lacks the SXIP motif and is supposed to be the minimal microtubule binding domain of SKAP, mediates SKAP localization to the mitotic spindle, whereas a construct encompassing amino acids 1 to 158 fails to localize to the spindle (Dunsch et al., 2011). These observations suggest that, besides binding microtubules via EB proteins, SKAP probably also contains a region for direct targeting to microtubules. There are other examples of proteins that combine a SXIP motif with a functional microtubule-binding domain, such as the mitotic centromere-associated kinesin (MCAK) (Akhmanova & Steinmetz, 2010). Indeed, in this study the microtubule-binding domain of SKAP was mapped to the region ranging from amino acid 135 to 225 (see section 3.3.2), which does not contain the SXIP motif. Since the residues 226 to 316 of SKAP are neither sufficient nor necessary for its microtubule binding (see section 3.3.1, figure 3.14, section 3.3.2, figure 3.17, and section 3.3.3, figure 3.18), the microtubule-binding domain of SKAP does not extend

to the very C-terminus as previously reported (Dunsch et al., 2011), but only to the end of its first predicted coiled-coil domain at amino acid 225. Conversely, extension towards the N-terminus up to amino acid 135 showed the highest binding affinity for microtubules with an apparent dissociation constant of around 0.58 µM (see section 3.3.3, figure 3.18). Thus, the microtubule-binding domain of SKAP extends N-terminally beyond the previously tested boundary at amino acid 157 (Dunsch et al., 2011).

In addition to SKAP, Astrin was also found to bind microtubules *in vitro* with its C-terminal region encompassing amino acids 955 to 1193 in previous studies (Schmidt et al., 2010). However, in this study, a very similar construct of Astrin ranging from amino acid 966 to 1175 showed no microtubule binding (see section 3.3.1, figure 3.15). This result is in agreement with the observation that the C-terminal segment of Astrin lacks spindle localization (Dunsch et al., 2011) and with the retained spindle localization of an Astrin construct that lacks this region (Mack & Compton, 2001). Since the N-terminal region of Astrin did not show microtubule binding either (see section 3.3.1, figure 3.15), and SKAP$^{159\text{-}316}$ exhibited an essentially identical affinity for microtubules in absence and presence of Astrin$^{482\text{-}850}$ (see section 3.3.1, figure 3.17), Astrin probably does not contribute to the microtubule binding of the Astrin/SKAP complex.

The binding sites of SKAP$^{135\text{-}225}$ on microtubules were mapped in crosslinking analyses to both the inter- and intra-tubulin dimer interface, which was confirmed by significantly decreased microtubule binding of SKAP to subtilisin-treated microtubules lacking the E-hooks of tubulin (see section 3.3.3). Interestingly, this is also the binding site of the major microtubule binder within the kinetochore, the Ndc80 complex (Alushin et al., 2010; Ciferri et al., 2008), suggesting a possible competitive behavior of SKAP and the Ndc80 complex upon microtubule binding. Indeed, in competition experiments SKAP was able to displace the Ndc80 complex from microtubules (see section 3.3.4). However, this apparent competition may not be physiologically relevant, since the kinetochore-microtubule interface provides enough space for both proteins to bind concomitantly. Thus, the significance of this observation is limited to demonstrating that SKAP and the Ndc80 complex bind to at least partly overlapping binding sites on microtubules. The observation that SKAP was not able to displace the Ndc80 complex completely in fluorescence microtubule flow cell experiments, while it did so at the very high concentrations used in the microtubule cosedimentation assay, suggests that SKAP may bind to the intra- and inter-tubulin interface with different affinities. SKAP binding to one interface of tubulin

might occur with higher affinity, so that SKAP is able to displace the Ndc80 complex from this interaction site, whereas its binding to the other interface may be much weaker and have less effect on Ndc80 binding, so that the competition at this site only gets detectable upon very high SKAP concentrations. Such a binding mode with two distinct binding sites of different affinity would facilitate a fine-tuning in the establishment of kinetochore-microtubule attachments, which may additionally be regulated by other factors or binding partners. The weaker binding to one interface might also be artificially created by the presence of the N-terminal mCherry-tag. In microtubule cosedimentation assays, the apparent dissociation constant of mCherry-SKAP$^{135-225}$ was basically identical to the one of untagged SKAP$^{135-225}$ (~0.8 µM for mCherry-SKAP$^{135-225}$ compared to ~0.6 µM for untagged SKAP$^{135-225}$), but the maximal bound fraction was reduced from ~1.0 to ~0.7, indicating that the tag may have some effect on microtubule binding. To test the influence of the mCherry-tag, SKAP$^{135-225}$ can be terminally labeled with a small dye via the sortase labeling approach instead of a large fusion protein, so that a possible steric hindrance can be excluded.

It was shown by mutational analyses *in vitro* and *in vivo* that microtubule binding of SKAP$^{135-225}$ requires several conserved positively charged residues including K140, K149, K161, K164, K168 and K170 (see section 3.3.5). Since a construct comprising amino acids 135 to 174, which contains all identified residues, as well as another construct ranging from amino acid 175 to 225 were not able to retain microtubule binding of SKAP (see section 3.3.5, figure 3.28), SKAP may possess a multipartite mode of microtubule binding, in which several residues are involved in addition to the identified ones. Such a multipartite binding mode may suggest the existence of several binding site on microtubules that SKAP binds to with different affinities as discussed above.

Depletion of SKAP by RNA interference revealed several spindle and chromosome alignment defects including a significant increase in the occurrence of multipolar spindles, the presence of pseudo-metaphase states with multiple misaligned chromosomes and a concomitant increase of the mitotic index indicating SAC activation (see section 3.3.5, figure 3.31, table 3.8). These experiments confirm the previously described phenotypes observed upon SKAP depletion (Gruber et al., 2002; Thein et al., 2007; Fang et al., 2009; Schmidt et al., 2010; Manning et al., 2010; Dunsch et al., 2011). In this study, it was shown that the ability of SKAP to exert its function in spindle organization and mitotic progression corresponds with the number of inserted mutations and thus with its ability to bind to microtubules. Thus,

this work demonstrates that SKAP contains a *bona fide* microtubule-binding domain, whose functional inactivation prevents rescuing the significant defects in spindle formation, chromosome congression and mitotic progression that are caused by depletion of SKAP.

It was demonstrated that SKAP is not only able to bind to microtubules, but also to tubulin in solution (see section 3.3.6, figures 3.32 and 3.33). Different assays pointed to the ability of $SKAP^{135-225}$ to promote tubulin polymerization by facilitating the nucleation and increasing the growth rates of microtubules, while the introduction of mutations, and thereby the reduction of its microtubule binding affinity, severely impairs these effects (see section 3.3.6, figures 3.34 and 3.35). The influence of SKAP on microtubule nucleation is a possible reason for its localization to centrosomes in early mitosis (Mack & Compton, 2001; Thein et al., 2007). SKAP may be part of the pericentriolar material that contains a network of proteins surrounding the centrosomes, including microtubule nucleation factors, such as the γ-tubulin ring complex (Moritz et al., 1995; Morgan, 2007). Here, it may assist in the nucleation of microtubules in prophase and prometaphase and subsequently facilitate the growth of the emerging microtubules by incorporating new α-/β-tubulin dimers in the microtubule lattice in a non-catalytic manner, which depends on the direct interaction of SKAP with the tubulin dimer.

Furthermore, it was shown that $SKAP^{135-225}$ assembles tubulin to cold stable microtubule bundles (see section 3.3.6, figures 3.36 to 3.38), which may be due to the multipartite binding mode of SKAP and its ability to form trimers. The microtubule stabilizing and bundling effect of SKAP may explain the importance of the Astrin/SKAP complex for spindle organization and its localization to the spindle midzone in anaphase and telophase (Mack & Compton, 2001), where it may assist in organizing the bipolar spindle by bundling interpolar microtubules. The key microtubule crosslinking proteins in mitosis are the motor proteins kinesin-5 and kinesin-14 that link interpolar, antiparallel microtubules (Peterman & Scholey, 2009; Morgan, 2007). Kinesin-5 slides the microtubules outwards apart from each other, thereby opposing the function of kinesin-14 that pulls the microtubules together. Also non-motor proteins have been identified to associate with the spindle midzone. After chromosome segregation, members of the Ase1p family of microtubule-associated proteins assist in organization of the spindle midzone and in spindle elongation in anaphase B (Schuyler et al., 2003; Peterman & Scholey, 2009). Like SKAP, these Ase1p proteins possess a microtubule-binding domain and coiled-coil domains, show oligomerization and are able to bundle microtubules. Thus, SKAP may participate in

the protein network at the spindle midzone that ensures maintenance of the spindle bipolarity and spindle elongation during anaphase. To test this hypothesis, live cell imaging of SKAP-depleted cells expressing GFP-SKAP wild type or mutants impaired in microtubule binding may be used to see whether these cells show a similar spindle collapse in anaphase as Ase1p-depleted cells (Schuyler et al., 2003). Also, in GFP-SKAP expressing cells, the localization of SKAP to the spindle midzone can be analyzed in more detail, and it can be tested in FRAP or photoactivation experiments whether SKAP shows similar diffusion properties along microtubules as Ase1p, with slower diffusion between crosslinked microtubules and faster diffusion on single microtubules (Schuyler et al., 2003). More detailed EM analysis on the microtubule bundles that form in the presence of SKAP may elucidate whether SKAP preferentially bundles parallel or antiparallel microtubules. In addition, cryo EM studies of SKAP and microtubules, as described in the optimized approach for studying the interaction of EB proteins with microtubules (Zhang et al., 2015), may be used to analyze how SKAP modulates the microtubule structure to achieve a stabilizing effect apart from microtubule bundling. The previously reported results that the stability of the microtubule lattice seems to be mainly regulated at the longitudinal inter-tubulin dimer interface (Alushin et al., 2014; Zhang et al., 2015) are in agreement with targeting of this interface by SKAP. SKAP may reverse the microtubule lattice compaction, which takes place upon GTP hydrolysis, and thereby release the destabilizing strain, similar to the effect observed for taxol. Alternatively, SKAP may stabilize microtubules in their compacted form by balancing the destabilizing tension through its binding. SKAP may even promote the microtubule lattice compaction, as observed in presence of EB proteins, and thereby induce fast GTP hydrolysis.

The identified microtubule-binding domain of SKAP presumably cooperates with the SXIP motif that targets the Astrin/SKAP complex to growing microtubule plus ends (Dunsch et al., 2011; Wang et al., 2012, Tamura et al., 2015). A possible functional significance of the combination of these binding motifs is that a specific function of the microtubule-binding domain is delivered specifically or preferentially to the plus ends of microtubules. The microtubule-binding domain of SKAP stabilizes microtubules and favors their growth *in vitro* (see section 3.3.6) and it is possible that this is the crucial activity of the Astrin/SKAP complex that needs to be delivered to plus ends of microtubules and to kinetochores. The hypothesis that the microtubule-binding domain of SKAP cooperates with the SXIP motif could be tested in tip tracking experiments with GFP-SKAP wild type and mutants as well as by

comparison of the microtubule localization of these constructs combined with a SXIP mutant that lacks EB interaction. These experiments are currently in progress.

Taken together, this work shows that SKAP bundles microtubules *in vitro* and points towards the ability of SKAP to nucleate the polymerization of microtubules and to favor microtubule growth. Thus, SKAP may be a microtubule-stabilizing factor with effects on nucleation and growth of microtubules explaining its functions in spindle organization and stabilization of kinetochore-microtubule attachments. The exact molecular mechanisms underlying the effects of SKAP on microtubules, which may include a conformational change within the microtubule lattice upon SKAP binding, will need to be clarified.

4.3 Kinetochore recruitment of the Astrin/SKAP complex

The conversion from the initial lateral attachments to the final end-on attachments requires a highly dynamic kinetochore-microtubule interface. Several proteins that are initially present at kinetochores before the establishment of kinetochore-microtubule attachments are released from kinetochores upon initial microtubule attachment, including the RZZ complex and its associated proteins Spindly and dynein/dynactin (Karess, 2005), or during conversion from lateral to end-on attachment, such as the microtubule depolymerases MCAK and Kif2b (Manning et al., 2010). Other proteins, like the Astrin/SKAP complex and the Ska complex, are only recruited to attached kinetochores and seem to play a role in the final stabilization of end-on attachment before anaphase onset (Thein et al., 2007; Fang et al., 2009; Schmidt et al., 2010; Dunsch et al., 2011; Hanisch et al., 2006). Aurora B was found to regulate this localization pattern, because it contributes to the recruitment of early kinetochore components and prevents the recruitment of late kinetochore components until it is spatially separated from its substrates, probably due to an increased intra-kinetochore tension upon establishment of biorientation (Liu et al., 2009). This is in agreement with the well-established function of Aurora B in the correction of erroneous kinetochore-microtubule attachments and in the establishment of chromosome biorientation (Carmena et al. 2012).

The NetPhos 2.0 server (Blom et al., 1999) predicts 14 potential phosphorylation sites on SKAP (9 serine and 5 threonine sites), including two Aurora B consensus sites with the motif (R/K)-X-(S/T) at threonines 16 and 108. For Astrin, 68 phosphorylation sites (53 serine and 15 threonine sites) are predicted, including 11 potential Aurora B consensus sites. These possible Aurora B targeting sites of

Astrin and SKAP are listed in table 4.1. Since they only amount to a small fraction of all potential phosphorylation sites, it may be that the localization pattern of the Astrin/SKAP complex is not only regulated by Aurora B, but also by other kinases, such as glycogen synthase kinase 3β (Cheng et al., 2008) and Aurora A (Chiu et al., 2014). Since the Aurora B consensus sites mainly lie outside the minimal kinetochore localization domains of Astrin and SKAP, Aurora B probably also regulates other functions of the Astrin/SKAP complex, such as fine-tuning of its microtubule-binding affinities or the binding to other interaction partners. *In vitro* kinase assays, in case of successful production of longer Astrin and SKAP constructs, or mass spectrometric analysis of the proteins purified from human cell extracts using appropriate antibodies may point to the sites that are indeed physiologically relevant.

Table 4.1: Potential Aurora B phosphorylation sites of SKAP and Astrin. Phosphorylation sites were predicted by the NetPhos 2.0 server (Blom et al., 1999). Potentially phosphorylated residues are indicated in bold type.

protein	site	sequence	score
SKAP	Thr16	VFRT**T**WLST	0.828
	Thr108	QTRA**T**SKSL	0.965
Astrin	Ser8	VKKL**S**LSLS	0.948
	Ser21	TGKP**S**MRTP	0.698
	Ser43	SGKR**S**PACS	0.933
	Ser115	TPKT**S**EEAV	0.991
	Ser183	GDRF**S**EVAA	0.981
	Ser289	HPKE**S**ETED	0.994
	Ser362	NLRQ**S**LSLP	0.840
	Ser411	GTKH**S**TSET	0.995
	Ser490	HLKE**S**HEMG	0.924
	Ser597	SQRI**S**QLEQ	0.996
	Ser1154	NLRR**S**DKEL	0.998

The kinetochore localization of the Astrin/SKAP complex was suggested not only to depend on Aurora B activity, but also on the presence of microtubules, since in cells that were treated with the microtubule-depolymerizing drug nocodazole as well as the Aurora B inhibitor ZM447493, SKAP was not detected at kinetochores (Schmidt et al., 2010). Confirming the dependency of the kinetochore localization of SKAP on

Aurora B, it was shown in this study that in cells treated with the proteasome inhibitor MG132 as well as the Aurora B inhibitor Hesperadin, SKAP exhibited a small but significant increase in kinetochore localization and also localized to unattached kinetochores (see section 3.4.1, figure 3.39). This observation indicates that Aurora B indeed counteracts the kinetochore localization of SKAP. In agreement with previously described results (Schmidt et al., 2010), SKAP localization at kinetochores was lost in the presence of the microtubule-depolymerizing drug nocodazole. On the other hand, contradicting former observations (Schmidt et al., 2010), when cells were treated with both nocodazole and Hesperadin, the localization of SKAP could be restored to about 50 %, suggesting that SKAP is also able to localize to kinetochores in the absence of microtubules. Thus, not only the attachment to microtubules brings SKAP to kinetochores, but there has to be an additional kinetochore receptor for SKAP.

The KMN network was suggested to be required for the kinetochore localization of SKAP, since depletion of subunits of the Ndc80 complex or the Mis12 complex significantly decreases SKAP levels at the kinetochore (Wang et al., 2012). In yeast two-hybrid experiments, immunoprecipitations and GST pull-downs, a direct interaction of SKAP with the Dsn1 and the Nsl1 subunits of the Mis12 complex was found (Wang et al., 2012). However, this reported interaction could not be verified in this study, since SKAP and the Mis12 complex did not show binding in GST pull-downs or size exclusion chromatography experiments (see section 3.4.2, figures 3.40 to 3.42). The MST experiments with $SKAP^{159-316}$, the Mis12 complex and the Ndc80 complex indicated interactions between SKAP and both complexes with similar dissociation constants in the nM range (see section 3.4.2, figure 3.44). Since these binding affinities are typical of very tight interactions, it would have been expected to observe binding of SKAP to the Mis12 and the Ndc80 complexes also in other binding assays, which instead was not the case. Therefore, we suspect that the MST experiments may not show real interactions, but only effects on changes in the hydration of the fluorescent probes that are probably not a direct cause of binding events, but of an altered surrounding upon addition of the unlabeled molecules. A similar discrepancy was observed during studies of the interaction between the Ndc80 complex and the Mis12 complex. This interaction was previously shown to be very tight with a dissociation constant of about 10 nM (Petrovic et al., 2010), but MST failed to detect it (see supplementary figure 6.17). Therefore, these observations suggest a cautious interpretation of binding data obtained from a single approach. Furthermore, GST pull-down, size exclusion chromatography and MST experiments

with SKAP$^{159-316}$ and Zwint suggested an interaction of SKAP and Zwint both on solid and phase in solution (see section 3.4.2, figures 3.40, 3.43 and 3.44). Since the observed interaction of SKAP and Zwint appeared to be weaker in the presence of the Zwint-interacting partner Knl1, the detected binding was probably due to an artificial coiled-coil interaction.

To identify other possible binding partners of the Astrin/SKAP complex, the complex and bound interacting partners can be enriched from human cell extracts, by using pull-down experiments with appropriate antibodies, and subsequently analyzed by mass spectrometry. Subsequent *in vitro* analysis of the interactions between the Astrin/SKAP complex and the detected proteins can be used to validate the identified hits.

Taken together, it was shown that the kinetochore localization of the Astrin/SKAP complex depends only marginally on the presence of microtubules as previously reported. No defined kinetochore receptor could be identified, suggesting that the recruitment of the Astrin/SKAP complex to kinetochores may rely on several weak interactions that are difficult to detect by *in vitro* studies. Therefore, fully reconstituted kinetochores may be necessary to further analyze the kinetochore recruitment of the Astrin/SKAP complex.

4.4 Structural characterization of the Astrin/SKAP complex

To gain an even deeper understanding of the function of the Astrin/SKAP complex and its underlying molecular mechanisms, it would be useful to obtain structural information of the Astrin/SKAP complex. First efforts into this direction are described in section 3.5 and are currently being continued.

It was shown by negative stain EM that the Astrin$^{482-850}$/SKAP$^{159-316}$ complex exhibits a highly elongated structure with a length of about 40-50 nm (see section 3.5.1). This is consistent with the previously reported rotary shadowing EM analysis of full-length Astrin refolded from bacterial inclusion bodies revealing an 80 nm ‘lollipop’ structure with a 35 nm central coiled-coil domain (Gruber et al., 2002). The presence of ring-like structures may suggest that the Astrin$^{482-850}$/SKAP$^{159-316}$ complex is able to form higher order structures, which is in agreement with previously reported oligomerization of Astrin (Gruber et al., 2002). As SKAP was shown to bundle

microtubules, or other components of the kinetochore, the ability of the Astrin/SKAP complex to oligomerize may contribute to its function in crosslinking microtubules. The high flexibility of the Astrin$^{482-850}$/SKAP$^{159-316}$ complex hampered further single particle analysis. Attempts to reduce its flexibility by binding the complex to microtubules were not successful because decoration of microtubules was unsuccessful. This was probably due to the low affinity of the Astrin$^{482-850}$/SKAP$^{159-316}$ complex for microtubules, which being in the low µM range may be too weak to achieve microtubule binding under conditions suitable for EM analysis. A crosslinking approach, in which the Astrin/SKAP complex is bound to microtubules at higher protein concentrations and subsequently crosslinked, may help to obtain decorated microtubules and to reveal the binding mode of the Astrin/SKAP complex. However, obtained results have to be critically evaluated because of potential artifacts due to the crosslinking reagent.

In order to get insight into the atomic structure of SKAP, attempts were made to solve the structure of truncated SKAP constructs by means of X-ray crystallography. Different SKAP constructs, including SKAP$^{135-225}$ wild type and a seleno-methionine version, the sextuple mutant SKAP$^{135-225}$ K140/149/161/164/168/170A as well as SKAP$^{159-225}$, were successfully crystallized by the vapor diffusion method with sitting and hanging drops (section 3.5.2). The subsequent diffraction analysis resulted in several data sets with a resolution up to 2.9 Å revealing a tetragonal space group - either $P4_1$ 2 2 or $P4_3$ 2 2 - of the crystals, with two short axes and one long axis. Such a highly elongated unit cell is consistent with the predicted coiled-coil structure of SKAP. However, attempts to solve the structure by isomorphous replacement were hampered by problems with high anisotropic diffraction and insufficient resolution and phasing power of the derivative data. Efforts to solve the structure of SKAP$^{135-225}$ by molecular replacement failed because of protein degradation of a mCherry-SKAP$^{135-225}$ fusion protein during the crystallization process and insufficient quality of the crystals obtained for the SKAP$^{135-225}$/tubulin/RB3 complex. In order to solve the crystal structure of SKAP, several efforts are currently in progress to further optimize the obtained crystals. A diffraction test at room temperature can show whether the obtained crystals reveal a better diffraction before cryo-cooling. If this is the case, the conditions for cryo-cooling can be further improved by testing other cryoprotectants. Furthermore, since SKAP and EB1 are supposed to interact directly (Wang et al., 2012; Tamura et al., 2015), it can be tested whether a SKAP construct containing the SXIP motif, such as the soluble SKAP$^{103-225}$, forms a tight complex

with EB1 that can be purified. Crystals of such an SKAP/EB1 complex could be later used to solve the structure of SKAP by molecular replacement.

Taken together, no atomic structure of SKAP or the Astrin/SKAP complex could be obtained, but a promising step towards the crystal structure of SKAP could be achieved by successful crystallization of different SKAP constructs. Further attempts to optimize the diffraction properties of the obtained crystals are currently in progress.

4.5 Physiological functions of the Astrin/SKAP complex in mitosis

Considering together all results, including those reported previously and those in this study, the diverse physiological functions of the Astrin/SKAP complex in mitosis may be summarized as follows:

Prior to mitosis, the Astrin/SKAP complex is recruited to centrosomes, through a possible interaction with Ninein during the S and G2 phases (Cheng et al., 2007), and may act as part of the pericentriolar material to assist in maintaining centrosome integrity. In early mitosis, the Astrin/SKAP complex may facilitate the nucleation of microtubules together with other nucleating factors, such as the γ-tubulin ring complex. By subsequent dissociation from Ninein and following binding to the emerging microtubules, the Astrin/SKAP complex may stabilize the growing microtubules and promote their polymerization by incorporating new α-/β-tubulin dimers in the microtubule lattice. Interaction with EB proteins via the SXIP-motif of SKAP recruits the Astrin/SKAP complex to microtubule plus ends, where it may further regulate microtubule dynamics by favoring their growth rate. Upon the establishment of chromosome biorientation, when the outer kinetochore components are spatially separated from the reach of the Aurora B kinase due to increasing intrakinetochore stretch, the Astrin/SKAP complex is recruited to kinetochores, possibly through multiple weak interactions, e.g. with KMN network components, in combination with its microtubule plus end binding. At kinetochores, the Astrin/SKAP complex may assist in the stabilization of proper end-on attachments together with other microtubule binders, such as the Ndc80 complex and the Ska complex, possibly by replacing a microtubule destabilizing Kif2b/CLASP1 complex with a stabilizing Astrin/CLASP1 complex (Manning et al., 2010). Thereby, the Astrin/SKAP

complex may help to ensure that kinetochore-microtubule attachments are robust enough to keep the kinetochores bound to the depolymerizing microtubule ends during anaphase. In addition, an interaction of the Astrin/SKAP complex with dynein may promote dynein-mediated transport of kinetochore components from microtubule plus ends toward spindle poles, which takes place upon microtubule attachment (Dunsch et al., 2011). After anaphase onset, the Astrin/SKAP complex may also participate in the protein network at the spindle midzone, together with kinesin-5, kinesin-14 and members of the Ase1p family, in order to ensure maintenance of the spindle bipolarity by bundling interpolar microtubules.

In summary, the work described in this thesis provides a first thorough *in vitro* analysis of the structure and function of the 2-subunit Astrin/SKAP complex. By using a combinatorial approach including biochemical, biophysical, cell biological and structural methods, the Astrin/SKAP complex was identified as a microtubule-stabilizing factor with effects on nucleation and growth of microtubules, explaining its functions in spindle organization and stabilization of kinetochore-microtubule attachments. Thereby, this work significantly advances our understanding of the functional role of the Astrin/SKAP complex during mitosis and the mechanisms leading to the establishment of functional end-on attachments.

5 MATERIALS AND METHODS

5.1 Materials

5.1.1 Chemicals

Table 5.1: List of used chemicals.

manufacturer	chemical
Applichem, Darmstadt, DE	acrylamide/bisacrylamide (37.5:1, 30 %), ammonium sulfate, ethylene glycol-bis-(β-aminoethyl ether)-N,N,N',N'-tetraacetic acid (EGTA), hydrochloric acid, L-glutathione reduced, magnesium chloride, piperazine-N,N'-bis(2-ethanesulfonic acid (PIPES)
BioRad, Hercules, US-CA	gel filtration standard, Precision Plus Protein Standard
Calbiochem, Darmstadt, DE	MG132, Mowiol
Cytoskeleton, Inc., Denver, US-CO	bovine brain α-/β-tubulin, porcine α-/β-tubulin
Fluka Analytical, Buchs, CH	polyethylene glycol (PEG) 200, PEG 6000, PEG 8000
GE Healthcare, Piscataway, US-NJ	Glutathione Sepharose 4 Fast Flow
Gerbu, Gaiberg, DE	ampicillin, 1,4-dithioerythritol (DTE), ethylenediamine tetraacetic acid disodium salt (EDTA), glycerol
GIBCO, Carlsbad, US-CA	penicillin, streptomycin
Gold Biotechnologie, St. Louis, US-MO	4-(2-Aminoethyl) benzenesulfonyl fluoride (AEBSF)
HellmaAnalytics, Müllheim, DE	Hellmanex III
Invitrogen, Carlsbad, US-CA	blasticidin, hygromycin, Sf-900 III SFM serum free medium complete, SYBRSafe DNA gel stain
J.T.Baker, Deventer, NL	2-propanol, sodium hydroxide
Life Technologies, Carlsbad, US-CA	AccuPrime Pfx DNA Polymerase, ECL western blotting substrate
Lonza, Rockland, US-ME	agarose
Merck, Darmstadt, DE	imidazole
New England Biolabs, Ipswich, US-MA	bovine serum albumin (BSA), Crimson Taq Polymerase, Q5 High Fidelity 2x Master Mix, restriction enzymes, T4 DNA ligase

Table 5.1 (continued): List of used chemicals.

manufacturer	chemical
Nippon Genetics EUROPE GmbH, Dueren, DE	Midori Green advanced DNA stain
Promega, Fitchburg, US-WI	FuGENE HD Transfection Reagent
Qiagen, Hilden, DE	HyPerFect transfection reagent, JCSG Core I-IV
Roth, Karlsruhe, DE	glycine, 2-(4-(2-hydroxyethyl)-1-piperazinyl)-ethanesulfonic acid (HEPES), isopropyl-β-D-1-thiogalactopyranoside (IPTG), milk powder, tris(hydroxymethyl)-aminomethane (Tris)
Serva Electrophoresis GmbH, Heidelberg, DE	ammonium persulfate, β-mercaptoethanol, bromphenol blue, coomassie brilliant blue R-250/G-250, DAPI, L-seleno-methionine, phenylmethyl sulfonyl fluoride (PMSF), protease inhibitor mix HP PLUS, sodium dodecyl sulfate (SDS), N,N,N',N'-tetramethylethylenediamine (TEMED), Tween-20, X-Gal
Sigma-Aldrich, St. Louis, US-MO	acetic acid, acetonitril (ACN), doxycycline, methanol, PEG 3350, poly-L-lysine, Ponceau S, subtilisin A
Thermo Fisher Scientific, Waltham, US-MA	Coomassie Protein Assay Reagent (Bradford solution), ethanol, GeneRuler 1 kb Plus DNA Ladder
VWR International, West Chester, US-PA	sodium chloride

5.1.2 Instrumentation

Table 5.2: List of used instruments.

instrument	model	manufacturer
centrifuges	Avanti J-20XP	Beckman Coulter, Palo Alto, US-CA
	Eppendorf Centrifuge 5424/5810 R	Eppendorf, Cologne, DE
	Hettich Universal 320R	Hettich Lab Technology, Tuttlingen, DE
	Sorvall RC3BP+	Thermo Fisher Scientific, Waltham, US-MA

Table 5.2 (continued): List of used instruments.

instrument	model	manufacturer
columns	GSTrap FF 5 ml HiLoad 16/600 Superdex 200 pg HisTrap FF 5 ml HiTrap Q FF 5 ml Superdex 200 5/150 GL Superose 6 10/300 GL Superose 6 prep grade XK 16/70 Superose 6 Tricorn 5/150 GL	GE Healthcare, Piscataway, US-NJ
concentrators	Amicon Ultra-15 Ultracel-10k/30k Vivacell 250, 10 000 MWCO inserts	Millipore, Billerica, US-MA Sartorius Stedim Biotech, Goettingen, DE
dialysis tubes	Snake Skin Dialysis Tubing, MWCO: 3.5 kDa, 7 kDa	Thermo Fisher Scientific, Waltham, US-MA
ESI-MS	Finnigan LCQ Advantage MAX	Thermo Fisher Scientific, Waltham, US-MA
FPLC instruments	ÄKTA Prime Plus ÄKTA Purifier ÄKTA Micro	GE Healthcare, Piscataway, US-NJ
imager for crystallization screens	Rock Imager 1000	Formulatrix, Waltham, US-MA
incubators	BD 53 Minitron	Binder, Tuttlingen, DE Infors-HAT, Bottmingen, CH
microscopes	DeltaVision Elite imaging system 3i Marianas system VisiTIRF Fluorescence Imaging System	Applied Precision, Issaquah, US-WA Intelligent Imaging Innovations, Göttingen, DE Visitron Systems GmbH, Puchheim, DE
NanoDrop spectrophotometer	ND-1000 Spectrophotometer	peQLab, Erlangen, DE

Table 5.2 (continued): List of used instruments.

instrument	model	manufacturer
nanoliter high-throughput robot	Mosquito	TPP LabTech, Melbourne, GB
PCR-Thermocycler	TProfessional TRIO Thermocycler	Biometra, Goettingen, DE
pH meter	pHenomenal pH 1000 L	VWR International, West Chester, US-PA
plate reader	POLARstar Omega	BMG Labtech, Ortenberg, DE
rotors	JA-30.50 Ti TLA 100.1 H6000A/HBB6	Beckman Coulter, Palo Alto, US-CA Thermo Fisher Scientific, Waltham, US-MA
SDS-PAGE	Mini-PROTEAN Tetra Cell NuPAGE SDS-PAGE gel system	BioRad, Hercules, US-CA Life Technologies, Carlsbad, US-CA
spectrophotometer	Bio Photometer	Eppendorf, Hamburg, DE
Stopped-Flow	SX.18MV-R	Applied Photophysics, Surrey, GB
thermomixer	Thermomixer comfort	Eppendorf, Köln, DE
ultracentrifuge	Beckman Optima L-70K	Beckman Coulter, Palo Alto, US-CA

5.1.3. Common used buffers and media

Table 5.3: Composition of common used buffers and media.

buffer/medium	composition
BRB80	80 mM Pipes 1 mM $MgCl_2$ 1 mM EGTA pH 6.8
DNA loading buffer	30 % (w/v) sucrose 20 % (v/v) glycerol 0.2 % (w/v) orange G

Table 5.3 (continued): Composition of common used buffers and media.

buffer/medium	composition
LB medium	0.5 % (w/v) yeast extract 1 % (w/v) trypton 1 % (w/v) NaCl pH 7.4 with NaOH
MES buffer	50 mM MES 50 mM Tris 0.1 % (w/v) SDS 1 mM EDTA pH 7.3
M9 minimal medium	50 mM Na_2HPO_4 x 2 H_2O 20 mM KH_2PO_4 10 mM NaCl 20 mM NH_4Cl 1 mM $MgSO_4$ 0.4 % (w/v) glucose 0.1 mM $CaCl_2$
PBS	137 mM NaCl 2.7 mM KCl 10 mM Na_2HPO_4 2 mM KH_2PO_4 pH 7.4
SDS-PAGE loading buffer (5x)	0.25 M Tris-HCl, pH 6.8 15 % (w/v) SDS 50 % (v/v) glycerol 25 % (v/v) β-mercaptoethanol 0.01 % (w/v) bromophenol blue
SDS-PAGE running buffer (10x)	0.25 M Tris-HCl 2 M glycine 1 % (w/v) SDS
SDS-PAGE separating buffer (4x)	1.5 M Tris-HCl, pH 8.8 0.4 % (w/v) SDS
SDS-PAGE stacking buffer (4x)	0.5 M Tris-HCl, pH 6.8 0.4 % (w/v) SDS

Table 5.3 (continued): Composition of common used buffers and media.

buffer/medium	composition
SDS-PAGE staining solution	0.5 % (w/v) coomassie brillant blue R-250 0.5 % (w/v) coomassie brillant blue G-250 7.5 % (v/v) acetic acid 50 % (v/v) ethanol
TAE buffer	40 mM Tris, pH 8.0 20 mM acetic acid 1 mM Na_2EDTA
TB medium	2.4 % (w/v) yeast extract 1.2 % (w/v) trypton 0.4 % (v/v) glycerol 17 mM KH_2PO_4 72 mM K_2HPO_4
TBS-T	20 mM Tris-HCl 150 mM NaCl 0.1 % (v/v) Tween-20
Western blot transfer buffer	25 mM Tris-HCl 200 mM glycine 20 % (v/v) methanol

5.1.4. Cell strains

Table 5.4: List of used cell strains.

cell strain (manufacturer)	genotype	manufacturer
BL21-CodonPlus (DE3)-RIL	*E. coli* B F^- *ompT hsdS*(r_B^- m_B^-) *dcm*$^+$ Tet^r *gal* λ(DE3) *endA* Hte [*argU ileY leuW* Cam^r]	Stratagene
One Shot OmniMAX 2-T1	*E. coli* F' {*pro*AB^+ *lacI*^{q} *lacZ*ΔM15 *Tn*10(Tet^R) Δ(*ccd*AB)} *mcr*A Δ(*mrr-hsd*RMS-*mcr*BC) ϕ80(*lacZ*)ΔM15 Δ(*lac*ZYA-*arg*F) U169 *end*A1 *rec*A1 *sup*E44 *thi*-1 *gyr*A96 *rel*A1 *ton*A *pan*D	Invitrogen
OverExpress C41(DE3)	*E. coli* F^- *ompT hsdS*$_B$(r_B^- m_B^-) *gal dcm* (DE3)	Lucigen
Rosetta 2(DE3)	*E. coli* F^- *ompT hsdS*$_B$(r_B^- m_B^-) *gal dcm* (DE3) pRARE2 (Cam^R)	Novagen

5.1.5. Expression vectors

All plasmids come from the Max Planck Institute of Molecular Physiology, Dortmund, department of mechanistic cell biology. Plasmids #1-46, #71-76, #86-89 and #119-128 originate from codon-optimized DNA sequences (Invitrogen, Carlsbad, US-CA), plasmids # 47-70, # 78-85 and # 90-111 from cDNA library sequences.

Table 5.5: List of used plasmids. h: human

plasmid #	expressed protein	vector
1	hAstrin f.l.	pST50Trc2-HISDHFR
2	hAstrin f.l.	pST50Trc2-HISNDHFR
3	hAstrin f.l.	pST50Trc2-DHFRHIS
4	hAstrin f.l.	pST50Trc3-HISDHFR
5	hSKAP f.l.	pST50Trc2-HISDHFR
6	hSKAP f.l.	pST50Trc2-HISNDHFR
7	hSKAP f.l.	pST50Trc2-DHFRHIS
8	hSKAP f.l.	pST50Trc3-HISDHFR
15	hAstrin f.l.	pGEX-6p-2rbs
16	hSKAP f.l.	pGEX-6p-2rbs
17	hAstrin f.l. (MCS1) + hSKAP f.l. (MCS2)	pGEX-6p-2rbs
18	hSKAP f.l. (MCS1) + hAstrin f.l. (MCS2)	pGEX-6p-2rbs
19	His_6-hAstrin f.l. + hSKAP f.l.	pST50Trc2-HISDHFR
20	His_6-TEV-hAstrin f.l. + hSKAP f.l.	pST50Trc2-HISNDHFR
21	His_6-hSKAP f.l. + hAstrin f.l.	pST50Trc2-HISDHFR
22	His_6-TEV-hSKAP f.l. + hAstrin f.l.	pST50Trc2-HISNDHFR
23	$hAstrin^{1-481}$	pGEX-6p-2rbs
24	$hAstrin^{1-239}$	pGEX-6p-2rbs
25	$hAstrin^{482-850}$	pGEX-6p-2rbs
26	$hAstrin^{482-903}$	pGEX-6p-2rbs
27	$hAstrin^{996-1175}$	pGEX-6p-2rbs
28	$hAstrin^{482-1175}$	pGEX-6p-2rbs
29	$hSKAP^{1-158}$	pST50Trc2-HISDHFR
30	$hSKAP^{1-225}$	pST50Trc2-HISDHFR
31	$hSKAP^{159-316}$	pST50Trc2-HISDHFR
32	$hSKAP^{159-225}$	pST50Trc2-HISDHFR
33	$hSKAP^{226-316}$	pST50Trc2-HISDHFR

Table 5.5 (continued): List of used plasmids. h: human

plasmid #	expressed protein	vector
34	hAstrin$^{482-850}$ (MCS1) + hSKAP$^{159-316}$ (MCS2)	pGEX-6p-2rbs
35	hAstrin$^{482-903}$ (MCS1) + hSKAP$^{159-316}$ (MCS2)	pGEX-6p-2rbs
36	hAstrin$^{482-1175}$ (MCS1) + hSKAP$^{159-316}$ (MCS2)	pGEX-6p-2rbs
37	hAstrin$^{1-850}$	pGEX-6p-2rbs
38	hAstrin$^{1-903}$	pGEX-6p-2rbs
39	hAstrin f.l.	pFH
40	hSKAP f.l.	pFH
41	hAstrin$^{482-850}$	pFH
42	hAstrin$^{482-903}$	pFH
43	hAstrin$^{482-1175}$	pFH
44	hAstrin$^{1-850}$	pFH
45	hAstrin$^{1-903}$	pFH
46	hAstrin$^{955-1193}$	pGEX-6p-2rbs
47	hAstrin f.l.	pGEX-6p-2rbs
48	hSKAP f.l.	pGEX-6p-2rbs
49	hDYNLL1 f.l.	pGEX-6p-2rbs
50	hAstrin f.l. (MCS1) + hSKAP f.l. (MCS2)	pGEX-6p-2rbs
51	hAstrin f.l. (MCS1) + hDYNLL1 f.l. (MCS2)	pGEX-6p-2rbs
52	hSKAP f.l. (MCS1) + hAstrin f.l. (MCS2)	pGEX-6p-2rbs
53	hSKAP f.l. (MCS1) + hDYNLL1 f.l. (MCS2)	pGEX-6p-2rbs
54	hDYNLL1 f.l. (MCS1) + hAstrin f.l. (MCS2)	pGEX-6p-2rbs
55	hDYNLL1 f.l. (MCS1) + hSKAP f.l. (MCS2)	pGEX-6p-2rbs
57	hSKAP f.l.	pFH
58	hDYNLL1 f.l.	pFH
59	hSKAP$^{1-158}$	pGEX-6p-2rbs
60	hSKAP$^{159-225}$	pGEX-6p-2rbs
61	hSKAP$^{159-316}$	pGEX-6p-2rbs
62	hSKAP$^{226-316}$	pGEX-6p-2rbs
63	hAstrin f.l.	pFH
64	hSKAP$^{159-316}$	pFH
65	hSKAP$^{146-225}$	pGEX-6p-2rbs
66	hSKAP$^{135-225}$	pGEX-6p-2rbs
67	hSKAP$^{120-225}$	pGEX-6p-2rbs
68	hSKAP$^{103-225}$	pGEX-6p-2rbs

Table 5.5 (continued): List of used plasmids. h: human

plasmid #	expressed protein	vector
69	hSKAP$^{74-225}$	pGEX-6p-2rbs
70	hSKAP$^{46-225}$	pGEX-6p-2rbs
71	GST-hAstrin$^{482-850}$	pFL
72	hAstrin$^{482-850}$-His$_6$	pFL
73	hSKAP$^{159-316}$	pFL
74	hSKAP$^{159-316}$-His$_6$	pFL
75	GST-hSKAP f.l.	pFL
76	hSKAP$^{159-316}$ (MCS1) + hAstrin$^{482-850}$-His$_6$ (MCS2)	pFL
78	hSKAP$^{135-225}$ L189M	pGEX-6p-2rbs
79	hSKAP$^{135-225}$ L210M	pGEX-6p-2rbs
80	hSKAP$^{135-225}$ L189/210M	pGEX-6p-2rbs
81	hSKAP$^{135-225}$ K140A	pGEX-6p-2rbs
82	hSKAP$^{135-225}$ K149A	pGEX-6p-2rbs
83	hSKAP$^{135-225}$ K161A	pGEX-6p-2rbs
84	hSKAP$^{135-225}$ K164A	pGEX-6p-2rbs
85	hSKAP$^{135-225}$ K161/164A	pGEX-6p-2rbs
86	hSKAP$^{159-316}$ K161A (MCS1) + hAstrin$^{482-850}$-His$_6$ (MCS2)	pFL
87	hSKAP$^{159-316}$ K164A (MCS1) + hAstrin$^{482-850}$-His$_6$ (MCS2)	pFL
88	hSKAP$^{159-316}$ K161/164A (MCS1) + hAstrin$^{482-850}$-His$_6$ (MCS2)	pFL
89	hSKAP$^{159-316}$ K267A (MCS1) + hAstrin$^{482-850}$-His$_6$ (MCS2)	pFL
90	GST-mCherry-hSKAP$^{135-225}$	pGEX-6p-2rbs
91	GST-mCherry-hSKAP$^{159-316}$	pGEX-6p-2rbs
92	hSKAP$^{135-225}$ K140/149A	pGEX-6p-2rbs
93	hSKAP$^{135-225}$ K140/161A	pGEX-6p-2rbs
94	hSKAP$^{135-225}$ K140/164A	pGEX-6p-2rbs
95	hSKAP$^{135-225}$ K149/161A	pGEX-6p-2rbs
96	hSKAP$^{135-225}$ K149/164A	pGEX-6p-2rbs
97	hSKAP$^{135-225}$ K140/161/164A	pGEX-6p-2rbs
98	hSKAP$^{135-225}$ K149/161/164A	pGEX-6p-2rbs

Table 5.5 (continued): List of used plasmids. h: human

plasmid #	expressed protein	vector
99	hSKAP$^{135-225}$ K140/149/161A	pGEX-6p-2rbs
100	hSKAP$^{135-225}$ K140/149/164A	pGEX-6p-2rbs
101	hSKAP$^{135-225}$ K140/149/161/164A	pGEX-6p-2rbs
102	hSKAP$^{135-316}$ (MCS1) + hAstrin$^{482-850}$-His$_6$ (MCS2)	pFL
103	hSKAP$^{135-225}$ K168A	pGEX-6p-2rbs
104	hSKAP$^{135-225}$ K170A	pGEX-6p-2rbs
105	hSKAP$^{135-225}$ K168/170A	pGEX-6p-2rbs
106	hSKAP$^{135-225}$ K140/149/161/164/168A	pGEX-6p-2rbs
107	hSKAP$^{135-225}$ K140/149/161/164/170A	pGEX-6p-2rbs
108	hSKAP$^{135-225}$ K140/149/161/164/168/170A	pGEX-6p-2rbs
109	hSKAP$^{135-216}$	pGEX-6p-2rbs
110	hSKAP$^{135-174}$	pGEX-6p-2rbs
111	hSKAP$^{175-225}$	pGEX-6p-2rbs
119	hSKAP$^{135-225}$	pCDNA5/FRT/TO-EGFP-IRES
120	hSKAP$^{135-225}$ K161/164A	pCDNA5/FRT/TO-EGFP-IRES
121	hSKAP$^{135-225}$ K140/149/161/164A	pCDNA5/FRT/TO-EGFP-IRES
122	hSKAP f.l.	pCDNA5/FRT/TO-EGFP-IRES
123	hSKAP f.l. K161/164A	pCDNA5/FRT/TO-EGFP-IRES
124	hSKAP f.l. K140/149/161/164A	pCDNA5/FRT/TO-EGFP-IRES
127	hSKAP$^{135-225}$ K140/149/161/164/168/170A	pCDNA5/FRT/TO-EGFP-IRES
128	hSKAP f.l. K140/149/161/164/168/170A	pCDNA5/FRT/TO-EGFP-IRES

5.2 Molecular biological methods

5.2.1 Transformation

Transformation is the uptake of genetic material into competent cells, i.e. cells that are able to receive the DNA from its surroundings by means of adequate stimuli (Lottspeich & Engels, 2006). This serves to amplify the transferred plasmids or to express encoded proteins. The transformation was performed via a heat shock in the presence of high Ca^{2+} concentrations. Pores are temporarily created in the bacterial plasma membrane with a sudden increase in temperature from 0 °C to 42 °C for 45 s thereby allowing the DNA to enter to cell. Afterwards, the cells were incubated in 800 µL LB medium for 45 min at 37 °C and subsequently selected on LB agar plates containing the respective antibiotics overnight at 37 °C.

5.2.2 Purification of DNA

5.2.2.1 Agarose gel electrophoresis

By means of agarose gel electrophoresis (Takahashi et al., 1969) DNA mixtures were separated with an electric field by the sieve effect of the agarose gel according to their size. 0.9 % agarose gels in TAE buffer were used and DNA was stained with SYBRSafe DNA gel stain or Midori Green advanced DNA stain. Samples were mixed with DNA loading buffer and separated by applying a voltage of 120 V to the agarose gel. For comparison, the GeneRuler 1 kb Plus DNA ladder (Thermo Fisher Scientific, Waltham, US-MA) was loaded in addition to the samples. DNA fragments were visualized by UV light.

5.2.2.2 Purification of plasmid DNA

Plasmid DNA was amplified in the *E. coli* cell strain One Shot OmniMAX 2-T1. After transformation a miniculture of a single colony in LB containing the respective antibiotics was incubated overnight at 37 °C. After cell harvest plasmid DNA was isolated from the bacterial cell pellet by use of the QIAprep Spin Miniprep Kit (Qiagen, Hilden, DE) according to the manufacturer's instructions. DNA was eluted with elution buffer (10 mM Tris, pH 8.0) and stored at -20 °C.

5.2.3 Polymerase chain reaction

With polymerase chain reaction (PCR) (Saiki et al., 1988) DNA was amplified analytically or preparatively. PCR reactions were carried out in a PCR thermocycler TProfessional TRIO (Biometra, Goettingen, DE).

5.2.3.1 Preparative PCR

For preparative PCR 50 µL reactions were used with 20 ng template DNA, 50 pmol of each primer, 10 nmol dNTPs and 1 unit AccuPrime Pfx DNA polymerase in AccuPrime Pfx reaction buffer. PCR was carried out with the following cycling parameters:

denaturation	2 min	95 °C	
denaturing	30 s	95 °C	30 cycles
annealing	30 s	~50 °C	
elongation	1 min/kb	68 °C	
elongation	5 min	68 °C	

Amplification products were purified via agarose gel electrophoresis. Appropriate bands were cut and processed with the QIAquick Gel Extraction Kit (Qiagen, Hilden, DE) according to the manufacturer's instructions. DNA was eluted with elution buffer (10 mM Tris, pH 8.0) and stored at -20 °C.

5.2.3.2 Colony PCR

The success of ligation (see paragraph 6.2.5) was checked via analytical PCR. For this purpose, single colonies of the transformation were dipped into a PCR tube and amplified in minicultures at 37 °C overnight. The cells in the PCR tube were mixed with 10 pmol of each primer, 2 nmol dNTPs and 0.5 units Crimson Taq polymerase in Crimson Taq reaction buffer. The PCR reaction was carried out with the protocol described in paragraph 6.2.3.1 and analyzed via agarose gel electrophoresis.

5.2.3.3 Site-directed mutagenesis

Site-directed mutagenesis was performed in order to selectively insert mutations into DNA sequences according to the Stratagene QuikChange site-directed mutagenesis protocol (Papworth et al., 1996). Self-complementary primers that contained the

desired mutations were used. In 25 µL reactions 50 ng template, 9 pmol of each primer, 3 % (v/v) DMSO and 12.5 µL 2x Q5 High Fidelity 2x Master Mix were incubated under the following cycling parameters:

denaturation	1 min	98 °C	
denaturing	1 min	98 °C	25 cycles
annealing	1 min	58 °C	
elongation	1 min/kb	72 °C	
elongation	10 min	72 °C	

To digest the parental methylated DNA, the samples were mixed with 1 unit DpnI for 1-3 h at 37 °C. After analysis via agarose gel electrophoresis the reaction mixture was transformed into One Shot OmniMAX 2-T1 cells.

5.2.3.4 DNA sequencing

Sequences of the cloned DNA constructs were verified via DNA sequencing by StarSEQ GmbH, Mainz, DE, or Beckman Coulter Genomics, Takeley, UK.

5.2.4 Restriction digest of DNA

Restriction digest (Lottspeich & Engels, 2006) was used to specifically cut DNA with the help of restriction enzymes in order to prepare the ligation of two DNA fragments (see paragraph 6.2.5). 0.5-1 µg of DNA were incubated with 1 unit of each restriction enzyme in a recommended buffer for 1-2 h at 37 °C. Digested DNA was purified with the QIAquick PCR Purification Kit (Qiagen, Hilden, DE) according to the manufacturer's instructions. DNA was eluted with elution buffer (10 mM Tris, pH 8.0) and stored at -20 °C. For digestion of plasmid DNA, 1 unit of shrimp alkaline phosphatase was added in addition to the restriction enzymes in order to dephosphorylate 5'-ends and minimize self-ligation of the vector. Purification of the cleaved plasmids was performed via agarose gel electrophoresis and subsequent gel extraction with the QIAquick Gel Extraction Kit (Qiagen, Hilden, DE) according to the manufacturer's instructions. DNA was eluted with elution buffer (10 mM Tris, pH 8.0) and stored at -20 °C.

5.2.5 DNA ligation

DNA ligation serves to covalently connect two DNA fragments after restriction digestion in order to obtain a covalently closed plasmid. Ligation was carried out using approximately 50 ng cleaved plasmid DNA, 3-5x molar excess of the digested insert and 1 unit of T4 DNA ligase in T4 DNA ligase reaction buffer. The reactions were incubated overnight at 16 °C followed by an incubation for 15 min at 65 °C and then transformed in competent *E. coli* One Shot OmniMAX 2-T1 cells.

5.3 Bioanalytical methods

5.3.1 Sodium dodecyl sulfate polyacrylamide gel electrophoresis (SDS-PAGE)

Sodium dodecyl sulfate (SDS) polyacrylamide gel electrophoresis (PAGE) (Laemmli, 1970) separates protein mixtures with an electric field by the sieve effect of the polyacrylamide gel according to their size. Hereby, the composition and purity of the samples can be analyzed. The used SDS-PAGE gels consisted of a ~ 40 cm^2 big 10-18 % separating gel and a stacking gel. In some cases NuPAGE SDS-PAGE was used with NuPAGE Novex 4-12 % Bis-Tris precast gradient gels (Life Technologies, Carlsbad, US-CA) in MES buffer. The samples were mixed with 5x SDS-PAGE loading buffer and denatured 5 min at 95 °C. For comparison a molecular weight marker (Precision Plus Protein Standard, Bio-Rad, Hercules, US-CA) was loaded in addition to the samples. The gels were placed into a Mini-PROTEAN Tetra Cell (Bio-Rad, Hercules, US-CA) with SDS-PAGE running buffer and a voltage of 120 V was applied till the dye of the loading buffer exited the gel. Proteins were visualized by Coomassie staining and subsequent destaining with 10 % (v/v) acetic acid.

5.3.2 Determination of protein concentration

5.3.2.1 Determination of protein concentration via Bradford assay

The determination of protein concentrations via the Bradford assay (Bradford, 1976) occurs colorimetrically by binding of the dye Coomassie brilliant blue G-250 to the cationic side chains of arginine, lysine and histidine. For this purpose, 1-10 µg of protein were mixed with 1 mL of Bradford solution (Thermo Fisher Scientific, Waltham, US-MA). After incubation for 5 min the absorbance at a wavelength of 595 nm was measured spectrometrically by comparison to a reference sample. The

protein concentration was determined by use of a standard curve with BSA of known concentration.

5.3.2.2 Determination of protein concentration via UV absorbance

The determination of protein concentrations via UV absorbance at a wavelength of 280 nm is based on the Beer-Lambert law. The required extinction coefficient for proteins can be calculated from the number of tryptophan, tyrosine and cysteine (Gasteiger et al., 2005). The measurement of absorbance was carried out with a NanoDrop spectrophotometer ND-1000 (peQLab, Erlangen, DE).

5.3.3 ESI mass spectrometry

Electrospray ionization (ESI) mass spectrometry (MS) (Fenn et al., 1989) serves to determine the molecular weight of molecules. For the analysis of protein samples, 0.3-0.5 nmol protein were used. The samples were desalted on a C_4 column (HPLC instrument LC1100, Agilent Technologies, Santa Clara, US-CA) and eluted a combination of 0.1 % TFA (trifluoroacetic acid) in H_2O (buffer A) and 0.08 % TFA in acetonitrile (buffer B). A linear gradient from 80 % buffer A and 20 % buffer B to 20 % buffer A and 80 % buffer B was employed. Subsequently, the MS analysis of the samples was carried out by a Finnigan LCQ Advantage MAX mass spectrometer (Thermo Fisher Scientific, Waltham, US-MA) in positive ion mode. The analysis of the MS spectra was done with Xcalibur and MagTran. The accuracy of the weight determination of proteins via ESI MS amounted to appromixately 7 Da.

5.3.4 Analytical size-exclusion chromatography

Analytical size-exclusion chromatography was used to analyze the binding of proteins in solution. Size-exclusion chromatography (SEC) (Porath & Flodin, 1959) separates molecules according to their hydrodynamic radius. The elution occurs with decreasing size, because small molecules preferentially enter the porous matrix of the column and are thereby retained longer. The SEC experiments were carried out using an ÄKTA micro (GE Healthcare, Piscataway, US-NJ) with a Superdex 200 5/150 GL or Superose 6 Tricorn 5/150 GL column (GE Healthcare, Piscataway, US-NJ), respectively.

For sample preparation the respective proteins were mixed at concentrations of 5-20 µM in size exclusion chromatography buffer in a final volume of 50 µL. Samples containing single proteins in size exclusion chromatography buffer served as controls. The samples were incubated at least for 1 h on ice before injecting onto the size exclusion chromatography column. The columns were equilibrated in size exclusion chromatography buffer and after injection the samples were eluted with one column volume of size exclusion chromatography buffer at a flow rate of 0.1-0.2 mL/min and fractionated. The eluted proteins were detected via their absorbance at a wavelength of 280 and 214 nm and subsequently analyzed via SDS-PAGE. Subsequently, the chromatograms and the corresponding SDS-PAGE gels of the samples were compared for the single proteins and the protein mixtures.

5.3.5 Western blot

Western blots were used to stain for specific proteins in cell lysates. For this purpose, protein samples were separated via SDS-PAGE and then transferred onto a PVDF membrane (Bio-Rad Laboratories, Munich, DE) via electrophoresis in 25 mM Tris, 200 mM glycine and 20 % (v/v) methanol by applying 100 V for 90 min. Protein transfer was checked by staining with Ponceau S. The membrane was blocked for 1 h at room temperature in TBS-T supplemented with 5 % (w/v) milk powder. Incubation with primary antibodies against α-tubulin (mouse monoclonal antibody, DM1A, Sigma-Aldrich, 1:10,000), SKAP (rabbit polyclonal anti-human SKAP$^{135\text{-}225}$ antibody, made in cooperation with Cogentech, Milan, IT, 1:2,000) or GFP (rabbit polyclonal antibody, generated in-house, 1:5,000) diluted in TBS-T supplemented with 5 % (w/v) milk powder was performed overnight at 4 °C. After three washes for 5 min with TBS-T the membrane was incubated for 1 h at room temperature HRP-conjugated donkey anti-rabbit antibody (Amersham Biosciences, Piscataway, US-NJ) or HRP-conjugated sheep anti-mouse antibody (Amersham Biosciences, Piscataway, US-NJ) diluted in TBS-T supplemented with 5 % (w/v) milk powder. The membrane was washed 4 times for 7 min with TBS-T, enhanced chemiluminescence western blotting substrate was added according to the manufacturer's instructions and signals were detected with a developer machine on film.

5.4 Biochemical methods

5.4.1 Protein expression and purification

For protein expression the cell strains and plasmids listed in tables 6.4 and 6.5 were used. Zwint, Knl1, RB3, TTL, the Mis12 complex (Petrovic et al., 2010) and the Ndc80 complex (Petrovic et al., 2010) were already purified and stored at -80 °C.

5.4.1.1 Protein expression in Escherichia coli

The protein constructs (see Table 5.5) were tested for expression in the cell strains Rosetta 2(DE3), OverExpress C41(DE3) or BL21-CodonPlus(DE3) RIL, respectively, after incubation with 0.1-0.2 mM IPTG and an overnight incubation at temperatures of 16-20 °C in LB or TB medium. For subsequent protein purification of the Astrin and SKAP constructs, an overnight expression in OverExpress C41(DE3) cells at 16 °C in LB medium was used. The expression was induced with 0.1 mM IPTG at an optical density at 600 nm of 0.5-0.8 absorbance units. Cells were harvested by centrifugation at 5,000 g for 15-20 min at 20 °C.

5.4.1.2 Seleno-methionine expression of SKAP$^{135-225}$ in Escherichia coli

By the seleno-methionine expression (Abergel et al., 2000) a protein can be labeled with selenium in order to solve the phase problem occurring during X-ray crystallography. For this purpose, 50 mL overnight culture of *E. coli* OverExpress C41(DE3) that were transformed with the pGEX-6p-2rbs-SKAP$^{135-225}$ plasmid were centrifuged and used to inoculate 5 L M9 minimal medium. At an optical density at 600 nm of 0.5 absorbance units the feedback inhibition of methionine biosynthesis was facilitated by the addition of 100 mg/L of phenylalanine, lysine and threonine as well as 50 mg/L of isoleucine, leucine and valine. After 15 min 60 mg/L L-seleno-methionine were added and after another 15 min the expression was induced with 0.1 mM IPTG. Seleno-methionine labeled protein was expressed overnight at 18 °C. Cells were harvested by centrifugation at 5,000 g for 15 min at 20 °C.

5.4.1.3 Protein expression in insect cells

5.4.1.3.1 Generation of bacmid

For generation of bacmid, DH10EMBacY cells, which are *E. coli* cells containing the EMBacY bacmid, were transformed with the gene-containing transfer plasmid - a MultiBac pFL-derived vector (Fitzgerald et al., 2006) - and recombination was allowed to take plate for 5 h at 37 °C. Selection for successful transposition into the bacmid was done via blue/white screening on LB agar containing kanamycin, gentamycin, tetracycline, X-gal and IPTG for 2 d at 37 °C. Bacmid was isolated from minicultures of white colonies with alkaline lysis of bacteria and subsequent pelleting of the bacmid with isopropanol. For this purpose, cell pellets of 4 mL overnight cultures were mixed with 300 µL each of the QIAprep Spin Miniprep Kit solution (Qiagen, Hilden, DE) according to the manufacturer's instructions and incubated 20 min on ice. Samples were centrifuged for 10 min at 20,000 g and subsequently the supernatant was centrifuged for another 10 min. 850 µL of isopropanol was added to the cleared supernatant and incubated at -20 °C overnight. After centrifugation for 20 min at 20000 g the pellet was washed with 70 % (v/v) ethanol. Under a sterile hood the ethanol was removed and the pellet allowed to dry before dissolving in TE buffer. The bacmid DNA was stored at -20 °C.

5.4.1.3.2 Transfection of insect cells and virus amplification

For transfection and virus amplification, the *Spodoptera frugiperda* cell line *Sf*9 (Invitrogen, Carlsbad, US-CA) was used. Bacmid was incubated for 20 min with FuGENE (Promega, Fitchburg, US-WI) in Sf-900 III SFM serum free medium (Invitrogen, Carlsbad, US-CA) and subsequently added to a 6-well plate containing $1x10^6$ cells per transfection in 2 mL Sf-900 III SFM. Cells were incubated at 27 °C for 3 d.

For virus amplification, the transfected cells were resuspended and added to 10 mL of fresh medium with $1x10^6$ Sf9 cells per mL. After incubation at 27 °C for 4 d the cells were centrifuged at 1,000 g for 5 min. The supernatant (V_0) was sterile filtered and stored at 4 °C. For further virus amplification, $1x10^6$ Sf9 cells per mL were incubated with 1:100 V_0 in Sf-900 III SFM for 4 d at 27 °C. Afterwards, cells and supernatant (V_1) were treated as mentioned above.

5.4.1.3.3 Protein expression in insect cells

For protein expression, the *Trichoplusia ni* cell line BTI-*Tnao*38 was used. $1x10^6$ cells per mL were incubated with different ratios (1:25 to 1:100) of V_1 virus in Sf-900 III SFM and incubated for 4 d at 27 °C. Cells were harvested by centrifugation at 420 g for 20 min at 20 °C.

5.4.1.4 Protein purification from Escherichia coli

Following protein expression, harvested cells were resuspended in 5 volumes of ice-cold lysis buffer (50 mM Hepes, pH 7.5, 300 mM NaCl, 10 % (v/v) glycerol, 1 mM $MgCl_2$, 0.1-0.2 % Triton X-100, DNaseI, protease inhibitor mix and 5 mM β-mercaptoethanol for His-tagged proteins or 5 mM DTE for GST-tagged proteins) and lyzed by sonication. The lysate was cleared by centrifugation at 100,000 g for 30 min at 4 °C in a JA-30.50 Ti rotor.

The subsequent protein purification was carried out with an ÄKTA prime plus and an ÄKTA purifier at 4 °C. The proteins were purified in a first step via affinity chromatography on a 5 mL GSTrap FF column for GST-tagged proteins or a 5 mL HisTrap FF column for His-tagged proteins. For this purpose, the cleared lysate was loaded onto the equilibrated column with a flow rate of 2 mL/min. Afterwards, the column was washed with at least 40 column volumes of buffer containing 50 mM Hepes, pH 7.5, 300 mM NaCl, 10 % (v/v) glycerol and 2 mM reducing agent as well as 20 mM imidazole for His-tagged proteins. His-tagged proteins were eluted with an imidazole gradient from 20-500 mM imidazole, fractionated and detected via absorbance at 280 nm. After analysis with SDS-PAGE appropriate fractions were dialyzed in buffer containing 20 mM Hepes, pH 7.5, 300 mM NaCl, 10 % (v/v) glycerol and 2 mM DTE overnight. GST-tagged proteins were eluted with buffer containing 20 mM Hepes, pH 7.5, 300 mM NaCl, 10 % (v/v) glycerol, 2 mM DTE and 50 mM GSH to keep the GST-tag or the tag was cleaved on the column by an adding of GST-tagged PreScission protease to the column-bound protein for approximately 16 h and the protein was subsequently eluted with 1.5 column volumes of buffer containing 20 mM Hepes, pH 7.5, 300 mM NaCl, 10 % (v/v) glycerol and 2 mM DTE.

The proteins were further purified by anion-exchange chromatography. They were loaded onto a 5 mL HiTrap Q FF equilibrated in buffer containing 20 mM Hepes, pH 7.5, 100-300 mM NaCl, 10 % (v/v) glycerol and 2 mM DTE. The flow-through was collected and the bound proteins eluted with a salt gradient up to 1 M NaCl over 20 column volumes. Proteins were detected via absorbance at 280 nm and analyzed

with SDS-PAGE. Fractions containing the protein of interest were concentrated in a VivaCell 250 (Sartorius Stedim Biotech, Goettingen, DE) at 4 °C and further purified via size exclusion chromatography. Depending on the amount and size of the proteins one of the following size exclusion chromatography columns was used: Superdex 200 5/150 GL, HiLoad 16/600 Superdex 200 pg, Superose 6 10/300 GL or Superose 6 prep grade XK 16/70. The columns were equilibrated in size exclusion chromatography buffer (20 mM Hepes, pH 7.5, 300 mM NaCl, 10 % (v/v) glycerol and 2 mM DTE) and after injection the samples were eluted with one column volume of size exclusion chromatography buffer and fractionated. The eluted proteins were detected via their absorbance at 280 nm and subsequently analyzed with SDS-PAGE. Fractions containing the protein of interest were concentrated in a VivaCell 250 (Sartorius Stedim Biotech, Goettingen, DE) at 4 °C, shock frozen in liquid nitrogen and stored at -80 °C.

5.4.1.5 Protein purification from insect cells

His-tagged Astrin$^{482-850}$/SKAP$^{159-316}$ complex was purified from insect cells. Cells were resuspended in 10 volumes of ice-cold lysis buffer (50 mM Hepes, pH 7.5, 300 mM NaCl, 10 % (v/v) glycerol, 1 mM $MgCl_2$, 0.5 % Triton X-100, DNaseI, protease inhibitor mix and 5 mM β-mercaptoethanol) and lyzed by sonication. The lysate was cleared by centrifugation at 100,000 g for 30 min at 4 °C in a JA-30.50 Ti rotor.

The subsequent protein purification was carried out with an ÄKTA prime plus and an ÄKTA purifier at 4 °C. The protein complex was purified in a first step via affinity chromatography on a 5 mL HisTrap FF column. For this purpose, the cleared lysate was loaded onto the equilibrated column at a flow rate of 2 mL/min. Afterwards, the column was washed with 30 column volumes of buffer containing 50 mM Hepes, pH 7.5, 300 mM NaCl, 10 % (v/v) glycerol, 0.5 % Triton X-100, 20 mM imidazole and 2 mM β-mercaptoethanol and subsequently with 20 column volumes of buffer without Triton X-100. Proteins were eluted with an imidazole gradient from 20-500 mM imidazole, fractionated and detected via absorbance at 280 nm. After analysis with SDS-PAGE appropriate fractions were dialyzed in buffer containing 20 mM Hepes, pH 7.5, 300 mM NaCl, 10 % (v/v) glycerol and 2 mM DTE for approximately 16 h.

The proteins were concentrated in a VivaCell 250 (Sartorius Stedim Biotech, Goettingen, DE) at 4 °C and further purified via size exclusion chromatography on Superose 6 10/300 GL or Superose 6 prep grade XK 16/70 columns. The columns were equilibrated in size exclusion chromatography buffer (20 mM Hepes, pH 7.5,

300 mM NaCl, 10 % (v/v) glycerol and 2 mM DTE) and after injection the samples were eluted with one column volume of size exclusion chromatography buffer and fractionated. The eluted proteins were detected via their absorbance at 280 nm and subsequently analyzed with SDS-PAGE. Fractions containing the proteins of interest were concentrated in a VivaCell 250 (Sartorius Stedim Biotech, Goettingen, DE) at 4 °C, shock frozen in liquid nitrogen and stored at -80 °C.

5.4.2 Microtubule cosedimentation assays

Microtubule cosedimentation assays were performed in order to analyze the ability of protein constructs to bind to microtubules. For this purpose, bovine α-/β-tubulin (Cytoskeleton, Inc., Denver, US-CO, #TL238) was diluted to a concentration of 50 µM in BRB80 buffer. The dissolved tubulin was mixed with 2.5 mM GTP and placed in a PCR thermocycler TProfessional TRIO (Biometra, Goettingen, DE) to allow polymerization at 34 °C for 1 h. Afterwards, 0.5 mM taxol was added to stabilize the microtubules and incubated for 1-2 h at 34 °C. In order to obtain subtilisin-treated microtubules, 6 µM taxol-stabilized microtubules were incubated with 100 µg/mL subtilisin A for 45 min at 30 °C. The reaction was quenched by the addition of 10 mM phenylmethyl sulfonyl fluoride. The digested microtubules were pelleted at 350,000 g for 10 min at 25 °C and resuspended in BRB80 buffer. Taxol-stabilized or subtilisin-treated microtubules were incubated with the protein of interest for 10 min at room temperature in a final reaction volume of 35 µL in 25 mM Hepes, pH 7.5, 150 mM NaCl, 1 mM $MgCl_2$, 1 mM EGTA and 2 mM DTE. The samples were placed on top of 100 µL cushion buffer (25 mM Hepes, pH 7.5, 150 mM NaCl, 1 mM $MgCl_2$, 1 mM EGTA, 50 % (v/v) glycerol and 50 µM taxol) and ultracentrifuged in a TLA 120.1 rotor at 350,000 g for 10 min at 25 °C. The upper 35 µL (soluble fraction) were mixed with 5x SDS loading buffer. The pellet was dissolved in 1x SDS loading buffer. Afterwards, the samples were analyzed with SDS-PAGE. The quantification of the pellet and soluble fraction was carried out with ImageJ 1.49 (NIH). To obtain normalized binding data, the values of the pellet fraction were divided by the sum of pellet and soluble fraction. The normalized data were fitted using Origin7.0 (OriginLab, Northampton, US-MA) to the following equation (Ciferri et al., 2008):

$$\text{fraction bound} = \frac{(B_t+K_d+x)-\sqrt{(B_t+K_d+x)^2-(4B_tx)}}{2}$$

B_t is the maximal fractional protein-tubulin complex, K_d is the dissociation constant and x is the concentration of tubulin dimer.

5.4.3 Microtubule cold shock assay

Microtubule cold shock assays were performed in order to test the influence of proteins on the stability of microtubules to a cold treatment. 10 µM bovine α-/β-tubulin (Cytoskeleton, Inc., Denver, US-CO) were incubated at 34 °C for 30 min either alone or in the presence of 10 µM protein of interest in a buffer containing 25 mM Hepes, pH 7.5, 150 mM NaCl, 5 % glycerol, 4 mM $MgCl_2$, 1 mM EGTA, 2 mM DTE and 2.5 mM GTP. Afterwards, the samples were incubated for 10 min on ice and centrifuged on top of 100 µL cushion buffer (25 mM Hepes, pH 7.5, 150 mM NaCl, 1 mM $MgCl_2$, 1 mM EGTA, 50 % (v/v) glycerol) in a TLA 120.1 rotor at 350,000 g for 10 min at 4 °C. As a control, samples with the same composition were treated without cold shock and centrifuged at 350,000 g for 10 min at 34 °C. Supernatants and pellets were analyzed with SDS-PAGE and the amount of polymerized tubulin was quantified as described in section 6.4.2.

5.4.4 Chemical crosslinking and MS analysis

Chemical crosslinking (Herzog et al., 2012) was performed in order to map lysine residues that lie close to each other and thereby point to the binding sites of the interacting proteins. An equimolar mixture of isotopically light and heavy labeled crosslinker bis(sulfosuccinimidyl)glutarate (BS2G-H6/D6, Creative Molecules, www.creativemolecules.com) or di(succinimidyl)suberate (DSS-H12/D12, Creative Molecules, www.creativemolecules.com) was dissolved in DMSO at a concentration of 50 µM. In an initial experiment the appropriate amount of crosslinker was determined. For this purpose, 10-15 µg of total protein was incubated with varying amounts of crosslinker (weight ratio of 10:1 to 1:10) in a final volume of 20-25 µL. After incubation for 30 min at 37 °C the reaction mixture was quenched by the adding of 100 mM ammonium bicarbonate and incubation for 15 min at 37 °C. Samples were analyzed for their extent of crosslinking via NuPAGE SDS-PAGE and promising reaction mixtures were repeated on a larger scale. In case of the $Astrin^{482-850}$/$SKAP^{159-316}$ complex 90 µg of protein were mixed in a 1:1 ratio with DSS or BS2G in a final volume of 130 µL. To analyze the SKAP-microtubule interaction, 10 µM $SKAP^{135-225}$ and 10 µM taxol-stabilized microtubules (170 µg total protein) were mixed with DSS in a ratio of 1:2.5 or with BS2G in a ratio of 1:1 in a final volume of 150 µL. Crosslinked samples were send to the lab of Franz Herzog (Gene Center Munich, LMU Munich, DE) for further mass spectrometric analysis of crosslinked peptides (Herzog et al., 2012). In brief, crosslinked proteins were

digested and the peptides were enriched and analyzed by liquid chromatography coupled to tandem mass spectrometry analysis. Crosslinks were identified via the *xQuest* database and visualized using the xVis web server (Grimm et al., 2015).

5.4.5 Fluorescence microtubule flow cell assays

For the purpose of studying the microtubule binding of different proteins at low concentrations, fluorescence microtubule flow cell assays were performed. To make a hydrophilic surface and achieve a homogenous coating, the cover slips were cleaned prior to usage as follows:

I. Sonication in isopropanol for 20 min.
II. Two times sonication in Millipore water for 5 min.
III. Sonication in 1 M KOH for 20 min.
IV. Storage in 1 M KOH overnight.
V. Sonication in Millipore water for 5 min before use.

The glass slides were cleaned in the following way:

I. Sonication in 1 % Hellmanex for 10 min.
II. Sonication in Millipore water for 5 min.
III. Sonication in 70 % ethanol for 10 min.
IV. Sonication in Millipore water for 5 min.
V. Repetition of I-III.
VI. Storage in ethanol until use.
VII. Sonication in Millipore water for 5 min before use.

Porcine tubulin (Cytoskeleton, Inc., Denver, US-CO) containing 10 % biotinylated tubulin and 10 % fluorescently labeled tubulin was polymerized for 30-60 min at 34 °C at a concentration of 10 mg/mL in BRB80 buffer containing 50 % glycerol. Glycerol was added in order to increase nucleation and to obtain a higher amount of shorter microtubules. Afterwards 12 µM taxol was added and the microtubules were incubated for about an hour at 34 °C.

All the following steps were carried out at room temperature. To functionalize the cover slips, two clean and dry cover slips were incubated with 5 % biotinylated poly-L-lysine-PEG at a concentration of 0.2 mg/mL for 30 min. Afterwards, flow cells were prepared by placing dry, functionalized coverslips on top of dry glass slides separated by double-sided tape so that the created flow cells had a width of around 5 mm and a volume of 10-15 µL. The surface of the flow cells was passivated with

poly-L-lysine-PEG for 30 min and subsequently with 1 % pluronic F-127 for 30-45 min. The chambers were then incubated with 0.33 mg/mL avidin, diluted in BRB80 buffer containing 1 % pluronic F-127, for 45 min. Afterwards, the flow cells were washed with at least 10 chamber volumes of reaction buffer containing 25 mM Hepes, pH 7.5, 150 mM NaCl, 10 % glycerol, 1 mM $MgCl_2$, 1 mM EGTA, 2 mM DTE and 10 µM taxol. 100-200 nM HiLyte 647-labeled microtubules were added for 10-20 min and the flow cell was washed with 3 chamber volumes. Fluorescently labeled proteins were added at the indicated concentrations together with 0.5 mg/mL BSA. The flow cells were sealed with wax and imaged with a 3i Marianas system (Intelligent Imaging Innovations Inc., Göttingen, DE) equipped with an Axio Observer Z1 microscope (Zeiss, Oberkochen, DE), a CSU-X1 confocal scanner unit (Yokogawa Electric Corporation, Tokyo, Japan), a Plan-Apochromat 100x/1.4NA DIC oil objective (Zeiss, Oberkochen, DE), an Orca Flash 4.0 sCMOS Camera (Hamamatsu, Hamamatsu City, Japan) and controlled by Slidebook Software 6.0 (Intelligent Imaging Innovations Inc., Göttingen, DE). Images were acquired as z-sections at 0.27 µm and maximal intensity projections were made with Slidebook Software 6.0 (Intelligent Imaging Innovations). Quantification was done with ImageJ 1.49 (NIH) and intensities were normalized to microtubule signals.

5.4.6 TIRF microscopy

Total internal reflection fluorescence (TIRF) microscopy was used to study the dynamics of microtubules in the absence and presence of different proteins. The glass slides, coverslips and flow cells were prepared as described in section 6.4.5. After incubation with avidin the chambers were washed with reaction buffer (25 mM Hepes, pH 7.5, 150 mM NaCl, 10 % (v/v) glycerol, 1 mM $MgCl_2$, 1 mM EGTA, 2 mM DTE) including an oxygen scavenger mix consisting of 4.5 mg/mL glucose, 0.2 mg/mL glucose oxidase, 35 µg/mL catalase and 10 mM DTE. Flow cells were incubated for 10-20 min with 20 µL of a microtubule seed mix containing 400 nM GMPCPP microtubule seeds (15 % biotinylated and 15 % alexa-647 labeled; incubated for 30 min at 34 °C with 1 mM GMPCPP), oxygen scavenger mix, 0.5 mg/mL casein and 0.1 % (w/v) methylcellulose in reaction buffer. After washing with 50 µL of reaction buffer including oxygen scavenger mix a tubulin mix (14 µM Rhodamine labeled tubulin, 2.5 mM GTP, oxygen scavenger mix, 0.35 mg/mL casein and 0.1 % (w/v) methylcellulose in reaction buffer) was added in the presence or absence of proteins of interest at the indicated concentrations. The chambers were sealed with wax and imaged at 25 °C with a VisiTIRF Fluorescence Imaging System

(Visitron Systems GmbH, Puchheim, DE) with a Nikon Eclipse Ti-E inverted microscope (Nikon, Tokyo, JP), an Apo-TIRF 100x/1.49NA oil objective (Nikon, Tokyo, JP) and an Evolve Delta camera (Photometrics, Tucson, US-AZ). 200 time points were imaged every 5 s at a penetration depth of 140 nm. Kymographs were made with ImageJ 1.49 (NIH).

5.4.7 Tubulin polymerization assays

Tubulin polymerization assays were performed to examine the influence of proteins on the polymerization of tubulin. The polymerization of tubulin was analyzed with a turbidity experiment (Mirigian et al., 2013) by measuring the change in light scattering that is caused by the microtubule suspension. For this purpose, the absorbance at 350 nm was followed in a POLARstar Omega plate reader (BMG Labtech, Ortenberg, DE). Bovine α-/β-tubulin (Cytoskeleton, Inc., Denver, US-CO) was incubated for 50 min at 37 °C in reaction buffer (20 mM Hepes, pH 7.5, 150 mM NaCl, 5 % glycerol, 4 mM $MgCl_2$, 2.5 mM GTP and 2 mM DTE) at a concentration of 5-15 µM either alone or in the presence of other proteins at the indicated concentrations. A sample with reaction buffer was used as blank and subtracted from the raw data.

5.4.8 GST pull-down assays

In order to study the binding of proteins on a solid support, GST pull-down assays were carried out. For this purpose, 10 µL GSH beads were washed with reaction buffer (20 mM Hepes, pH 7.5, 150-300 mM NaCl, 5-10 % glycerol and 2 mM DTE) and saturated with GST tagged proteins by incubation for at least 1 h at 4 °C under slight rotation. Subsequently, the beads were washed three times with 500 µL of reaction buffer containing 0.05 % Tween-20 and then incubated with possible interaction partners. After incubation for at least 1 h at 4 °C under slight rotation the beads were washed again three times with 500 µL of reaction buffer containing 0.05 % Tween-20 and the bound proteins were eluted with reaction buffer containing 50 mM GSH. Afterwards, the eluted proteins were analyzed via SDS-PAGE.

5.5 Cell biological methods

5.5.1 Cell line generation and cell culture

Codon-optimized SKAP genes (Invitrogen, Carlsbad, US-CA) were amplified by PCR and subcloned into a pCDNA5/FRT/TO-EGFP-IRES vector, a modified version (Krenn et al., 2012) of the pCDNA5/FRT/TO vector (Invitrogen, Carlsbad, US-CA). Mutations were introduced via site-directed mutagenesis. All plasmids were verified by DNA sequencing. Flp-In T-REx HeLa cells that were used to generate stable doxycycline-inducible cell lines were a gift from S.S. Taylor (University of Manchester, Manchester, England, UK). Flp-In T-REx HeLa host cell lines were maintained in DMEM (PAN Biotech, Aidenbach, DE) with 10 % tetracycline-free FBS (Clontech, part of Takara Bio group, Shiga, Japan) supplemented with penicillin and streptomycin. For generation of Flp-In T-REx HeLa expression cell lines 100 µL optiMEM medium and 6 µL XtremeGene were incubated for 5 min and mixed with 1.8 µg pOG44 and 0.2 µg of the pCDNA5/FRT/TO-EGFP-IRES expression plasmid. After 20 min the reaction mixture was added to the Flp-In T-REx HeLa host cells and incubated at 37 °C for 48 h. Afterwards, the cells were put under selection for two weeks in DMEM with 10 % tetracycline-free FBS supplemented with 250 µg/mL hygromycin and 5 µg/mL blasticidin. Cells of single colonies were maintained in DMEM with 10 % tetracycline-free FBS supplemented with hygromycin and blasticidin. HeLa cells were maintained in DMEM with 10 % tetracycline-free FBS.

5.5.2 Immunofluorescence and RNA interference

For the purpose of studying the cellular localization of SKAP, immunofluorescence experiments were performed either with GFP-SKAP WT and GFP-SKAP mutants or endogenous SKAP. For localization studies with endogenous SKAP HeLa cells were grown on coverslips precoated with poly-D-lysine and poly-L-lysine. Cells were treated with 10 µM MG132 or 3.3 µM nocodazole for 3 h and in some cases 500 nM Hesperadin was added for 1.5 h in order to inhibit AuroraB kinase. In case of GFP fusion constructs respective Flp-In T-REx HeLa cells were grown on coverslips precoated with poly-D-lysine and poly-L-lysine. To induce gene expression, 0.1 µg/mL doxycycline was added for 24 h. Afterwards, cells were treated for 2-3 h with 10 µM of the proteasome inhibitor MG132 to arrest the cells in metaphase. In order to analyze the phenotypes of SKAP-depleted cells Flp-In T-REx HeLa cells were treated with small interfering RNA (siRNA). For this purpose, 100 µL medium were mixed with 10 µL HyPerFect transfection reagent. After incubation for 5 min

siRNA duplexes (SKAP1: GAAAGAGUCCGAUUCCUAG[dT][dT], SKAP2: AGGCUACAAACCACUGAGUAA) were added for 20 min. Cells were transfected with 100 nM siRNA for 24 h, 48 h or 72 h. The efficiency of the siRNA treatment was analyzed with cell lysates via western blot and with immunofluorescence as described below. To study whether SKAP WT or mutants can rescue the observed phenotype, the expression of GFP fusion proteins in SKAP-depleted cells was induced for 24 h prior to fixation of the cells.

Cells were fixed with 4 % paraformaldehyde in PBS for 10 min and permeabilized with 0.1 % Triton X-100 in PBS for 5-10 min. Coverslips were blocked in 4 % BSA in PBS for 1 h at room temperature. Cells were stained for SKAP (rabbit polyclonal anti-SKAP$^{135-225}$ antibody made in cooperation with Cogentech, Milan, IT, 1:1,000), α-tubulin (mouse monoclonal anti-α-tubulin antibody, DM1A, Sigma-Aldrich, 1:500) and CREST/anti-centromere antibodies (Antibodies, Inc., Davis, US-CA, 1:100) diluted in 2 % BSA in PBS for 1.5 h at room temperature. After washing with PBS coverslips were incubated with donkey anti-rabbit Alexa Fluor 488 (Invitrogen, Carlsbad, US-CA, 1:200), goat anti-mouse Rhodamine Red-X (Jackson ImmunoResearch Laboratories, Inc., West Grove, US-PA, 1:200) and goat anti-human Alexa Fluor 647 (Invitrogen, Carlsbad, US-CA, 1:200) as secondary antibodies for 1 h at room temperature. DNA was stained with 0.5 µg/mL DAPI for 5 min. The coverslips were washed with PBS and water, airdried and mounted with Mowiol mounting media.

Cells were imaged using a DeltaVision Elite imaging system (Applied Precision, Issaquah, US-WA) with an inverted Olympus IX71 microscope (Olympus, Shinjuku, Tokyo, JP) equipped with a U Plan-Apochromat 60x/1.42NA oil objective (Olympus, Shinjuku, Tokyo, JP) and a CoolSNAP HQ2 camera (Photometrics, Tucson, US-AZ). Images were acquired as z-sections at 0.2 µm and the deconvolution and maximal intensity projections were carried out with softWoRx 5.0 (Applied Precision, Issaquah, US-WA). The quantification of fluorescence intensities at kinetochores and spindle microtubules was performed with unmodified z-series images using the spot and the surface function of Imaris 7.3.4 software (Bitplane, Zurich, CH). After background subtraction the GFP signals were normalized to those of the SKAP full-length WT cell line. For quantification of endogenous SKAP localization intensities obtained for SKAP were normalized to CREST signals.

5.6 Biophysical methods

5.6.1 Microscale thermophoresis

Microscale thermophoresis experiments (Jerabek-Willemsen et al., 2011) were performed to analyze protein-protein interactions. Protein samples were prepared as serial 1:1 dilutions with 150 nM mCherry-SKAP$^{159-316}$ as fluorescent binding partner and 1.53-12,500 nM Mis12 complex, 0.76-6,250 nM Ndc80 complex or 1.53-12,500 nM Zwint as unlabeled titrated binding partner, respectively. For the interaction of the Mis12 complex and the Ndc80 complex, 2 nM GFP-tagged Ndc80 complex were incubated with 0.12-500 nM Mis12 complex in 20 mM Hepes, pH 7.5, 150 mM NaCl, 5 % (v/v) glycerol, 0.05 % (v/v) Triton X-100 and 10 mM β-mercaptoethanol. Reactions were performed in 20 mM Hepes, pH 7.5, 150 mM NaCl, 0-5 % (v/v) glycerol, 0.5 mg/mL BSA and 2 mM DTE. After spinning for 5 min at 20,000 g samples were transferred to standard glass capillaries (NanoTemper Technologies GmbH, Munich, DE) and analyzed with a Monolith NT.115 instrument (NanoTemper Technologies GmbH, Munich, DE). Experiments were controlled with NT Control software and analyzed with NT Analysis software. The signals of the initial fluorescence or the thermophoresis and temperature jump were normalized to signals of sample with lowest concentration of titrated unlabeled protein. The normalized data were plotted against the concentration of titrated unlabeled protein and fitted with Origin7.0 (OriginLab, Northampton, US-MA) using following equation (NanoTemper Technologies GmbH, Munich, DE):

$$f(c) = \text{unbound} + \left((\text{bound} - \text{unbound}) \cdot \frac{\left(F+c+K_d - \sqrt{(F+c+K_d)^2 - 4Fc}\right)}{2F} \right)$$

with f(c) as concentration dependent signal, unbound as signal of unbound state, bound as signal of bound state, F as fluorophore concentration, c as concentration of titrated unlabeled protein and K_d as dissociation constant.

5.6.2 Sedimentation velocity analytical ultracentrifugation

Sedimentation velocity experiments were used to determine the molecular weight and thereby the oligomeric state of the analyzed proteins. The experiments were performed in an Optima XL-A analytical ultracentrifuge (Beckman Coulter, Palo Alto, US-CA) with Epon charcoal-filled double-sector quartz cells and an An-60 Ti rotor (Beckman Coulter, Palo Alto, US-CA). Before the analysis samples were dialyzed

against buffer (20 mM Hepes, pH 7.5, 300 mM NaCl, 10 % glycerol and 2 mM DTE) that was used as blank. Samples were centrifuged at 42,000 rpm at 20 °C and 500 radial absorbance scans at 280 nm were collected with a time interval of 1 min. The data were analyzed using the SEDFIT software (Schuck, 2000) in terms of continuous distribution function of sedimentation coefficients (c(S)). The protein partial specific volume was estimated from the amino acid sequence using the program SEDNTERP. Data were plotted using the program GUSSI.

5.7 Structural methods

5.7.1 Bioinformatic methods

A bioinformatic characterization of Astrin and SKAP was performed in order to obtain possible hints regarding the structural and functional organization of the two proteins, which could be used to design appropriate truncation constructs. For this purpose, the servers and programs listed in Table 5.6 were used.

Table 5.6: List of used servers and programs for the bioinformatic characterization of Astrin and SKAP.

program	predicted feature	homepage
Jpred (Cole et al., 2008)	secondary structure	http://www.compbio.dundee.ac.uk/www-jpred/
PSIPRED (Buchan et al., 2013)	secondary structure	http://bioinf.cs.ucl.ac.uk/psipred/
Phyre2 (Kelley & Sternberg, 2009)	tertiary structure	http://www.sbg.bio.ic.ac.uk/phyre2/
I-TASSER (Roy et al., 2010; Zhang, 2008)	tertiary structure	http://zhanglab.ccmb.med.umich.edu/I-TASSER/
Paircoil2 (McDonnell et al., 2006)	coiled-coil regions	http://groups.csail.mit.edu/cb/paircoil2/

5.7.2 X-ray crystallography

5.7.2.1 Protein crystallization

In order to determine the crystal structure of SKAP, crystallization experiments were performed with appropriately truncated SKAP constructs. For this purpose, the crystallization behavior of the proteins was first tested via sitting-drop vapor diffusion

with the screens JCSG Core I-IV (Qiagen, Hilden, DE) in 96-well Corning 3550 plates (Corning, New York, US-NY). In these initial crystallization experiments 100 nL protein solution were mixed with 100 nL reservoir solution with a Mosquito nanoliter high-throughput robot (TPP LabTech, Melbourne, GB) and incubated with 75 µL reservoir solution at 20 °C.

Successful conditions of the initial crystallization experiments were reproduced and refined via hanging-drop vapor diffusion in 24-well plates Linbro 24 Conical Flat Bottom Wells (MP Biomedicals, Santa Ana, US-CA). Therefor, 1 µL of protein solution was mixed with 1 µL of reservoir solution and incubated with 500 µL of reservoir solution at 20 °C.

5.7.2.2 Soaking with heavy atom derivatives

To obtain the phase information, heavy atoms were introduced into the crystals via soaking experiments with heavy atom derivatives, including K_2PtCl_4, $Pt(NH_3)_2Cl_2$, $UO_2(CH_3COO)_2$ and $Pb(CH_3COO)_2$. For this purpose, native $SKAP^{135-225}$ crystals were soaked with different concentrations of the heavy atom derivatives diluted in reservoir solution for 1-30 min before freezing the crystals.

5.7.2.3 Data collection and processing

Crystals were cryo-cooled in liquid nitrogen. If required, the crystals were soaked before with cryo solution containing reservoir solution and 20-30 % (v/v) glycerol or 30-40 % PEG 200 in order to avoid ice formation. Crystal diffraction was tested in-house at 100 K with a Nonius MICRO Star generator (Bruker AXS, Karlsruhe, DE) and a mar345 CCD detector (mar research, Norderstedt, DE). Data sets were collected on the beamline PXII of the Swiss Light Source (SLS) at the Paul Scherrer Institute, Villigen, CH, with a transmission of 20 %, an exposure time of 0.1 s, a rotation of 0.25°/image and a total rotation of 180-360°.

For data processing the following programs were used: XDS for indexing and integration of the reflections of all diffraction images; XSCALE for scaling the related intensities; XDSCONV to convert the hkl file to an mtz-file; Phenix AutoSol for identifying heavy atom positions and isomorphous replacement.

5.7.3 Negative stain electron microscopy

Prior to electron microscopy experiments Astrin$^{482-850}$/SKAP$^{159-316}$ complex was freshly purified and diluted appropriately after final size-exclusion chromatography. The specimens were prepared using the conventional negative staining procedure (Bröcker et al., 2012). For this purpose, 4 µl of the diluted sample were adsorbed for 40 s on a freshly glow-discharged 400 mesh copper grid (G2400C, Plano GmbH, Wetzlar, DE) that was covered with a thin carbon film. The excess solution was blotted by touching a Whatman filter paper. The specimens were washed three times with a drop of size-exclusion chromatography buffer and once with freshly prepared 0.75 % uranyl formate (SPI Supplies/Structure Probe, West Chester, US-PA). The samples were exposed to the staining solution for about 1 min. After removing the excess stain by blotting the specimen was air-dried. Image acquisition was performed with a Joel JEM-1400 electron microscope equipped with a LaB_6 cathode and operated at an acceleration voltage of 120 kV. Digital micrographs were recorded at a corrected magnification of 82,524x using a 4k x 4k CMOS camera F416 (TVIPS, Gauting, DE) at a pixel size of 1.89 Å/pixel under minimal dose conditions.

For experiments with Astrin$^{482-850}$/SKAP$^{159-316}$ complex on microtubules, GMPCPP-stabilized microtubule seeds were prepared as follows (Gell et al., 2010). 20 µM tubulin (Cytoskeleton, Inc., Denver, US-CO) was mixed with 1 mM GMPCPP in BRB80 buffer and incubated on ice for 5 min and then at 37 °C for 30 min. After spinning at 126,000 g for 5 min in a TLA 120.1 rotor the pellet was resuspended in BRB80 buffer and incubated on ice for 20 min. After addition of 1 mM GMPCPP the sample was again incubated on ice for 5 min and then at 37 °C for 30 min. After another centrifugation at 126,000 g for 5 min the pellet was dissolved in the size-exclusion chromatography buffer of the Astrin$^{482-850}$/SKAP$^{159-316}$ complex. The GMPCPP-stabilized microtubule seeds were mixed with the Astrin$^{482-850}$/SKAP$^{159-316}$ complex and incubated on the grid for 5 min at 37 °C. Subsequently, the negative stain specimens were prepared as described above. Digital micrographs were recorded at a corrected magnification of 34,110x at a pixel size of 4.66 Å/pixel.

To analyze the effect of SKAP on the structure of microtubules, 10 µM bovine tubulin (Cytoskeleton, Inc., Denver, US-CO) was mixed with 0-10 µM SKAP$^{135-225}$ in reaction buffer (25 mM Hepes, pH 7.5, 150 mM NaCl, 5 % (v/v) glycerol, 4 mM $MgCl_2$, 1 mM EGTA, 2 mM DTE and 2.5 mM GTP) and incubated 10 min at 34 °C. After addition of 50 µM taxol the samples were incubated for 30 min at 34 °C. 4 µL of undiluted samples were adsorbed onto grids for 10 s and prepared as described above.

6 SUPPLEMENT

6.1 Supplementary figures

Figure 6.1: Secondary structure of SKAP predicted by PSIPRED.

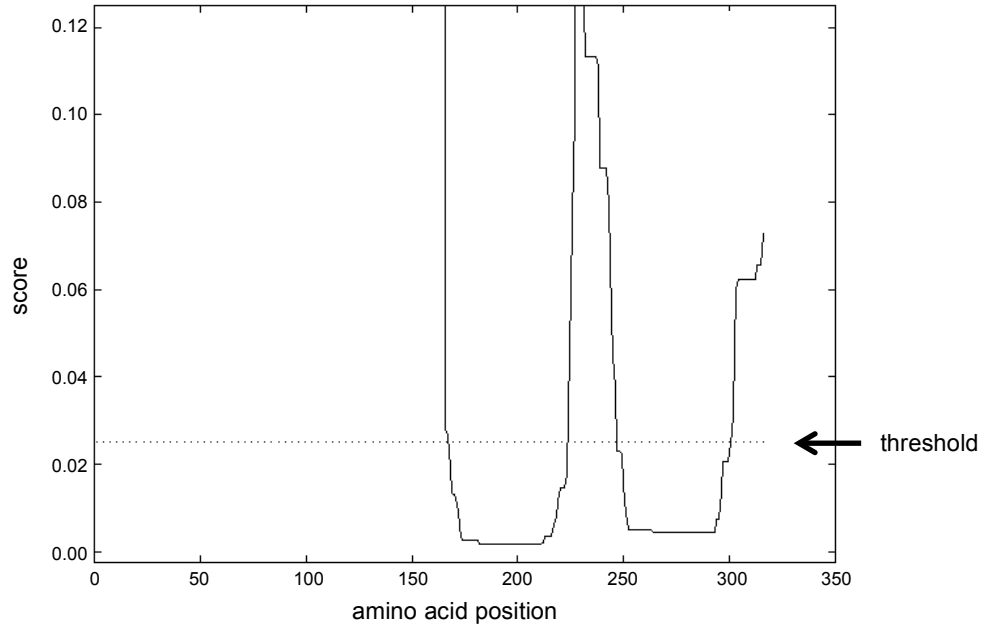

Figure 6.2: Coiled-coil domain prediction of SKAP performed with Paircoil2.

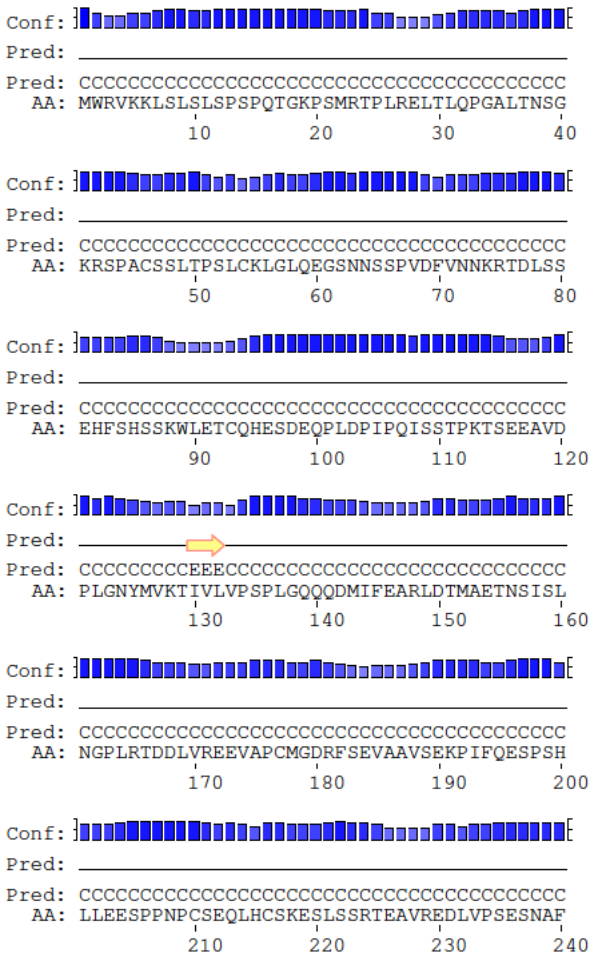

Figure 6.3: Secondary structure of Astrin predicted by PSIPRED.

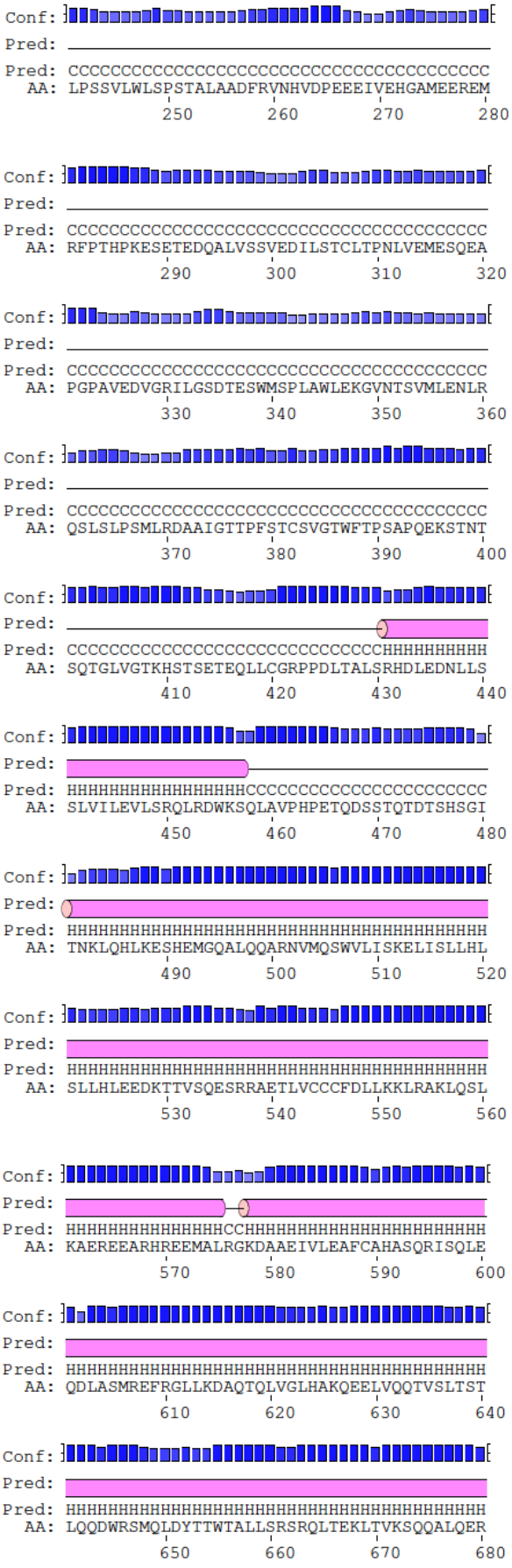

Figure 6.3 (continued): Secondary structure of Astrin predicted by PSIPRED.

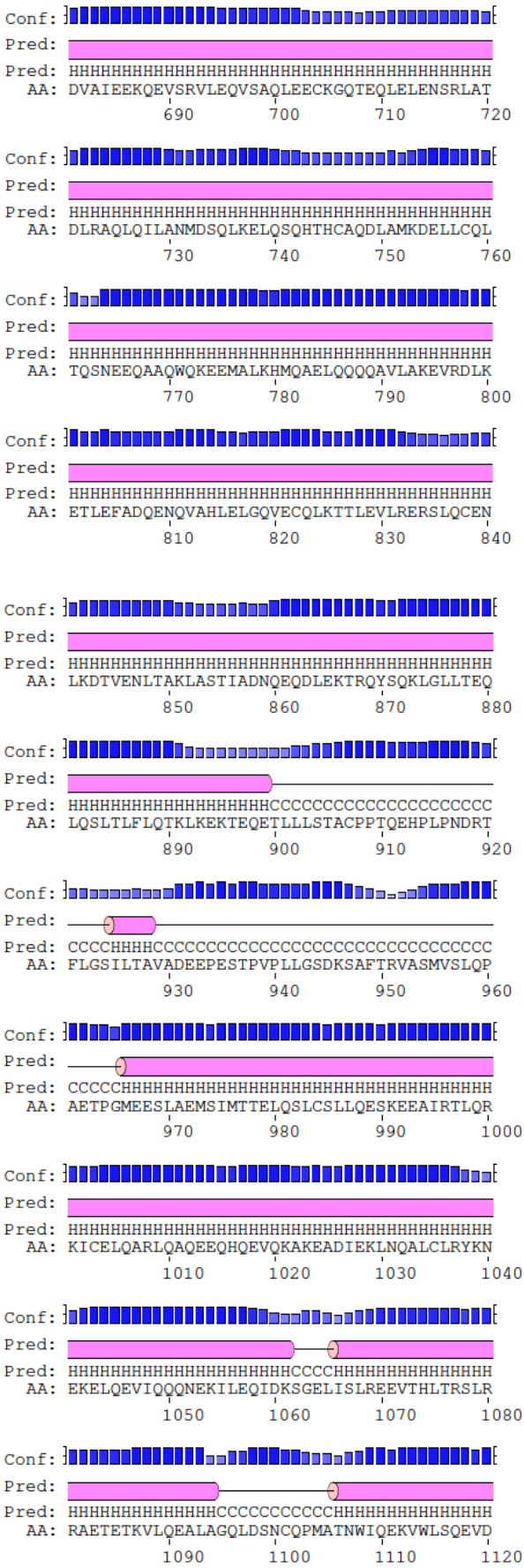

Figure 6.3 (continued): Secondary structure of Astrin predicted by PSIPRED.

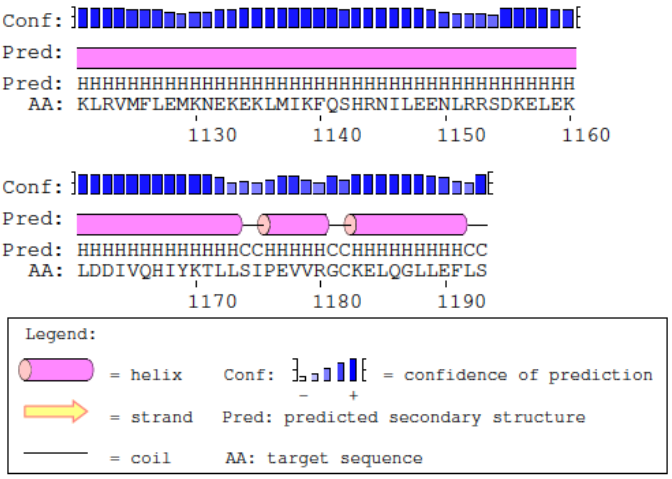

Figure 6.3 (continued): Secondary structure of Astrin predicted by PSIPRED.

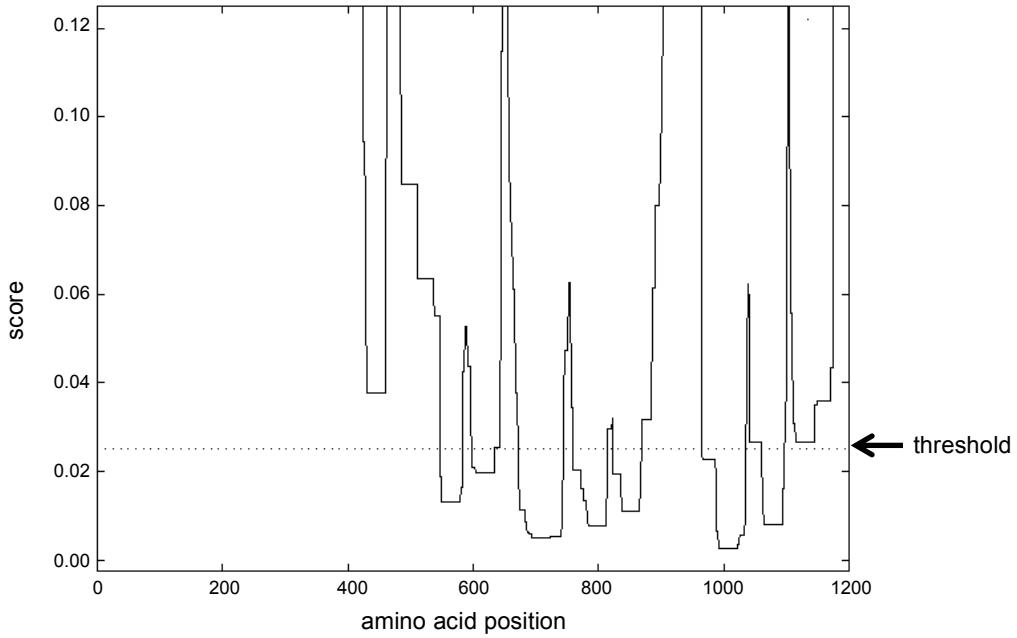

Figure 6.4: Coiled-coil domain prediction of Astrin performed with Paircoil2.

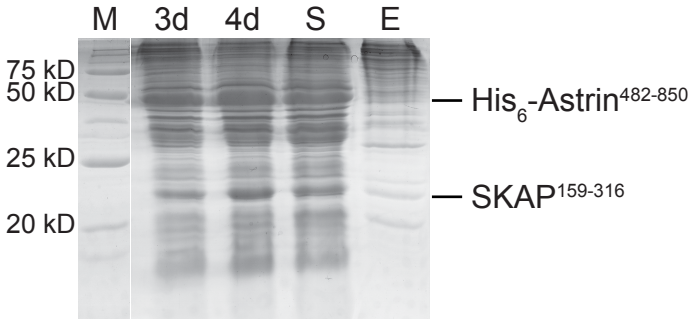

Figure 6.5: Test coexpression of His_6-Astrin$^{482-850}$ and SKAP$^{159-316}$ in Tnao38 cells. M: molecular weight marker with molecular weights indicated on the left, 3d and 4d: whole cell extracts after 3 and 4 days of expression, S: soluble fraction after clearing the cell lysate, E: eluate of the bead fraction.

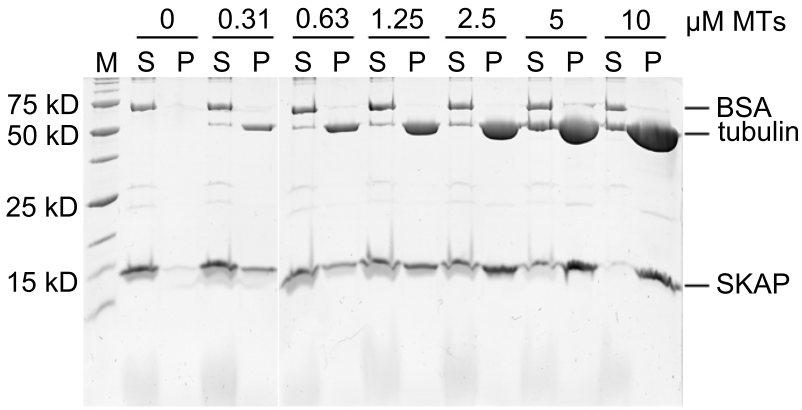

Figure 6.6: Microtubule cosedimentation assay of SKAP$^{135-225}$ K140A. Representative SDS-PAGE gels of microtubule cosedimentation assay with 0-10 µM taxol-stabilized microtubules (MTs) and 1 µM SKAP$^{135-225}$ K140A. S: soluble fraction with proteins not bound to microtubules. P: pellet fraction with microtubules and bound proteins. M: molecular weight marker with molecular weights indicated on the left.

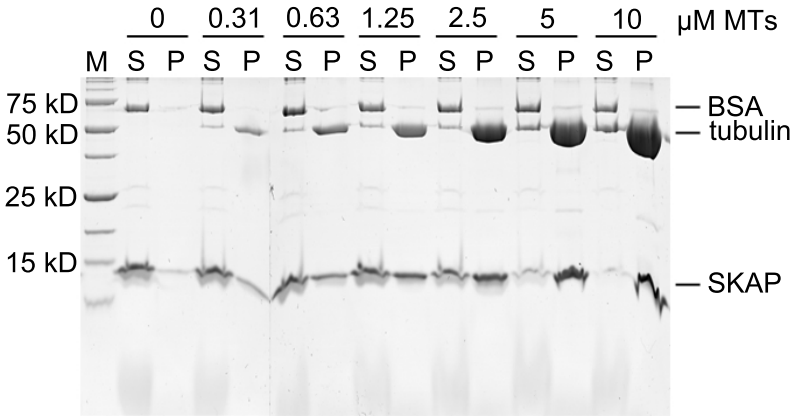

Figure 6.7: Microtubule cosedimentation assay of SKAP$^{135-225}$ K149A. Representative SDS-PAGE gels of microtubule cosedimentation assay with 0-10 µM taxol-stabilized microtubules (MTs) and 1 µM SKAP$^{135-225}$ K149A. S: soluble fraction with proteins not bound to microtubules. P: pellet fraction with microtubules and bound proteins. M: molecular weight marker with molecular weights indicated on the left.

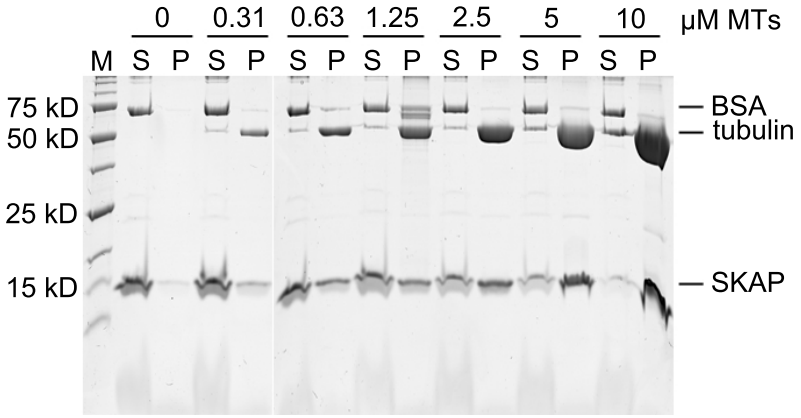

Figure 6.8: Microtubule cosedimentation assay of SKAP$^{135-225}$ K161A. Representative SDS-PAGE gels of microtubule cosedimentation assay with 0-10 μM taxol-stabilized microtubules (MTs) and 1 μM SKAP$^{135-225}$ K161A. S: soluble fraction with proteins not bound to microtubules. P: pellet fraction with microtubules and bound proteins. M: molecular weight marker with molecular weights indicated on the left.

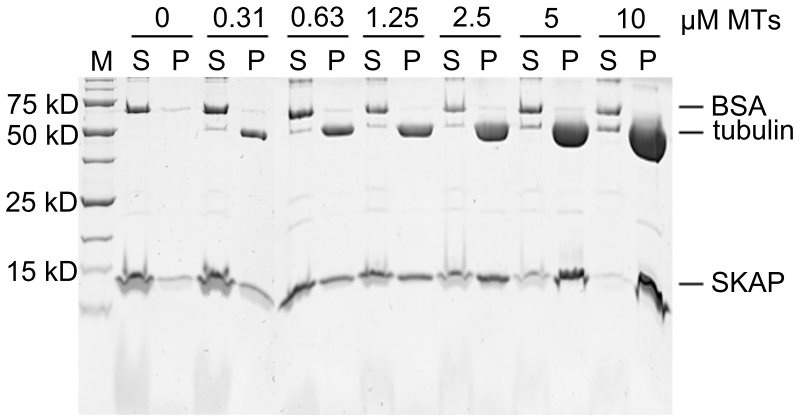

Figure 6.9: Microtubule cosedimentation assay of SKAP$^{135-225}$ K164A. Representative SDS-PAGE gels of microtubule cosedimentation assay with 0-10 μM taxol-stabilized microtubules (MTs) and 1 μM SKAP$^{135-225}$ K164A. S: soluble fraction with proteins not bound to microtubules. P: pellet fraction with microtubules and bound proteins. M: molecular weight marker with molecular weights indicated on the left.

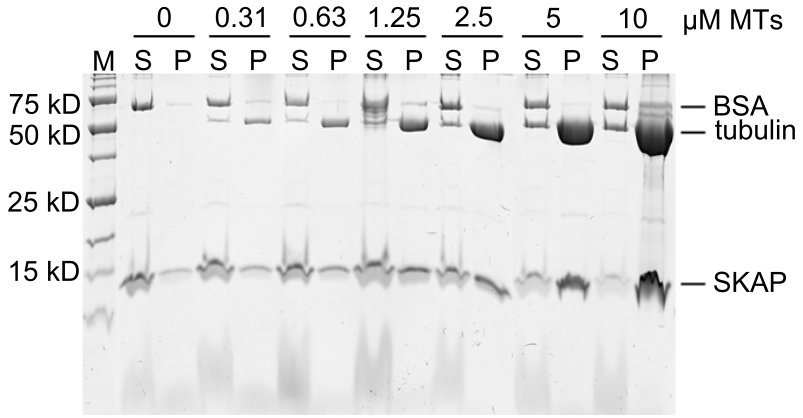

Figure 6.10: Microtubule cosedimentation assay of SKAP$^{135-225}$ K161/164A. Representative SDS-PAGE gels of microtubule cosedimentation assay with 0-10 µM taxol-stabilized microtubules (MTs) and 1 µM SKAP$^{135-225}$ K161/164A. S: soluble fraction with proteins not bound to MTs. P: pellet fraction with microtubules and bound proteins. M: molecular weight marker with molecular weights indicated on the left.

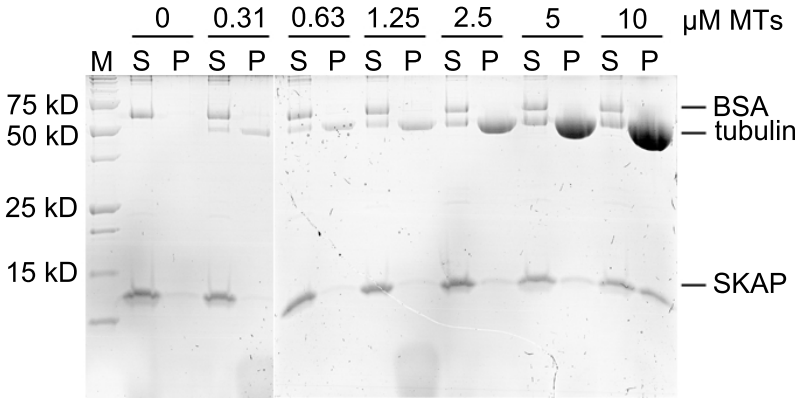

Figure 6.11: Microtubule cosedimentation assay of SKAP$^{135-225}$ K140/149/161/164A. Representative SDS-PAGE gels of microtubule cosedimentation assay with 0-10 µM taxol-stabilized microtubules (MTs) and 1 µM SKAP$^{135-225}$ K140/149/161/164A. S: soluble fraction with proteins not bound to microtubules. P: pellet fraction with microtubules and bound proteins. M: molecular weight marker with molecular weights indicated on the left.

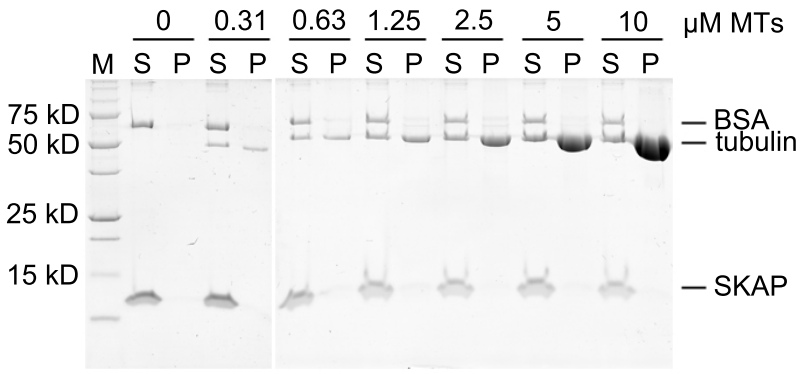

Figure 6.12: Microtubule cosedimentation assay of SKAP$^{135-225}$ K140/149/161/164/168/170A. Representative SDS-PAGE gels of microtubule cosedimentation assay with 0-10 µM taxol-stabilized microtubules (MTs) and 1 µM SKAP$^{135-225}$ K140/149/161/164/168/170A. S: soluble fraction with proteins not bound to microtubules. P: pellet fraction with microtubules and bound proteins. M: molecular weight marker with molecular weights indicated on the left.

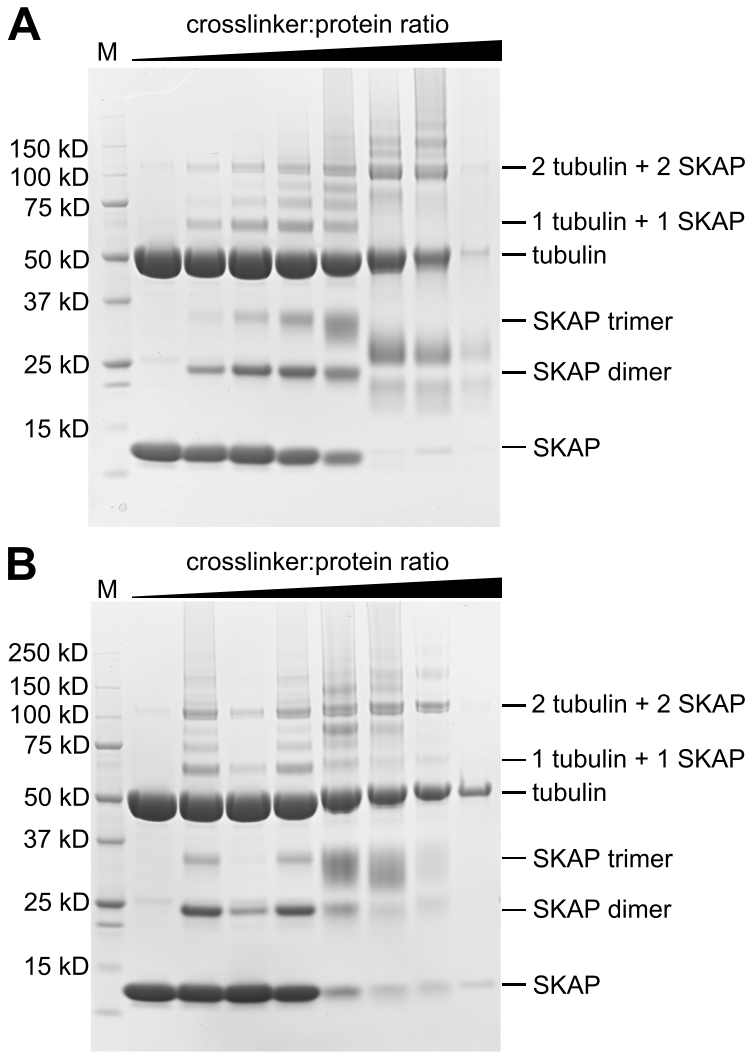

Figure 6.13: Screen of appropriate conditions for crosslinking analysis of microtubules and SKAP$^{135-225}$. SDS-PAGE gels of crosslinking reactions performed with 10 µM taxol-stabilized microtubules, 10 µM SKAP$^{135-225}$ and the crosslinkers BS2G (A) and DSS (B). Crosslinker:protein weight ratios from left to right were 0:1, 1:10, 1:5, 1:2.5, 1:1, 2.5:1, 5:1 and 10:1. M: molecular weight marker with molecular weights indicated on the left.

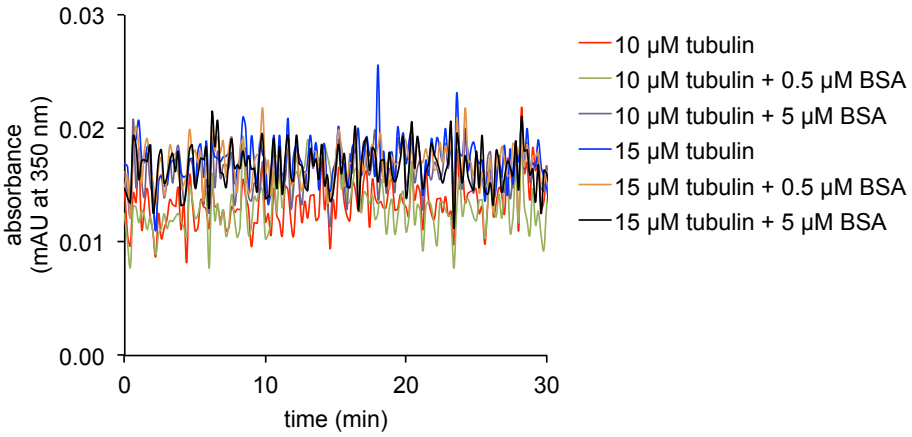

Figure 6.14: Tubulin and BSA controls for tubulin polymerization assay. Tubulin polymerization assays with 10-15 µM tubulin and 0-5 µM BSA. Tubulin polymerization was measured by following the absorbance at 350 nm at 37 °C.

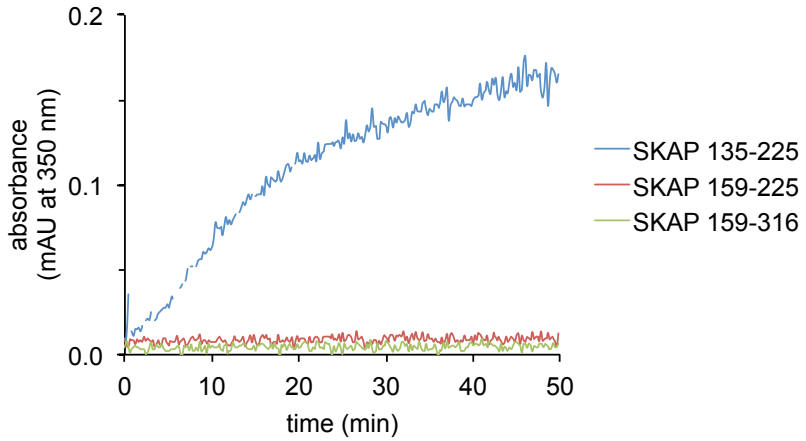

Figure 6.15: SKAP$^{159-225}$ and SKAP$^{159-316}$ do not promote tubulin polymerization. Tubulin polymerization assays with 5 µM tubulin and 1 µM of SKAP$^{135-225}$, SKAP$^{159-225}$ or SKAP$^{159-316}$. Tubulin polymerization was measured by following the absorbance at 350 nm at 37 °C.

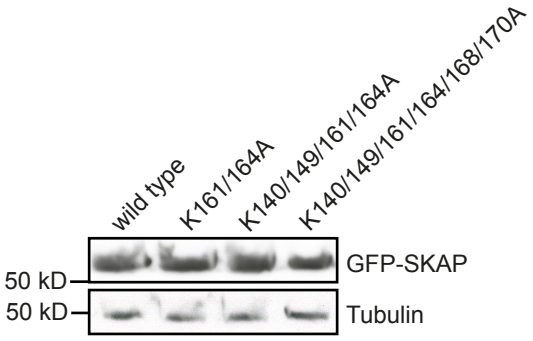

Figure 6.16: Levels of GFP-SKAP wild type and mutants after doxycycline induction. Western blots with cell lysates of stable Flp-In T-REx cell lines expressing GFP-SKAP full-length wild type or indicated mutants. Cells were treated with 0.1 µg/mL doxycycline for 24 h. Western blots were stained for GFP and tubulin as loading control.

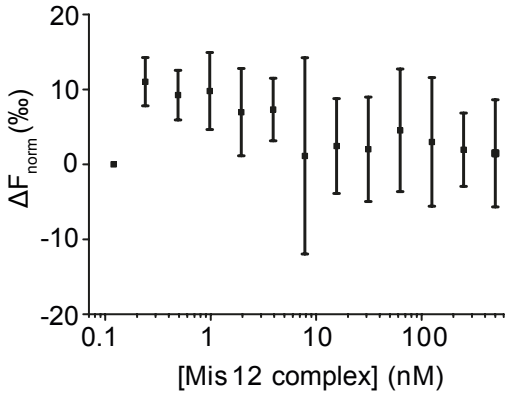

Figure 6.17: The Mis12 complex and the Ndc80 complex do not interact in MST. Quantification of microscale thermophoresis assay with 2 nM GFP-tagged Ndc80 complex and the Mis12 complex. Normalized difference in fluorescence for the thermophoresis and the temperature jump signal. Signals were analyzed with the NT Analysis software (NanoTemper Technologies GmbH, Munich, DE).

6.2 Supplementary tables

Table 6.1: Crosslinks between microtubules and SKAP$^{135-225}$ in presence of DSS. TIC: fraction of total ion current of fragment ion spectrum assigned to crosslink. Mz: mass to charge ratio. nseen: number of fragment ion spectra assigned to the crosslink in entire dataset.

Summary of intermolecular crosslinks

Crosslinked peptides	Protein 1	Protein 2	Aa pos 1	Aa pos 2	Mz	z	Error_rel [ppm]	nseen	TIC	ID score
FDLMYAKR-ITKLR-a7-b3	α-Tubulin	SKAP	401	140	453,512	4	-1,3	4	0,71	41,71
FDLMYAKR-GYKPLSK-a7-b3	α-Tubulin	SKAP	401	164	494,019	4	-2,8	4	0,65	41,22
LDHKFDLMYAK-ITKLR-a4-b3	α-Tubulin	SKAP	394	140	537,802	4	-1,9	2	0,59	40,22
LDHKFDLMYAKR-ITKLR-a11-b3	α-Tubulin	SKAP	401	140	461,664	5	-1,1	2	0,58	39,58
DVNAAIATIKTK-ITKLR-a10-b3	α-Tubulin	SKAP	336	140	671,408	3	-1,1	4	0,62	38,45
LSVDYGKK-ITKLR-a7-b3	α-Tubulin	SKAP	163	140	420,004	4	-2,1	2	0,64	38,28
GHYTIGKEIIDLVLDR-ITKLR-a7-b3	α-Tubulin	SKAP	112	140	653,131	4	-1,3	8	0,61	38,17
LDHKFDLMYAK-GYKPLSK-a4-b3	α-Tubulin	SKAP	394	164	578,31	4	-1,4	3	0,44	37,86
ENGQMKATDTATRR-LSVDYGKK-a6-b7	SKAP	α-Tubulin	149	163	525,871	5	-2	3	0,49	37,43
FDLMYAKR-KGYKPLSK-a7-b4	α-Tubulin	SKAP	401	164	526,043	4	-1,9	3	0,77	37,41
LSVDYGKK-SEEELKDK-a7-b6	α-Tubulin	SKAP	163	176	506,766	4	-1	2	0,44	36,81
LDHKFDLMYAKR-KGYKPLSK-a11-b1	α-Tubulin	SKAP	401	161	519,689	5	-2,1	2	0,57	36,51
HGKYMACCLLYR-KGYKPLSK-a3-b1	α-Tubulin	SKAP	311	161	658,091	4	-2,2	3	0,41	35,49
GHYTIGKEIIDLVLDR-KGYKPLSK-a7-b1	α-Tubulin	SKAP	112	161	725,662	4	-2,1	8	0,47	34,8
LSVDYGKK-QKSEEELK-a7-b2	α-Tubulin	SKAP	163	170	510,023	4	-3,2	4	0,5	34,75
HGKYMACCLLYR-ITKLR-a3-b3	α-Tubulin	SKAP	311	140	585,561	4	0,1	3	0,51	34,72
TIGGGDDSFNTFFSETGAGKHVPR-ITKLR-a20-b3	α-Tubulin	SKAP	60	140	653,738	5	-1,5	3	0,45	34,34

Crosslinked peptides	Protein 1	Protein 2	Aa pos 1	Aa pos 2	Mz	z	Error_rel [ppm]	nseen	TIC	ID score
FDLMYAKR-QKSEEELK-a7-b2	α-Tubulin	SKAP	401	170	543,531	4	-2	3	0,39	33,96
LDHKFDLMYAK-KGYKPLSK-a4-b1	α-Tubulin	SKAP	394	161	610,334	4	-1,7	1	0,34	33,76
GHYTIGKEIIDLVLDR-ENGQMKATDTATR-a7-b6	α-Tubulin	SKAP	112	149	681,152	5	-2,3	2	0,43	33,69
DVNAAIATIKTK-KGYKPLSK-a10-b4	α-Tubulin	SKAP	336	164	576,34	4	-1,3	2	0,52	33,68
DVNAAIATIKTK-KGYKPLSK-a10-b1	α-Tubulin	SKAP	336	161	576,34	4	-0,9	1	0,58	32,83
GHYTIGKEIIDLVLDR-GYKPLSK-a7-b3	α-Tubulin	SKAP	112	164	693,638	4	-2,3	5	0,5	32,39
GYKPLSKQK-LSVDYGKK-a7-b7	SKAP	α-Tubulin	168	163	419,842	5	-1,5	3	0,49	32,26
GHYTIGKEIIDLVLDR-RENGQMKATDTATR-a7-b7	α-Tubulin	SKAP	112	149	712,373	5	-2	4	0,46	31,86
KLAVNMVPFPR-FDLMYAKR-a1-b7	β-Tubulin	α-Tubulin	252	401	613,835	4	-3,3	2	0,51	31,74
LDHKFDLMYAKR-KGYKPLSK-a11-b4	α-Tubulin	SKAP	401	164	519,688	5	-2,2	1	0,39	31,08
DVNAAIATIKTK-GYKPLSK-a10-b3	α-Tubulin	SKAP	336	164	725,419	3	-1	2	0,56	30,87
KGYKPLSK-LSVDYGKK-a1-b7	SKAP	α-Tubulin	161	163	656,378	3	-2,4	2	0,34	30,65
ENGQMKATDTATRR-FDLMYAKR-a6-b7	SKAP	α-Tubulin	149	401	690,595	4	-1,4	1	0,46	30,58
ENGQMKATDTATR-HGKYMACCLLYR-a6-b3	SKAP	α-Tubulin	149	311	783,618	4	-1,5	2	0,37	30,21
DVNAAIATIKTK-QKSEEELK-a10-b2	α-Tubulin	SKAP	336	170	791,436	3	-0,4	2	0,29	29,75
KLAVNMVPFPR-VELLEKFR-a1-b6	β-Tubulin	SKAP	252	212	611,354	4	-1,1	6	0,49	29,52
ENGQMKATDTATR-KLAVNMVPFPR-a6-b1	SKAP	β-Tubulin	149	252	708,618	4	-2,2	2	0,44	29,1
QLFHPEQLITGKEDAANNYAR-KGYKPLSK-a12-b1	α-Tubulin	SKAP	96	161	695,37	5	-1,9	8	0,39	28,6
FDLMYAKR-KGYKPLSK-a7-b1	α-Tubulin	SKAP	401	161	701,055	3	-1	1	0,37	27,84
QLFHPEQLITGKEDAANNYAR-MSMKEVDEQMLNVQNK-a12-b4	α-Tubulin	β-Tubulin	96	324	1119,79	4	-1,4	3	0,31	27,71

Crosslinked peptides	Protein 1	Protein 2	Aa pos 1	Aa pos 2	Mz	z	Error_rel [ppm]	nseen	TIC	ID score
ENGQMKATDTATR-FDLMYAKR-a6-b7	SKAP	α-Tubulin	149	401	868,423	3	-2,6	3	0,26	27,25
LDHKFDLMYAKR-GYKPLSKQK-a11-b7	α-Tubulin	SKAP	401	168	545,301	5	-0,4	1	0,41	26,88
ENGQMKATDTATR-LDHKFDLMYAK-a6-b4	SKAP	α-Tubulin	149	394	735,861	4	-0,6	2	0,26	26,21
TLKLTTPTYGDLNHLVSATMSGVTTCLR-GDVVPKDVNAAIATIK-a3-b6	β-Tubulin	α-Tubulin	216	326	960,514	5	0	1	0,34	24,77
DNCLAILESKG-KLAVNMVPFPR-a10-b1	SKAP	β-Tubulin	224	252	876,8	3	-1,9	1	0,32	24,32
GHYTIGKEIIDLVLDR-QKSEEELK-a7-b2	α-Tubulin	SKAP	112	170	743,151	4	-0,9	3	0,31	23,92
VGINYQPPTVVPGGDLAKVQR-RENGQMKATDTATR-a18-b7	α-Tubulin	SKAP	370	149	785,613	5	-1,8	2	0,58	22,79

Summary of intramolecular crosslinks

Crosslinked peptides	Protein 1	Protein 2	Aa pos 1	Aa pos 2	Mz	z	Error_rel [ppm]	nseen	TIC	ID score
VELLEKFR-ITKLR-a6-b3	SKAP	SKAP	212	140	451,029	4	-1,4	7	0,73	44,44
VELLEKFR-GYKPLSK-a6-b3	SKAP	SKAP	212	164	491,536	4	-2,8	7	0,68	42,74
SEEELKDK-ITKLR-a6-b3	SKAP	SKAP	176	140	582,327	3	-2,2	4	0,62	42,49
SEEELKDK-GYKPLSK-a6-b3	SKAP	SKAP	176	164	477,506	4	-0,5	10	0,58	42,26
KGYKPLSK-SEEELKDK-a4-b6	SKAP	SKAP	164	176	407,825	5	-0,7	17	0,56	42,03
KGYKPLSK-ITKLR-a1-b3	SKAP	SKAP	161	140	422,767	4	-0,9	20	0,68	41,93
GYKPLSK-ITKLRR-a3-b3	SKAP	SKAP	164	140	429,768	4	-2,2	7	0,47	41,6
DLTQKVELLEKFR-ITKLR-a11-b3	SKAP	SKAP	212	140	597,357	4	-2	2	0,62	41,56

Crosslinked peptides	Protein 1	Protein 2	Aa pos 1	Aa pos 2	Mz	z	Error_rel [ppm]	nseen	TIC	ID score
QKSEEELK-GYKPLSK-a2-b3	SKAP	SKAP	170	164	480,763	4	-2,3	26	0,4	41,53
GYKPLSKQK-GYKPLSK-a7-b3	SKAP	SKAP	168	164	495,289	4	-1,8	7	0,54	41,14
GYKPLSKQK-KGYKPLSK-a7-b1	SKAP	SKAP	168	161	422,053	5	-0,7	6	0,55	40,94
GYKPLSKQK-SEEELKDK-a7-b6	SKAP	SKAP	168	176	721,723	3	-1,1	19	0,65	40,94
GYKPLSKQK-KGYKPLSK-a7-b4	SKAP	SKAP	168	164	422,052	5	-1,5	14	0,54	40,93
SEEELKDK-VELLEKFR-a6-b6	SKAP	SKAP	176	212	537,791	4	-2,2	6	0,59	40,86
KGYKPLSK-KGYKPLSK-a1-b4	SKAP	SKAP	161	164	495,299	4	-1,1	4	0,6	40,77
NQLLEAVNKQLHQK-ITKLR-a9-b3	SKAP	SKAP	187	140	486,889	5	-1,7	7	0,56	40,67
GYKPLSK-ITKLR-a3-b3	SKAP	SKAP	164	140	520,656	3	-0,2	3	0,6	40,64
DKNQLLEAVNK-DLTQKVELLEK-a2-b5	SKAP	SKAP	178	206	681,881	4	-1	2	0,48	40,58
DLTQKVELLEKFR-DLTQKVELLEK-a11-b5	SKAP	SKAP	212	206	768,685	4	-2,6	3	0,49	40,5
KGYKPLSK-GYKPLSK-a1-b3	SKAP	SKAP	161	164	463,275	4	-2	11	0,48	40,39
DLTQKVELLEK-VELLEKFR-a5-b6	SKAP	SKAP	206	212	622,358	4	-1,6	4	0,58	40,15
GYKPLSKQK-VELLEKFR-a7-b6	SKAP	SKAP	168	212	444,662	5	-1,7	2	0,56	40,1
KGYKPLSK-ITKLRR-a4-b3	SKAP	SKAP	164	140	461,793	4	0,6	10	0,52	39,75
DKNQLLEAVNK-ITKLR-a2-b3	SKAP	SKAP	178	140	510,552	4	-0,9	8	0,57	39,73
DKNQLLEAVNK-GYKPLSK-a2-b3	SKAP	SKAP	178	164	734,411	3	-0,9	8	0,53	39,39
QKSEEELK-VELLEKFR-a2-b6	SKAP	SKAP	170	212	541,049	4	-2	5	0,55	39,14
DLTQKVELLEK-GYKPLSK-a5-b3	SKAP	SKAP	206	164	562,073	4	-1,2	5	0,53	39,12
DLTQKVELLEK-KGYKPLSK-a5-b4	SKAP	SKAP	206	164	594,095	4	-2,7	7	0,6	39,02
KGYKPLSK-SEEELKDK-a1-b6	SKAP	SKAP	161	176	679,036	3	-1,2	14	0,48	38,87

Crosslinked peptides	Protein 1	Protein 2	Aa pos 1	Aa pos 2	Mz	z	Error_rel [ppm]	nseen	TIC	ID score
RENGQMKATDTATR-VELLEKFR-a7-b6	SKAP	SKAP	149	212	688,112	4	-2,7	13	0,67	38,76
KGYKPLSK-ITKLR-a4-b3	SKAP	SKAP	164	140	422,767	4	-1,4	13	0,61	38,62
LTETQGELKDLTQK-VELLEKFR-a9-b6	SKAP	SKAP	201	212	925,51	3	-1,7	4	0,46	38,31
NQLLEAVNKQLHQK-DKNQLLEAVNK-a9-b2	SKAP	SKAP	187	178	1024,57	3	0,4	7	0,42	38,26
DLTQKVELLEK-DNCLAILESKG-a5-b10	SKAP	SKAP	206	224	891,473	3	-1,8	4	0,52	38,25
QKSEEELK-ITKLR-a2-b3	SKAP	SKAP	170	140	440,255	4	-2	7	0,33	38,21
QLHQKLTETQGELK-DKNQLLEAVNK-a5-b2	SKAP	SKAP	192	178	613,137	5	-0,6	11	0,53	37,99
KGYKPLSKQK-KGYKPLSK-a8-b1	SKAP	SKAP	168	161	447,671	5	-1,5	2	0,51	37,95
DNCLAILESKG-VELLEKFR-a10-b6	SKAP	SKAP	224	212	797,427	3	0,4	34	0,5	37,8
LTETQGELKDLTQKVELLEK-VELLEKFR-a9-b6	SKAP	SKAP	201	212	697,992	5	-2,5	4	0,57	37,79
KGYKPLSKQK-SEEELKDK-a8-b6	SKAP	SKAP	168	176	764,421	3	-1,1	2	0,41	37,63
DLTQKVELLEK-ITKLR-a5-b3	SKAP	SKAP	206	140	521,565	4	-1,2	4	0,57	37,6
GYKPLSKQK-QKSEEELK-a7-b2	SKAP	SKAP	168	170	436,043	5	-1,9	10	0,31	37,53
DLTQKVELLEKFR-KGYKPLSK-a11-b1	SKAP	SKAP	212	161	669,889	4	-0,7	5	0,44	37,51
RENGQMKATDTATR-GYKPLSK-a7-b3	SKAP	SKAP	149	164	627,827	4	-1,8	16	0,44	37,38
DKNQLLEAVNK-VELLEKFR-a2-b6	SKAP	SKAP	178	212	814,791	3	-1,4	5	0,49	37,31
DKNQLLEAVNK-SEEELKDK-a2-b6	SKAP	SKAP	178	176	796,083	3	-1,1	6	0,47	37,3
QLHQKLTETQGELK-GYKPLSK-a5-b3	SKAP	SKAP	192	164	517,289	5	-2,2	7	0,37	37,16
ENGQMKATDTATR-VELLEKFR-a6-b6	SKAP	SKAP	149	212	649,087	4	-2,3	8	0,46	37,12
FRDNCLAILESKG-VELLEKFR-a12-b6	SKAP	SKAP	224	212	674,114	4	-1	14	0,44	37,05
ENGQMKATDTATR-DKNQLLEAVNK-a6-b2	SKAP	SKAP	149	178	708,609	4	-2,9	7	0,46	36,95

Crosslinked peptides	Protein 1	Protein 2	Aa pos 1	Aa pos 2	Mz	z	Error_rel [ppm]	nseen	TIC	ID score
KGYKPLSK-ITKLRR-a1-b3	SKAP	SKAP	161	140	461,792	4	-1,3	4	0,4	36,89
ENGQMKATDTATR-GPLGSVTKITK-a6-b8	SKAP	SKAP	149	137	887,466	3	-4	4	0,37	36,82
ENGQMKATDTATR-KGYKPLSK-a6-b1	SKAP	SKAP	149	161	827,434	3	2,2	30	0,35	36,8
LTETQGELKDLTQK-ITKLRR-a9-b3	SKAP	SKAP	201	140	506,295	5	-1,5	9	0,55	36,72
DLTQKVELLEKFR-DKNQLLEAVNK-a11-b2	SKAP	SKAP	212	178	1009,89	3	-2	5	0,36	36,48
LTETQGELKDLTQK-QKSEEELK-a9-b2	SKAP	SKAP	201	170	911,147	3	0,2	4	0,28	36,48
GPLGSVTKITK-VELLEKFR-a8-b6	SKAP	SKAP	137	212	757,78	3	-3,7	1	0,63	36,45
NQLLEAVNKQLHQK-GYKPLSK-a9-b3	SKAP	SKAP	187	164	648,868	4	-0,6	3	0,54	36,38
QKSEEELK-SEEELKDK-a2-b6	SKAP	SKAP	170	176	527,017	4	-1,8	5	0,53	36,35
KGYKPLSK-QKSEEELK-a1-b2	SKAP	SKAP	161	170	512,787	4	-1,6	54	0,26	36,28
QLHQKLTETQGELK-VELLEKFR-a5-b6	SKAP	SKAP	192	212	565,517	5	-2,7	12	0,36	36,27
DKNQLLEAVNK-KGYKPLSK-a2-b4	SKAP	SKAP	178	164	777,109	3	-0,1	18	0,44	36,23
ENGQMKATDTATRR-DKNQLLEAVNK-a6-b2	SKAP	SKAP	149	178	598,31	5	-1,1	4	0,48	36,11
KGYKPLSK-QKSEEELK-a4-b2	SKAP	SKAP	164	170	683,38	3	-2,2	54	0,3	35,92
QKSEEELKDK-KGYKPLSK-a8-b4	SKAP	SKAP	176	164	459,056	5	-1,2	13	0,48	35,91
DKNQLLEAVNK-KGYKPLSKQK-a2-b8	SKAP	SKAP	178	168	862,492	3	-2,9	2	0,51	35,78
QLHQKLTETQGELK-SEEELKDK-a5-b6	SKAP	SKAP	192	176	692,615	4	-0,4	6	0,31	35,72
DLTQKVELLEK-SEEELKDK-a5-b6	SKAP	SKAP	206	176	608,327	4	-0,6	4	0,45	35,47
RENGQMKATDTATR-DKNQLLEAVNK-a7-b2	SKAP	SKAP	149	178	598,31	5	-1,5	6	0,45	35,02
ENGQMKATDTATR-KGYKPLSK-a6-b4	SKAP	SKAP	149	164	620,826	4	0,2	16	0,41	35,02
ENGQMKATDTATR-DLTQKVELLEK-a6-b5	SKAP	SKAP	149	206	719,623	4	-0,9	6	0,45	34,92

Crosslinked peptides	Protein 1	Protein 2	Aa pos 1	Aa pos 2	Mz	z	Error_rel [ppm]	nseen	TIC	ID score
DKNQLLEAVNK-QKSEEELK-a2-b2	SKAP	SKAP	178	170	600,571	4	-2	13	0,43	34,92
GPLGSVTKITK-KGYKPLSK-a8-b1	SKAP	SKAP	137	161	432,463	5	-0,3	2	0,54	34,83
DLTQKVELLEK-ITKLRR-a5-b3	SKAP	SKAP	206	140	560,59	4	-1,6	2	0,57	34,69
LTETQGELKDLTQK-KGYKPLSK-a9-b4	SKAP	SKAP	201	164	887,829	3	-0,3	10	0,35	34,65
DLTQKVELLEK-QKSEEELK-a5-b2	SKAP	SKAP	206	170	611,584	4	-1,8	4	0,47	34,59
QLHQKLTETQGELK-ITKLR-a5-b3	SKAP	SKAP	192	140	484,884	5	-0,3	6	0,3	34,57
ENGQMKATDTATRR-ITKLR-a6-b3	SKAP	SKAP	149	140	470,056	5	-3	31	0,45	34,52
LTETQGELKDLTQK-DKNQLLEAVNK-a9-b2	SKAP	SKAP	201	178	1004,87	3	-2,5	4	0,46	34,51
ENGQMKATDTATRR-GYKPLSK-a6-b3	SKAP	SKAP	149	164	502,463	5	-1,6	23	0,38	34,5
ENGQMKATDTATR-GYKPLSK-a6-b3	SKAP	SKAP	149	164	784,734	3	-0,9	6	0,45	34,38
ENGQMKATDTATR-ITKLR-a6-b3	SKAP	SKAP	149	140	730,723	3	-1	22	0,32	34,38
DLTQKVELLEKFR-KGYKPLSK-a11-b4	SKAP	SKAP	212	164	536,112	5	-2,6	5	0,67	34,28
QLHQKLTETQGELK-QKSEEELK-a5-b2	SKAP	SKAP	192	170	927,493	3	-1,5	8	0,1	34,19
ENGQMKATDTATR-GYKPLSKQK-a6-b7	SKAP	SKAP	149	168	522,473	5	-1,9	12	0,21	34,19
NQLLEAVNKQLHQK-GYKPLSKQK-a9-b7	SKAP	SKAP	187	168	712,906	4	-1,4	5	0,38	34,08
QLHQKLTETQGELK-KGYKPLSK-a5-b1	SKAP	SKAP	192	161	678,384	4	-0,8	21	0,26	34,05
LTETQGELKDLTQK-GYKPLSKQK-a9-b7	SKAP	SKAP	201	168	930,514	3	-1,4	8	0,45	34,01
NQLLEAVNKQLHQK-QLHQKLTETQGELK-a9-b5	SKAP	SKAP	187	192	863,977	4	-0,6	5	0,28	33,98
QLHQKLTETQGELK-DNCLAILESKG-a5-b10	SKAP	SKAP	192	224	753,145	4	0,3	7	0,43	33,86
NQLLEAVNKQLHQK-VELLEKFR-a9-b6	SKAP	SKAP	187	212	945,205	3	1,7	3	0,49	33,77
ENGQMKATDTATR-SEEELKDK-a6-b6	SKAP	SKAP	149	176	846,406	3	-0,2	8	0,45	33,71

Crosslinked peptides	Protein 1	Protein 2	Aa pos 1	Aa pos 2	Mz	z	Error_rel [ppm]	nseen	TIC	ID score
DKNQLLEAVNK-DNCLAILESKG-a2-b10	SKAP	SKAP	178	224	876,79	3	-0,5	5	0,5	33,41
GPLGSVTKITK-ITKLRR-a8-b3	SKAP	SKAP	137	140	506,82	4	-0,8	2	0,59	33,37
LTETQGELKDLTQK-DNCLAILESKG-a9-b10	SKAP	SKAP	201	224	987,508	3	-1,4	2	0,49	33,32
DKNQLLEAVNK-GPLGSVTKITK-a2-b8	SKAP	SKAP	178	137	628,113	4	1,8	2	0,35	33,18
RENGQMKATDTATR-GYKPLSKQK-a7-b7	SKAP	SKAP	149	168	691,865	4	-1,1	7	0,64	33,15
ENGQMKATDTATRR-KGYKPLSK-a6-b4	SKAP	SKAP	149	164	528,082	5	-2	28	0,45	33,14
LTETQGELKDLTQK-ENGQMKATDTATR-a9-b6	SKAP	SKAP	201	149	1055,20	3	-1,6	4	0,37	33,1
LTETQGELKDLTQKVELLEK-KGYKPLSK-a9-b1	SKAP	SKAP	201	161	843,978	4	0,6	2	0,32	32,99
QLHQKLTETQGELK-ENGQMKATDTATR-a5-b6	SKAP	SKAP	192	149	803,912	4	0,4	13	0,33	32,98
DLTQKVELLEKFR-FRDNCLAILESKG-a11-b12	SKAP	SKAP	212	224	656,554	5	-1,6	11	0,46	32,92
NQLLEAVNKQLHQK-ENGQMKATDTATR-a9-b6	SKAP	SKAP	187	149	806,417	4	-2,5	5	0,32	32,9
LTETQGELKDLTQK-SEEELKDK-a9-b6	SKAP	SKAP	201	176	906,802	3	-1,8	2	0,4	32,87
ENGQMKATDTATRR-KGYKPLSK-a6-b1	SKAP	SKAP	149	161	659,851	4	-0,2	15	0,3	32,72
NQLLEAVNKQLHQK-KGYKPLSK-a9-b1	SKAP	SKAP	187	161	680,893	4	0,4	9	0,4	32,61
LTETQGELKDLTQK-KGYKPLSKQK-a9-b4	SKAP	SKAP	201	164	584,33	5	-1,4	4	0,39	32,6
DLTQKVELLEKFR-SEEELKDK-a11-b6	SKAP	SKAP	212	176	684,119	4	-1	1	0,48	32,58
NQLLEAVNKQLHQK-FRDNCLAILESKG-a9-b12	SKAP	SKAP	187	224	831,443	4	-2,5	8	0,42	32,57
DKNQLLEAVNKQLHQK-DKNQLLEAVNK-a11-b2	SKAP	SKAP	187	178	663,767	5	-1,7	3	0,42	32,45
QLHQKLTETQGELK-KGYKPLSKQK-a5-b4	SKAP	SKAP	192	164	742,423	4	0,3	3	0,31	32,43
QLHQKLTETQGELK-ITKLRR-a5-b3	SKAP	SKAP	192	140	516,104	5	-0,7	9	0,28	32,38
QLHQKLTETQGELK-RENGQMKATDTATR-a5-b7	SKAP	SKAP	192	149	674,551	5	-0,2	16	0,41	32,38

Crosslinked peptides	Protein 1	Protein 2	Aa pos 1	Aa pos 2	Mz	z	Error_rel [ppm]	nseen	TIC	ID score
FRDNCLAILESKG-DKNQLLEAVNK-a12-b2	SKAP	SKAP	224	178	977,846	3	-0,6	19	0,43	32,25
LTETQGELKDLTQK-KGYKPLSKQK-a9-b8	SKAP	SKAP	201	168	730,165	4	3,7	5	0,45	32,24
RENGQMKATDTATR-KGYKPLSK-a7-b1	SKAP	SKAP	149	161	528,081	5	-3,5	10	0,22	32,12
RENGQMKATDTATR-DNCLAILESKG-a7-b10	SKAP	SKAP	149	224	979,146	3	-1,1	5	0,44	32,04
QLHQKLTETQGELK-FRDNCLAILESKG-a5-b12	SKAP	SKAP	192	224	663,35	5	-1,6	17	0,37	31,87
ENGQMKATDTATR-QKSEEELK-a6-b2	SKAP	SKAP	149	170	850,751	3	0,1	8	0,26	31,66
NQLLEAVNKQLHQK-SEEELKDK-a9-b6	SKAP	SKAP	187	176	926,495	3	0,5	3	0,43	31,54
LTETQGELKDLTQK-NQLLEAVNKQLHQK-a9-b9	SKAP	SKAP	201	187	851,717	4	0,7	5	0,31	31,5
DLTQKVELLEK-GPLGSVTKITK-a5-b8	SKAP	SKAP	206	137	639,123	4	-2,3	2	0,42	31,41
NQLLEAVNKQLHQK-KGYKPLSKQK-a9-b8	SKAP	SKAP	187	168	744,93	4	-1,5	2	0,4	31,37
QKSEEELKDK-GYKPLSK-a8-b3	SKAP	SKAP	176	164	541,544	4	-1,4	8	0,2	31,31
LTETQGELKDLTQK-GYKPLSK-a9-b3	SKAP	SKAP	201	164	634,099	4	-2	2	0,36	31,23
NQLLEAVNKQLHQK-RENGQMKATDTATR-a9-b7	SKAP	SKAP	187	149	845,446	4	1,6	13	0,41	31,05
ENGQMKATDTATRR-QKSEEELK-a6-b2	SKAP	SKAP	149	170	542,073	5	-1,4	17	0,44	30,88
QKSEEELK-ITKLRR-a2-b3	SKAP	SKAP	170	140	479,28	4	-3,1	8	0,45	30,84
RENGQMKATDTATR-QKSEEELK-a7-b2	SKAP	SKAP	149	170	542,072	5	-3,3	13	0,27	30,79
ENGQMKATDTATR-FRDNCLAILESKG-a6-b12	SKAP	SKAP	149	224	1028,17	3	1,4	5	0,44	30,71
KGYKPLSKQK-KGYKPLSK-a8-b4	SKAP	SKAP	168	164	447,671	5	-1,1	1	0,39	30,7
LTETQGELKDLTQK-QLHQKLTETQGELK-a9-b5	SKAP	SKAP	201	192	849,208	4	-1,2	9	0,24	30,66
DLTQKVELLEK-KGYKPLSK-a5-b1	SKAP	SKAP	206	161	791,794	3	0,4	2	0,41	30,6
QLHQKLTETQGELK-GYKPLSKQK-a5-b7	SKAP	SKAP	192	168	568,521	5	-0,5	7	0,26	30,46

Crosslinked peptides	Protein 1	Protein 2	Aa pos 1	Aa pos 2	Mz	z	Error_rel [ppm]	nseen	TIC	ID score
ENGQMKATDTATRR-SEEELKDK-a6-b6	SKAP	SKAP	149	176	898,44	3	-0,5	7	0,27	30,41
QLHQKLTETQGELK-DLTQKVELLEK-a5-b5	SKAP	SKAP	192	206	777,182	4	-0,4	5	0,32	30,33
NQLLEAVNKQLHQK-QKSEEELK-a9-b2	SKAP	SKAP	187	170	558,906	5	-0,3	4	0,39	30,18
ENGQMKATDTATR-DNCLAILESKG-a6-b10	SKAP	SKAP	149	224	927,112	3	-1,4	6	0,34	30,16
FRDNCLAILESKG-KGYKPLSK-a12-b1	SKAP	SKAP	224	161	860,799	3	-1,4	13	0,37	30,06
LTETQGELKDLTQKVELLEK-DLTQKVELLEK-a9-b5	SKAP	SKAP	201	206	754,422	5	-0,4	2	0,38	30,01
ENGQMKATDTATRR-ITKLRR-a6-b3	SKAP	SKAP	149	140	501,277	5	-1,4	6	0,45	29,91
RENGQMKATDTATR-FRDNCLAILESKG-a7-b12	SKAP	SKAP	149	224	810,403	4	-1,4	14	0,29	29,76
DLTQKVELLEK-QKSEEELKDK-a5-b2	SKAP	SKAP	206	170	672,366	4	0	1	0,31	29,59
LTETQGELKDLTQK-DLTQKVELLEKFR-a9-b11	SKAP	SKAP	201	212	672,771	5	-2,1	1	0,3	29,46
LTETQGELKDLTQK-FRDNCLAILESKG-a9-b12	SKAP	SKAP	201	224	1088,57	3	-1,6	7	0,37	29,45
QKSEEELKDK-GYKPLSKQK-a8-b7	SKAP	SKAP	176	168	484,668	5	-0,5	5	0,47	29,25
DKNQLLEAVNKQLHQK-ITKLR-a11-b3	SKAP	SKAP	187	140	535,514	5	-1,5	1	0,48	29,19
GPLGSVTKITK-ITKLR-a8-b3	SKAP	SKAP	137	140	623,391	3	-0,9	1	0,4	29,02
FRDNCLAILESKG-QKSEEELKDK-a12-b8	SKAP	SKAP	224	176	579,498	5	-1,8	4	0,3	28,89
ENGQMKATDTATRR-GYKPLSKQK-a6-b7	SKAP	SKAP	149	168	553,694	5	-0,8	8	0,41	28,73
KGYKPLSKQK-QKSEEELKDK-a8-b8	SKAP	SKAP	168	176	637,605	4	-2,2	3	0,3	28,66
FRDNCLAILESKG-DLTQKVELLEK-a12-b5	SKAP	SKAP	224	206	744,65	4	-0,6	16	0,33	28,59
DKNQLLEAVNK-KGYKPLSKQK-a2-b4	SKAP	SKAP	178	164	647,122	4	-1,1	4	0,55	28,56
ENGQMKATDTATR-QKSEEELKDK-a6-b8	SKAP	SKAP	149	176	699,093	4	-2,7	5	0,27	27,74
QKSEEELKDK-ITKLR-a8-b3	SKAP	SKAP	176	140	501,036	4	-2,3	5	0,13	27,72

Crosslinked peptides	Protein 1	Protein 2	Aa pos 1	Aa pos 2	Mz	z	Error_rel [ppm]	nseen	TIC	ID score
DKNQLLEAVNK-QKSEEELKDK-a2-b8	SKAP	SKAP	178	176	661,353	4	-0,7	2	0,35	27,64
RENGQMKATDTATR-QKSEEELKDK-a7-b8	SKAP	SKAP	149	176	738,12	4	-0,6	9	0,33	27,54
LTETQGELKDLTQKVELLEK-DKNQLLEAVNK-a9-b2	SKAP	SKAP	201	178	931,759	4	-3,4	3	0,36	27,34
FRDNCLAILESKG-QKSEEELK-a12-b2	SKAP	SKAP	224	170	884,118	3	-0,5	7	0,28	26,82
DNCLAILESKG-KGYKPLSKQK-a10-b8	SKAP	SKAP	224	168	634,097	4	-2	3	0,36	26,66
QKSEEELKDK-QKSEEELK-a8-b2	SKAP	SKAP	176	170	473,047	5	-0,3	2	0,11	26,34
FRDNCLAILESKG-KGYKPLSKQK-a12-b1	SKAP	SKAP	224	161	568,113	5	-1,6	3	0,5	26,31
FRDNCLAILESKG-KGYKPLSK-a12-b4	SKAP	SKAP	224	164	860,799	3	-1,4	12	0,4	25,92
GYKPLSKQKSEEELK-GYKPLSK-a7-b3	SKAP	SKAP	168	164	898,496	3	-2,1	7	0,17	25,58
LTETQGELKDLTQKVELLEK-QLHQKLTETQGELK-a9-b5	SKAP	SKAP	201	192	1027,06	4	-3,5	2	0,25	25,29
RENGQMKATDTATR-KGYKPLSK-a7-b4	SKAP	SKAP	149	164	659,851	4	-0,4	7	0,2	25,01
DNCLAILESKG-QKSEEELK-a10-b2	SKAP	SKAP	224	170	783,06	3	-2,9	4	0,31	24,97
FRDNCLAILESKG-SEEELKDK-a12-b6	SKAP	SKAP	224	176	660,082	4	-0,9	3	0,24	24,79
FRDNCLAILESKG-KGYKPLSKQK-a12-b8	SKAP	SKAP	224	168	709,889	4	-2,1	3	0,35	24,6
FRDNCLAILESKG-GYKPLSK-a12-b3	SKAP	SKAP	224	164	818,102	3	-0,3	6	0,39	24,49
KGYKPLSKQK-SEEELKDK-a4-b6	SKAP	SKAP	164	176	573,568	4	-0,3	2	0,2	24,36
ENGQMKATDTATRR-DLTQKVELLEK-a6-b5	SKAP	SKAP	149	206	1011,20	3	-0,6	3	0,3	24,32
LTETQGELKDLTQKVELLEK-FRDNCLAILESKG-a9-b12	SKAP	SKAP	201	224	795,827	5	0,5	2	0,37	24,21
KGYKPLSKQK-QKSEEELKDK-a4-b8	SKAP	SKAP	164	176	637,606	4	-1,1	2	0,35	23,89
DLTQKVELLEKFR-DNCLAILESKG-a11-b10	SKAP	SKAP	212	224	595,922	5	0,7	9	0,25	23,86

Crosslinked peptides	Protein 1	Protein 2	Aa pos 1	Aa pos 2	Mz	z	Error_rel [ppm]	nseen	TIC	ID score
LTETQGELKDLTQKVELLEK-ENGQMKATDTATR-a14-b6	SKAP	SKAP	206	149	969,505	4	-0,3	2	0,32	23,76
FRDNCLAILESKG-KGYKPLSKQK-a12-b4	SKAP	SKAP	224	164	568,113	5	-1,8	2	0,36	22,62
LTETQGELKDLTQKVELLEK-QKSEEELK-a9-b2	SKAP	SKAP	201	170	689,374	5	-1	1	0,17	22,47
LTETQGELKDLTQKVELLEK-ENGQMKATDTATRR-a9-b6	SKAP	SKAP	201	149	1008,53	4	-0,2	1	0,26	22,32
LTETQGELKDLTQKVELLEK-DNCLAILESKG-a9-b10	SKAP	SKAP	201	224	918,737	4	-1,6	2	0,42	22,31
DLTQKVELLEKFR-QKSEEELK-a11-b2	SKAP	SKAP	212	170	687,377	4	-1,4	1	0,12	22,28
NQLLEAVNKQLHQK-QKSEEELKDK-a9-b8	SKAP	SKAP	187	176	759,16	4	-1,5	3	0,21	22,06
GDVVPKDVNAAIATIK-LSVDYGKK-a6-b7	α-Tubulin	α-Tubulin	326	163	665,123	4	-2,4	1	0,66	40,32
HGKYMACCLLYR-LDHKFDLMYAKR-a3-b11	α-Tubulin	α-Tubulin	311	401	649,923	5	-1,8	1	0,38	35,38
GHYTIGKEIIDLVLDR-HGKYMACCLLYR-a7-b3	α-Tubulin	α-Tubulin	112	311	710,964	5	-3,1	1	0,45	34,38
QLFHPEQLITGKEDAANNYAR-GHYTIGKEIIDLVLDR-a12-b7	α-Tubulin	α-Tubulin	96	112	733,22	6	0,1	3	0,4	28,34
QLFHPEQLITGKEDAANNYAR-GDVVPKDVNAAIATIK-a12-b6	α-Tubulin	α-Tubulin	96	326	833,44	5	-2,1	4	0,22	26,17
VGINYQPPTVVPGGDLAKVQR-HGKYMACCLLYR-a18-b3	α-Tubulin	α-Tubulin	370	311	980,006	4	-1	1	0,47	22,36
ALTVPELTQQMFDSKNMMAACDPR-KLAVNMVPFPR-a15-b1	β-Tubulin	β-Tubulin	297	252	1041,52	4	1,5	1	0,39	23,6

Table 6.2: Crosslinks between microtubules and SKAP$^{135-225}$ in presence of BS2G. TIC: fraction of total ion current of fragment ion spectrum assigned to crosslink. Mz: mass to charge ratio. nseen: number of fragment ion spectra assigned to the crosslink in entire dataset.

Summary of intermolecular crosslinks

Crosslinked peptides	Protein 1	Protein 2	Aa pos 1	Aa pos 2	Mz	z	Error_rel [ppm]	nseen	TIC	ID score
LDHKFDLMYAK-KGYKPLSK-a4-b1	α-Tubulin	SKAP	394	161	599,823	4	0,2	4	0,39	37,79
LSVDYGKK-GYKPLSK-a7-b3	α-Tubulin	SKAP	163	164	450	4	-1,8	4	0,61	36,77
LDHKFDLMYAK-ITKLR-a4-b3	α-Tubulin	SKAP	394	140	527,29	4	-2,5	3	0,56	36,6
HGKYMACCLLYR-ITKLR-a3-b3	α-Tubulin	SKAP	311	140	575,049	4	0,7	2	0,53	36,5
DVNAAIATIKTK-ITKLR-a10-b3	α-Tubulin	SKAP	336	140	657,393	3	-1,5	4	0,62	35,93
FDLMYAKR-ITKLR-a7-b3	α-Tubulin	SKAP	401	140	443	4	-1,9	2	0,6	35,62
FDLMYAKR-KGYKPLSK-a7-b4	α-Tubulin	SKAP	401	164	515,532	4	-0,4	1	0,61	35,39
GDVVPKDVNAAIATIK-ITKLR-a6-b3	α-Tubulin	SKAP	326	140	584,845	4	-0,1	4	0,56	34,19
FDLMYAKR-KGYKPLSK-a7-b1	α-Tubulin	SKAP	401	161	515,532	4	0,1	2	0,5	30,76
LSVDYGKK-SEEELKDK-a7-b6	α-Tubulin	SKAP	163	176	496,254	4	-1,9	2	0,25	30,1
QLFHPEQLITGKEDAANNYAR-ITKLR-a12-b3	α-Tubulin	SKAP	96	140	628,935	5	-2	1	0,3	29,71
GYKPLSKQK-LSVDYGKK-a7-b7	SKAP	α-Tubulin	168	163	514,039	4	-0,1	1	0,58	29,61
LDHKFDLMYAK-QKSEEELK-a4-b2	α-Tubulin	SKAP	394	170	617,312	4	0,2	1	0,24	29,4
ENGQMKATDTATRR-HGKYMACCLLYR-a6-b3	SKAP	α-Tubulin	149	311	649,908	5	1	4	0,39	28,41
ENGQMKATDTATR-HGKYMACCLLYR-a6-b3	SKAP	α-Tubulin	149	311	773,108	4	0,4	2	0,38	27,98
ENGQMKATDTATR-DVNAAIATIKTK-a6-b10	SKAP	α-Tubulin	149	336	921,473	3	1,8	2	0,3	27,16

Summary of intramolecular crosslinks

Crosslinked peptides	Protein 1	Protein 2	Aa pos 1	Aa pos 2	Mz	z	Error_rel [ppm]	nseen	TIC	ID score
VELLEKFR-ITKLR-a6-b3	SKAP	SKAP	212	140	440,518	4	0,1	8	0,65	42,41
GYKPLSK-ITKLRR-a3-b3	SKAP	SKAP	164	140	419,257	4	-0,7	6	0,6	42,28
KGYKPLSK-ITKLR-a4-b3	SKAP	SKAP	164	140	412,255	4	-1,7	6	0,47	41,08
DLTQKVELLEK-VELLEKFR-a5-b6	SKAP	SKAP	206	212	815,461	3	1,2	10	0,6	41,08
QKSEEELK-GYKPLSK-a2-b3	SKAP	SKAP	170	164	470,252	4	-1,2	3	0,44	41,03
GYKPLSKQK-KGYKPLSK-a7-b1	SKAP	SKAP	168	161	413,643	5	-0,3	5	0,44	40,62
DKNQLLEAVNK-VELLEKFR-a2-b6	SKAP	SKAP	178	212	800,775	3	-2,4	4	0,56	40,59
GYKPLSKQK-GYKPLSK-a7-b3	SKAP	SKAP	168	164	484,778	4	-1,1	2	0,51	40,51
GYKPLSK-ITKLR-a3-b3	SKAP	SKAP	164	140	506,641	3	0,9	2	0,54	40,42
GYKPLSKQK-SEEELKDK-a7-b6	SKAP	SKAP	168	176	707,708	3	-0,1	14	0,56	40,42
KGYKPLSK-SEEELKDK-a1-b6	SKAP	SKAP	161	176	499,018	4	0	7	0,73	40,36
SEEELKDK-ITKLR-a6-b3	SKAP	SKAP	176	140	568,313	3	0	4	0,7	40,35
KGYKPLSK-GYKPLSK-a1-b3	SKAP	SKAP	161	164	452,764	4	-0,9	5	0,57	40,35
VELLEKFR-GYKPLSK-a6-b3	SKAP	SKAP	212	164	481,025	4	-2,4	5	0,66	40,16
KGYKPLSK-ITKLR-a1-b3	SKAP	SKAP	161	140	412,256	4	-1	6	0,67	39,98
DKNQLLEAVNK-QKSEEELK-a2-b2	SKAP	SKAP	178	170	590,061	4	0	8	0,55	39,95
DLTQKVELLEK-ITKLR-a5-b3	SKAP	SKAP	206	140	681,068	3	-1,8	5	0,53	39,58
RENGQMKATDTATR-SEEELKDK-a7-b6	SKAP	SKAP	149	176	663,571	4	1,6	8	0,53	39,48
QLHQKLTETQGELK-DKNQLLEAVNK-a5-b2	SKAP	SKAP	192	178	755,657	4	-1,1	7	0,51	39,19
KGYKPLSK-SEEELKDK-a4-b6	SKAP	SKAP	164	176	665,021	3	-0,9	14	0,4	39,06

Crosslinked peptides	Protein 1	Protein 2	Aa pos 1	Aa pos 2	Mz	z	Error_rel [ppm]	nseen	TIC	ID score
ENGQMKATDTATR-SEEELKDK-a6-b6	SKAP	SKAP	149	176	832,392	3	0,7	7	0,42	38,57
GYKPLSKQK-ITKLR-a7-b3	SKAP	SKAP	168	140	444,27	4	-0,5	2	0,57	38,47
ENGQMKATDTATR-ITKLR-a6-b3	SKAP	SKAP	149	140	716,708	3	-0,1	13	0,45	38,43
QKSEEELK-ITKLR-a2-b3	SKAP	SKAP	170	140	429,745	4	0,3	4	0,35	38,21
SEEELKDK-GYKPLSK-a6-b3	SKAP	SKAP	176	164	466,994	4	-0,2	4	0,55	38,02
ENGQMKATDTATR-VELLEKFR-a6-b6	SKAP	SKAP	149	212	851,098	3	-1,4	8	0,42	37,65
QKSEEELK-SEEELKDK-a2-b6	SKAP	SKAP	170	176	516,507	4	0,3	9	0,39	37,56
DLTQKVELLEK-DNCLAILESKG-a5-b10	SKAP	SKAP	206	224	877,459	3	0,5	2	0,53	37,12
RENGQMKATDTATR-GYKPLSK-a7-b3	SKAP	SKAP	149	164	617,316	4	0,1	13	0,44	37,02
DKNQLLEAVNK-ITKLR-a2-b3	SKAP	SKAP	178	140	666,384	3	-1,9	8	0,45	36,73
DNCLAILESKG-ITKLR-a10-b3	SKAP	SKAP	224	140	649,018	3	-2	2	0,58	36,71
KGYKPLSK-QKSEEELK-a1-b2	SKAP	SKAP	161	170	402,023	5	0,4	19	0,32	36,68
LTETQGELKDLTQK-ITKLRR-a9-b3	SKAP	SKAP	201	140	622,106	4	-0,1	9	0,53	36,65
HGKYMACCLLYR-LSVDYGKK-a3-b7	α-Tubulin	α-Tubulin	311	163	644,817	4	-1,4	1	0,52	36,4
RENGQMKATDTATR-KGYKPLSK-a7-b1	SKAP	SKAP	149	161	519,673	5	-1	4	0,55	36,39
DKNQLLEAVNK-GYKPLSK-a2-b3	SKAP	SKAP	178	164	720,393	3	-3,3	7	0,56	36,37
DKNQLLEAVNK-SEEELKDK-a2-b6	SKAP	SKAP	178	176	782,068	3	0,4	7	0,48	36,36
QKSEEELK-VELLEKFR-a2-b6	SKAP	SKAP	170	212	707,048	3	-0,5	5	0,26	36,3
LTETQGELKDLTQK-DKNQLLEAVNK-a9-b2	SKAP	SKAP	201	178	990,862	3	2	3	0,46	36,23
DKNQLLEAVNK-KGYKPLSK-a2-b1	SKAP	SKAP	178	161	763,094	3	-0,3	2	0,48	36,2
ENGQMKATDTATR-GYKPLSKQK-a6-b7	SKAP	SKAP	149	168	856,104	3	0,9	5	0,42	36,02

Crosslinked peptides	Protein 1	Protein 2	Aa pos 1	Aa pos 2	Mz	z	Error_rel [ppm]	nseen	TIC	ID score
SEEELKDK-ITKLRR-a6-b3	SKAP	SKAP	176	140	465,511	4	-1,8	5	0,62	35,94
RENGQMKATDTATR-VELLEKFR-a7-b6	SKAP	SKAP	149	212	677,601	4	-1,5	4	0,58	35,87
GYKPLSKQK-QKSEEELK-a7-b2	SKAP	SKAP	168	170	534,291	4	0	5	0,3	35,8
QKSEEELKDK-KGYKPLSK-a8-b4	SKAP	SKAP	176	164	450,646	5	-1,2	5	0,47	35,76
KGYKPLSK-ITKLRR-a1-b3	SKAP	SKAP	161	140	451,281	4	0,2	4	0,39	35,52
KGYKPLSK-QKSEEELK-a4-b2	SKAP	SKAP	164	170	502,276	4	0,1	7	0,32	35,47
DKNQLLEAVNK-KGYKPLSK-a2-b4	SKAP	SKAP	178	164	763,095	3	1	11	0,44	35,39
LTETQGELKDLTQK-ITKLR-a9-b3	SKAP	SKAP	201	140	583,081	4	0,6	7	0,43	35,31
DKNQLLEAVNK-ITKLRR-a2-b3	SKAP	SKAP	178	140	539,067	4	2	14	0,55	35,29
NQLLEAVNKQLHQK-SEEELKDK-a9-b6	SKAP	SKAP	187	176	684,611	4	-0,5	4	0,57	35,19
QLHQKLTETQGELK-GYKPLSK-a5-b3	SKAP	SKAP	192	164	635,85	4	1	2	0,33	35,14
DLTQKVELLEKFR-DLTQKVELLEK-a11-b5	SKAP	SKAP	212	206	758,175	4	-0,6	3	0,44	35,08
QLHQKLTETQGELK-ITKLR-a5-b3	SKAP	SKAP	192	140	595,34	4	-1,8	4	0,3	35,06
NQLLEAVNKQLHQK-QKSEEELK-a9-b2	SKAP	SKAP	187	170	687,869	4	-0,2	5	0,4	35,06
ENGQMKATDTATRR-SEEELKDK-a6-b6	SKAP	SKAP	149	176	884,425	3	0,6	15	0,32	34,93
LTETQGELKDLTQK-NQLLEAVNKQLHQK-a9-b9	SKAP	SKAP	201	187	841,204	4	-1,6	4	0,39	34,85
QLHQKLTETQGELK-KGYKPLSK-a5-b1	SKAP	SKAP	192	161	534,501	5	2,8	9	0,4	34,83
LTETQGELKDLTQK-QLHQKLTETQGELK-a9-b5	SKAP	SKAP	201	192	671,16	5	0,9	8	0,42	34,65
LTETQGELKDLTQK-VELLEKFR-a9-b6	SKAP	SKAP	201	212	683,873	4	-0,7	4	0,43	34,59
DLTQKVELLEKFR-DNCLAILESKG-a11-b10	SKAP	SKAP	212	224	734,14	4	2	12	0,37	34,44
FRDNCLAILESKG-ITKLR-a12-b3	SKAP	SKAP	224	140	562,808	4	-1,2	8	0,6	34,37

Crosslinked peptides	Protein 1	Protein 2	Aa pos 1	Aa pos 2	Mz	z	Error_rel [ppm]	nseen	TIC	ID score
ENGQMKATDTATR-DKNQLLEAVNK-a6-b2	SKAP	SKAP	149	178	930,463	3	-0,6	5	0,45	34,37
ENGQMKATDTATR-KGYKPLSK-a6-b4	SKAP	SKAP	149	164	813,417	3	-0,3	1	0,38	34,34
ENGQMKATDTATRR-GYKPLSK-a6-b3	SKAP	SKAP	149	164	494,055	5	0,7	11	0,44	34,26
DLTQKVELLEKFR-FRDNCLAILESKG-a11-b12	SKAP	SKAP	212	224	648,147	5	1,1	6	0,55	34,04
QLHQKLTETQGELK-DLTQKVELLEK-a5-b5	SKAP	SKAP	192	206	766,67	4	0	5	0,4	34,02
FRDNCLAILESKG-VELLEKFR-a12-b6	SKAP	SKAP	224	212	663,605	4	3,1	5	0,52	33,97
RENGQMKATDTATR-DKNQLLEAVNK-a7-b2	SKAP	SKAP	149	178	982,496	3	-0,8	12	0,45	33,69
QLHQKLTETQGELK-SEEELKDK-a5-b6	SKAP	SKAP	192	176	682,104	4	1,1	5	0,32	33,52
LTETQGELKDLTQK-KGYKPLSK-a9-b4	SKAP	SKAP	201	164	655,613	4	1,3	3	0,44	33,43
RENGQMKATDTATR-DLTQKVELLEK-a7-b5	SKAP	SKAP	149	206	748,136	4	-1,3	3	0,38	33,43
QLHQKLTETQGELK-VELLEKFR-a5-b6	SKAP	SKAP	192	212	557,11	5	0,9	8	0,38	33,4
DNCLAILESKG-VELLEKFR-a10-b6	SKAP	SKAP	224	212	587,809	4	-1,4	43	0,54	33,32
LTETQGELKDLTQK-KGYKPLSK-a9-b1	SKAP	SKAP	201	161	524,691	5	0	6	0,53	33,28
LTETQGELKDLTQK-GYKPLSKQK-a9-b7	SKAP	SKAP	201	168	687,627	4	1,1	3	0,44	32,98
VELLEKFR-ITKLRR-a6-b3	SKAP	SKAP	212	140	639,056	3	1,5	5	0,29	32,97
QLHQKLTETQGELK-ITKLRR-a5-b3	SKAP	SKAP	192	140	507,694	5	-1,2	10	0,5	32,81
ENGQMKATDTATR-DNCLAILESKG-a6-b10	SKAP	SKAP	149	224	913,097	3	-0,3	2	0,34	32,75
NQLLEAVNKQLHQK-VELLEKFR-a9-b6	SKAP	SKAP	187	212	698,642	4	-0,3	1	0,5	32,66
ENGQMKATDTATR-QKSEEELK-a6-b2	SKAP	SKAP	149	170	836,736	3	1,6	9	0,29	32,34
DKNQLLEAVNK-DNCLAILESKG-a2-b10	SKAP	SKAP	178	224	862,773	3	-2,1	4	0,47	32,33
LTETQGELKDLTQK-GYKPLSK-a9-b3	SKAP	SKAP	201	164	623,588	4	-0,4	5	0,49	32,24

Crosslinked peptides	Protein 1	Protein 2	Aa pos 1	Aa pos 2	Mz	z	Error_rel [ppm]	nseen	TIC	ID score
ENGQMKATDTATRR-DKNQLLEAVNK-a6-b2	SKAP	SKAP	149	178	737,125	4	0,2	5	0,5	32,1
ENGQMKATDTATRR-ITKLR-a6-b3	SKAP	SKAP	149	140	461,648	5	-0,1	12	0,38	31,82
ENGQMKATDTATR-KGYKPLSK-a6-b1	SKAP	SKAP	149	161	488,453	5	-0,4	11	0,42	31,63
DNCLAILESKG-SEEELKDK-a10-b6	SKAP	SKAP	224	176	764,702	3	-0,2	2	0,49	31,2
ENGQMKATDTATR-GYKPLSK-a6-b3	SKAP	SKAP	149	164	578,291	4	-0,1	4	0,33	30,99
DKNQLLEAVNK-GYKPLSKQK-a2-b7	SKAP	SKAP	178	168	604,587	4	0,6	4	0,57	30,93
LTETQGELKDLTQK-DNCLAILESKG-a9-b10	SKAP	SKAP	201	224	973,494	3	-0,6	2	0,36	30,9
FRDNCLAILESKG-GYKPLSK-a12-b3	SKAP	SKAP	224	164	804,085	3	-2,2	3	0,33	30,88
KGYKPLSKQK-SEEELKDK-a8-b6	SKAP	SKAP	168	176	750,406	3	0,2	1	0,4	30,85
FRDNCLAILESKG-DKNQLLEAVNK-a12-b2	SKAP	SKAP	224	178	723,125	4	-0,9	4	0,4	30,73
KGYKPLSKQK-KGYKPLSK-a8-b1	SKAP	SKAP	168	161	439,262	5	-1,6	1	0,41	30,72
NQLLEAVNKQLHQK-KGYKPLSK-a9-b1	SKAP	SKAP	187	161	893,504	3	-1,3	2	0,35	30,66
ENGQMKATDTATR-KGYKPLSKQK-a6-b8	SKAP	SKAP	149	168	674,354	4	1,1	2	0,38	30,59
QLHQKLTETQGELK-FRDNCLAILESKG-a5-b12	SKAP	SKAP	192	224	654,943	5	1,4	9	0,4	30,56
ENGQMKATDTATRR-KGYKPLSK-a6-b1	SKAP	SKAP	149	161	519,674	5	0,3	6	0,48	30,53
FRDNCLAILESKG-SEEELKDK-a12-b6	SKAP	SKAP	224	176	865,76	3	0,9	4	0,35	30,4
RENGQMKATDTATR-ITKLR-a7-b3	SKAP	SKAP	149	140	461,648	5	-0,7	8	0,35	30,36
GDVVPKDVNAAIATIK-LDHKFDLMYAK-a6-b4	α-Tubulin	α-Tubulin	326	394	772,412	4	-0,3	2	0,56	30,36
LTETQGELKDLTQKVELLEK-ITKLR-a9-b3	SKAP	SKAP	201	140	760,934	4	-0,5	2	0,35	30,2
ENGQMKATDTATR-FRDNCLAILESKG-a6-b12	SKAP	SKAP	149	224	760,868	4	0,6	4	0,36	30,01
DKNQLLEAVNK-QKSEEELKDK-a2-b8	SKAP	SKAP	178	176	520,874	5	-1	7	0,55	29,97

Crosslinked peptides	Protein 1	Protein 2	Aa pos 1	Aa pos 2	Mz	z	Error_rel [ppm]	nseen	TIC	ID score
ENGQMKATDTATRR-GYKPLSKQK-a6-b7	SKAP	SKAP	149	168	681,355	4	0,6	5	0,44	29,85
LTETQGELKDLTQK-SEEELKDK-a9-b6	SKAP	SKAP	201	176	892,787	3	-0,4	1	0,46	29,83
RENGQMKATDTATR-QKSEEELK-a7-b2	SKAP	SKAP	149	170	666,83	4	1,8	5	0,36	29,8
ENGQMKATDTATRR-KGYKPLSKQK-a6-b8	SKAP	SKAP	149	168	713,379	4	1,7	2	0,37	29,62
LTETQGELKDLTQK-QKSEEELK-a9-b2	SKAP	SKAP	201	170	897,131	3	-0,1	3	0,25	29,52
FRDNCLAILESKG-DLTQKVELLEK-a12-b5	SKAP	SKAP	224	206	734,138	4	0,2	6	0,41	29,48
ENGQMKATDTATRR-ITKLRR-a6-b3	SKAP	SKAP	149	140	410,892	6	0,5	7	0,41	29,11
QLHQKLTETQGELK-ENGQMKATDTATR-a5-b6	SKAP	SKAP	192	149	793,401	4	1,2	8	0,35	29,04
RENGQMKATDTATR-ITKLRR-a7-b3	SKAP	SKAP	149	140	615,835	4	1,9	8	0,4	29
KGYKPLSK-KGYKPLSK-a1-b4	SKAP	SKAP	161	164	484,788	4	1,2	1	0,38	28,66
DKNQLLEAVNK-KGYKPLSKQK-a2-b8	SKAP	SKAP	178	168	636,611	4	-0,1	1	0,48	28,33
ENGQMKATDTATRR-QLHQKLTETQGELK-a6-b5	SKAP	SKAP	149	192	555,286	6	0,9	8	0,39	28,32
QLHQKLTETQGELK-RENGQMKATDTATR-a5-b7	SKAP	SKAP	192	149	666,142	5	0,8	5	0,35	28,01
NQLLEAVNKQLHQK-ENGQMKATDTATR-a9-b6	SKAP	SKAP	187	149	795,907	4	-0,8	4	0,4	28,01
QLHQKLTETQGELK-QKSEEELK-a5-b2	SKAP	SKAP	192	170	548,49	5	0	6	0,34	27,74
RENGQMKATDTATR-FRDNCLAILESKG-a7-b12	SKAP	SKAP	149	224	799,892	4	-0,9	3	0,38	27,73
KGYKPLSKQK-VELLEKFR-a4-b6	SKAP	SKAP	164	212	577,087	4	-0,9	1	0,54	27,6
LTETQGELKDLTQK-ENGQMKATDTATR-a9-b6	SKAP	SKAP	201	149	1041,18	3	-0,9	2	0,27	27,32
QKSEEELKDK-GYKPLSK-a8-b3	SKAP	SKAP	176	164	531,033	4	0,5	3	0,22	27,06
ENGQMKATDTATR-DLTQKVELLEK-a6-b5	SKAP	SKAP	149	206	709,112	4	0,1	1	0,3	26,81
ENGQMKATDTATRR-QKSEEELK-a6-b2	SKAP	SKAP	149	170	533,663	5	-1,7	15	0,39	26,72

Crosslinked peptides	Protein 1	Protein 2	Aa pos 1	Aa pos 2	Mz	z	Error_rel [ppm]	nseen	TIC	ID score
ENGQMKATDTATR-GPLGSVTKITK-a6-b8	SKAP	SKAP	149	137	873,454	3	0,3	1	0,3	26,66
QLHQKLTETQGELK-DNCLAILESKG-a5-b10	SKAP	SKAP	192	224	989,84	3	-1,5	1	0,24	25,93
NQLLEAVNKQLHQK-QLHQKLTETQGELK-a9-b5	SKAP	SKAP	187	192	853,466	4	0,1	2	0,23	25,92
VELLEKFRDNCLAILESK-FRDNCLAILESKG-a6-b12	SKAP	SKAP	212	224	759,797	5	1,8	1	0,32	25,61
NQLLEAVNKQLHQK-FRDNCLAILESKG-a9-b12	SKAP	SKAP	187	224	820,935	4	1,1	5	0,32	25,49
QKSEEELKDK-KGYKPLSK-a8-b1	SKAP	SKAP	176	161	563,057	4	0,6	2	0,33	25,26
LTETQGELKDLTQK-RENGQMKATDTATR-a9-b7	SKAP	SKAP	201	149	820,165	4	0,7	2	0,34	24,92
ENGQMKATDTATR-QKSEEELKDK-a6-b8	SKAP	SKAP	149	176	688,584	4	0,7	2	0,24	24,87
DKNQLLEAVNK-KGYKPLSKQK-a2-b4	SKAP	SKAP	178	164	636,611	4	0,6	1	0,44	24,15
FRDNCLAILESKG-QKSEEELK-a12-b2	SKAP	SKAP	224	170	870,102	3	-0,5	3	0,22	23,48
ENGQMKATDTATRR-QKSEEELKDK-a6-b8	SKAP	SKAP	149	176	582,289	5	0,2	5	0,3	23,35
ENGQMKATDTATR-ITKLRR-a6-b3	SKAP	SKAP	149	140	768,742	3	-0,1	4	0,31	23,24

6.3 Protein sequences

6.3.1 Astrin

```
   1 MWRVKKLSLS LSPSPQTGKP SMRTPLRELT LQPGALTNSG KRSPACSSLT 50
  51 PSLCKLGLQE GSNNSSPVDF VNNKRTDLSS EHFSHSSKWL ETCQHESDEQ 100
 101 PLDPIPQISS TPKTSEEAVD PLGNYMVKTI VLVPSPLGQQ QDMIFEARLD 150
 151 TMAETNSISL NGPLRTDDLV REEVAPCMGD RFSEVAAVSE KPIFQESPSH 200
 201 LLEESPPNPC SEQLHCSKES LSSRTEAVRE DLVPSESNAF LPSSVLWLSP 250
 251 STALAADFRV NHVDPEEEIV EHGAMEEREM RFPTHPKESE TEDQALVSSV 300
 301 EDILSTCLTP NLVEMESQEA PGPAVEDVGR ILGSDTESWM SPLAWLEKGV 350
 351 NTSVMLENLR QSLSLPSMLR DAAIGTTPFS TCSVGTWFTP SAPQEKSTNT 400
 401 SQTGLVGTKH STSETEQLLC GRPPDLTALS RHDLEDNLLS SLVILEVLSR 450
 451 QLRDWKSQLA VPHPETQDSS TQTDTSHSGI TNKLQHLKES HEMGQALQQA 500
 501 RNVMQSWVLI SKELISLLHL SLLHLEEDKT TVSQESRRAE TLVCCCFDLL 550
 551 KKLRAKLQSL KAEREEARHR EEMALRGKDA AEIVLEAFCA HASQRISQLE 600
 601 QDLASMREFR GLLKDAQTQL VGLHAKQEEL VQQTVSLTST LQQDWRSMQL 650
 651 DYTTWTALLS RSRQLTEKLT VKSQQALQER DVAIEEKQEV SRVLEQVSAQ 700
 701 LEECKGQTEQ LELENSRLAT DLRAQLQILA NMDSQLKELQ SQHTHCAQDL 750
 751 AMKDELLCQL TQSNEEQAAQ WQKEEMALKH MQAELQQQQA VLAKEVRDLK 800
 801 ETLEFADQEN QVAHLELGQV ECQLKTTLEV LRERSLQCEN LKDTVENLTA 850
 851 KLASTIADNQ EQDLEKTRQY SQKLGLLTEQ LQSLTLFLQT KLKEKTEQET 900
 901 LLLSTACPPT QEHPLPNDRT FLGSILTAVA DEEPESTPVP LLGSDKSAFT 950
 951 RVASMVSLQP AETPGMEESL AEMSIMTTEL QSLCSLLQES KEEAIRTLQR 1000
1001 KICELQARLQ AQEEQHQEVQ KAKEADIEKL NQALCLRYKN EKELQEVIQQ 1050
1051 QNEKILEQID KSGELISLRE EVTHLTRSLR RAETETKVLQ EALAGQLDSN 1100
1101 CQPMATNWIQ EKVWLSQEVD KLRVMFLEMK NEKEKLMIKF QSHRNILEEN 1150
1151 LRRSDKELEK LDDIVQHIYK TLLSIPEVVR GCKELQGLLE FLS
```

6.3.2 SKAP

```
  1 MAAPEAPPLD RVFRTTWLST ECDSHPLPPS YRKFLFETQA ADLAGGTTVA 50
 51 AGNLLNESEK DCGQDRRAPG VQPCRLVTMT SVVKTVYSLQ PPSALSGGQP 100
101 ADTQTRATSK SLLPVRSKEV DVSKQLHSGG PENDVTKITK LRRENGQMKA 150
151 TDTATRRNVR KGYKPLSKQK SEEELKDKNQ LLEAVNKQLH QKLTETQGEL 200
201 KDLTQKVELL EKFRDNCLAI LESKGLDPAL GSETLASRQE STTDHMDSML 250
251 LLETLQEELK LFNETAKKQM EELQALKVKL EMKEERVRFL EQQTLCNNQV 300
301 NDLTTALKEM EQLLEM
```

6.4 Gene sequences

6.4.1 Astrin

6.4.1.1 Wild type gene

ATGTGGCGAGTGAAAAAACTGAGCCTCAGCCTGTCGCCTTCGCCCCAGACGGGAAAACCATCTATGAGA
ACTCCTCTCCGTGAACTTACCCTGCAGCCCGGTGCCCTCACCAACTCTGGAAAAAGATCCCCCGCTTGC
TCCTCGCTGACCCCATCACTGTGCAAGCTGGGGCTGCAGGAAGGCAGCAACAACTCATCTCCAGTGGAT
TTTGTAAATAACAAGAGGACAGACTTATCTTCAGAACATTTCAGTCATTCCTCAAAGTGGCTAGAAACT
TGTCAGCATGAATCAGATGAGCAGCCTCTAGATCCAATTCCCCAAATTAGCTCTACTCCTAAAACGTCT
GAGGAAGCAGTAGACCCACTGGGCAATTATATGGTTAAAACCATCGTCCTTGTACCATCTCCACTGGGG
CAGCAACAAGACATGATATTTGAGGCCCGTTTAGATACCATGGCAGAGACAAACAGCATATCTTTAAAT
GGACCTTTGAGAACAGACGATCTGGTGAGAGAGGAGGTGGCACCCTGCATGGGAGACAGGTTTTCAGAA
GTTGCTGCTGTATCTGAGAAACCTATCTTTCAGGAATCTCCGTCCCATCTCTTAGAGGAGTCTCCACCA
AATCCCTGTTCTGAACAACTACATTGCTCCAAGGAAAGCCTGAGCAGTAGAACTGAGGCTGTGCGTGAG
GACTTAGTACCTTCTGAAAGTAACGCCTTCTTGCCTTCCTCTGTTCTCTGGCTTTCCCCTTCAACTGCC
TTGGCAGCAGATTTCCGTGTCAATCATGTGGACCCAGAGGAGGAAATTGTAGAGCATGGAGCTATGGAG
GAAAGAGAAATGAGGTTTCCCACACATCCTAAGGAGTCTGAAACAGAAGATCAAGCACTTGTCTCAAGT
GTGGAAGATATTCTGTCCACATGCCTGACACCAAATCTAGTAGAAATGGAATCCCAAGAAGCTCCAGGC
CCAGCAGTAGAAGATGTTGGTAGGATTCTTGGCTCTGATACAGAGTCTTGGATGTCCCCACTGGCCTGG
CTGGAAAAAGGTGTAAATACCTCCGTCATGCTGGAAAATCTCCGCCAAAGCTTATCCCTTCCCTCGATG
CTTCGGGATGCTGCAATTGGCACTACCCCTTTCTCTACTTGCTCGGTGGGGACTTGGTTTACTCCTTCA
GCACCACAGGAAAAGAGTACAAACACATCCCAGACAGGCCTGGTTGGCACCAAGCACAGTACTTCTGAG
ACAGAGCAGCTCCTGTGTGGCCGGCCTCCAGATCTGACTGCCTTGTCTCGACATGACTTGGAAGATAAC
CTGCTGAGCTCTCTTGTCATTCTGGAGGTTCTCTCCCGCCAGCTTCGGGACTGGAAGAGCCAGCTGGCT
GTCCCTCACCCAGAAACCCAGGACAGTAGCACACAGACTGACACATCTCACAGTGGGATAACTAATAAA
CTTCAGCATCTTAAGGAGAGCCATGAGATGGGACAGGCCCTACAGCAGGCCAGAAATGTCATGCAATCA
TGGGTGCTTATCTCTAAAGAGCTGATATCCTTGCTTCACCTATCCCTGTTGCATTTAGAAGAAGATAAG
ACTACTGTGAGTCAGGAGTCTCGGCGTGCAGAAACATTGGTCTGTTGCTGTTTTGATTTGCTGAAGAAA
TTGAGGGCAAAGCTCCAGAGCCTCAAAGCAGAAAGGGAGGAGGCAAGGCACAGAGAGGAAATGGCTCTC
AGAGGCAAGGATGCGGCAGAGATAGTGTTGGAGGCTTTCTGTGCACACGCCAGCCAGCGCATCAGCCAG
CTGGAACAGGACCTAGCATCCATGCGGGAATTCAGAGGCCTTCTGAAGGATGCCCAGACCCAACTGGTA
GGGCTTCATGCCAAGCAAGAAGAGCTGGTTCAGCAGACAGTGAGTCTTACTTCTACCTTGCAACAAGAC
TGGAGGTCCATGCAACTGGATTATACAACATGGACAGCTTTGCTGAGTCGGTCCCGACAACTCACAGAG
AAACTCACAGTCAAGAGCCAGCAAGCCCTGCAGGAACGTGATGTGGCAATTGAGGAAAAGCAGGAGGTT
TCTAGGGTGCTGGAACAAGTCTCTGCCCAGTTAGAGGAGTGCAAAGGCCAAACAGAACAACTGGAGTTG
GAAAACAGTCGTCTAGCAACAGATCTCCGGGCTCAGTTGCAGATTCTGGCCAACATGGACAGCCAGCTA
AAAGAGCTACAGAGTCAGCATACCCATTGTGCCCAGGACCTGGCTATGAAGGATGAGTTACTCTGCCAG
CTTACCCAGAGCAATGAGGAGCAGGCTGCTCAATGGCAAAAGGAAGAGATGGCACTAAAACACATGCAG
GCAGAACTGCAGCAGCAACAAGCTGTCCTGGCCAAAGAGGTGCGGGACCTGAAAGAGACCTTGGAGTTT
GCAGACCAGGAGAATCAGGTTGCTCACCTGGAGCTGGGTCAGGTTGAGTGTCAATTGAAAACCACACTG

GAAGTGCTCCGGGAGCGCAGCTTGCAGTGTGAGAACCTCAAGGACACTGTAGAGAACCTAACGGCTAAA
CTGGCCAGCACCATAGCAGATAACCAGGAGCAAGATCTGGAGAAAACACGGCAGTACTCTCAAAAGCTA
GGGCTGCTGACTGAGCAACTACAGAGCCTGACTCTCTTTCTACAGACAAAACTAAAGGAGAAGACTGAA
CAAGAGACCCTTCTGCTGAGTACAGCCTGTCCTCCCACCCAGGAACACCCTCTGCCTAATGACAGGACC
TTCCTGGGAAGCATCTTGACAGCAGTGGCAGATGAAGAGCCAGAATCAACTCCTGTGCCCTTGCTTGGA
AGTGACAAGAGTGCTTTCACCCGAGTAGCATCAATGGTTTCCCTTCAGCCCGCAGAGACCCCAGGCATG
GAGGAGAGCCTGGCAGAAATGAGTATTATGACTACTGAGCTTCAGAGTCTTTGTTCCCTGCTACAAGAG
TCTAAAGAAGAAGCCATCAGGACTCTGCAGCGAAAAATTTGTGAGCTGCAAGCTAGGCTGCAGGCCCAG
GAAGAACAGCATCAGGAAGTCCAGAAGGCAAAAGAAGCAGACATAGAGAAGCTGAACCAGGCCTTGTGC
TTGCGCTACAAGAATGAAAAGGAGCTCCAGGAAGTGATACAGCAGCAGAATGAGAAGATCCTAGAACAG
ATAGACAAGAGTGGCGAGCTCATAAGCCTTAGAGAGGAGGTGACCCACCTTACCCGCTCACTTCGGCGT
GCGGAGACAGAGACCAAAGTGCTCCAGGAGGCCCTGGCAGGCCAGCTGGACTCCAACTGCCAGCCTATG
GCCACCAATTGGATCCAGGAGAAAGTGTGGCTCTCTCAGGAGGTGGACAAACTGAGAGTGATGTTCCTG
GAGATGAAAAATGAGAAGGAAAAACTCATGATCAAGTTCCAGAGCCATAGAAATATCCTAGAGGAGAAC
CTTCGGCGCTCTGACAAGGAGTTAGAAAAACTAGATGACATTGTTCAGCATATTTATAAGACCCTGCTC
TCTATTCCAGAGGTGGTGAGGGGATGCAAAGAACTACAGGGATTGCTGGAATTTCTGAGC

6.4.1.2 Codon-optimized gene

ATGTGGCGTGTTAAAAAACTGAGCCTGAGCCTGTCACCGAGTCCGCAGACCGGTAAACCGAGCATGCGT
ACACCGCTGCGTGAACTGACCCTGCAGCCAGGTGCACTGACCAATAGCGGTAAACGTAGTCCGGCATGT
AGCAGCCTGACCCCGAGCCTGTGTAAACTGGGTCTGCAAGAAGGTAGCAATAATTCAAGTCCGGTTGAT
TTTGTGAACAACAAACGTACCGATCTGAGCAGCGAACATTTTAGCCATAGCAGCAAATGGCTGGAAACC
TGTCAGCATGAAAGTGATGAACAGCCGCTGGACCCGATTCCGCAGATTAGCAGCACCCCGAAAACCAGC
GAAGAAGCAGTTGATCCGCTGGGCAATTATATGGTTAAAACCATTGTTCTGGTTCCGTCACCGCTGGGT
CAGCAGCAGGACATGATTTTTGAAGCACGTCTGGATACAATGGCAGAAACCAATAGCATTAGCCTGAAT
GGTCCGCTGCGTACCGATGATCTGGTTCGTGAAGAGGTTGCACCGTGTATGGGTGATCGTTTTAGCGAA
GTTGCAGCAGTTAGCGAAAAACCGATTTTTCAAGAAAGCCCGAGCCATCTGCTGGAAGAAAGTCCGCCT
AATCCGTGTAGCGAACAGCTGCATTGTAGCAAAGAAAGCCTGAGTAGCCGTACCGAAGCAGTGCGTGAA
GATCTGGTGCCGAGCGAAAGCAATGCATTTCTGCCGAGCAGCGTTCTGTGGCTGAGCCCGAGCACCGCA
CTGGCAGCAGATTTTCGTGTTAATCATGTTGATCCGGAAGAAGAAATTGTTGAGCACGGTGCTATGGAA
GAACGTGAAATGCGTTTTCCGACCCATCCGAAAGAAAGCGAAACCGAAGATCAGGCACTGGTTAGCAGC
GTTGAAGATATTCTGAGCACCTGTCTGACACCGAATCTGGTTGAAATGGAAAGCCAAGAAGCACCGGGT
CCGGCAGTTGAAGATGTTGGTCGTATTCTGGGTAGCGATACCGAAAGCTGGATGAGTCCGCTGGCCTGG
CTGGAAAAAGGTGTTAATACCAGCGTTATGCTGGAAAACCTGCGTCAGAGCCTGAGTCTGCCGAGTATG
CTGCGTGATGCAGCAATTGGCACCACCCCGTTTAGCACCTGTAGCGTTGGCACCTGGTTTACCCCGAGC
GCACCGCAAGAAAAAAGCACCAATACCAGCCAGACAGGTCTGGTTGGCACCAAACATAGCACCAGTGAA
ACCGAACAACTGCTGTGTGGTCGTCCGCCTGATCTGACCGCACTGAGCCGTCATGATCTGGAAGATAAT
CTGCTGAGCAGCCTGGTTATTCTGGAAGTTCTGAGTCGTCAGCTGCGCGATTGGAAAAGTCAGCTGGCA
GTTCCGCATCCGGAAACCCAGGATAGCAGTACCCAGACCGATACCAGTCATAGCGGTATTACCAATAAA
CTGCAGCACCTGAAAGAAAGTCATGAAATGGGTCAGGCCCTGCAGCAGGCACGTAATGTTATGCAGAGC

TGGGTTCTGATTTCCAAAGAACTGATTAGTCTGCTGCATCTGTCACTGCTGCACCTGGAAGAGGATAAA
ACCACCGTTAGCCAAGAAAGTCGTCGTGCAGAAACCCTGGTTTGTTGCTGTTTTGATCTGCTGAAAAAA
CTGCGTGCAAAACTGCAGAGTCTGAAAGCCGAACGCGAAGAGGCACGTCATCGTGAAGAAATGGCACTG
CGTGGTAAAGATGCAGCCGAAATTGTGCTGGAAGCATTTTGTGCACATGCAAGCCAGCGTATTAGCCAG
CTGGAACAGGATCTGGCCAGCATGCGTGAATTTCGTGGCCTGCTGAAAGATGCACAGACCCAGCTGGTT
GGTCTGCATGCAAAACAAGAAGAACTGGTTCAGCAGACCGTGAGCCTGACCAGCACCCTGCAACAGGAT
TGGCGTAGTATGCAGCTGGATTATACCACCTGGACAGCACTGCTGAGCCGTAGCCGTCAACTGACCGAA
AAACTGACCGTTAAAAGCCAGCAGGCGCTGCAAGAGCGTGATGTTGCAATTGAAGAAAAACAAGAGGTT
AGCCGTGTTCTGGAACAAGTTAGCGCACAGCTGGAAGAGTGTAAAGGTCAGACCGAGCAACTGGAACTG
GAAAATAGCCGTCTGGCAACCGATCTGCGTGCCCAGCTGCAGATTCTGGCAAATATGGATAGTCAGCTG
AAAGAGCTGCAGAGCCAGCATACCCATTGTGCACAGGACCTGGCAATGAAAGATGAGCTGCTGTGCCAA
CTGACCCAGAGCAATGAAGAACAGGCAGCACAGTGGCAGAAAGAAGAGATGGCCCTGAAACACATGCAG
GCAGAACTGCAACAGCAGCAAGCAGTTCTGGCCAAAGAAGTTCGCGATCTGAAAGAGACACTGGAATTT
GCAGATCAAGAAAATCAGGTTGCACATCTGGAACTGGGTCAGGTTGAATGTCAACTGAAAACCACCCTG
GAAGTGCTGCGCGAACGTAGCCTGCAGTGTGAAAATCTGAAAGATACCGTGGAAAATCTGACCGCCAAA
CTGGCAAGCACCATTGCAGATAATCAAGAACAAGATCTGGAAAAAACCCGTCAGTATAGCCAGAAACTG
GGACTGCTGACCGAGCAGCTGCAGTCTCTGACCCTGTTTCTGCAGACAAAACTGAAAGAAAAAACCGAG
CAAGAAACACTGCTGCTGTCAACCGCATGTCCGCCTACCCAAGAACATCCGCTGCCGAATGATCGTACC
TTTCTGGGTTCAATTCTGACAGCCGTTGCCGATGAAGAACCGGAAAGCACACCGGTTCCGCTGCTGGGT
AGTGATAAAAGCGCATTTACCCGTGTTGCAAGCATGGTTAGTCTGCAGCCTGCCGAAACACCGGGTATG
GAAGAGTCACTGGCCGAAATGAGCATTATGACCACCGAACTGCAGTCACTGTGTTCTCTGCTGCAAGAA
TCAAAAGAAGAAGCAATTCGTACACTGCAGCGCAAAATTTGTGAACTGCAAGCGCGTCTGCAGGCACAA
GAGGAACAGCATCAAGAAGTGCAGAAAGCAAAAGAAGCCGATATTGAGAAACTGAATCAGGCGCTGTGT
CTGCGCTATAAAAACGAAAAAGAACTGCAAGAAGTGATCCAGCAGCAGAACGAAAAAATCCTGGAACAA
ATTGACAAAAGCGGTGAACTGATTTCACTGCGCGAAGAAGTTACCCATCTGACCCGTAGTCTGCGTCGT
GCCGAGACTGAAACCAAAGTTCTGCAAGAGGCCCTGGCAGGTCAGCTGGATAGCAATTGTCAGCCGATG
GCAACCAATTGGATTCAAGAAAAAGTTTGGCTGAGTCAAGAGGTGGATAAACTGCGCGTTATGTTTCTG
GAAATGAAAAATGAGAAAGAAAAACTGATGATCAAATTTCAGAGCCACCGCAATATCCTGGAAGAGAAC
CTGCGTCGTAGCGATAAAGAACTGGAAAAACTGGATGATATTGTGCAGCACATCTATAAAACCCTGCTG
AGTATTCCGGAAGTTGTTCGTGGTTGTAAAGAACTGCAGGGACTGCTGGAATTTCTGAGC

6.4.2 SKAP

6.4.2.1 Wild type gene

ATGGCGGCTCCCGAAGCCCCGCCCCTGGACAGAGTTTTCCGTACAACATGGCTGTCTACAGAGTGCGAT
TCCCACCCACTTCCGCCTAGCTACCGGAAGTTTCTATTTGAAACCCAGGCGGCCGACTTAGCCGGTGGC
ACGACAGTTGCTGCAGGGAATCTTTTAAACGAGAGCGAGAAGGACTGCGGGCAGGACCGGCGGGCTCCT
GGGGTTCAGCCGTGCCGCCTCGTTACGATGACCAGTGTGGTTAAGACAGTGTATAGCCTGCAGCCCCCC
TCTGCGCTGAGCGGCGGCCAGCCGGCAGACACACAAACTCGGGCCACTTCTAAGAGTCTCTTACCTGTT
AGGTCCAAAGAAGTCGATGTTTCCAAACAGCTTCATTCAGGAGGTCCAGAGAATGATGTTACAAAAATC
ACCAAACTGAGACGAGAGAATGGGCAAATGAAAGCTACTGACACTGCCACCAGAAGGAATGTCAGAAAA
GGCTACAAACCACTGAGTAAGCAAAAATCAGAGGAAGAGCTCAAGGACAAGAACCAGCTGTTAGAAGCC
GTCAACAAGCAGTTGCACCAGAAGTTGACTGAAACTCAGGGAGAGCTGAAGGACCTGACCCAGAAGGTA
GAGCTGCTGGAGAAGTTTCGGGACAACTGTTTGGCAATTTTGGAGAGCAAGGGCCTTGATCCAGCTTTA
GGCAGTGAGACCCTGGCATCACGACAAGAATCCACTACTGATCACATGGACTCTATGTTGCTGTTAGAA
ACTTTGCAAGAGGAGCTGAAGCTTTTTAACGAAACAGCCAAAAAGCAGATGGAGGAGTTACAGGCCTTA
AAGGTAAAGCTGGAGATGAAAGAGGAAAGAGTCCGATTCCTAGAACAGCAAACCTTATGTAACAATCAA
GTAAATGATTTAACAACAGCCCTTAAGGAAATGGAGCAGCTATTAGAAATG

6.4.2.2 Codon-optimized gene

ATGGCAGCACCGGAAGCACCGCCTCTGGATCGTGTTTTTCGTACCACCTGGCTGAGCACCGAATGTGAT
AGCCATCCGCTGCCTCCGAGCTATCGTAAATTTCTGTTTGAAACCCAGGCAGCAGATCTGGCAGGCGGT
ACAACCGTTGCAGCAGGTAATCTGCTGAATGAAAGCGAAAAAGATTGTGGTCAGGATCGTCGTGCACCG
GGTGTTCAGCCGTGTCGTCTGGTTACCATGACCAGCGTTGTTAAAACCGTTTATAGCCTGCAGCCACCG
AGCGCACTGAGCGGTGGTCAGCCTGCAGATACCCAGACCCGTGCAACCAGCAAAAGCCTGCTGCCGGTT
CGTAGCAAAGAAGTTGACGTTAGCAAACAGCTGCATAGTGGTGGTCCGGAAAATGATGTTACCAAAATT
ACCAAACTGCGTCGCGAAAATGGTCAGATGAAAGCAACCGATACCGCAACCCGTCGTAATGTTCGTAAA
GGTTATAAACCGCTGTCGAAACAGAAAAGCGAAGAGGAACTGAAAGATAAAAATCAGCTGCTGGAAGCC
GTTAATAAACAACTGCATCAGAAACTGACCGAAACACAGGGTGAGCTGAAAGATCTGACCCAGAAAGTT
GAACTGCTGGAAAAATTTCGTGATAACTGTCTGGCAATCCTGGAAAGCAAAGGTCTGGACCCTGCACTG
GGTAGCGAAACCCTGGCAAGCCGTCAAGAAAGCACCACCGATCACATGGATAGCATGCTGCTGCTGGAA
ACCCTGCAAGAAGAACTGAAACTGTTTAATGAAACCGCCAAAAAACAAATGGAAGAACTGCAGGCACTG
AAAGTGAAACTGGAAATGAAAGAAGAACGCGTCCGTTTTCTGGAACAGCAGACCCTGTGTAATAATCAG
GTTAATGATCTGACCACAGCCCTGAAAGAAATGGAACAGCTGCTGGAAATG

References

Abad MA, Medina B, Santamaria A, Zou J, Plasberg-Hill C, Madhumalar A, Jayachandran U, Redli PM, Rappsilber J, Nigg EA & Jeyaprakash AA. Structural basis for microtubule recognition by the human kinetochore Ska complex. Nature communications 5:2964, 2014.

Abergel C, Monchois V, Chenivesse S, Jeudy S & Claverie JM. Crystallization and preliminary crystallographic study of b0220, an 'ORFan' protein of unknown function from *Escherichia coli*. *Acta Crystallographica Section D-Biological Crystallography* 56:1694-5, 2000.

Akhmanova A & Steinmetz MO. Microtubule +TIPs at a glance. *Journal of cell science* 123:3415-9, 2010.

Alberts B, Johnson A, Lewis J, Raff M, Roberts K & Walter P. Molecular Biology of the Cell. *Garland Science*, 5th edition, chapter 17, 2008.

Alushin GM, Ramey VH, Pasqualato S, Ball DA, Grigorieff N, Musacchio A & Nogales E. The Ndc80 kinetochore complex forms oligomeric arrays along microtubules. *Nature* 467:805-10, 2010.

Alushin GM, Musinipally V, Matson D, Tooley J, Stukenberg PT & Nogales E. Multimodal microtubule binding by the Ndc80 kinetochore complex. *Nature structural & molecular biology* 19:1161-7, 2012.

Alushin GM, Lander GC, Kellogg EH, Zhang R, Baker D & Nogales E. High-resolution microtubule structures reveal the structural transitions in αβ-tubulin upon GTP hydrolysis. *Cell* 157:1117-29, 2014.

Asbury CL, Gestaut DR, Powers AF, Franck AD & Davis TN. The Dam1 kinetochore complex harnesses microtubule dynamics to produce force and movement. *Proceedings of the National Academy of Sciences of the United States of America* 103:9873-8, 2006.

Black BE & Bassett EA. The histone variant CENP-A and centromere specification. *Current opinion in cell biology* 20:91-100, 2008.

Blom N, Gammeltoft S & Brunak S. Sequence- and structure-based prediction of eukaryotic protein phosphorylation sites. *Journal of molecular biology* 294:1351-1362, 1999.

Bradford MM. A Rapid and Sensitive Method for the Quantification of Microgram Quantities of Protein Utilizing the Principle of Protein-Dye Binding. *Analytical Biochemistry* 72:248-54, 1976.

Brady DM & Hardwick KG. Complex formation between Mad1p, Bub1p and Bub3p is crucial for spindle checkpoint function. *Current biology : CB* 10:675-8, 2000.

Bröcker C, Kuhlee A, Gatsogiannis C, Balderhaar HJ, Hönscher C, Engelbrecht-Vandré S, Ungermann C & Raunser S. Molecular architecture of the multisubunit homotypic fusion and vacuole protein sorting (HOPS) tethering complex. *Proceedings of the National Academy of Sciences of the United States of America* 109:1991-6, 2012.

Brouhard GJ, Stear JH, Noetzel TL, Al-Bassam J, Kinoshita K, Harrison SC, Howard J & Hyman AA. XMAP215 is a processive microtubule polymerase. *Cell* 132:79-88, 2008.

Buchan DWA, Minneci F, Nugent TCO, Bryson K & Jones DT. Scalable web services for the PSIPRED Protein Analysis Workbench. *Nucleic Acids Research* 41:W340-8, 2013.

Carmena M, Wheelock M, Funabiki H & Earnshaw WC. The chromosomal passenger complex (CPC): from easy rider to the godfather of mitosis. *Nature reviews. Molecular cell biology* 13:789-803, 2012.

Carroll CW, Milks KJ & Straight AF. Dual recognition of CENP-A nucleosomes is required for centromere assembly. *The Journal of cell biology* 189:1143-55, 2010.

Chan YW, Jeyaprakash AA, Nigg EA & Santamaria A. Aurora B controls kinetochore-microtubule attachments by inhibiting Ska complex-KMN network interaction. *The Journal of cell biology* 196:563-71, 2012.

Cheeseman IM, Anderson S, Jwa M, Green EM, Kang Js, Yates JR, Chan CS, Drubin DG & Barnes G. Phospho-regulation of kinetochore-microtubule attachments by the Aurora kinase Ipl1p. *Cell* 111:163-72, 2002.

Cheeseman IM, Chappie JS, Wilson-Kubalek EM & Desai A. The conserved KMN network constitutes the core microtubule-binding site of the kinetochore. *Cell* 127:983-97. 2006.

Cheeseman IM & Desai A. Molecular architecture of the kinetochore-microtubule interface. *Nature reviews. Molecular cell biology.* 9:33-46, 2008.

Cheng TS, Hsiao YL, Lin CC, Hsu CM, Chang MS, Lee CI, Yu RC, Huang CY, Howng SL & Hong YR. hNinein is required for targeting spindle-associated protein Astrin to the centrosome during the S and G2 phases. *Experimental cell research* 313:1710-21, 2007.

Cheng TS, Hsiao YL, Lin CC, Yu CT, Hsu CM, Chang MS, Lee CI, Huang CY, Howng SL & Hong YR. Glycogen synthase kinase 3beta interacts with and phosphorylates the spindle-associated protein astrin. *The Journal of biological chemistry* 283:2454-64, 2008.

Chiu SC, Chen JM, Wei TY, Cheng TS, Wang YH, Ku CF, Lian CH, Liu CC, Kuo YC & Yu CT. The mitosis-regulating and protein-protein interaction activities of astrin are controlled by aurora-A-induced phosphorylation. *American journal of physiology. Cell physiology* 307:C466-78, 2014.

Ciferri C, De Luca J, Monzani S, Ferrari KJ, Ristic D, Wyman C, Stark H, Kilmartin J, Salmon ED & Musacchio A. Architecture of the human ndc80-hec1 complex, a critical constituent of the outer kinetochore. *The Journal of biological chemistry* 280:29088-95, 2005.

Ciferri C, Pasqualato S, Screpanti E, Varetti G, Santaguida S, Dos Reis G, Maiolica A, Polka J, De Luca JG, De Wulf P, Salek M, Rappsilber J, Moores CA, Salmon ED & Musacchio A. Implications for kinetochore-microtubule attachment from the structure of an engineered Ndc80 complex. *Cell* 133:427-39, 2008.

Civril F & Musacchio A. Spindly attachments. *Genes & development* 22:2302-7, 2008.

Cole C, Barber JD & Barton GJ. The Jpred 3 secondary structure prediction server. *Nucleic Acids Research* 35:W197-201, 2008.

Coudreuse D & Nurse P. Driving the cell cycle with a minimal CDK control network. *Nature* 468:1074-9, 2010.

Daum JR, Wren JD, Daniel JJ, Sivakumar S, McAvoy JN, Potapova TA & Gorbsky GJ. Ska3 is required for spindle checkpoint silencing and the maintenance of chromosome cohesion in mitosis. *Current biology : CB* 19:1467-72, 2009.

David-Pfeuty T, Erickson HP & Pantaloni D. Guanosinetriphosphatase activity of tubulin associated with microtubule assembly. *Proceedings of the National Academy of Sciences of the United States of America* 74:5372-6, 1977.

De Antoni A, Pearson CG, Cimini D, Canman JC, Sala V, Nezi L, Mapelli M, Sironi L, Faretta M, Salmon ED & Musacchio A. The Mad1/Mad2 complex as a template for Mad2 activation in the spindle assembly checkpoint. *Current biology : CB* 15:214-25, 2005.

DeLuca JG, Moree B, Hickey JM, Kilmartin JV & Salmon ED. hNuf2 inhibition blocks stable kinetochore-microtubule attachment and induces mitotic cell death in HeLa cells. *The Journal of cell biology* 159:549-55, 2002.

DeLuca JG, Gall WE, Ciferri C, Cimini D, Musacchio A & Salmon ED. Kinetochore microtubule dynamics and attachment stability are regulated by Hec1. *Cell* 127:969-82, 2006.

DeLuca JG & Musacchio A. Structural organization of the kinetochore-microtubule interface. *Current opinion in cell biology* 24:48-56, 2012.

Desai A & Mitchison TJ. Microtubule polymerization dynamics. *Annual review of cell and developmental biology* 13:83-117, 1997.

Desai A, Verma S, Mitchison TJ & Walczak CE. Kin I kinesins are microtubule-destabilizing enzymes. *Cell* 96:69-78, 1999.

Du J, Jablonski S, Yen TJ & Hannon GJ. Astrin regulates Aurora-A localization. *Biochemical and biophysical research communications* 370:213-9, 2008.

Dumontet C & Jordan MA. Microtubule-binding agents: a dynamic field of cancer therapeutics. *Nature review. Drug discovery* 9:790-803, 2010.

Dunsch AK, Linnane E, Barr FA & Gruneberg U. The astrin-kinastrin/SKAP complex localizes to microtubule plus ends and facilitates chromosome alignment. *The Journal of cell biology* 192:959-68, 2011.

Fang L, Seki A & Fang G. SKAP associates with kinetochores and promotes the metaphase-to-anaphase transition. *Cell Cycle* 8:2819-27, 2009.

Feng J, Huang H & Yen TJ. CENP-F is a novel microtubule-binding protein that is essential for kinetochore attachments and affects the duration of the mitotic checkpoint delay. *Chromosoma* 115:320-9, 2006.

Fenn JB, Mann M, Meng CK, Wong SF & Whitehouse CM. Electrospray Ionization for Mass Spectrometry of Large Biomolecules. *Science* 246:64-71, 1989.

Fitzgerald DJ, Berger P, Schaffitzel C, Yamada K, Richmond TJ & Berger I. Protein complex expression by using multigene baculoviral vectors. *Nature methods* 3:1021-32, 2006.

Flemming W. Zellsubstanz, Kern und Zelltheilung. *FCW Vogel, Leipzig*, 1882.

Foley EA & Kapoor TM. Microtubule attachment and spindle assembly checkpoint signalling at the kinetochore. *Nature reviews. Molecular cell biology* 14:25-37, 2013.

Gaitanos TN, Santamaria A, Jeyaprakash AA, Wang B, Conti E & Nigg EA. Stable kinetochore-microtubule interactions depend on the Ska complex and its new component Ska3/C13Orf3. *The EMBO Journal* 28:1442-52, 2009.

Gascoigne KE, Takeuchi K, Suzuki A, Hori T, Fukagawa T & Cheeseman IM. Induced ectopic kinetochore assembly bypasses the requirement for CENP-A nucleosomes. *Cell* 145:410-22, 2011.

Gasteiger E, Hoogland C, Gattiker A, Duvaud S, Wilkins MR, Appel RD, Bairoch A & Walker JM (ed). The Proteomics Protocols Handbook: Protein Identification and Analysis Tools on the ExPASy Server. *Humana Press*, 2005, S. 571-607.

Gavet O, Ozon S, Manceau V, Lawler S, Curmi P & Sobel A. The stathmin phosphoprotein family: intracellular localization and effects on the microtubule network. *Journal of cell science* 111:3333-46, 1998.

Gell C, Bormuth V, Brouhard GJ, Cohen DN, Diez S, Friel CT, Helenius J, Nitzsche B, Petzold H, Ribbe J, Schäffer E, Stear JH, Trushko A, Varga V, Widlund PO, Zanic M & Howard J. Microtubule dynamics reconstituted in vitro and imaged by single-molecule fluorescence microscopy. *Methods in cell biology* 95:221-45, 2010.

Gigant B, Curmi PA, Martin-Barbey C, Charbaut E, Lachkar S, Lebeau L, Siavoshian S, Sobel A & Knossow M. The 4 A X-ray structure of a tubulin:stathmin-like domain complex. *Cell* 102:809-16, 2000.

Gigant B, Wang C, Ravelli RB, Roussi F, Steinmetz MO, Curmi PA, Sobel A & Knossow M. Structural basis for the regulation of tubulin by vinblastine. *Nature* 435:519-22, 2005.

Griffis ER, Stuurman N & Vale RD. Spindly, a novel protein essential for silencing the spindle assembly checkpoint, recruits dynein to the kinetochore. *The Journal of cell biology* 177:1005-15, 2007.

Grimm M, Zimniak T, Kahraman A & Herzog F. xVis: a web server for the schematic visualization and interpretation of crosslink-derived spatial restraints. *Nucleic acids research* 43:W362-9, 2015.

Grishchuk EL, Efremov AK, Volkov VA, Spiridonov IS, Gudimchuk N, Westermann S, Drubin D, Barnes G, McIntosh JR & Ataullakhanov FI. The Dam1 ring binds microtubules strongly enough to be a processive as well as energy-efficient coupler for chromosome motion. *Proceedings of the National Academy of Sciences of the United States of America* 105:15423-8, 2008.

Gruber J, Harborth J, Schnabel J, Weber K & Hatzfeld M. The mitotic-spindle-associated protein astrin is essential for progression through mitosis. *Journal of cell science* 115:4053-9, 2002.

Guimaraes GJ, Dong Y, McEwen BF & Deluca JG. Kinetochore-microtubule attachment relies on the disordered N-terminal tail domain of Hec1. *Current biology : CB* 18:1778-84, 2008.

Hanisch A, Silljé HH & Nigg EA. Timely anaphase onset requires a novel spindle and kinetochore complex comprising Ska1 and Ska2. *The EMBO Journal* 25:5504-15, 2006.

Hauf S, Cole RW, LaTerra S, Zimmer C, Schnapp G, Walter R, Heckel A, van Meel J, Rieder CL & Peters JM. The small molecule Hesperadin reveals a role for Aurora B in correcting kinetochore-microtubule attachment and in maintaining the spindle assembly checkpoint. *The Journal of cell biology* 161:281-94, 2003.

Hayashi I & Ikura M. Crystal structure of the amino-terminal microtubule-binding domain of end-binding protein 1 (EB1). *The Journal of biological chemistry* 278:36430-4, 2003.

Hayden JH, Bowser SS & Rieder CL. Kinetochores capture astral microtubules during chromosome attachment to the mitotic spindle: direct visualization in live newt lung cells. *The Journal of cell biology* 111:1039-45, 1990.

Herzog F, Kahraman A, Boehringer D, Mak R, Bracher A, Walzthoeni T, Leitner A, Beck M, Hartl FU, Ban N, Malmström L & Aebersold R. Structural probing of a protein phosphatase 2A network by chemical cross-linking and mass spectrometry. *Science* 337:1348-52, 2012.

Holy TE & Leibler S. Dynamic instability of microtubules as an efficient way to search in space. *Proceedings of the National Academy of Sciences of the United States of America* 91:5682-5, 1994.

Honnappa S, Okhrimenko O, Jaussi R, Jawhari H, Jelesarov I, Winkler FK & Steinmetz MO. Key interaction modes of dynamic +TIP networks. *Molecular cell* 23:663-71, 2006.

Honnappa S, Gouveia SM, Weisbrich A, Damberger FF, Bhavesh NS, Jawhari H, Grigoriev I, van Rijssel FJ, Buey RM, Lawera A, Jelesarov I, Winkler FK, Wüthrich K, Akhmanova A & Steinmetz MO. An EB1-binding motif acts as a microtubule tip localization signal. *Cell* 138:366-76, 2009.

Hori T, Amano M, Suzuki A, Backer CB, Welburn JP, Dong Y, McEwen BF, Shang WH, Suzuki E, Okawa K, Cheeseman IM & Fukagawa T. CCAN makes multiple contacts with centromeric DNA to provide distinct pathways to the outer kinetochore. *Cell* 135:1039-52, 2008.

Hori T, Shang WH, Takeuchi K & Fukagawa T. The CCAN recruits CENP-A to the centromere and forms the structural core for kinetochore assembly. *The Journal of cell biology* 200:45-60, 2013.

Huang Y, Wang W, Yao P, Wang X, Liu X, Zhuang X, Yan F, Zhou J, Du J, Ward T, Zou H, Zhang J, Fang G, Ding X, Dou Z & Yao X. CENP-E kinesin interacts with SKAP protein to orchestrate accurate chromosome segregation in mitosis. *The Journal of biological chemistry* 287:1500-9, 2012.

Jerabek-Willemsen M, Wienken CJ, Braun D, Baaske P & Duhr S. Molecular interaction studies using microscale thermophoresis. *Assay and drug development technologies* 9:342-53, 2011.

Jeyaprakash AA, Santamaria A, Jayachandran U, Chan YW, Benda C, Nigg EA & Conti E. Structural and functional organization of the Ska complex, a key component of the kinetochore-microtubule interface. *Molecular cell* 46:274-86, 2012.

Joglekar AP, Bouck DC, Molk JN, Bloom KS & Salmon ED. Molecular architecture of a kinetochore-microtubule attachment site. *Nature cell biology* 8:581-5, 2006.

Johnson KA & Borisy GG. Kinetic analysis of microtubule self-assembly *in vitro*. *Journal of Molecular Biology* 117:1-31, 1977.

Karess R. Rod-Zw10-Zwilch: a key player in the spindle checkpoint. *Trends in cell biology* 15:386-92, 2005.

Kelley LA & Sternberg MJE. Protein structure prediction on the web: a case study using the Phyre server. *Nature Protocols* 4:363-71, 2009.

Khodjakov A, Copenagle L, Gordon MB, Compton DA & Kapoor TM. Minus-end capture of preformed kinetochore fibers contributes to spindle morphogenesis. *The Journal of cell biology* 160:671-83, 2003.

Kiefer B, Sakai H, Solari AJ & Mazia D. The molecular unit of the microtubules of the mitotic apparatus. *Journal of molecular biology*, 20:75-79, 1966.

Kirschner M & Mitchison T. Beyond self-assembly: from microtubules to morphogenesis. *Cell* 45: 329-42, 1986.

Kitagawa K & Hieter P. Evolutionary conservation between budding yeast and human kinetochores. *Nature reviews. Molecular cell biology* 2:678-87, 2001.

Kiyomitsu T, Obuse C & Yanagida M. Human Blinkin/AF15q14 is required for chromosome alignment and the mitotic checkpoint through direct interaction with Bub1 and BubR1. *Developmental cell* 13:663-76, 2007.

Kline SL, Cheeseman IM, Hori T, Fukagawa T & Desai A. The human Mis12 complex is required for kinetochore assembly and proper chromosome segregation. *The Journal of cell biology* 173:9-17, 2006.

Kops GJ, Kim Y, Weaver BA, Mao Y, McLeod I, Yates JR, Tagaya M & Cleveland DW. ZW10 links mitotic checkpoint signaling to the structural kinetochore. The *Journal of cell biology* 169:49-60, 2005.

Krenn V, Wehenkel A, Li X, Santaguida S & Musacchio A. Structural analysis reveals features of the spindle checkpoint kinase Bub1-kinetochore subunit Knl1 interaction. *The Journal of cell biology* 196:451-67, 2012.

Krenn V, Overlack K, Primorac I, van Gerwen S & Musacchio A. KI motifs of human Knl1 enhance assembly of comprehensive spindle checkpoint complexes around MELT repeats. *Current biology : CB* 24:29-39, 2014.

Laemmli UK. Cleavage of Structural Proteins during the Assembly of the Head of Bacteriophage T4. *Nature* 227;680-5, 1970.

Lengauer C, Kinzler KW & Vogelstein B. Genetic instabilities in human cancers. *Nature* 396:643-9, 1998.

Liu D, Vader G, Vromans MJ, Lampson MA & Lens SM. Sensing chromosome bi-orientation by spatial separation of aurora B kinase from kinetochore substrates. *Science* 323:1350-3, 2009.

London N, Ceto S, Ranish JA & Biggins S. Phosphoregulation of Spc105 by Mps1 and PP1 regulates Bub1 localization to kinetochores. *Current biology : CB* 22:900-6, 2012.

London N & Biggins S. Mad1 kinetochore recruitment by Mps1-mediated phosphorylation of Bub1 signals the spindle checkpoint. *Genes & development* 28:140-52, 2014.

Lottspeich F & Engels JW. Bioanalytik. Spektrum Akademischer Verlag, 2nd edition, 2006.

Mack GJ & Compton DA. Analysis of mitotic microtubule-associated proteins using mass spectrometry identifies astrin, a spindle-associated protein. *Proceedings of the National Academy of Sciences of the Unites States of America* 98:14434-9, 2001.

Maiato H, DeLuca J, Salmon ED & Earnshaw WC. The dynamic kinetochore-microtubule interface. *Journal of cell science* 117:5461-77, 2004.

Malvezzi F, Litos G, Schleiffer A, Heuck A, Mechtler K, Clausen T & Westermann S. A structural basis for kinetochore recruitment of the Ndc80 complex via two distinct centromere receptors. *The EMBO journal* 32:409-23, 2013.

Manning AL, Ganem NJ, Bakhoum SF, Wagenbach M, Wordeman L & Compton DA. The kinesin-13 proteins Kif2a, Kif2b, and Kif2c/MCAK have distinct roles during mitosis in human cells. *Molecular biology of the cell* 18:2970-9, 2007.

Manning AL, Bakhoum SF, Maffini S, Correia-Melo C, Maiato H & Compton DA. CLASP1, astrin and Kif2b form a molecular switch that regulates kinetochore-microtubule dynamics to promote mitotic progression and fidelity. *The EMBO journal* 29:3531-43, 2010.

Maresca TJ & Salmon ED. Intrakinetochore stretch is associated with changes in kinetochore phosphorylation and spindle assembly checkpoint activity. *The Journal of cell biology* 184:373-81, 2009.

Martin-Lluesma S, Stucke VM & Nigg EA. Role of Hec1 in spindle checkpoint signaling and kinetochore recruitment of Mad1/Mad2. Science 297:2267-70, 2002.

Maure JF, Komoto S, Oku Y, Mino A, Pasqualato S, Natsume K, Clayton L, Musacchio A, Tanaka TU. The Ndc80 loop region facilitates formation of kinetochore attachment to the dynamic microtubule plus end. *Current Biology : CB* 21:207-13, 2011.

McDonnell AV, Jiang T, Keating AE & Berger B. Paircoil2: Improved prediction of coiled coils from sequence. *Bioinformatics* 22:356-8, 2006.

McEwen BF, Dong Y & VandenBeldt KJ. Using electron microscopy to understand functional mechanisms of chromosome alignment on the mitotic spindle. *Methods in cell biology* 79:259-93, 2007.

Mimori-Kiyosue Y, Grigoriev I, Lansbergen G, Sasaki H, Matsui C, Severin F, Galjart N, Grosveld F, Vorobjev I, Tsukita S & Akhmanova A. CLASP1 and CLASP2 bind to EB1 and regulate microtubule plus-end dynamics at the cell cortex. *The Journal of cell biology* 168:141-53, 2005.

Mirigian M, Mukherjee K, Bane SL & Sackett DL. Measurement of in vitro microtubule polymerization by turbidity and fluorescence. *Methods in Cell Biology* 115:215-29, 2013.

Mitchison T & Kirschner M. Dynamic instability of microtubule growth. *Nature* 312:237-42, 1984.

Mitchison TJ & Salmon ED. Mitosis: a history of division. *Nature cell biology* 3:E17-21, 2001.

Moore MS & Blobel G. A G protein involved in nucleocytoplasmic transport: the role of Ran. *Trends in biochemical sciences* 19:211-6, 1994.

Morgan DO. The Cell Cycle: Principles of Control. *New Science Press Ltd*, 2007.

Moritz M, Braunfeld MB, Sedat JW, Alberts B & Agard DA. Microtubule nucleation by gamma-tubulin-containing rings in the centrosome. *Nature* 378:638-40, 1995.

Moyle MW, Kim T, Hattersley N, Espeut J, Cheerambathur DK, Oegema K & Desai A. A Bub1-Mad1 interaction targets the Mad1-Mad2 complex to unattached kinetochores to initiate the spindle checkpoint. *The Journal of cell biology* 204:647-57, 2014.

Murphy DB & Borisy GG. Association of high-molecular-weight proteins with microtubules and their role in microtubule assembly *in vitro*. *Proceedings of the National Academy of Sciences of the Unites States of America* 72:2696-700, 1975.

Musacchio A & Salmon ED. The spindle-assembly checkpoint in space and time. *Nature reviews. Molecular cell biology* 8:379-93, 2007.

Nezi L & Musacchio A. Sister chromatid tension and the spindle assembly checkpoint. *Current opinion in cell biology* 21:785-95, 2009.

Nicklas RB & Koch CA. Chromosome micromanipulation. 3. Spindle fiber tension and the reorientation of mal-oriented chromosomes. *The Journal of cell biology* 43:40-50, 1969.

Nijenhuis W, von Castelmur E, Littler D, De Marco V, Tromer E, Vleugel M, van Osch MH, Snel B, Perrakis A & Kops GJ. A TPR domain-containing N-terminal module of MPS1 is required for its kinetochore localization by Aurora B. *The Journal of cell biology* 201:217-31, 2013.

Nishino T, Takeuchi K, Gascoigne KE, Suzuki A, Hori T, Oyama T, Morikawa K, Cheeseman IM & Fukagawa T. CENP-T-W-S-X forms a unique centromeric chromatin structure with a histone-like fold. *Cell* 148:487-501, 2012.

Nishino T, Rago F, Hori T, Tomii K, Cheeseman IM & Fukagawa T. CENP-T provides a structural platform for outer kinetochore assembly. The EMBO journal 32:424-36, 2013.

Nogales E, Whittaker M, Milligan RA & Downing KH. High-resolution model of the microtubule. *Cell* 96:79-88, 1999.

Overlack K, Krenn V & Musacchio A. When Mad met Bub. *EMBO reports* 15:326-8, 2014.

Papworth C, Bauer JC, Braman J & Wright DA. Site-directed mutagenesis in one day with >80% efficiency. *Strategies* 9:3–4, 1996.

Perpelescu M & Fukagawa T. The ABCs of CENPs. *Chromosoma* 120:425-46, 2011.

Peterman EJ & Scholey JM. Mitotic microtubule crosslinkers: insights from mechanistic studies. *Current biology : CB* 19:R1089-94, 2009.

Peters JM. The anaphase promoting complex/cyclosome: a machine designed to destroy. *Nature reviews. Molecular cell biology* 7:644-56, 2006.

Petrovic, A., Pasqualato, S., Dube, P., Krenn, V., Santaguida, S., Cittaro, D., Monzani, S., Massimiliano, L., Keller, J., Tarricone, A., Maiolica, A., Stark, H. & Musacchio, A. The MIS12 complex is a protein interaction hub for outer kinetochore assembly. *The Journal of cell biology* 190:835-52, 2010.

Petrovic A, Mosalaganti S, Keller J, Mattiuzzo M, Overlack K, Krenn V, De Antoni A, Wohlgemuth S, Cecatiello V, Pasqualato S, Raunser S & Musacchio A. Modular assembly of RWD domains on the Mis12 complex underlies outer kinetochore organization. *Molecular cell* 53:591-605, 2014.

Porath J & Flodin P. Gel Filtration: A Method for Desalting and Group Seperation. *Nature* 183:1657-9, 1959.

Prota AE, Magiera MM, Kuijpers M, Bargsten K, Frey D, Wieser M, Jaussi R, Hoogenraad CC, Kammerer RA, Janke C & Steinmetz MO. Structural basis of tubulin tyrosination by tubulin tyrosine ligase. *The Journal of cell biology* 200:259-70, 2013.

Rieder CL & Salmon ED. The vertebrate cell kinetochore and its roles during mitosis. *Trends in cell biology*, 8:310-8, 1998.

Roy A, Kucukural A & Zhang Y. I-TASSER: a unified platform for automated protein structure and function prediction. *Nature Protocols* 5:725-38, 2010.

Saiki RK *et al.* Primer-Directed Enzymatic Amplification of DNA with a Thermostable DNA Polymerase. *Science* 239:487-91, 1988.

Santaguida S & Musacchio A. The life and miracles of kinetochores. *The EMBO journal* 28:2511-31, 2009.

Santaguida S, Vernieri C, Villa F, Ciliberto A & Musacchio A. Evidence that Aurora B is implicated in spindle checkpoint signalling independently of error correction. *The EMBO journal* 30:1508-19, 2011.

Saurin AT, van der Waal MS, Medema RH, Lens SM & Kops GJ. Aurora B potentiates Mps1 activation to ensure rapid checkpoint establishment at the onset of mitosis. *Nature communications* 2:316, 2011.

Schmidt JC, Kiyomitsu T, Hori T, Backer CB, Fukagawa T & Cheeseman IM. Aurora B kinase controls the targeting of the Astrin-SKAP complex to bioriented kinetochores. *The Journal of cell biology* 191:269-80, 2010.

Schmidt JC, Arthanari H, Boeszoermenyi A, Dashkevich NM, Wilson-Kubalek EM, Monnier N, Markus M, Oberer M, Milligan RA, Bathe M, Wagner G, Grishchuk EL & Cheeseman IM. The kinetochore-bound Ska1 complex tracks depolymerizing microtubules and binds to curved protofilaments. *Developmental cell* 23:968-80, 2012.

Schuck P. Size-distribution analysis of macromolecules by sedimentation velocity ultracentrifugation and lamm equation modeling. *Biophysical Journal* 78:1606–1619, 2000.

Schuyler SC, Liu JY & Pellman D. The molecular function of Ase1p: evidence for a MAP-dependent midzone-specific spindle matrix. Microtubule-associated proteins. The Journal of cell biology 160:517-28, 2003.

Screpanti, E., De Antoni, A., Alushin, G. M., Petrovic, A., Melis, T., Nogales, E. & Musacchio, A. Direct binding of Cenp-C to the Mis12 complex joins the inner and outer kinetochore. *Current biology : CB* 21:391-8, 2011.

Shao X, Xue J & van der Hoorn FA. Testicular protein Spag5 has similarity to mitotic spindle protein Deepest and binds outer dense fiber protein Odf1. *Molecular reproduction and development* 59:410-6, 2001.

Sharp DJ, Rogers GC & Scholey JM. Cytoplasmic dynein is required for poleward chromosome movement during mitosis in Drosophila embryos. *Nature cell biology* 2:922-30, 2000.

Shepperd LA, Meadows JC, Sochaj AM, Lancaster TC, Zou J, Buttrick GJ, Rappsilber J, Hardwick KG & Millar JB. Phosphodependent recruitment of Bub1 and Bub3 to Spc7/KNL1 by Mph1 kinase maintains the spindle checkpoint. *Current biology : CB* 22:891-9, 2012.

Shrestha RL & Draviam VM. Lateral to end-on conversion of chromosome-microtubule attachment requires kinesins CENP-E and MCAK. *Current biology : CB* 23:1514-26, 2013.

Sievers F, Wilm A, Dineen D, Gibson TJ, Karplus K, Li W, Lopez R, McWilliam H, Remmert M, Söding J, Thompson JD & Higgins DG. Fast, scalable generation of high-quality protein multiple sequence alignments using Clustal Omega. *Molecular Systems Biology* 7:539, 2011.

Starr DA, Williams BC, Hays TS & Goldberg ML. ZW10 helps recruit dynactin and dynein to the kinetochore. *The Journal of cell biology* 142:763-74, 1998.

Starr DA, Saffery R, Li Z, Simpson AE, Choo KH, Yen TJ & Goldberg ML. HZwint-1, a novel human kinetochore component that interacts with HZW10. *Journal of cell science* 113:1939-50, 2000.

Takahashi M, Ogino T & Baba K. Estimation of Relative Molecular Length of DNA by Electrophoresis in Agarose Gel. *Biochimica et Biophysica Acta* 174:183-7, 1969.

Tamura N, Simon JE, Nayak A, Shenoy R, Hiroi N, Boilot V, Funahashi A & Draviam VM. A proteomic study of mitotic phase-specific interactors of EB1 reveals a role for SXIP-mediated protein interactions in anaphase onset. *Biology open* 4:155-69, 2015.

Tanaka TU, Rachidi N, Janke C, Pereira G, Galova M, Schiebel E, Stark MJ & Nasmyth K. Evidence that the Ipl1-Sli15 (Aurora kinase-INCENP) complex promotes chromosome bi-orientation by altering kinetochore-spindle pole connections. *Cell* 108:317-29, 2002.

Tanaka K, Mukae N, Dewar H, van Breugel M, James EK, Prescott AR, Antony C & Tanaka TU. Molecular mechanisms of kinetochore capture by spindle microtubules. *Nature* 434:987-94, 2005.

Tanaka TU. Bi-orienting chromosomes: acrobatics on the mitotic spindle. *Chromosoma* 117:521-33, 2008.

Tanaka TU. Kinetochore-microtubule interactions: steps towards bi-orientation. *The EMBO Journal* 29:4070-82, 2010.

Thein KH, Kleylein-Sohn J, Nigg EA & Gruneberg U. Astrin is required for the maintenance of sister chromatid cohesion and centrosome integrity. *The Journal of cell biology* 178:345-54, 2007.

Theis M, Slabicki M, Junqueira M, Paszkowski-Rogacz M, Sontheimer J, Kittler R, Heninger AK, Glatter T, Kruusmaa K, Poser I, Hyman AA, Pisabarro MT, Gstaiger M, Aebersold R, Shevchenko A & Buchholz F. Comparative profiling identifies C13orf3 as a component of the Ska complex required for mammalian cell division. *The EMBO Journal* 28:1453-65, 2009.

Tien JF, Umbreit NT, Gestaut DR, Franck AD, Cooper J, Wordeman L, Gonen T, Asbury CL & Davis TN. Cooperation of the Dam1 and Ndc80 kinetochore complexes enhances microtubule coupling and is regulated by aurora B. *The Journal of cell biology* 189:713-23, 2010.

Varma D & Salmon ED. The KMN protein network-chief conductors of the kinetochore orchestra. *Journal of cell science* 125: 5927-36, 2012.

Vleugel M, Tromer E, Omerzu M, Groenewold V, Nijenhuis W, Snel B & Kops GJ. Arrayed BUB recruitment modules in the kinetochore scaffold KNL1 promote accurate chromosome segregation. *The Journal of cell biology* 203:943-55, 2013.

Waizenegger IC, Hauf S, Meinke A, and Peters J-M. Two distinct pathways remove mammalian cohesin from chromosome arms in prophase and from centromeres in anaphase. *Cell* 103:399-410, 2000.

Wang X, Zhuang X, Cao D, Chu Y, Yao P, Liu W, Liu L, Adams G, Fang G, Dou Z, Ding X, Huang Y, Wang D & Yao X. Mitotic regulator SKAP forms a link between kinetochore core complex KMN and dynamic spindle microtubules. *The Journal of biological chemistry* 287:39380-90, 2012.

Wei RR, Sorger PK & Harrison SC. Molecular organization of the Ndc80 complex, an essential kinetochore component. *Proceedings of the National Academy of Sciences of the United States of America* 102:5363-7, 2005.

Weisenberg RC, Deery WJ & Dickinson PJ. Tubulin-nucleotide interactions during the polymerization and depolymerization of microtubules. *Biochemistry* 15:4248-54, 1976.

Welburn JP & Cheeseman IM. Toward a molecular structure of the eukaryotic kinetochore. *Developmental cell* 15:645-55, 2008.

Welburn JP, Grishchuk EL, Backer CB, Wilson-Kubalek EM, Yates JR 3rd & Cheeseman IM. The human kinetochore Ska1 complex facilitates microtubule depolymerization-coupled motility. *Developmental cell* 16:374-85, 2009.

Welburn JP, Vleugel M, Liu D, Yates JR 3rd, Lampson MA, Fukagawa T & Cheeseman IM. Aurora B phosphorylates spatially distinct targets to differentially regulate the kinetochore-microtubule interface. Molecular cell 38:383-92, 2010.

Westermann S, Avila-Sakar A, Wang HW, Niederstrasser H, Wong J, Drubin DG, Nogales E & Barnes G. Formation of a dynamic kinetochore-microtubule interface through assembly of the Dam1 ring complex. *Molecular cell* 17:277-90, 2005.

Westermann S, Wang HW, Avila-Sakar A, Drubin DG, Nogales E & Barnes G. The Dam1 kinetochore ring complex moves processively on depolymerizing microtubule ends. *Nature* 440:565-9, 2006.

Westermann S, Drubin DG & Barnes G. Structures and functions of yeast kinetochore complexes. *Annual review of biochemistry* 76:563-91, 2007.

Westermann S & Schleiffer A. Family matters: structural and functional conservation of centromere-associated proteins from yeast to humans. *Trends in cell biology* 23:260-9, 2013.

Wittmann T, Hyman A & Desai A. The spindle: a dynamic assembly of microtubules and motors. *Nature cell biology* 3:E28-34, 2001.

Wollman R, Cytrynbaum EN, Jones JT, Meyer T, Scholey JM & Mogilner A. Efficient chromosome capture requires a bias in the 'search-and-capture' process during mitotic-spindle assembly. *Current biology : CB* 15:828-32, 2005.

Yamagishi Y, Yang CH, Tanno Y & Watanabe Y. MPS1/Mph1 phosphorylates the kinetochore protein KNL1/Spc7 to recruit SAC components. *Nature cell biology* 14:746-52, 2012.

Yuan J, Li M, Wei L, Yin S, Xiong B, Li S, Lin SL, Schatten H & Sun QY. Astrin regulates meiotic spindle organization, spindle pole tethering and cell cycle progression in mouse oocytes. *Cell Cycle* 8:3384-95, 2009.

Zhang Y. I-TASSER server for protein 3D structure prediction. *BMC Bioinformatics* 9:40, 2008.

Zhang R, Alushin GM, Brown A & Nogales E. Mechanistic Origin of Microtubule Dynamic Instability and Its Modulation by EB Proteins. *Cell* 162:1-11, 2015.

Acknowledgements

First of all, I am grateful to my supervisor Prof. Andrea Musacchio for giving me the opportunity to work in his laboratory and for his constant support and scientific guidance throughout the years. My second supervisor Prof. Roland Winter as well as my internal advisors Prof. Roger S. Goody and Prof. Stefan Raunser are also highly acknowledged for helpful discussions and critical evaluation of my work.

Thanks to past and present members of the MPI Dortmund, especially departments I and III, for help in the lab, sharing reagents and ideas as well as the nice working atmosphere. In particular, I want to acknowledge Dr. Alex Faesen, who was always a great help in the lab, especially with microtubule cosedimentation, microtubule flow cell and TIRF assays, and who was always there for fruitful discussions. I also want to express my gratitude to Dr. Pim Huis in 't Veld and Daniel Prumbaum for the EM analyses and to Dr. Arsen Petrovic for the AUC experiments. Thanks to Sabine Wohlgemuth for purification of the Ndc80 and Mis12 complexes and for introducing me to the insect cell culture, to Dr. Marion Pesenti for providing the RB3 and TTL proteins and to Dr. Jenny Keller for Zwint proteins. I also want to acknowledge Suzan van Gerwen and Beate Voß for the big help in the tissue culture. Thanks to Dr. Stefano Maffini for introducing me to the microscopes, to Dr. Anne Kuhlee for help with MST, to Arthur Porfetye for support with fishing crystals and to Dr. Kerstin Klare for help with western blots. My gratitude also goes to Dr. Ingrid Vetter for crystallographic discussions and her attempts to solve the structure of SKAP. I want to thank Georg Holtermann for invaluable technical assistance. Thanks to all the people who analyzed my numerous crystals at the SLS and to the beamline staff for help with the data collection at the SLS. I want to acknowledge our student assistant Hendrik Hausmann, who prepared a huge amount of SDS-PAGE gels and buffers for me. My deep gratitude also goes to Antje Peukert and Christa Hornemann for support outside the lab, help with overcoming bureaucratic barriers and nice talks during lunchtime.

I appreciate the collaborations with Dr. Franz Herzog and Josef Fischböck of the LMU Munich, who did the crosslinking analyses that were a great help for my work, and with Giuseppe Ossolengo of the antibody facility at the IFOM-IEO in Milan, who was a big help with the production of the SKAP antibody.

I want to acknowledge the Fonds of the Chemical Industry and the International Max Planck Research School (IMPRS) for financial support.

Last but not least I want to express my warmest gratitude to my family and friends, who always supported me and believed in me. Special thanks go to my mother Barbara Rose, who is there for me in every circumstance and who is like a best friend to me. My warmest thanks also go to my husband Timon Friese, who lovingly supports me wherever he can and thereby is the basis for the success of this work.

Affidavit (Eidesstattliche Versicherung)

Friese, Alexandra — 0101647

Name, Vorname (Surname, first name) — Matrikel-Nr. (Enrolment number)

Belehrung:	Official notification:
Wer vorsätzlich gegen eine die Täuschung über Prüfungsleistungen betreffende Regelungen einer Hochschulprüfungsordnung verstößt, handelt ordnungswidrig. Die Ordnungswidrigkeit kann mit einer Geldbuße von bis zu 50.000,00 € geahndet werden. Zuständige Verwaltungsbehörde für die Verfolgung und Ahndung von Ordnungs-widrigkeiten ist der Kanzler/die Kanzlerin der Technischen Universität Dortmund. Im Falle eines mehrfachen oder sonstigen schwerwiegenden Täuschungs-versuches kann der Prüfling zudem exmatrikuliert werden, § 63 Abs. 5 Hochschul-gesetz NRW.	Any person who intentionally breaches any regulation of university examination regulations relating to deception in examination performance is acting improperly. This offence can be punished with a fine of up to EUR 50,000.00. The competent administrative authority for the pursuit and prosecution of offences of this type is the chancellor of the TU Dortmund University. In the case of multiple or other serious attempts at deception, the candidate can also be unenrolled, Section 63, paragraph 5 of the University Act of North Rhine-Westphalia.
Die Abgabe einer falschen Versicherung an Eides statt ist strafbar.	The submission of a false affidavit is punishable.
Wer vorsätzlich eine falsche Versicherung an Eides statt abgibt, kann mit einer Freiheitsstrafe bis zu drei Jahren oder mit Geldstrafe bestraft werden, § 156 StGB. Die fahrlässige Abgabe einer falschen Versicherung an Eides statt kann mit einer Freiheitsstrafe bis zu einem Jahr oder Geldstrafe bestraft werden, § 161 StGB.	Any person who intentionally submits a false affidavit can be punished with a prison sentence of up to three years or a fine, Section 156 of the Criminal Code. The negligent submission of a false affidavit can be punished with a prison sentence of up to one year or a fine, Section 161 of the Criminal Code.
Die oben stehende Belehrung habe ich zur Kenntnis genommen:	I have taken note of the above official notification:

Ort, Datum (Place, date) — Unterschrift (Signature)

Titel der Dissertation:
(Title of the thesis):

Molecular dissection of the spindle and kinetochore associated Astrin/SKAP complex

Ich versichere hiermit an Eides statt, dass ich die vorliegende Dissertation mit dem Titel selbstständig und ohne unzulässige fremde Hilfe angefertigt habe. Ich habe keine anderen als die angegebenen Quellen und Hilfsmittel benutzt sowie wörtliche und sinngemäße Zitate kenntlich gemacht.	I hereby swear that I have completed the present dissertation independently and without inadmissible external support. I have not used any sources or tools other than those indicated and have identified literal and analogous quotations.
Die Arbeit hat in gegenwärtiger oder in einer anderen Fassung weder der TU Dortmund noch einer anderen Hochschule im Zusammenhang mit einer staatlichen oder akademischen Prüfung vorgelegen.	The thesis in its current version or another version has not been presented to the TU Dortmund University or another university in connection with a state or academic examination.*

*Please be aware that solely the German version of the affidavit (“Eidesstattliche Versicherung”) for the PhD thesis is the official and legally binding version.

Ort, Datum (Place, date) — Unterschrift (Signature)